Theoretical Investigations of the Role of Ion-Ion Correlations and Ion-Specific Interactions in Electric Double Layers

Erik Wernersson

Thesis for the Degree of Doctor of Philosophy in Chemistry
in the Field of Physical Chemistry

This thesis is to be defended in English on the 2:nd of October 2009
at 10:15 in room 10:an, kemivägen 10, Göteborg.

Faculty opponent is Dr. Luc Belloni,
LIONS, CEA/SACLAY, France.

UNIVERSITY OF GOTHENBURG
DEPARTMENT OF CHEMISTRY
2009

ISBN 978-91-628-7869-6

ISBN 978-91-628-7869-6

Typeset with LaTeX.
Printed by Chalmersbibliotekets reproservice,
Göteborg, Sweden 2009

Abstract

Electric double layers are ubiquitous, arising in some form in almost every situation involving an interface with an aqueous electrolyte solution. In order to gain insight into the behavior of electrolytes and electric double layers, simple models of bulk and inhomogeneous electrolyte solutions are considered in this thesis. As the main focus is on situations where mean field theory is not applicable, due to high concentration, strong electrostatic interactions, polarization of the interface or a combination of these, the spatial correlation between ions is explicitly considered.

This is done within the framework of integral equation theory. The hypernetted chain (HNC) approximation is employed, which may be regarded as an approximate expression for the relation between the correlation functions and the potential of mean force. The excess contribution to the chemical potential is readily obtainable in the HNC approximation. By exploiting the fact that the ideal contribution to the chemical potential only depends on the local concentration and that thermodynamic equilibrium requires that the total chemical potential is equal everywhere, the concentration profile for each species of ion can be determined. Thus, the HNC approximation gives rise to a theory for electric double layers as well as for bulk electrolytes.

The model of ions and interfaces is based on the assumption that the ions are hard, charged spheres that are embedded in a dielectric continuum that represents the solvent. This type of model obviously ignores any effect of the atomic granularity of the solvent, but takes into account both electrostatic and excluded volume effects that together give rise to several interesting and counter-intuitive phenomena. These have implications for both single interface properties and interface-interface interactions.

Any contrast in dielectric properties on each side of the interface gives rise to forces on the ions in the vicinity, which may also be of importance for the behavior of the system. Dispersion interactions between ions and interfaces are present whenever the ions have a nonzero polarizability. Each ionic charge in the vicinity of an interface also causes polarization, creating a charge distribution that gives rise to forces on all ions in the vicinity. Thus, such polarization modifies the forces amongst ions as well as those between ions and interfaces. Both dispersion forces and the polarization of interfaces are explicitly considered in this thesis.

List of Papers

I. **On the Effect of Image Charges and Ion-Wall Dispersion Forces on Electric Double Layer Interactions**
Erik Wernersson and Roland Kjellander
J. Chem. Phys. **2006**, 125, 154702.

II. **Image Charges and Dispersion Forces in Electric Double Layers: The Dependence of Wall-Wall Interactions on Salt Concentration and Surface Charge Density**
Erik Wernersson and Roland Kjellander
J. Phys. Chem. B **2007**, 111, 14279.

III. **Ion Correlation Forces Between Uncharged Dielectric Walls**
Erik Wernersson and Roland Kjellander
J. Chem. Phys. **2008**, 129, 144701.

IV. **Charge Inversion and Ion-Ion Correlation Effects at the Mercury/Aqueous $MgSO_4$ Interface: Towards the Solution of a Long-Standing Issue**
Erik Wernersson, Roland Kjellander and Johannes Lyklema
Submitted to J. Phys. Chem. C.

V. **On the Applicability of Simple Electrolyte Models to Solutions of Divalent Metal Sulfates**
Erik Wernersson and Zareen Abbas
Submitted to J. Phys. Chem. B.

Acknowledgments

First of all I would like to thank my advisor Roland Kjellander, without the aid from whom this work would scarcely have been possible to complete.

Second, I would like to thank Hans Lyklema for instigating and following through with the line of inquiry that led to Paper IV and Zareen Abbas for the long and fruitful discussions about bulk electrolytes that eventually led to Paper V.

I would also like to thank my co-advisor Johan Bergenholtz for reading and commenting on my manuscripts, George Bacskay and Itai Panas for helping me with the quantum mechanical calculations in Paper I, Lee White for providing me with data on the dielectric functions of polystyrene and water, David Schiffrin for making the component of charge data from his thesis available to me and Luboš Vrbka for helping me to detect an improper generalization in the latest version of my HNC-solving code.

The members of the physical chemistry group deserve great thanks for making my time there enjoyable and interesting. This applies equally to the old guard: Erik Abrahamsson, Bodil Ahlström, Andreas Bäck, Carina Bäcktorp, William Eek, Björn Forsberg, Kai Lüder, Daniel Nilsson, Sture Nordholm, Gunnar Nyman, Jens Poulsen, Staffan Wall, Anna Zackrisson and Malin Zackrisson, as to the neophytes: Sergey Antipov, Magnus Gustafsson, Huaqing Li, Moheb Nayeri and Rasmus Persson, as well as to the wandering scholars: Stefan Andersson (also a member of the old guard), Terry Francombe, Jan Franz, Zhiying Li and Soheil Sharifi. Special thanks to Staffan Wall for teaching me to find and identify the delicious mushroom *cantharellus tubaeformis*, Erik Abrahamsson for finagling a comfortable chair for me and Carina Bäcktorp for bestowing on me the illustrious office of toastmaster at her disputation party.

Last but not least, I would like to thank my family for their enduring support and encouragement.

Marta, kocham cię.

Contents

Chapter 1

Introduction

Typically, a particle becomes charged due to adsorption or desorption of ions when immersed in water or a similar solvent. The counterions to a particle that has acquired a net charge remain in the vicinity, forming an "ionic atmosphere" around the particle. Together with the charge on the surface itself, this "atmosphere" is usually referred to as an *electric double layer*. This double layer is best described in terms of the local concentration of each species of ion as a function of position relative to the surface. The concentration of counterions typically decreases from a high concentration close to the surface to the bulk concentration with increasing distance from the surface. Conversely, the concentration of co-ions is typically low close to the surface and approaches the bulk concentration from below for large distances. The exact structure of the double layer is determined by a subtle balance between minimizing the Coulomb energy and maximizing the configurational entropy of the ions. Therefore, the properties of electric double layers are sensitive to the conditions in the bulk solution. Most notably, the concentration of electrolyte is the main factor that determines the spatial extent of the ionic atmosphere. Under experimentally attainable conditions, the thickness of the double layer can be as small as less than a nanometer or as large as hundreds of nanometers. Thus, a charged particle in solution together with its counterions form an electroneutral unit that can be many times larger than the particle itself or negligibly different from the particle in size, depending on the salt concentration. In light of this, it is not surprising that many properties of colloidal systems and interfaces that are dependent on salt concentration are related to electric double layers; it is the electric double layer that connects such seemingly disparate phenomena as electrokinesis, colloidal interactions and electrocapillarity.

For many systems of interest to colloid science, it is sufficient to treat the

consequences of the presence of charge on a mean field level of theory, where it is assumed that each ion sees its surroundings only in terms of their average behavior. This is a good approximation in situations where the typical interactions between ions are so weak that any individual ion does not perturb its environment strongly. This thesis is mainly about situations where this is not the case, where *ion-ion correlations* are important. The behavior of individual ions then depends on the details of how each ion affects the spatial distribution of its neighbors. This occurs for high densities, strong interactions or both and has important consequences in the bulk solution as well as in the vicinity of charged, or uncharged, surfaces. Depending on the details of *how* each ion affects its surroundings, the deviations from mean field behavior can be very different. Often, these deviations can give rise to phenomena that are qualitatively different from what would be expected from mean field theory. The limit of the range in concentration where mean field theory can be fruitfully applied tends to coincide, at least roughly, with the range of concentration in which the details of the interionic interactions are relatively unimportant. Above this limit one must take on the dual challenge of finding the details of the interionic interaction potential and working out the consequences of these details on the ion-ion correlations in order to find satisfactory descriptions of double layers and bulk electrolytes.

Any contrast in dielectric properties between the interior of a particle and the surrounding medium gives rise to forces on any ion in the vicinity of the particle surface. The *dynamic* polarization of the surface in response to charge density fluctuations in the ion gives rise to dispersion forces whereas the *static* polarization of the surface gives rise to so called image forces. If a charge is brought close to an interface between two dielectric media the compromise between the polarization of each medium will lead to a charge distribution on the surface. For planar interfaces, the field from this surface charge distribution is the same as the field from a charge that is located at the position of the "mirror image" of the original charge. The fictitious charge is referred to as an "image charge", hence the name "image forces". Because these forces are electrostatic in nature, the image charges are screened in the presence of electrolyte. This is a consequence of ion-ion correlations; in order for the screening to come out correctly in any theoretical treatment, ion-ion correlations must be taken into account. Dispersion interactions, on the other hand, are due to correlated charge density fluctuations on time scales so short that the ions cannot respond. Therefore, dispersion interactions are not subject to electrostatic screening. The effective range of these interactions does not depend strongly on the salt concentration. In papers I and II the consequence of image forces and dispersion forces for the interaction between

charged surfaces is explored. In paper III a similar investigation is carried out for uncharged surfaces.

Ions of higher valency than monovalent tend to interact so strongly that mean field theory is valid only in a very narrow range of concentration and surface charge density. This has consequences both in bulk and near surfaces. Counter-intuitively, strong repulsion between counterions near a surface causes the amount of counterions in the vicinity of the surface to be *larger* than for more weakly interacting counterions. This can have the consequence that an enrichment of co-ions occurs some distance from the surface, so that the surface appears to have a charge of the opposite sign compared to the actual surface charge to an observer in the bulk solution. This situation is referred to as charge inversion or overcharging. While this have been observed for simple models of electrical double layers since the early 1980s, the existence of this phenomenon *as a consequence of ion-ion correlations* in real systems has not yet been unambiguously demonstrated in experiments. In part, the dearth of experimental proof is due to the existence of alternative mechanisms for overcharging, notably adsorption of ions due to non-electrostatic interactions. The need to discriminate between different mechanisms places a great demand on the comparison between experiment and theory in that the comparison must be quantitative rather than qualitative. In paper IV an attempt is made to test the predictions of double layer models that charge inversion can occur as a consequence of ion-ion correlations. This is done by making a comparison between model predictions for surface thermodynamic properties and experimental data for the interface between mercury and aqueous solutions of magnesium sulfate. In the course of this work the question was raised to what extent the primitive model can be applied as a quantitative model of divalent salt solutions. This question is addressed in Paper V along with a possible modification to the model.

Chapter 2

Electrolytes and Electric Double Layers

> "All animals are equal, but some animals are more equal than others."
>
> -George Orwell, *Animal Farm* (1945)

Electrolytes are different from solutions containing only uncharged particles. Most obviously, electrolytes are electric conductors whereas non-electrolytes are insulators. Practically and historically, this is the defining property of an electrolyte. A closer look at the physico-chemical properties reveal more differences from ordinary solutions: thermodynamic properties of electrolytes such as activity coefficients and osmotic pressure (see definitions in Section 2.1) differ measurably from ideal solution behavior even for very low concentrations, where neutral solutes would behave ideally. Both these observations can be explained by the special properties of electrostatic interactions.

The electrostatic force between particles with charges of the same sign is repulsive whereas it is attractive for particles with charges of opposite signs. In both cases the magnitude of the force is proportional to the product of the magnitudes of the charges and to the inverse square of the distance between them. Electric charge is quantized so that the charge of any particle is $\pm ne_0$ where n is an integer and e_0 is a constant. There is no known process in which charged particles are created or destroyed that does not preserve the total charge. One can therefore reasonably suspect that the amount of positive charge in the universe is equal to the amount of negative charge, down to the last e_0. These facts are so familiar that they appear

self-evident. Yet these laws are very remarkable, both with respect to their simple structure and far-reaching consequences. This is especially so since it is hard to imagine another set of laws of interaction that would from charged building blocks produce the macroscopic world as we see it: as composed of uncharged objects.

That we only occasionally encounter charged objects in a world where electrostatic interactions are ubiquitous and decisive for the properties of matter is due to the phenomenon of *screening*. Because unlike charges attract over long distances, ions tend to arrange themselves so that oppositely charged ions sit close to each other. The charges then appear to compensate each other when viewed from a sufficient distance. The most obvious example of this is an ionic crystal, where each ion has a well-defined position on a lattice of alternating anions and cations. Individual atoms also constitute an example of screening as the electrons shield the charge of the nucleus. Because the laws of quantum mechanics prohibit it, the exact positions of each electron in an atom cannot be known. Our knowledge is limited to the continuous probability distributions of positions of electrons, essentially the charge density. This situation of screening by a diffuse distribution of charge is also seen in electrolytes, but for completely different reasons that will be explained below.

In the macroscopic world, just a minuscule amount of excess charge of either sign on an object is required to produce measurable, and sometimes spectacular, effects. This extra charge has no counter-charge to screen it and so brings the long-range character of electrostatic interactions into the macroscopic world. While it is easy enough to put a small amount of extra charge on an object, for instance by rubbing two insulators (e.g. comb and hair) together in reasonably dry air, it does not correspond to an equilibrium situation. Whenever the opportunity arises, electric current will spontaneously flow to eliminate any unscreened charge. The condition that a system in equilibrium contains equal amounts of positive and negative charge is called the *electroneutrality condition*.

In electrolyte solutions the charges on the ions are screened by two different mechanisms. On one hand, the field from the ions orient the dipolar solvent molecules with the net result that the mean force between ions in pure solvent is for large distances of the same form as between charges in vacuum but significantly weaker. This is referred to as dielectric screening. On the other hand, the ions arrange themselves to effect mutual screening. It is this mechanism that is referred to when the word "screening" is used without qualifier. Because of the dielectric screening from the solvent, the strength of the net electrostatic interactions between ions is brought down

from its vacuum value to a magnitude comparable to the energy scale of the thermal motion. In this situation the configurational entropy of the ions is not insignificant compared to the entropy gain that can be obtained by the ions arranging themselves in the minimum-energy configuration and thereby dissipating the maximum heat. To find the equilibrium properties of the system both "entropic" and "energetic" contributions to the free energy has to be considered. The contribution from the configurational entropy acts to spread the ions evenly over the available volume and therefore counteracts screening for length scales smaller than that associated with that volume. The energetic contribution acts, as already established, to order ions into an arrangement with ions of different signs close to each other and those of the same sign further away. The actual distribution of ions is determined by a compromise between these two tendencies. A useful measure of the strength of electrostatic interactions in relation to the thermal energy is the Bjerrum length,

$$l_B = \frac{e_0^2}{4\pi\epsilon\epsilon_0 k_B T}, \tag{2.1}$$

where T is the temperature, k_B is Boltzmann's constant, ϵ_0 is the vacuum permittivity, and ϵ is the relative permittivity of the solvent, that is a measure of dielectric screening (hence the alternative name dielectric constant). The Bjerrum length may be interpreted as the distance between unit charges for which their interaction energy compared to infinite separation is exactly $k_B T$. In vacuum, l_B is 560 Å at room temperature. In water l_B is roughly eighty times shorter, about 7 Å under the same conditions. Because the typical size of ions is a few Å in diameter, the expectation is that for monovalent salts the electrostatic interaction does not reach more than a few $k_B T$ at any point in space. This cannot be taken for granted, however, as the characterization of the solvent by just its relative permittivity is not necessarily justified for distances of the order of the size of the solvent molecules, see Section 3.

A charged surface in contact with an electrolyte solution always has a diffuse region of counter-charge associated with it, that together with the surface charge forms an electric double layer. This name derives from that the double layer was originally thought to literally consist of two charged planes some distance from each other. The concept is originally due to Quincke [1] but the name "double layer" (actually *doppelschicht*) was coined by Helmholtz [2]. The modern picture of the electric double layer is that there is a continuously varying deviation in concentration of each species of ion from the bulk concentration. Close to the surface there is a region where the solution is not locally electroneutral, but has a total charge that exactly compensates the surface charge, preserving global electroneutrality. The excess charge in

the region outside the surface can arise both from enrichment of counterions to the surface and by depletion of co-ions. All charged particles, including individual ions, disturb their environments in this way. A theory for electric double layers is therefore by necessity also a theory for electrolyte solutions, and vice versa. The structure of an electric double layer is best described by the *concentration profiles* associated with it. We write the concentration profile of ions of species i as $n_i(\mathbf{r})$ and interpret it simply as the local concentration of that species of ion at point $\mathbf{r}$. Far from any interface the concentration profile approaches the bulk concentration, denoted n_i^{bulk}, and thus becomes independent of position. Related to the concentration profile is the pair distribution function $g_{ij}(\mathbf{r}, \mathbf{r}')$, with the interpretation that $n_i(\mathbf{r})g_{ij}(\mathbf{r}, \mathbf{r}')$ is the concentration of ions of species i at $\mathbf{r}$ given that there is an ion of species j at $\mathbf{r}'$. In bulk, $\mathbf{r}'$ can be taken as the origin of the coordinate system and $n_i^{bulk}g_{ij}(\mathbf{r})$ can be interpreted as the concentration profile around any given ion. These concepts will be introduced in a more formal way and discussed in Chapter 4. Examples of pair distribution functions relevant for the system considered in Paper IV are shown in Figure 2.1. Note that the cation-anion pair distribution function for the 2:2 salt is very strongly peaked at contact, much more so than the corresponding function for the 1:1 salt.

There are certain restrictions that the set of distribution functions in an electrolyte solution has to obey, most obviously the electroneutrality condition. The distribution of charge around an ion of species i in bulk solution is

$$\rho_i(\mathbf{r}) = \sum_j q_j n_j^{bulk} g_{ij}(\mathbf{r}), \tag{2.2}$$

where q_j is the charge of an ion of species j and the sum is over all charged species in solution. Because electroneutrality dictates that the total charge of an ion and the charge distribution around it is zero, the distribution must contain a total amount of charge that is equal in magnitude and opposite in sign to the charge of the central ion. This condition leads to the sum rule

$$\frac{\sum_i q_i n_i^{bulk} \sum_j q_j n_j^{bulk} \int g_{ij}(\mathbf{r})\, d\mathbf{r}}{\sum_i q_i^2 n_i^{bulk}} = -1 \tag{2.3}$$

for the pair distribution functions. From the connection between the distribution functions and the response to external fields, that is mentioned in Chapter 4 as eq. (4.18), together with the fact that electrolytes behave as conductors on a macroscopic scale, a less obvious sum rule that can be derived [3],

$$\frac{\sum_i q_i n_i^{bulk} \sum_j q_j n_j^{bulk} \int r^2 g_{ij}(\mathbf{r})\, d\mathbf{r}}{\sum_i q_i^2 n_i^{bulk}} = -\frac{6}{\kappa^2}, \tag{2.4}$$

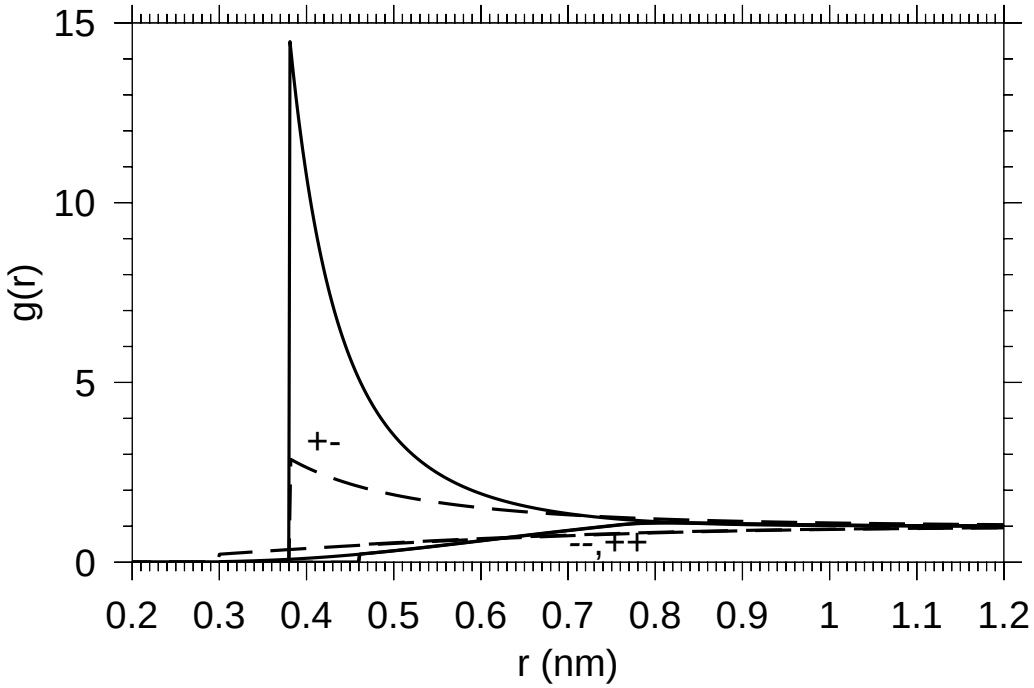

Figure 2.1: Pair distribution functions for the model 2:2 electrolyte (solid lines) considered in Paper IV and an analogous model 1:1 electrolyte (dashed lines) with the same ion sizes for 0.5 M bulk concentration calculated within the HNC approximation, see Section 4.2. The cation-anion distribution function is marked by "+−" and the anion-anion and cation-cation distributions functions are marked with "−−" and "++", respectively. Note that the like-ion distribution functions are indistinguishable on the scale of the figure in the range where they overlap (the cations are smaller than the anions) for each type of salt.

with κ defined by

$$\kappa^2 = \frac{1}{k_B T \epsilon \epsilon_0} \sum_i q_i^2 n_i^{bulk}. \tag{2.5}$$

The quantity κ^{-1} may be considered the characteristic length scale of screening in an electrolyte and has a prominent place in mean-field theories of electrolytes and electric double layers, discussed in Section 2.2 below. Notably, κ is proportional to the square root of the ionic strength. Both eqs. (2.3) and (2.4) are consequences of the special properties of electrostatic interactions; there are no counterparts for solutions of uncharged solutes. Note however that eq. (2.3) would be valid even if the potential for electrostatic interaction decayed as fast as $1/r^3$, whereas eq. (2.4) requires the interaction potential

to decay as $1/r$ to hold.

Electrolytes and electric double layers can be probed experimentally in a variety of ways. Of special interest for double layers are direct and indirect measures of the interaction between charged surfaces. Section 2.3 contains a discussion about the effect of electric double layers on interactions between surfaces. Direct measurements of interactions between surfaces are just that: surfaces are brought together and the force between them is recorded as a function of distance [4, 5]. While this is naturally a difficult kind of experiment to perform, the current state of the art is that a high level of sophistication have been reached, to the degree that for some surfaces the force curves can be recorded with a distance resolution of less than one Å [6]. Indirect measures of interactions include measurement of the stability, phase behavior or structural properties of colloidal suspensions from which the interactions can be inferred.

Another important type of experiments is electrokinetic measurements, the most well-known example of which is electrophoresis. This technique is based on subjecting a suspension of particles to an electric field and measuring the velocity with which the particles move in response to it. The information about the electric double layer that can be obtained by this technique is model dependent. This is so because assumptions have to be made about the deviation in the viscosity of the solvent close to a particle surface from the bulk value in order to work out the connection between the double layer and the hydrodynamic drag forces on the particle. In the close vicinity of the particle the solvent is effectively stagnant with respect to the particle surface and any ions in this region will move with the particle and effectively add to its surface charge. Because the concentration profiles tend to decay quickly close to the surface, small differences in the assumptions about the width of the stagnant solvent layer can give rise to large changes in conclusions about the "actual" charge on the surface. Under conditions where the use of mean field theory, discussed in Section 2.2, is justifiable these difficulties are sometimes surmountable. Under such conditions the conclusions about surface charge from interaction studies tend to agree with those from electrokinetic experiments.

Not surprisingly, the methods of electrochemistry are useful in studying electric double layers. This is especially so if one electrode can be made such that no reaction takes place on its surface. In this way, reliable information about the dependence of surface thermodynamic properties can be obtained as functions of the potential and surface charge density. In Section 2.1 the relevant thermodynamic relations are discussed together with one of the most useful experimental systems for the study of double layers: the mercury elec-

trode. In that section some important bulk thermodynamic properties are introduced and the principle for their experimental determination outlined

2.1 Thermodynamics of Charged Systems

Due to the electroneutrality condition, the thermodynamic treatment of systems containing charged particles is slightly different compared to systems composed of neutral particles. Nevertheless, the thermodynamic properties of both bulk and interfacial electrolyte systems can be measured using standard techniques. Of special interest are those bulk properties that are directly related to the interactions between solute particles, mainly the chemical potential of the salt and solvent. The intensive properties of a system are related to each other by the Gibbs-Duhem equation,

$$0 = -VdP + SdT + \sum_i N_i d\mu_i, \tag{2.6}$$

where S is the entropy, V is the volume and P is the pressure. The sum is over all components and N_i and μ_i are the number of particles and chemical potential of species i, respectively. If a solution is placed in contact with a reservoir of pure solvent in such a way that only solvent and not solute particles can diffuse between the solution and the reservoir, eq. (2.6) implies that the pressure in the solution is different from that in the reservoir. The pressure thus exerted is called the osmotic pressure. Incidentally, it was the interpretation of osmotic data in terms of kinetic theory that first led to the conclusion that salts dissociate into free ions on dissolution [7]. Often, the osmotic pressure is expressed as the *osmotic coefficient*, that is here defined as the quotient of the actual bulk osmotic pressure, P^{bulk}, and the osmotic pressure for an ideal solute of the same concentration

$$\phi = \frac{P^{bulk}}{k_B T \sum_i n_i}, \tag{2.7}$$

where the sum is over *solute* species only. Note that this is a non-standard definition of this quantity. The reason for adopting this definition and its relationship with the standard one is discussed in Chapter 3. The chemical potential of solute species is usually expressed in terms of *activity coefficients*, f, defined by

$$\mu_i = \mu_i^0 + k_B T \ln f_i n_i^{bulk}, \tag{2.8}$$

where μ_i^0 is the chemical potential in the standard state. The interpretation of the argument of the logarithm is that it is the concentration of an ideal

solute that would have the same chemical potential as the real solute. Implicit in this definition is that the standard state is chosen as an ideal system at unit concentration in whatever unit is chosen for n_i^{bulk}, here taken as 1 M unless otherwise stated.

For constant temperature and pressure eq. (2.6) states that the chemical potential of a component of the system cannot be varied independently of the chemical potential of the other components. Exploiting this relation, the chemical potential of dissolved salt can be obtained from that of the solvent. This forms the basis of *isopiestic* determination of salt activity coefficients [8]. A solution with a known amount of salt is placed in a gas-tight, thermostated chamber together with a reference solution of a substance for which the chemical potential as a function of concentration is known with high accuracy. The solutions are then left alone until equilibrium is established, typically for several days. In both solutions, the solvent now has the same chemical potential. If the solute is non-volatile so that only solvent is exchanged, the equilibrium compositions can be established simply by weighing the solutions. If this is repeated for several starting concentrations, the activity coefficients of the solute can be obtained from integration of eq. (2.6). To obtain the proper integration constant, the osmotic coefficient must be known down infinite dilution where the system behaves ideally and $\ln(f_i) = 0$. Obviously, this cannot be done in practice and extrapolation must be used at some stage. In the case of the isopiestic method the lowest concentration that can be reliably treated is around 0.1 m, which cannot be considered close to infinite dilution. The extrapolation must therefore be carried out over a considerable concentration interval, thus introducing an appreciable uncertainty in the integration constant. This problem is most severe for electrolytes containing ions of higher valence types, where the range of validity of the Debye-Hückel limiting law, see eq. (2.25) below, is very narrow.

Note that the chemical potential of individual ionic species is *not* unambiguously obtainable by the isopiestic method or by any other known experiment. Because the electroneutrality condition allows only electroneutral combinations of ions to be added to a system, the number of particles of different ionic species are not independent quantities. What can be determined is therefore the chemical potential of such electroneutral combination of ions, denoted μ_{salt}. The activity coefficients of electrolytes are usually given in terms of the mean activity coefficients, $f_\pm$, defined for a binary electrolyte by

$$f_\pm^{(s_+ + s_-)} = f_+^{s_+} f_-^{s_-} \tag{2.9}$$

where s_i is the stoichiometric coefficient. The chemical potential of the salt

is given in terms of $f_\pm$ by

$$\mu_{salt} = \mu^0_{salt} + (s_+ + s_-)k_B T \ln f_\pm n^{bulk}, \tag{2.10}$$

where n^{bulk} is the bulk concentration of the salt. There are some subtleties inherent in relating experimentally determined activity coefficients to those calculated in models without an explicit solvent component. These are discussed in Chapter 3.

At an interface, the interfacial excess properties are related to each other by the thermodynamic relation, analogous to the Gibbs-Duhem equation, known as the Gibbs adsorption isotherm,

$$0 = Ad\gamma + S^{(s)}dT + \sum_i N_i^{(s)} d\mu_i, \tag{2.11}$$

where γ is the interfacial tension and $S^{(s)}$ and $N^{(s)}$ are the interfacial excess entropy and number of particles, respectively. The sum is over all components in the system. In this context "interfacial excess" means the difference in a thermodynamic quantity between two bulk phases and the system containing two phases with an interface between them, with each phase having the same volume in each case. The position of the interface used to determine the volumes is arbitrary, but can always be chosen uniquely in such a way that the interfacial excess number of particles of one component is zero. The surface excesses are then said to be with respect to that component, that will be referred to as the solvent. At constant temperature, the Gibbs adsorption isotherm can be written in a more convenient form,

$$-d\gamma = \sum_i \Gamma_i d\mu_i \tag{2.12}$$

where $\Gamma_i = N_i^{(s)}/A$ is referred to as the "surface excess"of species i and the sum may be regarded as being over all species except the solvent, as Γ of the solvent is zero by construction. For electrified interfaces the surface excesses are subject to the electroneutrality condition,

$$0 = \sum_i q_i \Gamma_i. \tag{2.13}$$

If the system is such that the charged components of the phases (denoted "I" and "II") on each side of the interface are negligibly soluble in the other phase, one can assign each of the ionic species to one of the phases. The thermodynamic surface charge can then be defined as

$$\sigma = \sum_i {}^{I} q_i \Gamma_i = -\sum_i {}^{II} q_i \Gamma_i, \tag{2.14}$$

where each of the summations is over components present in phase I or phase II only.

Let us consider such a system composed of a chemically inert electrode connected to a reference electrode, both immersed in a binary electrolyte. If one defines the potential difference between electrode and reference electrode as the difference in chemical potential of the charge carrier (electrons) per unit charge,

$$E_{\pm} = -(\mu_{e^-} - \mu_{e^-}^{ref}), \tag{2.15}$$

where the subscript on $E_{\pm}$ denotes that the reference electrode is *reversible* to either the cations or the anions. In other words, a reaction forming either the cation or the anion by reduction or oxidation of a solid substance can occur reversibly at that electrode. The chemical equilibrium between ions in solution and in the reference electrode connects the chemical potential of the salt with that of electrons in the reference electrode. Thus only two chemical potentials can be varied independently, that of the salt and that of electrons in the measuring electrode. One can use this to write the Gibbs adsorption isotherm as

$$-d\gamma = \sigma dE_{\pm} + \Gamma_{\mp} d\mu_{salt}. \tag{2.16}$$

From this form of the isotherm the Lippmann equation immediately follows,

$$\sigma = -\left.\frac{\partial\gamma}{\partial E_{\pm}}\right|_{T,\mu_{salt}}, \tag{2.17}$$

where the subscript $\pm$ on $E_{\pm}$ indicates that the equation is equally valid for reference electrodes reversible to cations or anions. For the surface excess of the ionic species to which the reference electrode is *not* reversible an analogous relation exists,

$$\Gamma_{\mp} = -\left.\frac{\partial\gamma}{\partial\mu^{salt}}\right|_{T,E_{\pm}}. \tag{2.18}$$

Thus, for any electrode for which the surface tension is measurable both the surface charge density and the surface excess of each ionic species is experimentally accessible. For double layers, the surface excesses of co- and counterions are often expressed weighted by the ionic charges as *components of charge*,

$$\sigma_{\pm} = q_{\pm}\Gamma_{\pm}. \tag{2.19}$$

The advantage of expressing surface excesses in terms of the components of charge is that they give the contribution of each ionic species to the countercharge to the surface charge, that makes a natural connection to the electroneutrality condition, eq. (2.14).

An experimental system that is regarded by many as the canonical system for the study of the electric double layer is the dropping mercury electrode and similar experimental set-ups [9]. The main advantage of using a liquid metal electrode is that the surface tension can be measured as a function of either the potential of the mercury electrode or the chemical potential of the bulk solution, while keeping the other quantity constant. From such measurements along with the Gibbs adsorption isotherm the surface charge density as well as the components of charge are available. Since the differential capacitance,

$$C = \left.\frac{\partial \sigma}{\partial E_{\pm}}\right|_{T,\mu_{salt}}, \tag{2.20}$$

is independently measurable, the surface charge density can, given an integration constant, be obtained also from this quantity. By comparing the surface charge densities obtained from the "surface tension" and "capacitance" route, the robustness of the experimental method can be tested.

Since quantities obtained from the mercury electrode are derived by the use of exact thermodynamic relations they are model independent and therefore suitable for testing the predictions of models. It is unfortunate that the mercury electrode does not readily lend itself to either interaction studies or electrokinetic experiments. Had this been the case, a large degree of uncertainty in the interpretation of such experiments could be removed by measurement of the thermodynamic surface charge density.

During the last century, a large body of data on the mercury/aqueous electrolyte system has been collected. It has been found that the properties of the double layer associated with this interface tend to show a strong ion specificity for positive polarization, where the anions are counterions, but only a weak ion specificity for sufficiently negative polarization, where the cations are counterions. The conclusion is that anions are attracted to the surface to a degree that depends on the identity of the ion but that this is not the case for cations. For negative polarization the mercury surface appears to be well approximated by models without ion-specific attractive interactions between the surface and the ions of the electrolyte.

2.2 Mean-Field Theory and Its Limitations

In some cases where the interaction between ions is weak the Poisson-Boltzmann (PB) theory gives an adequate description of the concentration profiles of ions

close to charged surfaces [10, 11]. The PB theory for planar surfaces is sometimes called Gouy-Chapman (GC) theory in the colloid science literature, and since only planar surfaces are considered here these names will be used interchangeably in this thesis. The fundamental assumption of PB theory is that the mean force on an ion at any point is equal to the force due to the electric field from the average charge distribution. The concentration profiles are then given by

$$n_i(\mathbf{r}) = n_i^{bulk} e^{-\frac{q_i \Psi(\mathbf{r})}{k_B T}}, \tag{2.21}$$

where $\Psi(\mathbf{r})$ is the mean electrostatic potential at point $\mathbf{r}$, given by

$$\Psi(\mathbf{r}) = \psi(\mathbf{r}) + \frac{1}{4\pi\epsilon\epsilon_0} \sum_i \int \frac{q_i n_i(\mathbf{r})}{|\mathbf{r} - \mathbf{r}'|} \, d\mathbf{r}', \tag{2.22}$$

where $\psi(\mathbf{r})$ is the potential from the charge on the surface. The mean electrostatic potential can be calculated using Poisson's equation and the fact that the mean charge distribution can be calculated from the concentration profiles, leading to the differential equation

$$-\epsilon\epsilon_0 \nabla^2 \Psi(\mathbf{r}) = \sum_i q_i n_i^{bulk} e^{-\frac{q_i \Psi(\mathbf{r})}{k_B T}}, \tag{2.23}$$

from which the concentration profiles can be determined through $\Psi(\mathbf{r})$. Eq. (2.21) would be exact if the ions were point charges and did not perturb their local environment, which would only be the case if their charge were infinitesimally small. Of course, due to the quantization of charge there is no such thing as an infinitesimal charge. Because the interaction between ions is only taken into account as the interaction between an ion and the mean field, that is zero in bulk, the PB theory contains the implicit assumption that the bulk electrolyte behaves as an ideal gas. For electrolytes, this is a severe approximation even for moderate concentrations. The PB approximation may be thought of as a mapping of an interacting system onto a non-interacting system in an external field that depends on the concentration profiles.

In the GC theory, the possibility that ions may adsorb due to specific interactions with the surface is not taken into account explicitly. The charge on the surface enters the problem only through the boundary conditions to eq. (2.23), typically of either the "constant potential" or the "constant surface charge density" type. To account for the common situation that the charge on the surface comes from a layer of ions adsorbed on the surface due to non-electrostatic interactions, the GC theory is often combined with a *Stern layer* where ions are assumed to be adsorbed by some non-electrostatic mechanism [12]. The assumption is that there is a chemical equilibrium between free

ions and ions in the Stern layer. The free energy of adsorption corresponding to this equilibrium is typically used as a fitting parameter. The resulting theory is referred to as Gouy-Chapman-Stern (GCS) theory. For an exhaustive account of this theory, see ref. [13]. Because, as will be discussed in Section 2.4, the presence of specific adsorption is the rule rather than the exception in colloid and interface science, GCS theory finds wider application than GC theory itself. The practice of using the parameters specifying the Stern layer as fitting parameters also means that agreement between GCS theory and experiment at best provides information about the magnitude of the free energy of adsorption. To establish the mechanism of adsorption requires additional information. This problem is similar to the problem that is faced for bulk electrolytes, discussed in Section 3, that the physical interpretation of the parameters that determine the short range interaction between ions is very hard to ascertain by comparison with macroscopic measurements.

If $\Psi(\mathbf{r})$ is small everywhere, the exponential function in eqs. (2.21) and (2.23) can be linearized to give

$$\nabla^2\Psi(\mathbf{r}) = \kappa^2\Psi(\mathbf{r}), \tag{2.24}$$

where κ^2 is the same quantity as given by eq. (2.5). This theory predicts that the concentration profiles for a flat surface decay exponentially to bulk concentration with a decay length κ^{-1}. For this reason, eq. (2.24) is recovered from eq. (2.23) wherever the potential is small in magnitude. Consequently, the long distance asymptotic decay of the concentration profiles always have the same exponential form if the concentration is low enough for eq. (2.24) to be valid. In this limit, electric double layers are well understood in the sense that a theoretical framework exist that can accommodate a large body of evidence from a wide variety of experimental techniques.

By applying eq. (2.24) to the case where $\psi(\mathbf{r})$ is the potential from an ion of species i a theory for the distribution functions $g_{ij}(\mathbf{r})$ in a bulk electrolyte is obtained. (Recall that $n_i^{bulk}g_{ij}(\mathbf{r})$ can be interpreted as the concentration profile of ions of species i around an ion of species j.) This theory is known as the Debye-Hückel (DH) theory [14]. As can be imagined, it is in many ways quite crude. For instance, the theory predicts unphysical negative values for the distribution function between like-charged ions under some conditions. What is not obvious, but can be shown [15], is that the DH theory is exact in the limit of low concentration of salt. The properties of electrolyte solutions in this limit are generic; the chemical idiosyncrasies of a given system plays a negligibly small role for its behavior. What matters under these conditions are the ionic charges and κ. For instance, the activity coefficients are given

in the DH theory in the low concentration limit by

$$\ln f_i = -\tfrac{1}{2} Z_i^2 \kappa l_B, \tag{2.25}$$

where $Z_i = q_i/e_0$ is the *valency* of an ion of species i. Comparison between activity coefficient from eq. (2.25), often referred to as the Debye-Hückel limiting law (DHLL), and experiment reveals that the range of validity of this theory is rather limited, especially so for salts containing ions of valencies greater than one. Incidentally, eq. (2.25) is also obtained in the limit of zero ion-size. That a finite result is obtained at all in this limit is due to the strictly linear treatment of the Coulomb interactions. An exact treatment of a model with point ions would give negative infinity for $\ln f_i$, see Section 3.1. At least for 1:1 salts, the range where agreement with experiments is found can be extended considerably by taking the finite ion size into account, as was done in the original derivation of the theory.

In situations of high surface charge density or high electrolyte concentration as well as for strongly interacting ions the assumption underlying the PB theory that the ions behaves as point ions that do not perturb their local environment is not realistic. Under such conditions the mean-field approach cannot be sustained; each ion have a strong influence on its surroundings and this has to be taken into account when computing the average force on each ion. It is instructive to note that the PB approximation can be derived from an exact statistical mechanical expression by setting $g_{ij}(\mathbf{r}, \mathbf{r}')$ identically equal to one and ignoring any interaction between ions except the Coulomb interaction [16]. When $g_{ij}(\mathbf{r}, \mathbf{r}')$ differs significantly from one in an appreciable volume the PB theory is a poor approximation. This is true regardless of *how* the pair distribution functions differ from one. In what way the true concentration profiles differ from the PB-concentration profiles, *does* depend strongly on the details of $g_{ij}(\mathbf{r}, \mathbf{r}')$.

The exponential form of the distribution functions that is obtained whenever eq. (2.24) is valid tends to be retained up to relatively high concentration. The relation between the decay length and the electrolyte concentration is in general more complicated than in DH theory, however, even for simple electrolyte models [17, 18, 19]. For high concentrations the pair distribution functions develop oscillations. The structure of the solution becomes such that the ions are ordered in what might be called a "diffuse lattice": each ion is surrounded by an ionic atmosphere with regions of alternating sign of the average charge density because alternating layers of depletion and enrichment of anion and cations are formed. Interestingly, it can be concluded that the pair distribution functions cannot be monotonic for arbitrarily large

concentrations on the basis of only eq. (2.4) and the assumption that the ions have a finite size [20].

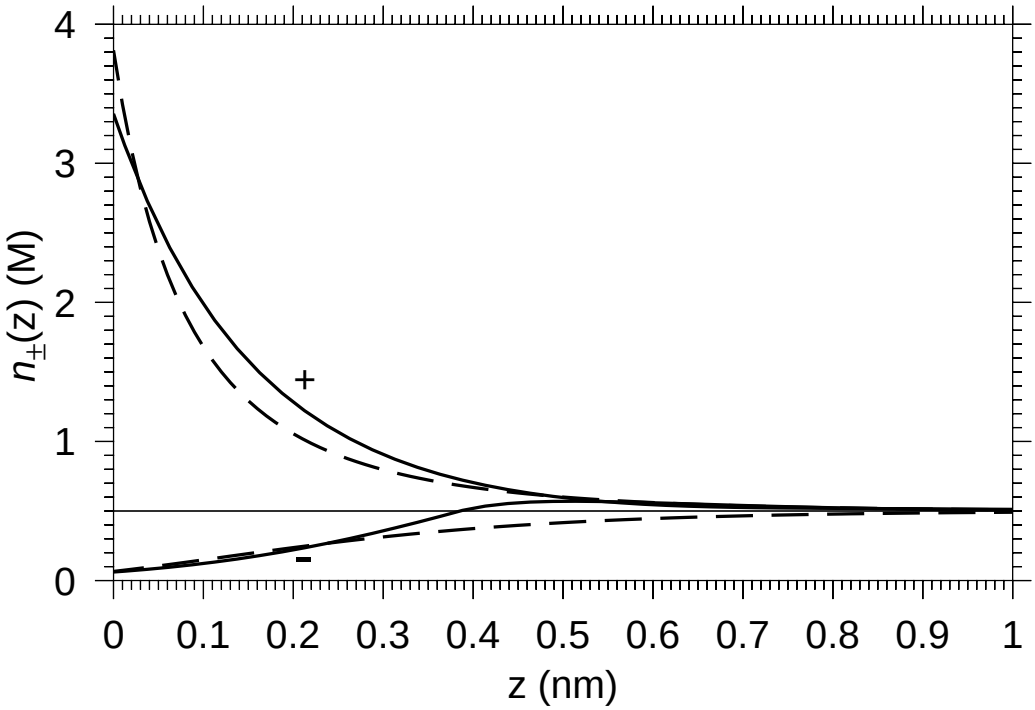

Figure 2.2: Concentration profiles for the model 2:2 electrolyte considered in Paper IV for 0.5 M bulk concentration and a surface charge density close to -10 µC cm^{-2} calculated within the HNC approximation, see Section 4.2. The dashed lines are the concentration profiles from PB theory for the same system. The cation (counterion) profiles are marked with a plus-sign and the anion (co-ion) profiles are marked with a minus-sign.

For situations characterized by strong electrostatic interactions, mean field theories are inaccurate even at very moderate concentration, both for bulk and surface properties. In such situations the the electrostatic interactions between anions and cation make the distribution function $g_{+-}(\mathbf{r}, \mathbf{r}')$ very large for small separations. This situation has been dubbed "ion pairing". Aqueous salt solutions containing only monovalent ions tend to be "weakly interacting" whereas systems containing divalent (or higher) ions tend to be "strongly interacting", in the sense that in the former case but not in the latter, mean field theory usually works reasonably well. Nevertheless, a modification of the DH theory by Bjerrum where ion pairing is explicitly considered in terms of a chemical equilibrium between "free" and "paired"

ions significantly improves the predictions of the bulk properties of binary salt solutions where both the cation and the anion are divalent. [21].

Strong electrostatic interactions also have consequences close to surfaces. Simple double layer models, discussed in Section 3.1 below, show that when the repulsion between counterions is sufficiently strong, the behavior of the electric double layer is qualitatively different from the predictions of mean field theory. Counter-intuitively, stronger interactions between counterions give rise to a larger enrichment of counterions close to the surface than weaker interactions. A situation that is typical for polyvalent counterions is that for sufficiently large surface charge densities there is an enrichment of co-ions compared to counterions in the region beyond a few Å from the surface. The co-ion concentration profile then approaches the bulk concentration from above at large distances from the the surface. To an observer in the bulk solution, the surface can then appear to have charge of opposite sign to that of the actual surface charge. For this situation to arise, the electroneutrality condition dictates that there must be a larger amount of counter-charge than is required to neutralize the surface charge in the region close to the walls. Therefore, the phenomenon is often referred to as *overcharging*. In Figure 2.2 the concentration profiles for a model system where overcharging is taking place are shown together with the concentration profiles from PB theory. Notice especially the difference in the co-ion profile compared to its PB counterpart. Overcharging can also arise due to attractions of a chemical nature between counterions and the surface. Such interactions, discussed further in Section 2.4, are common in real systems and frequently gives rise to overcharging that is strong compared to the overcharging from ion-ion correlations that can be expected for aqueous systems near room temperature for reasonable ion valencies. For this reason together with a scarcity of model systems that are sufficiently well characterized with respect to, for instance, the surface charge density, it has been difficult to find experimental systems to test the model predictions of overcharging due to ion-ion correlations.

Another counter-intuitive prediction of simple electrolyte models is that the potential difference between the surface and the electrolyte bulk need not be a monotonic function of the surface charge density. The potential can have an extremum, beyond which the potential varies with surface charge density in a direction opposite to what would be expected from simple electrostatics. Under some conditions, making the surface charge density more positive can thus have the effect of making the potential *less* positive. For surface charge densities in the experimentally attainable range this behavior is seen for divalent [22] and multivalent counterions. That the potential as a function of surface charge density has an extremum carries the implication that

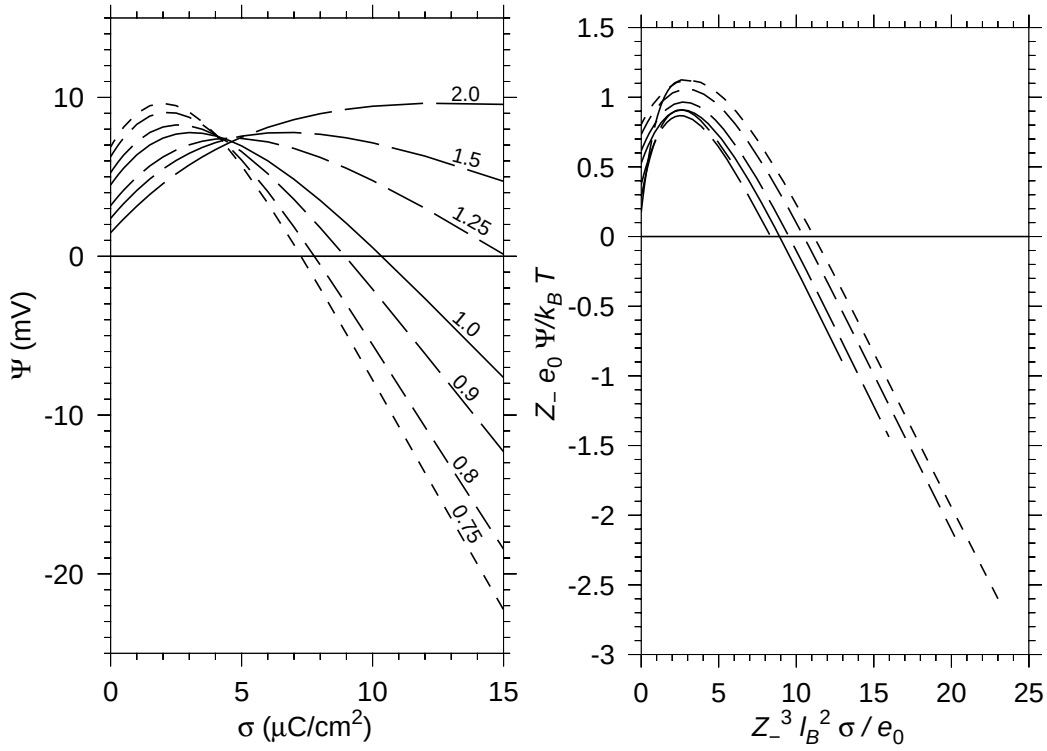

Figure 2.3: Potential drop over a double layer in the presence of a primitive model 1:3 salt of 0.25 M concentration. The ion diameters are $d_{++} = 3.6$, $d_{+-} = 5.0$ and $d_{--} = 6.4$ Å, see Section 3.1. The permittivity of the solvent is taken to be 2.0, 1.5, 1.25, 1.0, 0.9, 0.8 and 0.75 times that of water, as indicated in the left figure. In the right figure the potential and surface charge density are given in reduced units. The reduced potential is the work required to increase the surface charge by the charge of one counterion divided by k_BT. The reduced surface charge density is the quotient between the area of a quadratic grid such that the counterions can be placed on it so far apart that their mutual interaction energy is exactly k_BT divided by the area per counterion.

the differential capacitance of the double layer is negative for surface charge densities beyond the extremum. A negative capacitance is incompatible with thermodynamic equilibrium [23], so surface charge densities for which the total capacitance is negative could not be obtained in a real system. In Figure 2.3 an example of a set of systems displaying a potential maximum is shown. The relative permittivity varies between 0.75 and 2.0 times that of water in order to assess the effect of changes in the strength of the electrostatic interactions. It is important to note, however, that the potential associated with

the part of the double layer on the electrolyte side is in general not the only contribution to the potential of the surface, see Section 4.3. Assuming that the contributions to the capacitance can be added together as capacitors in series, which is consistent with additivity of the corresponding contributions to the potential, the condition that precludes equilibrium is that the double layer capacitance is negative and smaller in magnitude than the total of all other contributions to the capacitance. Even the very reasonable assumption that the surface charge is situated at a distance comparable to molecular dimensions from, rather than directly at, the plane of closest approach of the ions would give a positive contribution to the capacitance could make the total capacitance positive for the cases shown in the figure. It is interesting to note that in the reduced units used in the right portion of the figure the potential maxima occur at nearly the same reduced surface charge density. Moreover, the slope of the curves beyond the maximum in reduced units is almost equal for all the permittivities considered where sufficiently large reduced surface charge densities are reached. This quasi-universality suggests that the lateral correlation among counterions is the origin of the anomalous behavior of the potential as a function of surface charge density.

2.3 Double Layer Interactions and Colloidal Stability

The term "colloidal suspension" refers to a liquid suspension of particles that are large compared to atomic dimensions, yet small on the macroscopic scale. The size range of particles to which the word "colloidal" is generally applied is 1 - 1000 nm. Suspensions of particles in this size range appear homogeneous and sedimentation is slow or absent. Dilute colloidal suspensions can thus be mistaken for homogeneous solutions on casual inspection while concentrated suspensions can have the appearance of a paste. The distinction between solution and suspension is not always easy to make, as molecules and molecular aggregates are frequently so large that they fall into the colloidal size range. Many substances that we come into contact with in our daily lives are in fact colloidal suspensions. Examples are milk, where the white color is caused by the scattering of light by micrometer-sized fat globules, and solutions of macromolecules, that make up a large portion of our own bodies.

From a physical perspective, the defining characteristic of a colloidal system is a large interfacial area per unit volume of the dispersed phase. This is a purely geometrical consequence of the small size of the particles. As a unit

area is proportional to the square of the unit length and a unit volume is proportional to the cube of the unit length (as the name of these powers suggests) a system that is inhomogeneous on small length scales must necessarily have a large surface to volume ratio. The properties of the interfaces are therefore of much greater importance for the macroscopic properties of colloidal systems than for comparable homogeneous systems. Because an interface between two phases is associated with a positive contribution to the free energy, colloidal suspensions are often not equilibrium phases but may lower their free energy by precipitating the particles. If the particles repel each other sufficiently strongly for the activation barrier against precipitation to be insurmountable in practice, colloidal suspension can often be metastable even if they are out of equilibrium. This is a property that distinguishes suspensions from solutions, as the latter are almost always equilibrium phases. Thus, knowledge of the interactions between colloidal particles is of paramount importance for answering the question of whether a particular suspension is stable or not. Beside the basic question of stability, the interactions between colloidal particles are important for the determination of many properties of suspensions, such as flow behavior and sedimentation velocity.

Interaction between particles in a colloidal suspension may arise from several physical mechanisms, of which two are almost always present. These are double layer and van der Waals forces, that are usually repulsive and usually attractive, respectively. Charged particles in solution interact due to overlap between the diffuse part of the double layers around them. As a charged particle and its counterions form an electroneutral unit, interaction between them is not primarily electrostatic but due to the osmotic pressure exerted by the ions in the double layer. Therefore, the distance dependence of the pressure follows that of the concentration profiles, rather than the "Coulomb's law" form expected from simple electrostatics. When the surfaces are far apart the concentration profile in the space between them is approximately the sum of the concentration profiles of two individual surfaces. As one might expect, this approximation becomes worse the closer the surfaces come to each other. Nevertheless the behavior of the concentration profiles near individual surfaces is very useful for understanding the distance dependence of the force between surfaces. For systems where the DHLL is valid in the bulk solution, for instance, the range of the interactions is determined by κ. For two equal infinite planar surfaces at sufficiently large separation, D, the pressure between the surfaces is proportional to $e^{-\kappa D}$.

Apart from double layer interactions, colloidal particles interact also via van der Waals forces, that are caused by fluctuations in the charge density dis-

tribution of the particles in time and space. If two particles are close to each other, a random fluctuation in charge density in one of the particles will give rise to an electric field that induces a fluctuation in charge density in the other particle that will in turn polarize the first particle and so on. Such correlated charge density fluctuations give rise to an attractive force between the particles, generally called the van der Waals force [24]. Such forces are ubiquitous in nature and van der Waals forces between atoms and molecules play a key role in such mundane phenomena as the formation of condensed phases and friction between surfaces. Compared to the forces associated with covalent bonds and unscreened electrostatic interactions, van der Waals forces are weak. But as the interactions between neighboring atoms in a typical condensed phase are comparable in magnitude to the thermal energy, k_BT, at room temperature it is easy to see that van der Waals forces can be important in colloidal systems. The strength of the van der Waals force between colloidal particles depends on the dielectric properties of the particles as well as those of the medium between them. For the geometry of two parallel planar walls at small and intermediate separations, the potential for this attraction decays as D^{-2}. For typical colloidal systems, the van der Waals force is strong enough to be important for separations as large as tens of nanometers or more. For separations that are so large that the time it takes for the field to propagate between the particles is comparable to the time scale of the charge density fluctuations, the decay of the potential is faster, proportional to D^{-3} [25, 26].

What may be regarded as the first successful theory for the interaction between colloidal particles is the Derjaguin-Landau-Verwey-Overbeek (DLVO) theory [27, 28]. In DLVO theory the interaction between colloidal particles is assumed to be the sum of the contributions from the two physical mechanisms above (i.e. double layer and van der Waals interactions.) Furthermore, these contributions are calculated, on some level of approximation, as if they were independent of each other. Generally, the "double layer" part of the problem is treated within the PB approximation, as was done in the original versions of this theory. That is, the pressure is repulsive and decays for large separations as $e^{-\kappa D}$ with κ proportional to the square root of the ionic strength for all salt concentrations. The pressure due to the van der Waals attraction, on the other hand, is attractive and decays as D^{-3}.

Thus, the total interaction between particles depends on a balance between repulsive double layer forces and attractive van der Waals forces. This balance is influenced by the particle surface charge density and dielectric properties and, importantly, on the salt concentration that controls the range and strength of the double layer interactions. The DLVO theory tends to

predict the dependence of the stability of colloidal suspensions on the salt concentration correctly in situations of modest surface charge density and small concentration of monovalent salt. The predictions of DLVO theory have been tested by direct force measurements, confirming its validity in the low salt concentration regime [29, 30, 5, 31].

Under conditions where ion-ion correlations are important, the interactions between charged particles in electrolyte solution becomes more complicated. For electrolyte concentrations so large that the correlation functions turn oscillatory in bulk, the simple exponential form of the distance dependence for large distances is replaced by an exponentially damped oscillatory decay. The pressure between surfaces due to the double layer is then attractive for some separations. This is a reflection of the fact that the concentration profiles take on the behavior of the bulk distribution functions in the large distance asymptotic regime.

For smaller distances between surfaces, less can be said about their interaction on the basis of the bulk electrolyte properties. Under such conditions the interaction can have many features that are inexplicable in terms of mean field theory. One counter-intuitive consequence of correlations, that has been predicted from computer simulations as well as theory for simple double layer models, is that strong electrostatic interaction between counterions can give rise to attraction between surfaces for some separations at sufficiently high surface charge density. This is partly due to van der Waals-like forces arising from correlations between counterions on opposite surfaces and partly due to that the correlation between counterions on the same surface allows a greater amount of ions to get close to each surface, decreasing the concentration further out. The net effect is that the repulsion due to the ideal contribution to the osmotic pressure becomes small and gives way for the attractive correlation pressure, resulting in a net attraction. At least the qualitative features of these predictions are borne out by experiments. For instance, the fact that the swelling of clays is very different in the presence of divalent counterions compared to monovalent is consistent with double layer attraction with divalent ions [32, 33]. Forces between charged surfaces in the presence of divalent ions have also been measured using two different techniques, confirming the existence of an attractive well [34].

A confounding factor in the interpretation of the short-ranged double layer interactions is the presence of solvation forces. These interactions are due to the work required to displace the solvent between the surfaces in response to a small change in the distance between the surfaces. Depending on the interactions between the surface and the solvent molecule these interactions can be attractive, repulsive or oscillatory. The last situation is common

and is due to packing constraint on the distribution of solvent molecules. Solvophobic surfaces tend to attract and solvophilic surfaces tend to repel. An oscillatory component may be present even in the case where there is and overall attraction or repulsion. See ref. [35] for an overview of solvation forces.

Another type of interaction that fits under the label of "correlation forces" is depletion interactions of electrostatic origin. A short ranged attraction due to depletion of ions by repulsive image charge interactions has been predicted for uncharged dielectric surfaces in the presence of salt [36]. For uncharged surfaces the contribution to the surface-surface interaction due to the osmotic pressure may be regarded as analogous to solvation forces. In addition, the image charge interactions affects the van der Waals interactions by screening the contributions from zero frequency modes [37], see also Section 3.2. The net effect is that the zero frequency contribution to the van der Waals attraction is replaced by a exponentially decaying depletion attraction. The screening of the van der Waals force has been demonstrated experimentally in lipid bi-layer systems [38], confirming the predictions of theory.

2.4 Ion Specificity and Non-Electrostatic Interactions

While many of the properties of electrolytes and double layers are determined by electrostatic interactions, they cannot be the end of the story. For one thing, the formation of a double layer is often driven by the preferential adsorption of one species of ion over others due to short ranged "chemical" forces. Many of the systems usually employed in colloid science have a surface charge density that depends on the concentration of a specific type of ion, the potential determining ion, in a way that suggest chemical equilibrium. Examples of this are silver iodide sols, where the surface potential varies linearly with the chemical potential of silver ions in the solutions, and oxides, including silica, where the surface potential is determined by the pH.

It is in such situations that the GCS theory finds its greatest application. Because the adsorption is often so strong that a minuscule concentration of the potential determining ion is required to reach a particular value of the surface charge density, the concentration of indifferent (not potential determining) electrolyte can be kept low. The GC theory can then be applied with some confidence, at least for monovalent salts and not too high surface charge density. For low salt concentration the length scale characterizing

the diffuse part of the electric double layer is much larger than the range of the interactions that give rise to specific adsorption and the assumption inherent in GCS theory that ions are adsorbed as a monolayer is not greatly in error. For higher concentrations or surface charge densities, the latter corresponding to a large local concentration of counterions, ion specificity is also seen for ions that are not potential determining. While also this type of ion specificity fit into the GCS framework, the interpretation is not clear cut because the GC theory is less reliable for higher concentrations. In this regime there is a risk that deviations of GCS theory from experiments due to failures of GC theory are erroneously ascribed to specific adsorption.

It has been known for well over a century that the chemical identity of "indifferent" ions play a role in a large range of phenomena involving moderate to high electrolyte concentrations. The first systematic study of ion specificity was performed by Franz Hofmeister in 1888. It was shown that the concentration of salt required to precipitate chicken egg white albumin depends on the type of salt used [39]. Hofmeister arranged ions (actually salts with a common counterion) in a sequence based on their "precipitating power" into what is known today as the Hofmeister series. For example, the ability of the halides to precipitate albumin was in Hofmeisters original experiment found vary as the series $F^- > Cl^- > Br^- > I^-$. This means that a lower concentration of F^- compared to, for instance, Cl^- is required to precipitate protein from solution.

Since then, it has been found that the ion specificity of a large range of properties and phenomena, including enzymatic activity [40, 41, 42, 43], surface-surface interactions [44] and colloidal stability [45], and the interfacial tension of electrolytes [46, 47, 48], follow either a similar or the reverse sequence. Also the bulk properties differ greatly between different salts for moderate to large concentrations [49]. This variation have in some cases been found to correlate with the variation in the effect of salt on surface properties [45, 50]. The near-universality of the Hofmeister series together with its correlation with bulk properties suggest that this type of ion specificity is strongly influenced by the properties of the individual species of ions. This gives some hope that the ion specificity of a given phenomenon might one day be rendered predictable on the basis of those properties.

It has long been widely believed, particularly in biochemistry, that the ion specificity of protein solubility, precipitation and denaturation result from competition for solvating water between the protein and salt components of the solution [51]. In this picture, the origin of ion-specificity would be the difference in solvation strength of different species of ions. Small ions allow the charge on the ion to get close to the dipolar (quadrupolar, etc.) solvent

molecules, allowing strong electrostatic interaction and thereby strong hydration. Large ions, on the other hand, interact less strongly with the solvent molecules. Strongly hydrated ions have an ordered shell of water molecules around them whereas large ions are believed to break up the hydrogen bond network in water. Therefore small well-hydrated ions are often referred to as "kosmotropes" and large weakly hydrated ions as "chaotropes". If competition for solvating water molecules were the only mechanism for precipitation of proteins one would expect kosmotropes to be stronger salting-out agents than chaotropes. This is consistent with the order of the "original" Hofmeister series, but that order is not universal. For some proteins (and colloidal suspensions) the corresponding series have the reverse order. It is even the case that the opposite series is found above and below the pI of for the same protein. This would not be the case if competition for hydration of the protein was the main explanation for ion-specificity as both negatively and positively charged proteins are hydrated (though not necessarily to the same extent). Thus, one can conclude that competition for hydration is not enough to explain ion specificity in protein precipitation, let alone ion-specific effects that are not directly related to solubility.

Relatively recently, ion specificity and the Hofmeister series have received much attention from the physical chemistry community. A view has emerged in which direct, specific interaction between ions and macromolecules or interfaces, that are weaker but more long-ranged than the interactions that give rise to the surface charge, are seen as the main mechanism for ion-specificity. Direct interactions between ions and surfaces (or macromolecules) affect the concentration profiles of ions and therefore the surface thermodynamic (and other) properties as well as the interaction between surfaces. Analysis of experimental data in terms of Kirkwood-Buff theory lend support to this view [52, 53]. Some authors even go so far as to claim that the effect of salt on the bulk properties, including the "solvating ability", of water are so small as to be unimportant [54].

In this thesis the term "specific interaction" is used for all interactions that depend on the chemical idiosyncrasies of a system. These include donor-acceptor bonding, dispersion forces, solvent mediated interactions and excluded volume effects. That these classes of interactions are here grouped together in this way is not to be taken as an assertion that they necessarily have similar effects on a system, however. Both the strength and the distance dependence of the interactions may be of importance, and these differ wildly between the mechanisms mentioned above. While for instance dispersion forces are much shorter in range than (unscreened) Coulomb interactions, they tend to be more long-ranged than the "site-binding" interactions that

makes some ions potential determining. Thus, one must distinguish between different types of specific interactions that differ in both strength and distance dependence. Strong, short ranged forces simply act to create a surface charge by adsorption of ions in the way envisioned by GCS theory. Longer range interactions, on the other hand, can affect the spatial distribution of ions in the outer part of the double layer even if the interaction is too weak to affect the number of adsorbed ions to a large extent. A detailed description of the electric double layer on the implicit-solvent level would require the full solvent averaged interaction potential between an ion and the surface, as well as that between ions. Unfortunately, these interaction potentials are imperfectly known in all cases. Assumptions and approximations must therefore be made.

In order to get a feel for at what concentration specific interactions starts becoming non-negligible in comparison to the long-range electrostatic ones, it is instructive to consider the typical length scales characterizing the solution. If the ions in a 100 mM salt solution, corresponding to maybe one ion pair per 550 water molecules, were placed on a simple cubic lattice the lattice spacing of would be about 20 Å. In the same solution κ^{-1} is about 10 Å. In a 1 M solution, with in the order of 55 water molecules per ion pair, the corresponding lattice spacing and κ^{-1} would be around 9 Å and around 3 Å, respectively. Taking into account that ions have a size in the order of one to a few Å (or, if one counts the first layer of coordinating water molecules, as it is frequently argued that one should, several Å) it is not surprising that the chemical character of the ions becomes increasingly important in the concentration range between 0.1 and 1 M, which is something that is frequently seen in experiments. Electrostatic interactions are then screened to ranges comparable to the size of the ions.

The starting point of the recent interest in direct ion-surface interactions can be traced back to the suggestion by Ninham and Yaminsky that the ordering of the Hofmeister series might be explained by (dispersion) van der Waals forces between the ions and interfaces [55]. The strength of such force depends on the difference in polarizability of the ion and the solvent as well as the polarizability of the interface. This idea is made plausible by the fact that the ionic polarizability varies over a wide range for the small, inorganic ions that are commonly employed as background electrolyte within colloid science, particularly for anions. Anions tend to be more polarizable, and have a larger variation in polarizability, than comparable cations [56]. It is noteworthy that the polarizability of ions tend to correlate with their size. A classification of ions in terms of polarizability would thus be likely to yield the same sequence as a classification of ions based on solvation.

Ion-wall dispersion forces distinguish themselves from other ion-specific forces in that they are of relatively long range, the potential decaying as d^{-3} where d is the ion-wall distance. In the case of interaction between two surfaces, such interactions give rise to contributions to the wall-wall pressure that are as long-ranged as the wall-wall van der Waals force. Furthermore, the strength of the ion-wall van der Waals forces can be calculated within the same theoretical framework as the wall-wall van der Waals interaction in the limit of large wall-ion distances. This idea has been investigated in a number of recent publications [57, 58, 59, 60, 61, 62, 63, 64, 65, 66].

Computer simulations consistently show that the potential of mean force between ions have an oscillatory component that is due to the the solvent structure and analogous to the oscillatory solvation force sometimes seen between surfaces. The strength of the solvent mediated interactions is often greater than the dispersion interactions and the difference in solvation structure of ions give rise to a variability in the interactions between ions that makes this mechanism a viable alternative as an explanation to the ordering of the Hofmeister series. This is closely related to the concepts of kosmotropicity and chaotropicity. Regardless of whether the bulk water structure is significantly influenced by ion hydration it is tautologically true that the local structure in the vicinity of ions is. The experimentally observed correlation between chaotropicity/kosmotropicity and ion specific phenomena has lead to the formulation of heuristic rules based on this concept. The most recent is probably the "law of matching water affinities" [67], that states that chaotropes attract other chaotropes and kosmotropes attract other kosmotropes while chaotropes and kosmotropes repel each other. The rationale is that a small ion can replace a solvating water molecule near another small ion, the strong attraction between the small ions compensating for the large solvation energy. Similarly, a large ion can come close to another large ion because neither is strongly solvated. Large ions cannot, however, replace the solvating water molecules of small ions because the Coulomb energy at contact is not sufficient to compensate for the loss of hydration energy. Obviously, computer simulations could in principle render this qualitative picture quantitative. The technical difficulties are unfortunately such that this goal has not yet been reached. Nevertheless, this is an active area of research and some progress have recently been made. This is discussed further in Section 3.1.

Simulations using all-atom models indicate that large, polarizable ions tend to enrich in a narrow region close to the air-water interface, even though there is a negative surface excess overall [68]. The wrong order of the halides emerge for the effect on surface tension in the air-water interface when only

dispersion forces are included [57]. When the difference in solvation energy of the ions is taken into account in an *ad hoc* manner the correct sequence could be obtained [69]. Essentially the same conclusion was recently drawn on the basis of surface selective spectroscopic measurements with gracing incidence X-ray fluorescence that provides a measure of the surface excess of ions: data could only be fitted if a short-ranged interaction was included together with the dispersion interactions [70]. The ion-specific surface pressure of a phospholipid film over aqueous electrolyte could be well fitted using the strength of the dispersion interactions as fitting parameters [71]. An equally good fit could be obtained from the assumption that ions penetrate into the phospholipid film to a different degree, however, but *not* from assuming binding to discrete sites.

In ref. [60] it was found that dispersion forces between ions and surfaces have opposite effect on the interaction pressure between surfaces when acting on the co-ion compared to when acting on the counterion. Mechanistically, this is explained by attractive interactions with the co-ion that effectively increases the surface charge density by drawing co-ions close to the surface. An attractive interaction acting on the counterions, on the other hand, draws them closer to the surface than electrostatic forces alone would. In the former case there is an increase in repulsion at short separations whereas in the latter case there is a decrease in repulsion for such separations. This mechanism might explain the observation that the precipitation of lysozyme follows a reverse Hofmeister series for pH below pI (i.e. for positive surface charge) and a direct Hofmeister series above pI (i.e. for negative surface charge). In ref. [72] it was shown that the same observation could be explained by solvent-mediated interactions, as also these can give rise to attractive interactions between ions and surfaces. This is another example of how models containing completely different interaction mechanisms lead to the same prediction; it seems that this prediction is not very sensitive to the distance dependence of the interaction potential.

The resulting state of the art is that it is reasonably certain that the main reason for the ordering of the Hofmeister series are weak (a fraction of k_BT to a few k_BT) and short ranged (less than 1 nm) direct interactions between ions or between ions and interfaces. The quantitative, mechanistic understanding of these interactions, however, is much less certain. While the bulk of this thesis does not deal directly with ion specific phenomena, the study of these forms the context and background of this work. In Papers I-III the effects of dispersion forces are investigated. The main focus is the effects of strong asymmetry in the ion-wall interactions between the cation and anion. A difficulty in most treatments of this problem to date is that the effect of

the static polarization of the dielectric interfaces due to that the ions cannot be treated consistently within mean field theories, that are usually favored for their simplicity. When ion-ion correlations are considered explicitly, as is done in this thesis, a consistent treatment of the continuum model of interfaces is possible. While the model of the interface employed in Papers I-III is likely too crude to result in quantitative predictions for real systems the consistent treatment of this model is nevertheless of interest. The role of specific adsorption as a mechanism for overcharging forms the background for Paper IV, wherein ion-ion correlations are considered as an alternative source of overcharging. In order to device a test to determine whether overcharging due to ion-ion correlation is indeed present in real systems it was necessary to ascertain the absence of strong specific adsorption as a confounding factor. Comparison with experimental data indicate that the relatively modest overcharging seen for negative surface charge densities for the mercury/aqueous $MgSO_4$ interface [73, 74] is explainable while the strong overcharging seen for many salts, including $MgSO_4$, for positively polarized mercury electrodes is not. This is consistent with notion that the mercury surface is free from specific adsorption for sufficiently negative surface charge densities.

Chapter 3

Continuum Models

"Auream quisquis mediocritatem diligit... "

-Quintus Horatius Flaccus, *Carmina* (23 BC)

A complete description of any substance would require explicit consideration of the properties of the constituent particles. But such a description is often not practically feasible. A typical situation in which atomic models tend to be intractable is one that is characterized by some length scale that is much larger than the length scale of the interaction between individual atoms. Such systems are often modeled by describing some or all the substances involved by their averaged properties, disregarding the inherent discreteness of the constituent atoms. When the disparity in length scales is large, such as for systems of macroscopic dimensions, the utility and validity of this approach is evident. Very rarely do we need to take into account the individuality of atoms when *describing* the macroscopic properties of substances; explicit consideration of the nature of and interaction between the atomic building blocks is needed only when we seek to *explain* those properties. Even on colloidal length scales, a continuum picture often gives an excellent description. In the lower end the colloidal size range the continuum description of matter cannot, however, be accepted *prima facie*. For such length scales or smaller, any continuum description is an approximation, the validity of which is an empirical question. Nevertheless, in models of electrolyte solutions the solvent is often described as a dielectric continuum.

A justification for why it is an acceptable approximation to only treat the ions and not the solvent explicitly when modeling electrolyte solutions can be obtained from an argument by McMillan and Mayer [75]. It was shown

by them that a solution in equilibrium with pure solvent can be treated as a fluid composed of only solute particles, interacting by the potential of mean force between solute particles in the solution in question. In general this potential of mean force is not limited to pairwise additive interactions, even if the interactions between constituent particles are pairwise additive. Also, the potential of mean force is unknown *a priori* because it has to be calculated as an ensemble average in the full system. Treating a system *exactly* by McMillan-Mayer theory does not necessarily simplify the problem and may well complicate it. Rather, McMillan-Mayer theory usually serves as a starting point for approximate theories, where an ansatz is made for the solvent-averaged interaction potential that serves as a definition for a particular model. McMillan-Mayer type models thus contain no explicit reference to the solvent particles. In general, this engenders great simplification of the treatment of the statistical-mechanical problem of going from interaction potentials to thermodynamic properties. Rather than having to deal with the multi-component, molecular fluid at liquid state densities that is the actual system, a McMillan-Mayer type model has the appearance of a gas of solute particles with one fewer components than the full system. This is an important conceptual as well as technical simplification.

McMillan-Mayer type models have been found to be suitable for modeling electrolyte systems, at least for low concentrations. This is so because the long-range Coulomb interactions are dominant in this type of systems. Thus, a large portion of the interactions that determine the properties of the system take place over distances corresponding to several atomic diameters. The procedure of treating the interactions between solute ions as averaged over all configurations of the solvent particles is then easy to justify. The expectation that the form of the interaction between charges in a solvent is the same as that in vacuum, but scaled down by the relative permittivity to account for dielectric screening, is in fact correct for interactions over large distances [76], as if the solvent behaved as a macroscopic dielectric. This observation naturally leads to a class of models where it is taken at face value; where the solvent is actually is modeled as a dielectric continuum. The primitive model that is presented below, in Section 3.1, is an example of this approach. The physical assumption of treating the solvent as a dielectric continuum is also made in the Lifshitz theory of van der Waals interaction, discussed in Section 3.2. These models are thus constructed on the same conceptual foundation, which is why they are discussed together here.

The relation between the thermodynamic properties in McMillan-Mayer type models and those of real electrolyte solutions is simple but not quite trivial. As the solvent molecules are not explicitly part of these models, the nat-

ural way to specify the concentration is as a number density, that can be expressed as molar concentration (moles per liter of solution). The actual *composition* of the system, and therefore the molal concentration (moles per kilogram of solvent), is generally unknown in McMillan-Mayer type models because the amount of solvent is not specified. Furthermore, the McMillan-Mayer argument that justifies replacing the solvent component with effective ion-ion potentials requires the solvent degrees of freedom to be integrated out at constant solvent chemical potential. The conditions that McMillan-Mayer-type theory may be best thought to describe is a solution enclosed in a container of constant volume with semi-permeable walls immersed in a large excess of pure solvent. These conditions we refer to as McMillan-Mayer conditions. Experiments, on the other hand, are usually carried out under what we refer to as Lewis-Randall conditions, where the pressure is held constant and the solution composition is expressed as molal concentration (moles per kilogram of solvent), denoted m. Note that constant molar concentration under McMillan-Mayer conditions do not necessarily correspond to constant composition whereas constant molal concentration under Lewis-Randall conditions do.

A system under Lewis-Randall conditions is most conveniently described using a thermodynamic potential with temperature, pressure and composition as its natural variables, i.e. the normal Gibbs free energy, G. Under McMillan-Mayer conditions, on the other hand, a system is best described by a thermodynamic potential, denoted M, with the natural variables temperature, volume, number of solute particles and chemical potential of the solvent. The two thermodynamic potentials G and M are related by a Legendre transformation

$$M(\{N^s\}, \mu^0, V, T) = G(\{N\}, P, T) - PV - N^0\mu^0, \tag{3.1}$$

where $\{N\}$ is the set of the number of particles of each component, $\{N^s\}$ is the set of the number of particles of each *solute* component and μ^0 and N^0 are the solvent chemical potential and number of particles, respectively. In terms of M the chemical potential under McMillan-Mayer conditions is given by the relation

$$\left(\frac{\partial M}{\partial N_i}\right)_{\{N^s_{j\neq i}\},T,\mu^0,V} = \mu_i(\{N^s\}, T, \mu^0, V) = \mu_i^0 + k_B T \ln f_i n_i^{bulk}. \tag{3.2}$$

The activity coefficient f in this equation is the same as that in eq. (2.8).

The corresponding expression for Lewis-Randall conditions is

$$\left(\frac{\partial G}{\partial N_i}\right)_{\{N_{j\neq i}\},T,P} = \mu_i(\{N\},T,P) = \mu_i^0 + k_B T \ln f_i^{LR} m_i \tag{3.3}$$

that defines the Lewis-Randall activity coefficient f^{LR}. Note that the two definitions of the activity coefficient corresponds to different concentration scales and that the definition of activity coefficients that is usually used for tabulated data corresponds to f^{LR}. For a given temperature and composition, $\mu_i(\{N^s\},T,\mu^0,V)$ is not in general equal to $\mu_i(\{N\},T,P)$ because the pressures and chemical potentials of the solvent are not in general equal. In order to correct for this one can use thermodynamic integration along a path of constant temperature and composition

$$\mu_i(\{N\},P^0,T) = \mu_i(\{N\},P^0+P^{bulk},T) - \int_{P^0}^{P^0+P^{bulk}} \frac{\partial \mu_i}{\partial P'} dP', \tag{3.4}$$

where P^0 is the "external" pressure and P^{bulk} is the bulk osmotic pressure. Because $\frac{\partial \mu_i}{\partial P}$ is equal to the partial molar volume, v_i of species i, eq. (3.4) can be written as

$$\mu_i(\{N\},P^0,T) = \mu_i(\{N\},P^0+P^{bulk},T) - P^{bulk} v_i \tag{3.5}$$

for incompressible fluids. Under the assumption of incompressibility the relation between f_i^{LR} and f_i is thus

$$\ln(m_i f_i^{LR}) = \ln(n_i f_i) - \frac{P^{bulk} v_i}{k_B T} \tag{3.6}$$

where n_i and m_i correspond to the same composition.

For notational and conceptual convenience the quantity that is referred to as the osmotic coefficients in McMillan-Mayer-type models is given by the quotient of the bulk osmotic pressure, P^{bulk}, and the osmotic pressure of an ideal solute as given by eq. (2.7). The standard definition of osmotic coefficient, appropriate under Lewis-Randall conditions, is

$$\phi^{LR} = -\frac{\Delta\mu^0}{k_B T M^0 \sum_i m_i} \tag{3.7}$$

where M^0 is the molar mass of the solvent and $\Delta\mu^0$ is the difference in chemical potential of the solvent compared to pure solvent. The relation between ϕ^{LR} and ϕ is thus

$$\phi^{LR} M^0 \sum_i m_i = \phi v^0 \sum_i n_i, \tag{3.8}$$

where v^0 is the solvent partial molar volume. The difference in the form of the Gibbs-Duhem equation under McMillan-Mayer conditions,

$$VdP^{bulk} = \sum_i N_i^s d\mu_i^s, \tag{3.9}$$

and under Lewis-Randall conditions,

$$-N^0 d\mu^0 = \sum_i N_i^s d\mu_i^s, \tag{3.10}$$

ensure that these definitions of the osmotic coefficient correspond to analogous relationships between osmotic and activity coefficients under McMillan-Mayer conditions and Lewis-Randall conditions.

McMillan-Mayer type models contain no way to determine the amount of solvent in the system, or even the solvent chemical potential. Experimental volumetric data must therefore be available if the model thermodynamic data are to be compared with corresponding experimental data. The most convenient way to do so is to convert the experimental data to McMillan-Mayer conditions and compare directly to the model predictions.

3.1 The Primitive Model

Within the primitive model of electrolyte solutions and electric double layers the ions are modeled as charged hard spheres in a dielectric continuum solvent. The pair interaction potential between two ions of species i and j at coordinates $\mathbf{r}$ and $\mathbf{r}'$ is thus given by

$$u_{ij} = u_{ij}^{Coul} + u_{ij}^{core} \tag{3.11}$$

where

$$u_{ij}^{Coul}(\mathbf{r}, \mathbf{r}') = \frac{q_i q_j}{4\pi\epsilon\epsilon_0 \left|\mathbf{r} - \mathbf{r}'\right|}, \tag{3.12}$$

The 'hard sphere' potential, u_{ij}^{core}, is infinite if $|\mathbf{r} - \mathbf{r}'| < a_{ij}$ where a_{ij} is distance between ion centers when an ion of species i is in contact with an ion of species j, and zero otherwise. In general the ion radii may be additive, that is $a_{ij} = (a_{ii} + a_{jj})/2$ for all i and j, or non-additive. It is common to choose all ion radii to be equal, $a_{ij} = a$ for all i and j, to reduce the number of parameters in the model.

When considering interfacial systems in the primitive model one often seeks to model only one side of the interface. The interactions with the particles

of the other phase are treated using external potentials. This simplification carries the cost that the actual location of the Gibbs surface of the solvent cannot be obtained from the model. Instead, the location of the Gibbs plane must be taken as a model assumption. In this thesis the part of the electric double layer that is on the solution side is of interest, and therefore we model only the ions in solution explicitly. This type of model is compatible with the conceptual framework of GCS theory, where a distinction is made between the *inner* and *diffuse* parts of the double layer. The primitive model in the form presented here may be regarded as a model of the diffuse part.

The potential from a single charged surface with surface charge density σ located at $z = z^\sigma$ is given by

$$\nu_i^{Coul}(z) = -\frac{q_i \sigma}{2\epsilon\epsilon_0}|z - z^\sigma|. \tag{3.13}$$

Note that any choice of z^σ on the surface side of the plane of closest approach of the ions gives the same concentration profiles. This is also true if the surface charge is spread out in space as long as the surface charge distribution does not overlap with the ion distribution. In this thesis it is assumed that the walls are "hard" in the same sense as the ion cores, so that the interaction energy is infinite whenever an ion is closer than a certain distance from any wall. Note in this context that different origins of the coordinate system are used for cases where wall-wall interactions are considered and for cases where single-wall properties are considered. In the former case the origin is placed in the mid-plane between walls and in the latter case it is placed in the plane of closest approach of the ions to the walls.

The form of equation (3.12) is correct in bulk for large ionic separation; the approximations are the assumption that this form is valid for all separations up to hard-core contact and the use of the permittivity of pure solvent. For finite concentrations, the permittivity appropriate for the solution is in general not equal to the bulk permittivity of the pure solvent. Unfortunately, the bulk permittivity of the *solvent* in an electrolyte solution of finite concentration is an ill-defined quantity because the presence of free charges makes the solution a conductor with infinite permittivity. The form of the short range interaction potential, u_{ij}^{core}, is justified by the fact that ions cannot overlap due to Pauli repulsion. The interaction energy for very small separations must thus be so strongly repulsive compared to the thermal energy that it may as well be considered infinite. If this feature of the potential is not reproduced it would lead to the so-called 'Coulomb catastrophe'. As the interaction between cations and anions is infinitely attractive for zero ion-ion separation, the cation-anion correlation function would diverge at this point

in the absence of an additional interaction that is infinitely repulsive. The primitive model may thus in some sense be regarded as the simplest physically sound model of electrolyte solutions. While the very short-ranged and very long-ranged ion-ion interactions are reproduced faithfully, the primitive model interaction potential is no doubt a rather poor approximation of the true intermediate-range interactions. Thus, one would expect the primitive model to work well in situations where the long-range Coulomb interactions are dominant.

To calculate structural and thermodynamic properties of a primitive model by statistical mechanics is a non-trivial problem, despite the simplicity of the interaction potential. Fortunately, this is a problem that has attracted the attention of many workers over the last century and today theoretical as well as simulation methods that reliably gives the properties of the primitive model for a large range of parameters have been developed. The theories that tend to be most successful for primitive model electrolytes (and other simple fluids) belongs to the class of theoretical methods known as integral equation theories. These are discussed in Section 4.1. Furthermore, a number of general conclusions about the primitive model, some of which also applies to electrolytes in general, can be drawn on the basis of the long range nature of the Coulomb potential. Examples of such are sum rules for the zeroth and second moment of the charge density distribution around an ion [3] and the analytic form of the pair distribution function in the long-distance asymptotic limit [17].

Due to the finite size of the ions, the primitive model takes into account excluded volume effects. It has been found that the decay length of the bulk distribution functions for primitive model electrolytes depend on the ion sizes in a rather complicated fashion [77]. Thus, the ion size is a possible source of ion specificity. Using the ion sizes as fitting parameters, the primitive model has been found to be able to describe bulk thermodynamic data for many real electrolyte solutions quite well up to about 1 M concentration, sometimes much higher [78]. If a sufficiently large set of salts is investigated, it becomes apparent that the ionic radii that give the best fit are not in general transferable between salts, nor are they simply related to the radius of ions in crystalline compounds. Thus, the primitive model must be employed with the caveat that the ionic size parameter cannot be interpreted as a true geometric property of an ion.

The primitive model applied to electrolytes near interfaces is an important model for the electric double layer. While the same theoretical methods can be applied to this situation as to bulk electrolytes, the interfacial problem is far more technically demanding than the bulk problem. This is due to the in-

homogeneity and anisotropy of the solution close to an interface that breaks some of the spatial symmetries that can be used to simplify the bulk problem. Simulations of primitive model double layers [79, 80] and similar models [16] have been possible since the early 1980s. For monovalent counterions at moderate concentration near moderately charged surfaces, the results are in qualitative agreement with the predictions of the PB approximation and other mean-field theories. For divalent counterions (or counterions of even higher valency) the predictions of the PB approximation differ qualitatively from the predictions of primitive model simulations [81, 82]. This has implications for the interaction pressure between walls due to the ions, that is sometimes attractive [83, 84] rather than always repulsive, as is the case in DLVO theory, as well as for surface excess thermodynamic properties. These qualitative differences from mean field theory are discussed in Sections 2.2 and 2.3 above.

For more sophisticated models, realistic pairwise interaction potentials between ions may well differ sufficiently between different species of ions that they are the main source of ion specificity under some conditions. There are two principal methods for developing improved model interaction potentials. One is to make assumptions about the mathematical form of the interaction potential and use a fit to experimental data to determine the values of the parameters defining the details of the interaction. The other is to actually try to calculate the effective potential in some thermodynamic state using simulation or advanced theory and then try to generalize this form to other states.

The former approach have been extensively investigated, particularly for 1:1 salts [85, 86, 87, 88]. This research program has resulted in models in good agreement with bulk thermodynamic data. The approach does, however, suffer from the problem that many different forms of the interaction potential can give similar fits to experimental data. This was realized early on, as stated by Ramanathan and Friedman in ref. [85]:

> It seems to us that the main barrier to further advancement of our understanding of ionic solutions lies in the expectation that a vast number of equally attractive but distinguishable models can be found which are equally consistent with thermodynamic data.

Fits to data from macroscopic measurements can thus reveal general features of the interaction potential, but are blunt tools for obtaining detailed mechanistic information. As the form of an interaction potential, dictated

by theory, for one mechanism may give an equally good fit as the form corresponding to a completely different mechanism, definite conclusions can rarely be drawn.

The latter approach of deriving the effective interaction potential from more detailed models, on the other hand, shows some promise in giving mechanistic information but suffers from that thermodynamic properties of solutions at high concentrations are often very sensitive to small errors in the magnitude of the interaction potential. (The insensitivity of the possibility of fitting bulk thermodynamic data is to the form of the interaction potential does not contradict sensitivity of thermodynamic properties to its magnitude for a given form.) Thus, it is difficult to obtain an interaction potential that accurately gives the thermodynamic properties of solutions of a given salt by this route. Nevertheless, this kind of calculations have yielded important information about the general features of the effective interactions between ions in aqueous solutions. It seems to be a general feature that such interaction potentials have an oscillatory component due to ordering of water molecules that is superimposed on the Coulomb interaction [89, 90, 91, 92, 93, 94, 95, 96, 97, 98, 50, 72, 99]. This solvent mediated interaction may be considered analogous to the solvation force between surfaces [35]. As noted in Section 2.4, differences in this solvent induced interaction is one of the major candidates for explaining the ordering of the Hofmeister series. Interaction potentials from simulations have been applied to the modeling of inhomogeneous systems [100, 101].

3.2 Polarizable Interfaces and van der Waals Forces

As stated in the introduction, van der Waals forces are caused by correlated fluctuations in the charge density distribution of bodies that may be as small as atoms and as large as macroscopic objects. The fluctuations in charge density may arise from the displacement of either electrons or nuclei. Due to the difference in mass between nuclei and electrons, these mechanisms differ greatly in time scale. The electronic fluctuations can have frequencies well above those associated with visible light while the fluctuations associated with the nuclei occur at frequencies comparable to those associated with infrared radiation or smaller. Because the time scale associated with electronic motion can be much smaller than that of nuclear motion, the electrons move with the nuclei. The displacement of nuclei can thus only effect a significant fluctuation in charge density if those nuclei are part of polar molecules. Even

in such cases, the high frequency fluctuations associated with the electronic motion tend to give rise to the dominant contribution to the van der Waals force [35]. This is commonly called the dispersion force. In this thesis, the term "dispersion force" is used only for the contribution to the van der Waals force due to high frequency fluctuations. As we shall see in the following section, however, the same theoretical framework can be used regardless of the time scale of the fluctuations.

When electrolyte is present, it is vital to distinguish between the "high frequency" (dispersion) and "zero frequency" (that is due to very low frequency fluctuations in charge density) contribution to the wall-wall van der Waals force. The ions in an electrolyte cannot respond to the former, other than by changing their polarization state, because the vast majority of the fluctuations causing it happen on a timescale that is too short for the ions to move significantly in response. However, the ions can respond to the "zero frequency" contribution, and it is therefore screened by electrolyte much like other electrostatic interactions. This screening is automatically taken into account if the effects of image forces are included consistently in the treatment of the intervening electrolyte.

The first quantitative theoretical treatment of dispersion forces is due to London, who derived an approximate expression for the dispersion interaction between two atoms [24]. This expression predicted that the strength of the dispersion forces is proportional to the product of the atomic polarizabilities and that the potential for this force decays as the inverse sixth power of the interatomic distance for large distances, which is correct for distances that are sufficiently small that negligible error is introduced if the speed of light is taken to be infinite. The distance dependence of the van der Waals attraction between two macroscopic spheres was successfully predicted by Hamaker [102] by simply summing the average contribution from each individual volume element, as given by the London expression for dispersion forces and the average density. This procedure can of course be applied to any geometry. Despite this success, Hamaker's approach proved incapable of reliably predicting the strength of the van der Waals attraction between macroscopic bodies. This is to a large extent due to the fact that for the densities of typical condensed phases, the London expression, that pertains to two atoms in vacuum, is not valid. When atoms are close together, neighboring atoms will affect each other's polarization states in a complicated manner. Thus, the apparent polarizability of an individual atom will depend on the average polarization states of surrounding atoms, that in turn depends on the polarization states of the atoms surrounding them. As can be imagined, the problem of calculating this quantity quickly becomes very complex as the

density is increased. Note however that the problem of many-body polarization in connection to the (static) dielectric constant of polarizable liquids can be expressed as an integral equation similar to the integral equations for the correlation functions that appear in liquid state theories [103], see Section 4.1 below.

A theory for van der Waals forces that takes these considerations into account was developed in the 1950's by Lifshitz [104]. This theory was originally formulated in terms of quantum electrodynamics, but due to the approximations involved it can also be formulated in terms of classical electrodynamics with quantization of energy [25, 105, 26]. Within Lifshitz theory, materials are characterized by their macroscopic dielectric functions that contain the effects of many-body interactions on the response of the material to electric fields. These dielectric functions depend on the time scale on which the field varies and are usually expressed as functions of frequency. Thus, Lifshitz theory is a continuum theory where the molecular "granularity" of the wall and particle media is neglected, much in the same way as is done in the primitive model of electrolyte solutions.

The boundary condition that the electric field must satisfy at the interface between two media is determined by the dielectric functions of the media, as well as their geometries. If two interfaces are brought close to each other the need to satisfy the boundary conditions for both interfaces places a limitation on the wavelengths that "fit" between the interfaces. The partition function of the electric field is given by

$$Q = \prod_j \sum_l e^{-\frac{(l+1/2)\,\hbar\,\omega_j}{k_B T}} = \prod_j \frac{1}{2\sinh\left(\frac{\hbar\omega_j}{2k_B T}\right)}, \tag{3.14}$$

where ω_j denotes the frequency of the j-th allowed mode and l is an integer, corresponding to the number of photons in the mode. The free energy of the field is thus

$$A = -k_B T \ln Q = k_B T \sum_j \ln\left(2\sinh\left(\frac{\hbar\,\omega_j}{2k_B T}\right)\right). \tag{3.15}$$

As the frequencies of the allowed modes depend on the separation between the interfaces, the free energy of the field is also dependent on the separation. It is possible to rationalize why the van der Waals force is generally attractive by noting that the number of modes that fit between the interfaces generally becomes smaller as the interfaces are brought closer. Since most modes have an energy $\hbar\omega_j$ that is much larger than $k_B T$ for the temperature range that is of interest within colloid science, decreasing the number of modes correspond

to a decrease in the free energy. In order to obtain F as a function of distance one could solve the electrodynamic boundary value problem to find the frequencies of the allowed modes, which is generally a difficult problem, and substitute the frequencies into eq. (3.15). The problem can be simplified by writing the free energy of the modes associated with a certain magnitude of the wave vector in terms of the dispersion relation, $\mathscr{D}(\omega, k)$ (that has the property that the frequencies of the allowed modes satisfy $\mathscr{D}(\omega, k) = 0$) for imaginary frequencies

$$A(k) = k_B T \sum_{l=0}^{\infty}{}' \mathscr{D}\Big(i\frac{2\pi l k_B T}{\hbar}, k\Big), \tag{3.16}$$

where i is the imaginary unit and the prime on the summation symbol indicate that the term with $l = 0$ is to be given half weight. The proof of the equivalence between eq. (3.15) and eq. (3.16) relies on Cauchy's residue theorem and can be found in [106]. For two planar, parallel interfaces the dispersion relation is given by[1]

$$\mathscr{D}(\omega, k) = 1 - \epsilon_D^2(\omega) e^{-2kD}, \tag{3.17}$$

where k is the magnitude of the wave vector and

$$\epsilon_D(\omega) = \frac{\epsilon(\omega) - \epsilon_{wall}(\omega)}{\epsilon(\omega) + \epsilon_{wall}(\omega)}, \tag{3.18}$$

where $\epsilon(\omega)$ and $\epsilon_{wall}(\omega)$ are the frequency-dependent dielectric functions of the solvent and the wall material, respectively. These are related to the dielectric constants by $\epsilon(0) = \epsilon$ and $\epsilon_{wall}(0) = \epsilon_{wall}$ and may be thought of as a generalization of the concept of dielectric constant that applies to fields that vary in time. To obtain the total interaction free energy due to van der Waals forces as a function of D, eq. (3.16) can be integrated with respect to k, yielding

$$A(D) = \frac{k_B T}{8\pi D^2} \sum_{l=0}^{\infty}{}' \sum_{s=1}^{\infty} \frac{\epsilon_D^{2s}(i\omega_l)}{s^3}, \tag{3.19}$$

with $\omega_l = l\, 2\pi\, k_B T/\hbar$. In order to obtain the pressure due to van der Waals forces, the free energy is differentiated with respect to D, which gives the result

$$P^{vdW}(D) = -\frac{k_B T}{4\pi D^3} \sum_{l=0}^{\infty}{}' \sum_{s=1}^{\infty} \frac{\epsilon_D^{2s}(i\omega_l)}{s^3}. \tag{3.20}$$

[1]This dispersion relation is valid only if the speed of light can be taken as infinite, which is a good approximation for small D.

In what follows it will be important to distinguish between the $l = 0$ term in the sum, the zero-frequency van der Waals pressure, denoted P_0^{vdW} and the rest of the sum, the high-frequency van der Waals pressure, denoted P_{hf}^{vdW}. The zero-frequency van der Waals pressure is screened by the presence of electrolyte, whereas the high frequency van der Waals pressure is not. As it turns out, this screening is intimately related to the correlation of ions and their image charges. This screening effect is discussed below.

In most systems, the zero-frequency van der Waals pressure is small compared to the high-frequency van der Waals pressure, but hydrocarbon/water systems are an exception. As this is one of the types of system studied in this thesis (Papers I-III), the screening of the former term may thus have a large influence on the magnitude of the total pressure. For the particular system that is studied here, polystyrene/water, the zero-frequency van der Waals pressure contributes about a third of the total van der Waals pressure. The dielectric functions used here are taken from ref. [107].

Lifshitz theory can in principle be applied to any geometry. It can therefore be used to calculate the interaction free energy between a surface and a polarizable point particle a distance d from the surface. The interaction free energy for such a situation is [55]

$$A_i^{disp}(d) = -\frac{\hbar}{(4\pi)^2\epsilon_0 d^3}\int_0^\infty d\omega\, \frac{\alpha_i^*(i\omega)}{\epsilon(i\omega)}\epsilon_D(i\omega) = \frac{B_i}{d^3} \tag{3.21}$$

where $\hbar$ is Planck's constant divided by 2π, $\alpha_i^*(i\omega)$ is the dynamic excess polarizability of the ion and ω has the same meaning as in eq. (3.19). The meaning of excess polarizability is the polarizability of the ion in solution, $\alpha(\omega)$, less the polarizability of the solvent displaced by the ion. The polarizability of an ion can be inferred from spectroscopic data or quantum mechanical calculations using [25]

$$\alpha(\omega) = \frac{e_0^2}{4\pi\epsilon_0 m_e}\sum_l \frac{f_{0,l}}{\omega_{0,l}^2 - \omega^2}, \tag{3.22}$$

where m_e is the electron mass, $\omega_{0,l}$ is the frequency associated with the electronic excitation from the ground state to state l and $f_{0,l}$ is the oscillator strengths of that excitation. The quantities $f_{0,l}$ and $\omega_{0,l}$ can be calculated using quantum-mechanical density functional theory [108, 109]. It is on the basis of such calculations that the values of B_i that are used here are chosen. For details, see Paper I.

Equation (3.21) is strictly valid only for an isolated ion interacting with a single wall. Many-body interactions will be present in the case of two walls

and for finite salt concentrations. This is due to the fact that the environment of the ion will affect its polarization state, as discussed previously. Here, such many-body contributions are neglected. Under this approximation, the interaction potential due to dispersion forces acting on an ion between two walls is given by

$$\nu_i^{disp}(z|D) = B_i\left(\frac{1}{|z+D/2|^3} + \frac{1}{|z-D/2|^3}\right), \tag{3.23}$$

where B_i has the same meaning as in equation (3.21). This can be expected to be a good approximation, at least in situations where the density of ions is small and the walls are far apart.

When an ion is brought close to an interface between two dielectric materials the dielectrics on either side of the interface will be polarized to a different extent. This difference in polarization gives rise to surface charge distribution that can either repel or attract the ion, depending on which one of the dielectrics has a higher dielectric constant. An ion in a medium of high dielectric constant will be repelled from an interface with a medium of lower dielectric constant, and attracted in the reverse case.

The static polarization of the walls due to the ionic charges can be taken into account by the method of images. This method derives its name from the fact that for certain geometries, the field due to the surface polarization induced by a charge is identical to that from a charge placed at the position where the mirror image of the original charge would appear to be if the surface were a mirror. The method of images is very convenient when solving boundary value problems is simple geometries, such as that of a charge near a single planar interface. When the geometry of the interface is more complicated, the method of images often gives the field due to the surface polarization from a point charge as the field from an infinite array of image charges. The situation is illustrated in Figure 3.1. Often, the evaluation of such a sum is too cumbersome to make the method of images useful in practice. The situation with an infinite number of image charges is encountered even in the relatively simple geometry of two parallel walls considered here. Fortunately, the Hankel transform of the potential due to the infinite sum over image charges can be evaluated analytically.

Because the numerical procedure used to find the ionic distribution functions employs Hankel transforms, see Section 4.2 below, no extra difficulty is introduced from a potential function that is known only in k-space. The polarization of the walls gives rise to contributions to both the ion-ion interaction potential and the ion-wall interaction potential. The contribution due

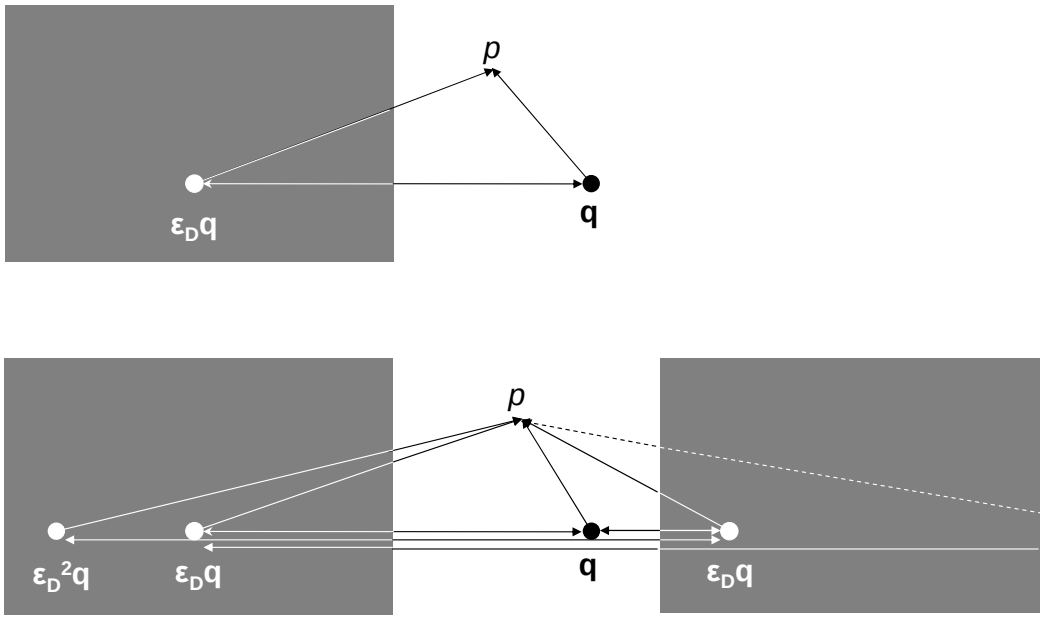

Figure 3.1: Schematic representation of the method of images. The charge of magnitude $\mathbf{q}$ and the image charges of magnitude $\epsilon_D^n \mathbf{q}$ (where n is an integer) all contribute to the potential at the point p. In the situation with a single dielectric wall in the upper part of the figure only a single image charge is needed to give the correct potential. In the second situation with two dielectric walls an infinite number of image charges, of which the first three are shown and the existence of a forth outside the right edge of the picture is hinted, are needed to give the potential at the point p.

to image charges to the ion-ion interaction potential is given by [84]

$$\begin{aligned} \hat{u}_{ij}^{im}(k,z,z'|D) &= \frac{q_i\, q_j}{\epsilon_{sol}\epsilon_0\, k}\left[\frac{\epsilon_D}{e^{kD}-\epsilon_D}\cosh(kz)\cosh(kz')\right. \\ &+ \left.\frac{\epsilon_D}{e^{kD}+\epsilon_D}\sinh(kz)\sinh(kz')\right] \end{aligned} \tag{3.24}$$

where $\epsilon_D = \epsilon_D(0)$. The contribution to the ion-wall interaction potential is given by the interaction between an ion and its own image charges,

$$\nu_i^{im}(z|D) = \frac{1}{2}u_{ii}^{im}(0,z,z|D), \tag{3.25}$$

and will be referred to the self-image interaction. From equation (3.18) we see that if the solvent has a higher dielectric constant than the walls, the self-image interaction will be repulsive. Under the same conditions, the image

charges will give also rise to an extra repulsion between like-charged ions and an extra attraction between oppositely charged ions.

If only the effect of the self-image interaction on the concentration profiles were to be taken into account, one would conclude that the contribution to the potential of mean force due to image charges would be long-ranged, decaying as d^{-1} in the case of a single wall. In reality, however, the image forces are screened much like the Coulomb interaction between ions in bulk. The exact nature of the screening depends on the ionic correlation functions that are themselves influenced by the presence of image charges. Thus, in order to treat the screening of image charges consistently the correlation functions must be considered explicitly. This fact makes integral equation theory well suited for the study of interfaces with a dielectric discontinuity, see Sections 4.1 and 4.2 below.

If the correlation between ions in the presence of image charges is treated consistently, a repulsive contribution to the pressure that exactly cancels the zero-frequency van der Waals pressure for large wall-wall separations will be present [37, 36]. For small separations, the image forces give rise to contributions to the pressure that have a shorter range than the the van der Waals pressure and can be either attractive or repulsive. The net effect is thus that the zero-frequency van der Waals pressure is replaced by a contribution that has a shorter range and depends on the effect of image charges on the ion distribution between the walls, see 4.3 below. For monovalent electrolyte at moderate concentrations between uncharged surfaces this contribution has the form of an exponentially decaying attraction [36]. For charged surfaces it can be repulsive, however, see Figure 4 of Paper II.

Chapter 4

Distribution Function Theory

"Reasoning is but reckoning."

-Thomas Hobbes, *Leviathan* (1651)

Equilibrium statistical mechanics is a field of study that aims to derive thermodynamic properties of substances from the interactions between the constituent particles. Using the concept of ensembles, collections of systems characterized by the same thermodynamic state but with the particles arranged differently on the microscopic scale, thermodynamic quantities can be obtained as averages over a suitable ensemble. The central relation between statistical mechanics and thermodynamics is that there is a one-to-one correspondence between each ensemble and a thermodynamic potential. This relation is most easily illustrated for the *microcanonical ensemble*, defined by constant number N of identical particles, volume V, and energy U, corresponding to a closed, isolated system with rigid walls. The entropy, S, is related to the number of quantum states available to the system, Ω, by

$$S = k_B \ln \Omega. \tag{4.1}$$

Boltzmann's constant, k_B, is included for the expression to be consistent with the practice of expressing the temperature in Kelvins rather than in a regular unit for energy, which is considered desirable for historical reasons. In the thermodynamic limit, where all extensive properties of the system are made infinite while preserving their ratio, S becomes equal to the corresponding quantity in classical thermodynamics. Since the natural variables of S are N, V, and U all thermodynamic observables of the system can be calculated if one knows how the number of possible quantum states of the system changes as N, V, and U are varied.

The one-to-one correspondence between ensembles and thermodynamic potentials is not limited to the entropy and the microcanonical ensemble. Relations analogous to eq. (4.1) can be derived for ensembles characterized by holding other thermodynamic quantities fixed. In the thermodynamic limit, all ensembles that correspond to the same thermodynamic state must give identical results for all thermodynamic observables, regardless of which quantities are held constant. The criterion for selecting an ensemble to work with is thus simply expedience with respect to the task at hand.

The ensemble defined by a fixed N, V and T is often referred to as the *canonical ensemble*. The fundamental quantity characterizing this ensemble is the canonical partition function, given in the classical approximation by

$$Q_N = \frac{1}{h^{3N}N!}\int\cdots\int e^{-\frac{H_N(\mathbf{r}_1,\cdots,\mathbf{r}_N,\mathbf{p}_1,\cdots,\mathbf{p}_N)}{k_BT}} d\mathbf{r}_1\cdots d\mathbf{r}_N d\mathbf{p}_1\cdots d\mathbf{p}_N \qquad (4.2)$$

where $\mathbf{r}_i$ is the position and $\mathbf{p}_i$ is the momentum of particle i. The prefactor ensures that indistinguishably of the particles is taken into account and that the expression is consistent with its quantum mechanical analogue in the applicable limit. The Hamiltonian, H_N, is given by

$$H_N(\mathbf{r}_1,\cdots,\mathbf{r}_N,\mathbf{p}_1,\cdots,\mathbf{p}_N) = \sum_i \frac{|\mathbf{p}_i|^2}{2m} + U_N(\mathbf{r}_1,\cdots,\mathbf{r}_N) \qquad (4.3)$$

where m is the mass of the particles, the first term gives the kinetic energy and U_N is the potential energy of the system.

The canonical partition function is related to the thermodynamic potential that has N, V and T as its natural variables, the Helmholtz free energy, A, by

$$A = -k_BT\ln Q_N. \qquad (4.4)$$

The direct relation between the canonical partition function and A establishes the relation with the second law. We recall that the minimum in a system's Helmholtz free energy corresponds to the state of a system that corresponds to a maximum in entropy of the system and its surroundings. This link to the surroundings is also present in eq. (4.2): the integrand is related to the availability of energy for transfer to the system from the surroundings. Distributions of positions and momenta characterized by values of the Hamiltonian that are large compared to k_BT carries less weight in the integral because of the decrease in entropy associated with transferring energy from the surroundings to the system as heat.

In order to study surface thermodynamic properties we will consider another ensemble that is suitable for this task: the *grand canonical ensemble*. This

ensemble is characterized by constant chemical potential, μ, rather than constant N. As in the canonical ensemble, V and T are held fixed. The partition function in this ensemble is defined in terms of the canonical partition function by

$$\Xi = \sum_{N=0}^{\infty} e^{\frac{\mu N}{k_B T}} Q_N. \tag{4.5}$$

The physical interpretation of the relationship with the canonical partition function can be grasped by noting that in the grand canonical ensemble, particles as well as energy can be exchanged with the surroundings. Much like all possible values of the total energy are taken into account in the canonical partition function, all possible numbers of particles are taken into account in the grand canonical partition function. Hence the sum over N. For bulk systems the thermodynamic potential that is related to Ξ is $-PV$, through the relation

$$PV = k_B T \ln \Xi, \tag{4.6}$$

that is analogous to eq. (4.4). The differential form of eq. (4.6) is the Gibbs-Duhem equation, eq. (2.6). The grand canonical ensemble can be extended to treat interfacial systems by making sure that an interface of specified area, $\mathscr{A}$, is present so that the resulting ensemble is characterized by fixed μ, V, $\mathscr{A}$ and T. This ensemble leads to the Gibbs adsorption isotherm, eq. (2.11). This explains why this close relative of the grand canonical ensemble is well suited for interfacial systems.

The form of eq. (4.3), with the kinetic energy contribution being independent of the potential energy contribution, implies that eq. (4.2) can be factorized into one factor that contains the kinetic energy only and one factor that contains only the potential energy. The "kinetic energy" part is identical to the partition function of an ideal gas where the potential energy is zero for all configurations. Eq. (4.4) then implies that the free energy, and therefore *all* thermodynamic quantities, can be expressed as a term that is equal to that of an ideal system and a term that contains all the contributions from interactions amongst the particles. Because the ideal contribution to any thermodynamic quantity can be written as an algebraic expression, usually a very simple one, the remainder of this section will be devoted to methods for evaluating the remaining, *excess*, contribution.

The probability density, p_N, for a subsystem of the canonical ensemble to be in a given configuration, defined by the particle coordinates $\mathbf{r}_1, \cdots, \mathbf{r}_N$, is

[110]

$$p_N(\mathbf{r}_1, \cdots, \mathbf{r}_N) = \frac{e^{-\frac{U(\mathbf{r}_1,\cdots,\mathbf{r}_N)}{k_B T}}}{\int \cdots \int e^{-\frac{U(\mathbf{r}_1,\cdots,\mathbf{r}_N)}{k_B T}} \, d\mathbf{r}_1 \cdots d\mathbf{r}_N}, \tag{4.7}$$

where $U(\mathbf{r}_1, \cdots, \mathbf{r}_N)$ is the potential energy associated with the configuration. The denominator in this expression is known as the *configuration integral* and is denoted by Z_N. This quantity is related to the excess Helmholtz free energy, A^{ex}, in analogy with eq. (4.4) via

$$A^{ex} = -k_B T \ln \frac{Z_N}{V^N}, \tag{4.8}$$

and thus contains all information about the effect of interactions on thermodynamic quantities. The configurational ensemble average of a quantity, F, say, is denoted $\langle F \rangle$ and can be expressed in terms of eq. 4.7 as

$$\langle F \rangle = \int \cdots \int F(\mathbf{r}_1, \cdots, \mathbf{r}_N) p_N(\mathbf{r}_1, \cdots, \mathbf{r}_N) \, d\mathbf{r}_1 \cdots d\mathbf{r}_N. \tag{4.9}$$

The excess contributions to thermodynamic quantities such as P can be calculated in terms of such ensemble averages, see Section 4.3.

4.1 Distribution Functions and Correlation Functions

A central part in statistical mechanics is the concept of distribution functions. These functions are closely linked to many experimentally measurable properties and are therefore a suitable starting point for statistical mechanical theories. In this section, the canonical ensemble is used to introduce the theory of distribution functions in terms of ensemble averages of the local concentration.

The particle density, i.e. "concentration", at position $\mathbf{r}$, $\mathfrak{n}(\mathbf{r})$, in any configuration is infinite at the particle positions and zero everywhere else, thus it can be written as

$$\mathfrak{n}(\mathbf{r}) = \sum_{i=1}^{N} \delta(\mathbf{r} - \mathbf{r}_i), \tag{4.10}$$

where $\delta(\mathbf{r})$ is the (three-dimensional) Dirac delta distribution[1]. The probability density of finding a particle at $\mathbf{r}$ at a given time, $n^{(1)}(\mathbf{r})$ is the ensemble

[1] That is infinite for $\mathbf{r} = 0$ and zero otherwise and has the property $\int \phi(\mathbf{r}')\delta(\mathbf{r} - \mathbf{r}')d\mathbf{r}' = \phi(\mathbf{r})$, where ϕ is a continuous function.

average of $\mathfrak{n}(\mathbf{r})$,

$$\begin{aligned} n^{(1)}(\mathbf{r}) = \langle \mathfrak{n}(\mathbf{r}) \rangle &= \frac{1}{Z_N} \int \cdots \int \sum_{i=1}^{N} \delta(\mathbf{r} - \mathbf{r}_i) e^{-\frac{U(\mathbf{r}_1, \cdots, \mathbf{r}_N)}{k_B T}} d\mathbf{r}_1 \cdots d\mathbf{r}_N \\ &= \frac{N}{Z_N} \int \cdots \int e^{-\frac{U(\mathbf{r}, \mathbf{r}_2, \cdots, \mathbf{r}_N)}{k_B T}} d\mathbf{r}_2 \cdots d\mathbf{r}_N. \end{aligned} \tag{4.11}$$

The fact that the particles are indistinguishable has been used to simplify the expression by noting that each of the N terms in the sum is identical. Similarly, the probability densities of finding one particles at $\mathbf{r}$ and one particle at $\mathbf{r}'$ simultaneously, $n^{(2)}(\mathbf{r}, \mathbf{r}')$, is given by

$$\begin{aligned} n^{(2)}(\mathbf{r}, \mathbf{r}') &= \left\langle \sum_{i=1}^{N} \sum_{\substack{j=1 \\ j \neq i}}^{N} \delta(\mathbf{r} - \mathbf{r}_i) \delta(\mathbf{r}' - \mathbf{r}_j) \right\rangle \\ &= \frac{N(N-1)}{Z_N} \int \cdots \int e^{-\frac{U(\mathbf{r}, \mathbf{r}', \mathbf{r}_3, \cdots, \mathbf{r}_N)}{k_B T}} d\mathbf{r}_3 \cdots d\mathbf{r}_N. \end{aligned} \tag{4.12}$$

Again, use has been made of the fact that the $N(N-1)$ terms are identical. By the same argument, the *l-particle distribution function*, $n^{(l)}(\mathbf{r}, \cdots, \mathbf{r}^{(l)})$, the corresponding probability density of finding l particles at $\mathbf{r}, \cdots, \mathbf{r}^{(l)}$ is given by

$$n^{(l)}(\mathbf{r}, \cdots, \mathbf{r}^{(l)}) = \frac{N!}{(N-l)! Z_N} \int \cdots \int e^{-\frac{U(\mathbf{r}, \cdots, \mathbf{r}^{(l)}, \mathbf{r}_{l+1}, \cdots, \mathbf{r}_N)}{k_B T}} d\mathbf{r}_{l+1} \cdots d\mathbf{r}_N. \tag{4.13}$$

From the 1- and l-particle densities the *normalized l-particle distribution function*[2], $g^{(l)}(\mathbf{r}, \cdots, \mathbf{r}^{(l)})$ can be defined by

$$n^{(l)}(\mathbf{r}, \cdots, \mathbf{r}^{(l)}) = n^{(1)}(\mathbf{r}) \cdots n^{(1)}(\mathbf{r}^{(l)}) g^{(l)}(\mathbf{r}, \cdots, \mathbf{r}^{(l)}). \tag{4.14}$$

As might be expected, the manipulation of higher order distribution functions quickly becomes intractably complex with increasing order. Fortunately, $n^{(1)}(\mathbf{r})$ and $g^{(2)}(\mathbf{r}, \mathbf{r}')$ are the distribution functions of greatest importance. Below, the superscripts on these symbols are suppressed whenever there is no risk of confusion and the functions they represent will be referred to as the *concentration profile* and the *pair distribution function*, respectively. In order to appreciate the physical significance of these functions, it is useful to note how they are interrelated. The product $n(\mathbf{r}')g(\mathbf{r}, \mathbf{r}')$ gives the average

[2]This naming convention is not universal, sometimes the name "distribution function" is reserved for the $g^{(l)}$ functions. In this case $n^{(l)}$ is called the l-particle density.

concentration at $\mathbf{r}'$, given that there is a particle at $\mathbf{r}$, which is the same thing as the concentration profile around a fixed particle. This interpretation of $g(\mathbf{r}, \mathbf{r}')$ gives rise to an elegant way of connecting the properties of homogeneous and inhomogeneous fluids already alluded to in Chapter 2. A theory that gives $n(\mathbf{r})$ for an arbitrary external potential is also a theory for $g(\mathbf{r}, \mathbf{r}')$ of a bulk fluid because the external potential can be chosen as the potential from a particle held fixed at a point $\mathbf{r}'$ (that may as well be taken as the origin of the coordinate system). The concentration profile in this situation corresponds to $n^{bulk} g(\mathbf{r}, \mathbf{r}')$.

The distributions functions are closely related to the *density-density correlation functions*, defined by

$$H^{(l)}(\mathbf{r}, \cdots, \mathbf{r}^{(l)}) = \Big\langle \big(\mathfrak{n}(\mathbf{r}) - n(\mathbf{r})\big) \cdots \big(\mathfrak{n}(\mathbf{r}^{(l)}) - n(\mathbf{r}^{(l)})\big) \Big\rangle. \tag{4.15}$$

The density-density correlation function of greatest interest and importance in practice is, as with the distribution functions, the one of lowest order, $l = 2$. This function is related to the distribution functions by

$$H^{(2)}(\mathbf{r}, \mathbf{r}') = n(\mathbf{r})\delta(\mathbf{r} - \mathbf{r}') + n(\mathbf{r})n(\mathbf{r}')h(\mathbf{r}, \mathbf{r}') \tag{4.16}$$

where $h(\mathbf{r}, \mathbf{r}')$ is the *total correlation function* related to $g(\mathbf{r}, \mathbf{r}')$ by

$$g(\mathbf{r}, \mathbf{r}') = h(\mathbf{r}, \mathbf{r}') + 1. \tag{4.17}$$

These functions are thus equivalent with respect to the physical information that they contain.

The density-density correlation function is closely related to the *linear response function*, $\chi(\mathbf{r}, \mathbf{r}')$, that determines how a fluid responds to a small change in an external field. The change in density at $\delta n(\mathbf{r})$ due to a small change in external potential $\delta\nu(\mathbf{r}')$ is given by

$$\delta n(\mathbf{r}) = \int \chi(\mathbf{r}, \mathbf{r}')\delta\nu(\mathbf{r}')d\mathbf{r}' = -\frac{1}{k_B T} \int H^{(2)}(\mathbf{r}, \mathbf{r}')\delta\nu(\mathbf{r}')d\mathbf{r}'. \tag{4.18}$$

This is an example of an application of the fluctuation-dissipation theorem that states that the response of a system to a weak external perturbation is determined by the fluctuations in the equilibrium system, see ref. [111].

The fact that the density-density correlation function determines the response of the fluid to a weak external field implies that it determines how the fluid interacts with radiation. Thus, at least for bulk systems where the concentration profiles are constant, the density-density correlation function,

and thereby the total correlation function, can be measured more or less directly in scattering experiments.

If the interaction potential is pairwise additive, i.e. it can be written as a sum where each term depends on at most two particle coordinates according to

$$U(\mathbf{r}_1, \cdots, \mathbf{r}_N) = \sum_{i=1}^{N} \nu_i(\mathbf{r}_i) + \frac{1}{2} \sum_{i=1}^{N} \sum_{\substack{j=1 \\ j \neq i}}^{N} u_{ij}(\mathbf{r}_i, \mathbf{r}_j), \tag{4.19}$$

where the factor 1/2 corrects for the fact that each pairwise interaction is counted twice, the thermodynamic properties of the fluid depend on $n(\mathbf{r})$, $h(\mathbf{r}, \mathbf{r}')$ and the interaction potential only [110]. While the interaction potential in real systems is not pairwise additive in general, pairwise additive model potentials have been shown to give results in good agreement with experimental data in many cases, see for instance ref. [112].

Over the last century, several predictive theories for $h(\mathbf{r}, \mathbf{r}')$ in terms of $n(\mathbf{r})$ and $u(\mathbf{r}, \mathbf{r}')$ have been developed. Commonly, such theories are expressed in terms of an equation where an unknown, typically $h(\mathbf{r}, \mathbf{r}')$, appears in an integrand, i.e. as an integral equation. The approach that has proved most fruitful for obtaining accurate approximations for $h(\mathbf{r}, \mathbf{r}')$ is to combine the exact Ornstein-Zernike (OZ) equation [113]

$$h(\mathbf{r}, \mathbf{r}') = c(\mathbf{r}, \mathbf{r}') + \int h(\mathbf{r}, \mathbf{r}'') n(\mathbf{r}'') c(\mathbf{r}'', \mathbf{r}') d\mathbf{r}'', \tag{4.20}$$

where $c(\mathbf{r}, \mathbf{r}')$ is called the *direct correlation function*, with a second, approximate, expression relating $h(\mathbf{r}, \mathbf{r}')$ and $c(\mathbf{r}, \mathbf{r}')$.

The direct correlation function may be considered defined by eq. (4.20), but an equivalent, more physically transparent definition is given by eq. (4.23) below. The relation between the total and direct correlation functions can be illustrated by recursively substituting the OZ equation into itself, yielding

$$h(\mathbf{r}, \mathbf{r}') = c(\mathbf{r}, \mathbf{r}') + \int c(\mathbf{r}, \mathbf{r}'') n(\mathbf{r}'') c(\mathbf{r}'', \mathbf{r}') d\mathbf{r}'' + \cdots . \tag{4.21}$$

The result is an expression for $h(\mathbf{r}, \mathbf{r}')$ as an infinite series of multi-centered integrals of products of $c(\mathbf{r}, \mathbf{r}')$ and $n(\mathbf{r})$. Thus, the total correlation function can be interpreted as the sum of the direct correlation and all indirect correlations.

For a system with an arbitrary number of components the OZ equation takes the form of a system of equations with one equation for each pair of species,

$$h_{ij}(\mathbf{r}, \mathbf{r}') = c_{ij}(\mathbf{r}, \mathbf{r}') + \sum_m \int h_{im}(\mathbf{r}, \mathbf{r}'') n_m(\mathbf{r}'') c_{mj}(\mathbf{r}'', \mathbf{r}') d\mathbf{r}'', \tag{4.22}$$

where i and j are species indexes and the summation is over all species. The indexed correlation functions refer to correlations between particles of species i and j in the sense that $n_j(\mathbf{r}')(h_{ij}(\mathbf{r},\mathbf{r}')+1) = n_j(\mathbf{r}')g_{ij}(\mathbf{r},\mathbf{r}')$ gives the average concentration of particles of species j at $\mathbf{r}'$ given that a particle of species i is held fixed at $\mathbf{r}$. Because the correlation functions are symmetric with respect to interchange of the species indexes, $h_{ij}(\mathbf{r},\mathbf{r}') = h_{ji}(\mathbf{r},\mathbf{r}')$ and similarly for $c_{ij}(\mathbf{r},\mathbf{r}')$, for an N-component system there are $N(N+1)/2$ equations. Since we are interested in binary electrolytes it is eq. (4.22) that is used in all calculations. We will continue to assume a one component system in the discussion below for notational simplicity. The generalization to multi-component systems is straight forward.

The direct correlation function can be expressed in terms of a functional derivative of the excess chemical potential with respect to the concentration profile,

$$\frac{1}{k_BT}\frac{\delta\mu^{ex}(\mathbf{r})}{\delta n(\mathbf{r}')} = -c(\mathbf{r},\mathbf{r}'), \tag{4.23}$$

where $\mu^{ex}(\mathbf{r})$ denotes the local excess chemical potential, the reversible work required to insert a particle into the system at $\mathbf{r}$ due to interactions with other particles. The corresponding relation for the ideal contribution to the chemical potential is

$$\frac{1}{k_BT}\frac{\delta\mu^{id}(\mathbf{r})}{\delta n(\mathbf{r}')} = \frac{\delta(\mathbf{r}-\mathbf{r}')}{n(\mathbf{r})}. \tag{4.24}$$

The OZ equation can be justified as follows by noting that equation (4.18) implies that[3]

$$k_BT\frac{\delta n(\mathbf{r})}{\delta\nu(\mathbf{r}')} = -H^{(2)}(\mathbf{r},\mathbf{r}'). \tag{4.25}$$

If the fluid is maintained in equilibrium at constant chemical potential, μ, so that

$$\mu = \mu^{id}(\mathbf{r}) + \mu^{ex}(\mathbf{r}) + \nu(\mathbf{r}), \tag{4.26}$$

is not changed by the change in external field, the change in the *intrinsic chemical potential*, $\mu^{int}(\mathbf{r}) = \mu^{id}(\mathbf{r}) + \mu^{ex}(\mathbf{r})$, the contribution to the chemical potential that is not due to external fields, must exactly cancel the change in $\nu(\mathbf{r})$,

$$\delta\mu^{id}(\mathbf{r}) + \delta\mu^{ex}(\mathbf{r}) = \delta\mu^{int}(\mathbf{r}) = -\delta\nu(\mathbf{r}). \tag{4.27}$$

Thus, the functional derivative of the density with respect to $\delta\mu^{int}(\mathbf{r})$ is

$$k_BT\frac{\delta n(\mathbf{r})}{\delta\mu^{int}(\mathbf{r}')} = H^{(2)}(\mathbf{r},\mathbf{r}'). \tag{4.28}$$

[3]According to the definition of functional derivative, $\delta F = \int \phi(\mathbf{r})\delta\psi(\mathbf{r})d\mathbf{r}$ implies that $\frac{\delta F}{\delta\psi(\mathbf{r})} = \phi(\mathbf{r})$

We note that the sum of eqs. (4.23) and (4.24) and eq. (4.28) are each others functional inverse, which means that they fulfill

$$\begin{aligned}\delta(\mathbf{r}-\mathbf{r}') &= \int k_B T \frac{\delta n(\mathbf{r})}{\delta \mu^{int}(\mathbf{r}'')}\Big(\frac{1}{k_B T}\frac{\delta \mu^{id}(\mathbf{r}'')}{\delta n(\mathbf{r}')}+\frac{1}{k_B T}\frac{\delta \mu^{ex}(\mathbf{r}'')}{\delta n(\mathbf{r}')}\Big)d\mathbf{r}'' \qquad (4.29)\\ &= \int n(\mathbf{r})(\delta(\mathbf{r}-\mathbf{r}'')+h(\mathbf{r},\mathbf{r}'')n(\mathbf{r}''))\Big(\frac{\delta(\mathbf{r}''-\mathbf{r}')}{n(\mathbf{r}'')}-c(\mathbf{r}'',\mathbf{r}')\Big)d\mathbf{r}'',\end{aligned}$$

from which the OZ equation, eq. (4.20), can be recovered. See ref. [111] for a complete proof.

In order to show how a second relation between $h(\mathbf{r},\mathbf{r}')$ and $c(\mathbf{r},\mathbf{r}')$ to supplement the OZ equation can be found, we note that the pair distribution function can be written as

$$g(\mathbf{r},\mathbf{r}') = e^{-\frac{\omega(\mathbf{r},\mathbf{r}')}{k_B T}}, \qquad (4.30)$$

where $\omega(\mathbf{r},\mathbf{r}')$ called the *potential of mean force*. As the name suggests, this function has the physical interpretation that it serves as the potential for the average force that two fixed particles, one at $\mathbf{r}$ and one at $\mathbf{r}'$, appears to exert on each other, including both the direct interactions between the particles and the average over the interaction with all other particles. The potential of mean force can be written as

$$\omega(\mathbf{r},\mathbf{r}') = u(\mathbf{r},\mathbf{r}') - k_B T \ln y(\mathbf{r},\mathbf{r}') \qquad (4.31)$$

where $y(\mathbf{r},\mathbf{r}')$ is the so-called *cavity correlation function* that has the physical interpretation that it is the pair distribution function between two imaginary particles that interacts normally with all other particles in the system, but do not interact with each other. The quantity $-k_B T \ln y(\mathbf{r},\mathbf{r}')$ may be interpreted as the *indirect* contribution to the potential of mean force. Thus, the problem has been reduced to finding $\ln y(\mathbf{r},\mathbf{r}')$ in terms of $h(\mathbf{r},\mathbf{r}')$ and $c(\mathbf{r},\mathbf{r}')$. It can be shown that [111]

$$\ln y(\mathbf{r},\mathbf{r}') = h(\mathbf{r},\mathbf{r}') - c(\mathbf{r},\mathbf{r}') + b(\mathbf{r},\mathbf{r}') \qquad (4.32)$$

where $b(\mathbf{r},\mathbf{r}')$ is called the *bridge function*. Although $b(\mathbf{r},\mathbf{r}')$ can be written as an infinite series where each term is given by a multi-centered integral over some product composed of $h(\mathbf{r},\mathbf{r}')$ and $n(\mathbf{r})$, experience has shown that this series tends to converge slowly while the computational complexity increases sharply with each term. Thus, the exact solution for $h(\mathbf{r},\mathbf{r}')$ is rendered intractable by our inability to calculate $b(\mathbf{r},\mathbf{r}')$ and in practice one must resort to approximations at this stage. Such approximations are often called *closures* in the literature because they are made in order to get a closed set of equations for $h(\mathbf{r},\mathbf{r}')$ and $c(\mathbf{r},\mathbf{r}')$.

4.2 The HNC Approximation

One closure that was proposed independently by several authors in the middle of last century [114, 115, 116] is the hypernetted chain (HNC) approximation, where $b(\mathbf{r}, \mathbf{r}')$ is simply set to zero. To get a feel for the physical implications of this approximation it instructive to note that the Ornstein-Zernike equation allows the HNC approximation for $\omega(\mathbf{r}, \mathbf{r}')$ to be written as

$$\begin{aligned} \omega^{HNC}(\mathbf{r}, \mathbf{r}') &= u(\mathbf{r}, \mathbf{r}') - k_B T\big(h(\mathbf{r}, \mathbf{r}') - c(\mathbf{r}, \mathbf{r}')\big) \\ &= u(\mathbf{r}, \mathbf{r}') - k_B T \int h(\mathbf{r}, \mathbf{r}'')n(\mathbf{r}'')c(\mathbf{r}'', \mathbf{r}')d\mathbf{r}''. \end{aligned} \tag{4.33}$$

The factor $h(\mathbf{r}, \mathbf{r}'')n(\mathbf{r}'')$ in the integrand can be interpreted as the deviation in density at $\mathbf{r}'$ caused by the presence of a particle at $\mathbf{r}$. Together with the definition of $c(\mathbf{r}, \mathbf{r}')$, eq. (4.23), this leads to the interpretation of the integral for the indirect contribution to the potential of mean force in eq. (4.33) as the change in excess chemical potential at $\mathbf{r}'$ resulting from change in density induced by the presence of a particle at $\mathbf{r}$ *if this change in density was infinitesimally small*. In reality that change in density is, of course, finite. The HNC approximation thus has the character of a mean field approximation in $c(\mathbf{r}, \mathbf{r}')$. The bridge function may be interpreted as containing all the higher order effects of the density response on the indirect part of the potential of mean force.

Empirically, it is known that the HNC approximation is suitable for systems where the pair interaction potential is long-ranged, e.g. Coulomb systems, where it gives result in close agreement with simulations under a wide range of conditions [117]. On the other hand, the HNC approximation does not perform well for short-ranged interaction potentials dominated by harsh repulsion, such as Lennard-Jones particles and "hard spheres" [118]. That the performance of an approximate closure depends critically on the form of the interaction potential is generally the case. A way to rationalize these observations is that the long-range character of the Coulomb potential makes the mean-field treatment of $c(\mathbf{r}, \mathbf{r}')$ justified. It is generally believed, but to the authors knowledge it has not been proved in all generality, that $c(\mathbf{r}, \mathbf{r}')$ behaves as

$$c(\mathbf{r}, \mathbf{r}') \approx -\frac{u(\mathbf{r}, \mathbf{r}')}{k_B T} \tag{4.34}$$

when $|\mathbf{r} - \mathbf{r}'|$ becomes large. It is therefore reasonable to expect that the long range of the Coulomb interactions makes the region where eq. (4.34) is a good approximation and the direct correlation function is close to the pair potential comparatively important.

A situation where the hypernetted chain approximation fails is for strongly attractive Coulomb interactions. This coincides with the development of a large peak in the cation-anion correlation function, that can be interpreted as "ion pairing". Given that the approximation in eq. (4.33) relies on the deviation from bulk density to be small, it is easy to see why the HNC approximation should fail under these conditions. The deviation from bulk concentration of one type of ions around an ion of the opposite sign is then very far from being small. For severe cases, i.e. very strong cation-anion interactions, there is no solution to the OZ equation with the HNC closure for for the primitive model in a range of concentrations [119]. For weaker interactions the height of the peak in the cation-anion distribution function is typically underestimated and there is a spurious peak in the like-ion distribution functions for a separation of about two ions diameters [120]. This occurs for parameters corresponding to aqueous 2:2 electrolytes close to room temperature for concentrations below a few hundred mM. For higher concentrations these deficiencies are much less pronounced.

The usual method of solving the OZ equations for a given closure and a given constant density is to simplify the equation by computing its Fourier transform. The Fourier transform, $\hat{\phi}(\mathbf{k})$, of an arbitrary function $\phi(\mathbf{r})$ is defined in l dimensions by

$$\hat{\phi}(\mathbf{k}) = \int \phi(\mathbf{r}) e^{-i\mathbf{k}\cdot\mathbf{r}} d\mathbf{r} \tag{4.35}$$

with the inverse relation

$$\phi(\mathbf{r}) = \frac{1}{(2\pi)^l} \int \hat{\phi}(\mathbf{k}) e^{i\mathbf{k}\cdot\mathbf{r}} d\mathbf{k}, \tag{4.36}$$

where i is the imaginary unit and $\mathbf{k}$ is the wave vector. The Fourier transform may be considered as an expansion of a function on an infinite basis set of standing waves, transforming a function of position $\mathbf{r}$ into a function of wave vector $\mathbf{k}$. The Fourier transform has the property that if

$$\psi(\mathbf{r}) = \int \phi(\mathbf{r}')\Phi(\mathbf{r} - \mathbf{r}')d\mathbf{r}' \tag{4.37}$$

then

$$\hat{\psi}(\mathbf{k}) = \hat{\phi}(\mathbf{k})\hat{\Phi}(\mathbf{k}). \tag{4.38}$$

This can be used to obtain an algebraic equation in terms of the Fourier transforms of the direct and total correlation functions. For homogeneous

fluids where $h_{ij}(\mathbf{r},\mathbf{r}') = h_{ij}(r)$ (and similarly for $c_{ij}(\mathbf{r},\mathbf{r}')$), $r = |\mathbf{r}' - \mathbf{r}|$ and the concentration n is a constant,

$$\hat{h}_{ij}(k) = \hat{c}_{ij}(k) + \sum_m \hat{h}_{im}(k) n_m \hat{c}_{mj}(k), \tag{4.39}$$

This equation can be written as a matrix equation

$$\hat{H}(k) = \hat{C}(k) + \hat{H}(k) N \hat{C}(k) \tag{4.40}$$

where the elements of $\hat{H}(k)$ are $\hat{h}_{ij}(k)$, the elements of $\hat{C}(k)$ are $\hat{c}_{ij}(k)$ and the elements of N are given by $n_i\delta_{ij}$ where δ_{ij} is the Kronecker delta. The solution to this equation for $\hat{H}(k)$ in terms of $\hat{C}(k)$ is

$$\hat{H}(k) = \hat{C}(k)[\mathbf{1} - N\hat{C}(k)]^{-1} \tag{4.41}$$

where $\mathbf{1}$ is the unit matrix. Thus, the OZ equation has a simpler structure in k-space than in r-space. The closure relation, on the other hand, is generally more easily expressed in r-space. Furthermore, analytical solutions are not possible for most closures, including HNC, so the problem has to be solved numerically. A common approach is to solve the set of equations iteratively, starting from a guess for $\hat{c}_{ij}(k)$ in Fourier space and calculating $\hat{h}_{ij}(k)$. The Fourier transform is then inverted and a new guess for $\hat{c}_{ij}(r)$ can be calculated from the old $\hat{h}_{ij}(r)$ and $\hat{c}_{ij}(r)$ using eqs. (4.30), (4.31), (4.32) and the closure relation. The Fourier transform of $c_{ij}(r)$ is calculated and the process is repeated until convergence is attained [121, 122]. Because the procedure requires multiple Fourier transforms (and inverse Fourier transforms) the fast Fourier transform algorithm is usually used.

The OZ equation is valid for both isotropic and anisotropic fluids and can therefore be applied to situations where the concentration profiles are not constant but functions of position. Thus, it can be applied to fluids near interfaces if the concentration profile is known. The concentration profile near an interface is in general unknown *a priori*, however. In order to find the equilibrium ionic concentration profiles an additional relation between the concentration profiles and correlation functions is needed. Several such relations exist, for instance the Lovett-Mou-Buff-Wertheim equation [123, 124]. A particularly convenient relation can be obtained in the special case where the HNC closure is used for the correlation functions. For this closure, the excess chemical potential of ions of species i at position $\mathbf{r}$, $\mu_i^{ex}(\mathbf{r})$, can be written in terms of the correlation functions as follows [125]

$$\begin{aligned} \mu_i^{ex}(\mathbf{r}) &= k_B T \sum_j \int n_j(\mathbf{r}') \Big(\frac{1}{2}(h_{ij}(\mathbf{r},\mathbf{r}'))^2 - c_{ij}(\mathbf{r},\mathbf{r}') - \frac{u_{ij}(\mathbf{r},\mathbf{r}')}{k_B T} \Big) d\mathbf{r}' \\ &+ \frac{k_B T (1 + c_{ij}(\mathbf{r},\mathbf{r}))}{2}. \end{aligned} \tag{4.42}$$

The equilibrium condition for the electrolyte in the slit is that the chemical potential for each species is equal everywhere

$$\mu_i = \mu_i^{id}(\mathbf{r}) + \mu_i^{ex}(\mathbf{r}) + \nu_i(\mathbf{r}), \tag{4.43}$$

Because the ideal part of the chemical potential depends on the concentration profile only, according to

$$\mu_i^{id}(\mathbf{r}) = k_B T \ln(\Lambda^3 n_i(\mathbf{r})), \tag{4.44}$$

where $\Lambda = h/(mk_BT)^{1/2}$ is the thermal wave length, equation (4.43) can be used to determine the concentration profiles. The choice of the actual value of the chemical potential corresponds to specifying the bulk concentration of an electrolyte solution that is in equilibrium with the electrolyte between the walls. For systems where each component is electrically neutral the chemical potential for each species can be specified independently, and correspondingly any thermodynamically possible mixture of the components is allowed. For binary electrolytes this is not the case. The components must here be present in such proportions that the electrolyte solution is uncharged overall. Thus, if the chemical potential of either species is fixed, the chemical potential of the other is also fixed to the value that gives an electroneutral combination of densities. Only the chemical potential in bulk salt need therefore be specified. The chemical potential of each species in the inhomogeneous system is then

$$\mu_i = \frac{s_i \mu_{salt}}{s_+ + s_-} + q_i \Delta\Psi, \tag{4.45}$$

where $\Delta\Psi$ is the electric potential difference with respect to bulk solution. The condition that the walls should have a fixed charge density, σ, and that the system should be electroneutral overall can be used to determine $\Delta\Psi$.

In the case of a primitive model electrolyte between two walls it is appropriate to adopt a coordinate system such as the one shown in Figure 4.1. The lateral distance is denoted $R = \sqrt{(x-x')^2 + (y-y')^2}$ and the coordinate perpendicular to the walls is z, with its origin in the mid-plane between the walls. The OZ equation in this geometry, in terms of the two dimensional Fourier transforms[4] of the correlation functions in the directions parallel to the walls, has the form

$$\hat{h}_{ij}(k, z, z') = \hat{c}_{ij}(k, z, z') + \sum_m \int \hat{h}_{im}(k, z, z'') n_m(z'') \hat{c}_{mj}(k, z'', z') dz''. \tag{4.46}$$

[4]For cylindrically symmetric functions these are equivalent to the zeroth-order Hankel transforms.

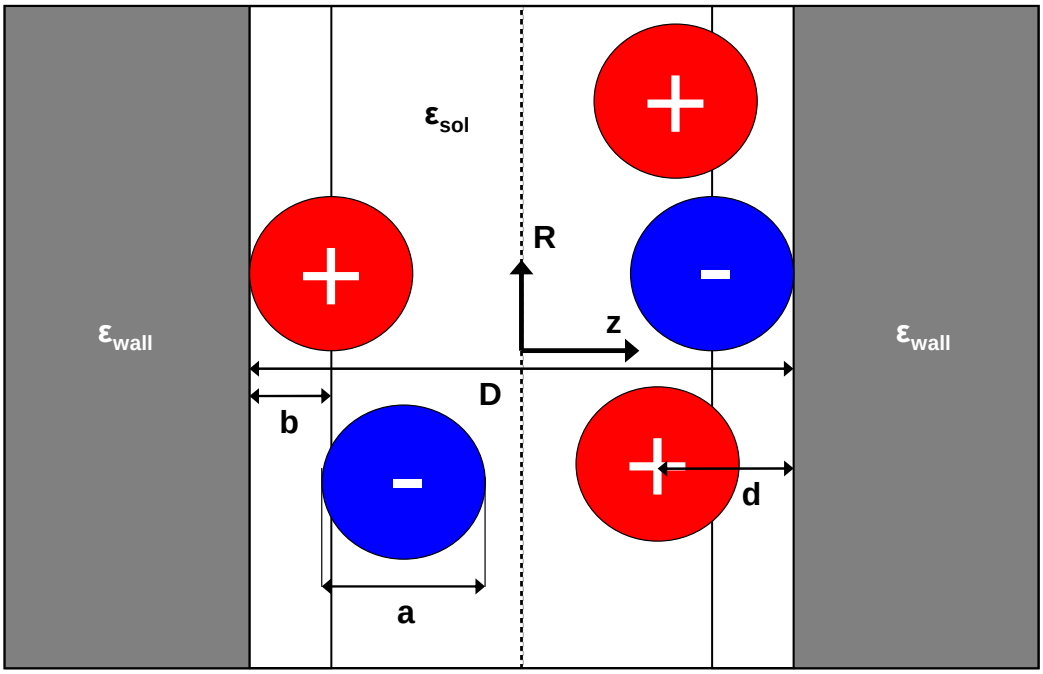

Figure 4.1: The geometry and notation used in calculations of the wall-wall pressure. $R = \sqrt{(x-x')^2 + (y-y')^2}$ is the lateral distance and z is the coordinate perpendicular to the wall. The distance between the dielectric interfaces is D the ion radius is a, the ion-wall distance is sometimes denoted d and the minimum ion-wall distance is denoted b.

If the integration is approximated by a Riemann sum, the equation becomes

$$\hat{h}_{ij}(k, z_o, z_p) = \hat{c}_{ij}(k, z_o, z_p) + \sum_m \sum_l \hat{h}_{im}(k, z_o, z_l) n_m(z_l) \hat{c}_{mj}(k, z_l, z_p) \Delta z_l, \tag{4.47}$$

where the indexed z coordinates denote the centers of intervals with width Δz, all of which need not be equal. Comparison with eq. (4.39) reveals that the OZ-equation for a three dimensional system that is inhomogeneous in one direction has the same form as two dimensional system with as many components as there are terms in the sum over m and l. If l is taken sufficiently large, eq. (4.47) becomes equivalent to eq. (4.46) for all intents and purposes. Thus, the same method that is used for bulk mixtures can be used to solve the OZ-equation in the inhomogeneous case, with a fixed concentration profile. The formal equivalence between an inhomogeneous three dimensional fluid and a multi-component two dimensional fluid is demonstrated in ref. [126].

Since the concentration profiles can be calculated from eq. (4.42) and the

equilibrium condition, eq. (4.43) the problem of finding the equilibrium concentration profiles and correlation functions can be solved by iteration: starting from a guess for the concentration profiles and correlation functions, the set of correlation functions that are consistent with the concentration profiles is calculated. From those, new concentration profiles are calculated and the set of correlation functions that are consistent with these are computed. If the starting guess for the set of concentration profiles and correlation functions is sufficiently close to the equilibrium distribution functions the solution will converge to these. For details regarding the numerical procedure, see refs. [126, 127, 128].

This method of calculating the distribution functions for inhomogeneous systems is usually referred to as the anisotropic HNC (AHNC) method. The concentration profiles and correlation functions obtained from AHNC calculations have been compared to simulation results and has been found to be in close agreement with these under most conditions [129]. (Even for cases where mean-field theories, such as the PB approximation, fail *qualitatively*.) The exception is when the local density is very high, such as for instance the counterion density close to a highly charged surface, where the contact values of the correlation functions between ions of different sign is overestimated.

The AHNC procedure can be modified to allow other closures than HNC, but this requires a different method of calculating the concentration profiles as eq. (4.42) is valid only within the HNC approximation. A notable example of another closure that has been applied to inhomogeneous electrolyte systems is the reference HNC approximation where the bridge function is not neglected but taken from a reference system [130]. Most of the shortcomings of the HNC approximation are absent for this closure [131, 132].

4.3 Calculation of Experimental Observables

Due to the prominent role of the chemical potential in the Gibbs adsorption isotherm, eqs. (2.11) and (2.12), surface thermodynamic properties are most easily handled within the grand canonical ensemble. To treat a general interface one would adopt an ensemble of systems containing an interface between phases that are both treated in molecular detail.

The surface excess number of particles is given by the difference in number of particles between a system that contains an interface at one of its boundaries and one that does not. This is a slightly different situation compared to that where both phases are treated in all atomic detail, see Section 2.1. In the

grand canonical ensemble the concentration profiles have the normalization property

$$\int n_i(\mathbf{r})d\mathbf{r} = \langle N_i \rangle. \tag{4.48}$$

The surface excess number of particles of species i can therefore be written as

$$N_i^s = \langle N_i \rangle_{surf} - \langle N_i \rangle_{bulk} = \int (n_i(\mathbf{r}) - n_i^{bulk}) d\mathbf{r}, \tag{4.49}$$

where the subscript "surf" means that the ensemble average is for a system containing a surface whereas the subscript "bulk" refers to the average in a homogeneous system of the same volume and chemical potential. For a planar surface, it follows that the surface excess in the primitive model, Γ_i^d (the superscript d stands for "diffuse"), is given by

$$\Gamma_i^d = \int_0^\infty (n_i(z) - n_i^{bulk}) dz, \tag{4.50}$$

where the origin of the z-coordinate is placed in the plane of closest approach of the ions to the surface. This formula is based on the assumption that the Gibbs surface separating the two phases is located at a negative z-coordinate, so that the ions cannot penetrate into the wall material. It is generally the case that the plane of closest approach of the ions to the surface does not coincide with the Gibbs plane in experimental systems. In this case, there will be a negative contribution to each Γ_i from the "ion-free layer" between those planes. This contribution is given simply by

$$\Gamma_i^i = n_i^{bulk} z^{solv}, \tag{4.51}$$

z^{solv} is the coordinate of the Gibbs plane of the solvent, which is negative by construction in the case considered here. The superscript i stands for "inner". If all charged species can approach the surface equally closely, the presence of an ion-free layer does not affect the concentration profiles. Thus, the inner and diffuse contributions to the surface excess are additive,

$$\Gamma_i = \Gamma_i^d + \Gamma_i^i. \tag{4.52}$$

Similarly, the drop in mean electrostatic potential over the diffuse region, the work per unit charge to bring an infinitesimal charge from the bulk solution to the point plane of closest approach of the ions, is

$$\Psi^d = -\frac{1}{\epsilon\epsilon_0} \sum_i q_i \int_0^\infty z n_i(z)\, dz. \tag{4.53}$$

This quantity does not depend on the actual distribution of charge on the surface side of the plane of closest approach of the ions. The corresponding contribution from the inner layer, Ψ^i, does, however, depend on the details of that distribution. If the assumptions of the primitive model are taken at face value and the surface charge is taken to be located in a single plane located at z^σ, then Ψ^i is given by

$$\Psi^i = -\frac{\sigma z^\sigma}{\epsilon\epsilon_0}. \tag{4.54}$$

Like z^{solv}, z^σ has a negative sign by construction. Note, however, that there is no physical reason to think that these coordinates should exactly coincide. As for the surface excess, the inner and diffuse contributions to the potentials are additive,

$$\Psi = \Psi^d + \Psi^i. \tag{4.55}$$

In the situation with two walls, the pressure between them can be calculated in terms of the distribution functions and interaction potentials. The interaction pressure in the slit between the walls is equivalent to the perpendicular component of the stress tensor at some plane between the walls [126]. Because the electrolyte is in equilibrium, the pressure must be independent of where in the slit it is evaluated. The choice where to evaluate the pressure is therefore one of convenience and numerical expedience. Two planes stand out in this respect: $z = \pm(D/2 - b)$ and $z = 0$, i.e. at wall-ion contact or in the middle of the slit. (Keep in mind that the coordinate system is different compared to the one-wall case, see Figure 4.1.) The former choice has been found to be numerically more difficult for charged surfaces due to the difficulty in evaluating the contact concentration with sufficient accuracy [84]. Therefore, the second alternative will be considered here. For a primitive model electrolyte in the presence of ion-wall dispersion interactions the pressure due to the ions between the walls may be written as a sum of contributions, each arising from one type of interaction,

$$P^{ion} = P^{ion}_{kin} + P^{ion}_{Coul} + P^{ion}_{core} + P^{ion}_{im} + P^{ion}_{disp}. \tag{4.56}$$

P^{ion}_{kin} is the ideal contribution to the pressure, given by $P^{ion}_{kin} = k_B T \sum_i n_i(0)$ (recall that $n_i(0)$ is the concentration of ions of species i in the mid-plane between the walls.) P^{ion}_{Coul} is the wall-wall interactions due to electrostatic ion-ion interactions across the mid-plane, given by

$$\begin{aligned} P^{ion}_{Coul} &= -\sum_{i,j} \int_0^{D/2} dz \int_{-D/2}^{0} dz' \int d\mathbf{R}\, n_i(z) n_j(z') \\ &\times \; h_{ij}(R, z, z') \frac{\partial u^{Coul}_{ij}(R, z, z')}{\partial z}. \end{aligned} \tag{4.57}$$

P^{ion}_{core} is the pressure contribution due to the ionic cores colliding across the mid-plane, the explicit expression for which is

$$\begin{aligned} P^{ion}_{core} &= 2\pi\, k_B T \sum_{i,j} \int_0^a dz \int_{z-a}^0 dz'\, n_i(z) n_j(z')\,(z-z') \\ &\times \quad g_{ij}([a_{ij}^2 - (z-z')^2]^{1/2}, z, z'). \end{aligned} \tag{4.58}$$

The three pressure contributions above approach finite values as the wall-wall separation goes to infinity. These values are of course identical to the corresponding contributions to the osmotic pressure of a bulk electrolyte and are given by $k_B T \sum_i n_i^{bulk}$, $-\sum_{i,j} \frac{n_i^{bulk} n_j^{bulk}}{6} \int_{r=a}^{r=\infty} d\mathbf{r}\, r h_{ij}^{bulk}(r) \frac{du_{ij}^{Coul}(r)}{dr}$ and $2\pi a^3\, k_B T \sum_{i,j} n_i^{bulk} n_j^{bulk}\, g_{ij}^{bulk}(a)/3$ for P^{ion}_{kin}, P^{ion}_{Coul} and P^{ion}_{core}, respectively. The sum of P^{ion}_{kin}, P^{ion}_{Coul} and P^{ion}_{core} is denoted P^{ion}_{osm} and referred to as the osmotic pressure below. Generally, it is not the absolute value of the pressure components but the deviation from the bulk value that is of interest. Whenever any of the above pressure components are prefixed by a capital Δ it is the value of that pressure component minus the corresponding bulk value that is referred to.

The pressure components P^{ion}_{im} and P^{ion}_{disp} are the pressure components due to image forces and wall-ion dispersion forces, respectively. Because these contributions to the pressure are dependent on wall-ion interactions, both are obviously zero in bulk. P^{ion}_{im} is given by [84]

$$\begin{aligned} P^{ion}_{im} = &-\tfrac{1}{2} \textstyle\sum_i \int_0^{D/2} dz\, n_i(z) \frac{\partial \nu_i^{im}(z|D)}{\partial z} - \tfrac{1}{2} \sum_i \int_{-D/2}^{D/2} dz\, n_i(z) \frac{\partial \nu_i^{im}(z|D)}{\partial D} \\ &-\tfrac{1}{2\pi} \textstyle\sum_{i,j} \int_0^{D/2} dz \int_{-D/2}^0 dz' \int_0^\infty dk\, n_i(z) n_j(z') \hat{h}_{ij}(k,z,z')\, k\, \frac{\partial \hat{u}_{ij}^{im}(k,z,z'|D)}{\partial z} \\ &-\tfrac{1}{4\pi} \textstyle\sum_{i,j} \int_{-D/2}^{D/2} dz \int_{-D/2}^{D/2} dz' \int_0^\infty dk\, n_i(z) n_j(z') \hat{h}_{ij}(k,z,z')\, k\, \frac{\partial \hat{u}_{ij}^{im}(k,z,z'|D)}{\partial D} \end{aligned} \tag{4.59}$$

and P^{ion}_{disp} is given by (see Paper I)

$$\begin{aligned} P^{ion}_{disp} &= -\sum_i \int_0^{D/2} dz\, n_i(z) \frac{\partial A_i^{disp}(z + D/2)}{\partial z} \\ &+ \quad \sum_i \int_{-D/2}^0 dz\, n_i(z) \frac{\partial A_i^{disp}(|z - D/2|)}{\partial z}. \end{aligned} \tag{4.60}$$

These last two pressure components could equally well be regarded as part of the wall-wall van der Waals pressure as of the double layer pressure.

Chapter 5

Results and Discussion

"The purpose of computation is insight, not numbers."

-Richard W. Hamming, *Numerical Methods for Scientists and Engineers* (1962)

5.1 Summary of Papers

Paper I

In Paper I the effect of image charges and dispersion forces on the pressure between two charged, planar walls is investigated. The main purpose of this study is to ascertain whether the consistent treatment of image charges affects the influence of dispersion forces on the system.

The pressure between two dielectric walls with charge ± 4.5 µC cm^{-2} (357 Å^2 per unit charge) in equilibrium with a bulk electrolyte of 0.5 M concentration is calculated as a function of the wall-wall separation using the AHNC method. The electrolyte model is symmetric in all respects except the dispersion interactions with the walls, that only acts on the anions. This choice of electrolyte model is made in order to mimic the situation where the cations are much less polarizable than the anions, which is believed to be common in real systems, while minimizing the complexity of the model.

In order to ensure that the polarizability of the model ions fall into the range that is realistic for small ions, the polarizability of iodine is calculated from quantum mechanical density functional theory. Iodide is chosen as it is the most polarizable atomic ions that is in common use for experimental work

in colloid and interface science, making it appropriate as an example of a highly polarizable ion. Based on these considerations the values 0, -20 and -40 kJ Å^3 mol^{-1} are chosen for B_-, of which the last correspond to iodide, an example of a highly polarizable ion, in aqueous solution interacting with a polystyrene wall.

It is found that the interaction pressure is less repulsive for positively charged surfaces when dispersion forces are included compared to when they are neglected. The opposite trend is found for negative surfaces, but the difference in pressure is much smaller. Image forces tend to make the pressure more repulsive and thus tend to counteract the effect of dispersion forces for positive surfaces. The magnitude of the pressure due to image charges is remarkably insensitive to the strength of the wall-ion dispersion force despite the fact that they have a large influence on the ionic concentration profiles.

Note that two formulas are erroneously reproduced in Paper I: In eq. (6) there should be a factor 1/2 on the right hand side and in eq. (17) the two first terms on the right hand side are missing a factor $1/(2\pi)^2$. Both equations are given correctly in this thesis as eqs. (3.25) and (4.59), respectively. None of these errors are made in the actual calculations.

Paper II

In Paper II, the same model system as in Paper I is investigated for a wider range of bulk electrolyte concentrations, 0.125, 0.250 and 0.500 M, and surface charge densities in the interval -6.4 to 6.4 µC cm^{-2} (250 Å^2 per unit charge).

It is found that for low surface charge densities, the image charges give rise to depletion of salt close to the surfaces. In the same regime dispersion forces, when present, give rise to an enrichment of ions for larger distances from the surface. Consequently, dispersion forces give rise to an increase in wall-wall repulsion for large separation and image forces give rise to a wall-wall attraction for small separation. Both these effects become stronger with increasing bulk electrolyte concentration. With an increase of the magnitude of the surface charge density, the net contribution to the pressure from the image charge becomes progressively less attractive and then turns repulsive, regardless of the sign of the surface charge. This behavior is caused by the fact that the exclusion of salt from the slit due to image forces has a smaller effect on the total pressure for larger surface charge densities, where a larger part of the repulsion is due to counterions, which must remain between the walls to satisfy the electroneutrality condition. As the concentration of counterions

increases, P_{im}^{ion} becomes more repulsive due to the self-image interaction. The relative importance of image charges for the magnitude of the total pressure tend to decrease with increasing surface charge density.

For negative surfaces, where the dispersion forces act on the co-ions, the pressure is found to become more repulsive with increasing strength of the dispersion forces. This tendency is strongest for large wall separation and high bulk concentration. For smaller separations, the exclusion of co-ions by electrostatic forces tend to dominate the attractive dispersion forces drawing ions into the slit. Thus, dispersion forces have little influence on the pressure in this regime. For positive surface charge densities, dispersion forces act on the counterions, drawing them closer to the surface than electrostatics alone would. This gives rise to a significant decrease in repulsion between the walls for intermediate separations as ΔP_{osm}^{ion} is smaller than for the case without wall-ion dispersion forces for these separations. Apart from the effect of dispersion forces on the osmotic interactions between the walls there is also a contribution to the pressure due to the direct wall-ion dispersion forces, P_{disp}^{ion}, that is always attractive. For the cases of negative and small positive surface charge densities P_{disp}^{ion} tend to counteract the change in P_{osm}^{ion}, making the net contribution to the pressure small. In the case of moderate to large positive surface charge densities P_{osm}^{ion} and P_{disp}^{ion} tend to act in the same direction, making the pressure less repulsive. It is under these conditions that the largest effect of wall-ion dispersion forces on the wall-wall pressure are seen.

Paper III

In Paper III the distance dependence of the interaction pressure between uncharged walls in the presence of electrolyte of 0.25 - 1.0 M concentration is investigated. Electrolytes of valence types 1:1, 2:2 and 1:2 are considered. The effect of the polarizability of the interface is taken into account, both with respect to the image forces and to the dispersion forces in the same way as in Papers I and II. It is found that for electrolytes that are symmetric in every respect, i.e. both with respect to the charge and to the dispersion interactions with the wall, the net contribution from the electrolyte to the interaction pressure is attractive. This is due to depletion of electrolyte between the walls caused by both the repulsive image forces and the loss of "favorable" correlations. In the bulk solution the correlation between ions tend to give rise to a large negative contribution to the chemical potential. In the vicinity of a surface, this negative contribution is smaller because ions cannot correlate with ions on the "surface" side. Thus, ions tend to be excluded from the region close to a surface as well as from any confined

space of dimensions smaller than the typical correlation length. This gives rise to an attractive depletion interaction between surfaces. There is one exception to this behavior: for 1 M 1:1 salt the concentration profiles are non-monotonic and for some separation there is sufficient enrichment at the mid-plane to give rise to a repulsive pressure.

For asymmetric electrolytes, again both with respect to valencies and dispersion interactions with the walls, the situation is different in that in all cases there is a repulsive contribution to the pressure from the electrolyte. In a few cases this repulsive contribution even exceeds the attraction from the wall-wall van der Waals interaction. In the case of electrolytes of asymmetric valence type the repulsion is due to that monovalent ions are depleted to a lesser degree than divalent ions in the region close to the wall. Thus, there is a net excess of charge of the same sign as that of the monovalent ions close to the walls. Due to electroneutrality, this charge has to be compensated by an opposite charge somewhere further away from the surface. A situation resembling that of a charged surface is thus created. In the case of dispersion interactions between ions and surfaces the same situation arises due to enrichment of one of the ion species close to the surface by direct dispersion attraction. The strongest repulsion is seen for large concentrations of asymmetric electrolyte where the monovalent ions are attracted to the surface by dispersion forces. In this case both mechanisms conspire to create a large charge separation *and* the concentration profiles are oscillatory so that the enrichment of ions at the mid-plane becomes disproportionately large for certain wall-wall separations.

Paper IV

In Paper IV a comparison is made between experimental data on the mercury/aqueous $MgSO_4$ interface from refs. [74, 73] and results from AHNC calculations using the primitive model. This experimental system is especially suitable for such a comparison because the surface excesses of co-ions and counterions can be obtained in a model-independent way. The aim of the comparison is to test the predictions from primitive model calculations that overcharging, i.e. an apparent change in sign of the surface charge, can arise as a consequence of ion-ion correlations. To this end the primitive model results and GC results are simultaneously compared to the experimental data under the constraint that identical assumptions about the Stern layer are made in both cases. This comparison between the agreement with experiment of GCS theory and an entirely analogous theory where the "diffuse"

part of the double is treated with ion-ion correlations taken into account is meant to assess the importance of such correlations.

The effect of ion-ion correlations is qualitatively different depending on the surface charge density. For small or zero surface charge density, depletion is predicted in the region close to the surface. For larger surface charge densities the depletion of electrolyte close to the surface persists but beyond a certain surface charge density there is an onset of enrichment of co-ions in a region further out. Due to electroneutrality this must be accompanied by an enrichment of counterions in excess of what is needed to compensate for the surface charge, i.e. overcharging. This behavior is not predicted by GC theory, which gives concentration profiles that are equal to the bulk concentration all the way up to the surface for zero surface charge density and depletion of co-ions everywhere for finite surface charge densities. This behavior of the concentration profiles is reflected in the component of charge of the co-ion, that is predicted to increase monotonically to an asymptotic value by GC theory and to go through a maximum by the primitive model.

It is found that the primitive model but not GC theory fits the trend that the dependence of the surface excess of sulfate tends to become less negative with increasing magnitude of the surface charge density. With the assumption of an ion-free layer of thickness between 3.0 and 3.5 Å (depending on whether image charges are taken into account or not in the primitive model calculations) the results of the primitive model calculations are in reasonable quantitative agreement with experimental data. For positive surface charges the GC and primitive model calculations are both in poor agreement with the experimental surface excesses. This is consistent with the predominating view in the literature that sulfate is adsorbed on the mercury surface for anodic polarization.

Paper V

In Paper V the ability of the primitive model to fit the concentration dependence of the bulk activity coefficients of a series of sulfates with divalent metal cations is investigated. Also a variant of the primitive model where the effect of the molecular granularity of the solvent is taken into account in an *ad hoc* manner, referred to as the "solvent structure primitive model" (SSPM), is considered. The HNC approximation is used to evaluate the properties of the model for the purpose of fitting the model parameters to experimental data for moderate concentrations. As this approximation has some known defects relevant for 2:2 salts in a large portion of the concentration range that is ex-

perimentally accessible, the HNC calculations are supplemented with Monte Carlo simulations in the regions where the accuracy or the approximation cannot be taken for granted and in regions where no solution exist (which is the case for the primitive model for low concentration).

It is found that the primitive model is capable of reproducing the key features of the concentration dependence of the osmotic coefficient. The model is not quite capable of quantitatively reproducing the trend in the details of the concentration dependence of the osmotic coefficient over the set of sulfates considered. While the primitive model might not be accurate enough for applications where activity coefficients are needed with very high accuracy, the comparison with experiment shows that it is a fairly life-like model in many respects. The SSPM gives a slightly better fit to the osmotic coefficients than does the PM; the position of the minimum in the osmotic coefficient as a function of concentration is better reproduced by the SSPM.

The activity coefficients of the salt for lower concentrations are calculated using the model parameters that gives the best fit for high concentration. The calculated activity coefficients are compared to activity coefficients derived from EMF measurements. This comparison reveals that both the primitive model and SSPM gives good agreement with the *relative* activity coefficient (the activity coefficients relative to those for a finite concentration) but that the primitive model and SSPM give significantly different predictions for the *absolute* activity coefficients (relative to a non-interacting standard state). These paradoxical observations are reconciled by noting that while the models behave similarly both for moderate to high concentrations and for very low concentrations (as they must due to the DHLL) there is an intermediate region where the primitive model activity coefficients depend more strongly on concentration than the SSPM activity coefficients do. Thus, comparison between both of the models and experiments in the low concentration regime (0.1-10 mM) can in principle determine which model is superior. Unfortunately, the congruency between different experimental studies is relatively poor and the outcome of such an analysis depends on what weight is assigned to each experimental study. The sensitivity of the activity coefficient to the details of the model assumptions has relevance for the interpretation of experimental data in that some theory-assisted extrapolation is often needed to put the activity coefficients on an absolute scale. The conclusions about the absolute activity coefficients thus seem to depend on the form of the interaction potential. This is especially problematic since the two models investigated are members of a class of models that has a vast number of members of similar *a priori* plausibility.

5.2 Discussion

The feature that unites Papers I-V is that a situation in which mean field theory is inadequate in one or more respect is investigated in each of them. This is not to be construed as implying that mean field theory is suitable only as a straw man to be cut down by more worthy theories. Rather, mean field theory, in the form of PB and DH theory, has illuminated so effectively many phenomena related to double layers and electrolyte solutions that if one is not careful, one risks being blinded to those phenomena that are still in the shadow. If one grows too accustomed to the conceptual simplicity afforded by declaring the electric potential and the potential of mean force as being one and the same animal, as one does in PB theory, it is easy to find oneself in an alien landscape when one encounters one of the many situations where they clearly are not the same. When this is the case, typically when the interactions are strong or the concentration is high, difficulties abound. Here, not only does the problem of calculating experimental observables from interactions potentials become difficult but details of the interaction potential that could sometimes be ignored with impunity become important. This forces the connection to be made with ion specificity in bulk and interfacial systems that, as is becoming increasingly clear, depend critically on non-electrostatic interactions. While none of the Papers included in this thesis deals with the ion-specificity in real systems directly, all are at least partly motivated by the need to disentangle the interactions that give rise to the idiosyncratic behavior of different ionic species.

In Papers I and II the presence of image charges necessitates the consideration of correlations between ions. If one were to include image charges in a PB-type theory, one would have to either neglect their screening and get absurd result or make some *ad hoc* assumption about the screening. It is found, however, that the effect of image charges on the wall-wall pressure is quantitative rather than qualitative for charged surfaces: while the inclusion of image charges is necessary to even get the correct sign of the surface-surface interaction pressure for some surface charge densities, the difference between "images" and "no images" is quantitative rather than qualitative for most surface charge densities. A notable exceptions to this is the region around zero surface charge density where image charges give rise to an attractive contribution to the pressure due to depletion of electrolyte.

An interesting feature of the double layer pressure in the presence of attractive dispersion (or other) forces is that such forces acting on the co-ion tend to increase repulsion while attractive forces on the counterions tend to decrease repulsion. This observation is by no means novel, see for instance

refs. [60] and [72] that are discussed in Section 2.4 in connection with the Hofmeister series, but still deserves closer discussion. The way to understand this paradoxical behavior is to note that any attractive force between ions and walls will give rise to an increase in ion concentration between the walls, that in turn gives rise to repulsion between the walls. Such ion-wall interactions will also give rise to attraction between the walls due to direct interactions between the ions in each double layer and the opposite wall. Which of these tendencies is dominant depends the details of the system. That attractive dispersion forces acting on the counterions give rise to a decrease in repulsion is due both to that there is a high density of counterions that can interact with the opposite wall and that the concentration profiles gets distorted (compared to the case with only electrostatic forces) so that there is a higher density of counterions close to the walls and a lower density in the mid-plane. In the case where the co-ions are attracted to the walls, the wall-wall attraction caused by direct ion-wall dispersion attraction is relatively small because the co-ions are excluded for electrostatic reasons. The change in the concentration profiles induced by dispersion forces tends to increase the concentration in in the mid-plane and thus give rise to repulsion. This is the dominant contribution to the net change in pressure in this case. In this latter case, with dispersion interactions between walls and co-ions, the two kinds of changes brought about by dispersion forces tend to counteract each other, and the total change in pressure is small. In the case where the dispersion forces act between walls and counterions, however, both of the contributions to the change in pressure act in the same direction, at least for a range of surface-surface separations and the magnitude of the total change in pressure is larger. The experimental predictions is that not only should any Hofmeister series for surface interaction be expected to be reversed when the the surface charge density changes sign, as discussed in Section 2.4, the magnitude of the specificity is expected to be dramatically different as well.

The long-range asymptotic expressions for the wall-wall pressure in the presence of dispersion forces derived in ref. [66] in the DH limit are interesting in this context. These expressions indicate that dispersion forces give rise to a repulsion (in the case of attractive dispersion forces) that decay in the same way as the wall-wall van der Waals interaction. The repulsive effect on the concentration profiles is thus dominant compared to the attraction due to wall-ion interactions in this limit. Both contributions to the pressure have the same distance dependence and the ratio of their magnitudes is 8/7. As the contributions have opposite signs this implies that the total pressure is 1/8 of the pressure due to the change in the concentration pro-

files, the remaining 7/8 being canceled by the pressure due to direct ion-wall interactions. The magnitude of the pressure is determined by the arithmetic mean of the strength of the dispersion interaction acting on each species of ion. These observations have the implication that the apparent Hamaker constant should be dependent on the concentration of salt if there are strong dispersion interactions between ions and walls, but only weakly so. The long-range behavior of the pressure is independent of the sign and magnitude of the surface charge density, in contrast to the observations for short to intermediate separations made above.

In Paper III the interaction between uncharged surfaces is investigated. The finding that the osmotic contribution to the interaction pressure changes from attractive to repulsive for a range of separations when salt of asymmetric valence type is present is non-trivial. The reason for the appearance of a repulsive pressure is that a double layer, of sorts, is formed outside the surface. This is not due to the preferential adsorption of ions on the surface but rather to an asymmetric *depletion* of ions close to the surface. This depletion is caused by both to repulsive image charges and correlation effects, both of which effectively repel ions from the surface.

While it may appear reasonable that charge separation close to a surface gives rise to repulsion that can be likened to the double layer repulsion between charged surfaces, it is not obvious that this repulsion should overcome the attraction that is expected due to overall depletion. That repulsion is seen is ultimately a consequence of the electroneutrality condition: the net excess of charge due to monovalent ions close to the walls has to be compensated by an excess of divalent ions somewhere. For surface-surface separations, where this "somewhere" turns out to be around the mid-plane between the walls, there can be a net enrichment there, corresponding to a net repulsive ideal contribution to the pressure.

To ascribe the resulting repulsive barrier to the ideal contribution alone is overly simplistic and would not be correct, however. Careful analysis of the contributions to the pressure shows that the maximum in the pressure curve occurs for a separation where there is already a net depletion and that non-ideal contributions to the pressure are decisive. These contributions come from both hard core collisions and loss of "favorable" electrostatic correlations. In the cases where there are additional attractive forces between the ions and walls in the form of dispersion interactions, the effect of these depends strongly on whether they oppose or act in concert with the charge separation due to asymmetry in ionic valency. In the cases where the dispersion interactions act on divalent ions they give rise to a smaller enrichment close to the walls than when they act on monovalent ions. In addition, the

dispersion interactions tend to enhance the charge separation in the former case but not in the latter. The net result is that dispersion interactions on monovalent ions give rise to a much more dramatic shift in the height of the repulsive barrier.

It is in some sense unfortunate that the most dramatic effects are seen for surface-surface separation where the applicability of the continuum description of the solvent cannot be taken for granted and solvation forces may be dominant. Nevertheless, the qualitative features of the model can be tested. A type of experiment that may be useful in this regard is measurements of the swelling of multilamellar phospholipid vesicles in response to osmotic stress of the type described in ref. [38]. In such an experiment the separation for which the system is in mechanical equilibrium is measured for a given external osmotic pressure, that is controlled by adding high molecular weight compounds that do not penetrate into the interlamellar spaces of the vesicles. The pressure as a function of separation is predicted to turn oscillatory for much smaller concentration for salts of asymmetric valence type than for salts of symmetric valence type. This difference could used to test the model. An experiment could be performed where the dependence on salt concentration of the equilibrium separation for a given osmotic pressure is measured for salts of different valence type in order to assess this qualitative predictions of the model. In principle, one could also investigate salt solutions composed of different combinations of the same species of ions. If the model predictions from the model are accurate, combinations giving salts of symmetric valence type should make the force between lamellae more attractive and combinations of asymmetric valence type should make it more repulsive.

The system investigated in Paper IV appears at first sight very different from that in Paper III. The results can to a large extent be discussed in terms of the same mechanisms, however. For low surface charge densities a depletion is seen. For high concentrations this is the case even in the presence of *attractive* image charge interactions. This is so because in order to approach the surface, the ionic atmosphere of each ion has to be distorted so that there is more charge on the "solution" side than on the "surface" side of the ion. The asymmetry of the ionic atmosphere gives rise to a force that effectively repels the ion from the surface. (It is noteworthy that for high concentrations of very large ions, a situation also considered in Paper IV, there is a net enrichment of ions close to the walls. In this situation the hard core collisions dominate the electrostatic force.)

For higher surface charge densities the situation is the opposite: there are more ions close to the walls than mean field theory predicts. The situation

with depletion of ions close to the walls for low surface charge densities and a relative enrichment for higher surface charge densities may be considered a "signature" for overcharging due to ion-ion correlation as opposed to overcharging due to direct, chemical interactions between ions and walls. The consequence of overcharging by the ion-ion correlation mechanism for the component of charge of the anions is that it first increases sharply as the surface charge density is made more negative (starting from zero), reaches a maximum and then decrease with a rate that is dependent on the strength of the electrostatic interactions between ions. That this behavior is seen for the co-ion is due to the electroneutrality condition, as each increase in the magnitude of the surface charge density gives rise to an opposite and greater change in the magnitude of the counterion component of charge, the depletion of co-ions must at the same time become smaller. For negative surfaces, this corresponds to a decrease in the anionic component of charge that in turn corresponds to an increase in the anionic surface excess. This pattern should be at least close to universal; salts with similar bulk properties, such as activity coefficients, should show a similar behavior of the surface excess for any surface where there is no strong specific adsorption.

It is unfortunate that few experimental systems are sufficiently well characterized to allow an analysis analogous to the one in Paper IV. Because the details of surface excess of ions as a function of surface charge density is needed to judge whether ion correlation constitute a likely mechanism in any particular instance of overcharging. Thus, the surface charge density has to be measurable with a high accuracy. Moreover, the surface charge density must be variable over a broad range and the surface charge has to be uniform. This precludes most of the model systems in use in colloid and interface science; the mercury electrode appears unique in the respect that it fulfills these requirements. Any variation of the experimental system would thus have to be made on the solution side, barring any unforeseen advance.

Correlation effects become more important with increasing ionic valency, suggesting that solutions of salts with such exotic (for salts in solutions) valence types as 3:2 should be studied. Examples of such salts that are reasonably soluble are $Al_2(SO_4)_3$ and $La_2(SO_4)_3$. At least for the latter, some experimental data exist [133]. In that work the dependence of capacitance on electrolyte concentration is investigated and it is found that the variation is well described by a modified version of GC theory where thermodynamic consistency is enforced [134], but not by the original GC theory. This is consistent with ion-ion correlations being important. More than this cannot be said because the modified GC theory does not contain an explicit model of the electrolyte interaction potentials. An analysis of the same system in

terms of such a model, like the one in Paper IV, would be of great interest. A confounding factor for highly charged ions is that hydrolysis cannot be excluded *a priori*. The pH has to be controlled in order to establish that the highly charged cations are not present as hydration complexes of lower total charge. While this problem need not be insurmountable, it severely limits the interpretability of data from experiments where the pH is not controlled.

A different type of systems where overcharging due to ion-ion correlations is expected to take place is non-aqueous electrolyte solutions with sufficiently low permittivity. All other features of the interaction potential being equal, a 1:1 salt in a solvent with permittivity around 20, a value that cannot be considered extreme for polar organic solvents, should behave in the same way as a 2:2 salt in water in terms of bulk properties. A double layer in the same non-aqueous solution should be similar to a double layer in an aqueous solution of 2:2 salt for a surface charge density that is twice as high. Even lower permittivity solvents could be used; the limiting factors are whether suitable salts can be found that are soluble and whether high surface charge densities are obtainable in the solvent in question. At the cost of introducing another component into the system and thereby making the thermodynamic analysis more complicated, the permittivity can be varied continuously by using a mixed solvent system. This would allow a very detailed test of the predictions of the model that should be sensitive to the permittivity.

These considerations are also closely related to the bulk systems considered in Paper V. Just as the correlations that gives rise to overcharging are to be expected to be similar in inhomogeneous systems with similar strength of the electrostatic interactions, the correlations that give rise to deviations from ideal solution behavior should be similar in corresponding bulk systems. It is an implicit assumption in the primitive model that any chemical idiosyncrasies of the solvent will merely modify the optimal ion radius slightly. We note in that lithium perchlorate in 2-propanol, for which the activity coefficients have been determined [135], is in some key aspects very similar to magnesium sulfate in water: the bare ion sizes are almost the same [136], the geometry of perchlorate is nearly identical to that of sulfate (these species are even isoelectronic) and 2-propanol has a dielectric constant that is almost exactly one fourth of that of water. Thus, the electrostatic interactions for a 1:1 salt in 2-propanol are identical to those for a 2:2 salt in water to the extent that the representation of the solvent as a dielectric continuum is accurate. What is not equal in water and 2-propanol is, of course, the structure of the solvent and any solvation complex. Comparison between bulk thermodynamic data for the two solvents may well reveal to what extent such details are important for the behavior if the electrolytes. In Figure 5.1

such a comparison is made. A remarkable similarity is found, which lends support to the use of the primitive model. If other systems displaying the same conformity could be found, it would allow a systematic evaluation of the primitive model. Particularly, the range in concentration for which the assumptions underlying the model are valid could be established.

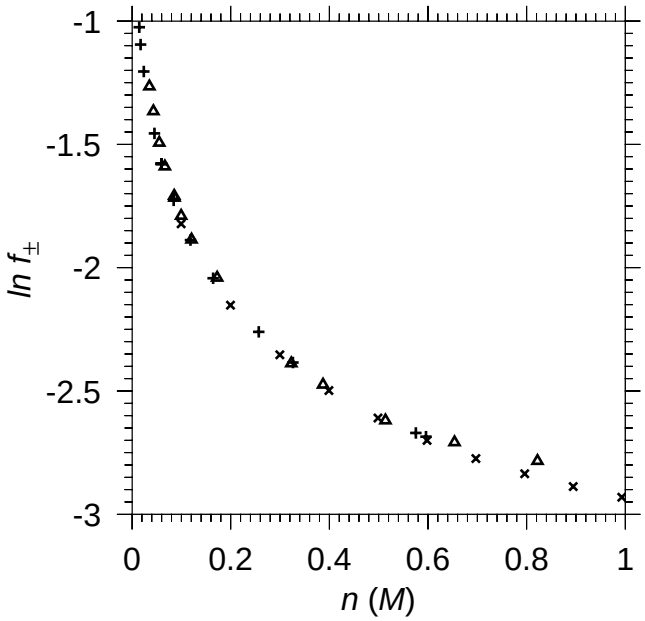

Figure 5.1: Comparison between activity coefficients for aqueous $MgSO_4$ and $LiClO_4$ in 2-propanol, taken from the literature. "+" and "x" symbols are for $MgSO_4$ taken from refs. [137] and [138], respectively. Triangles are for $LiClO_4$, taken from ref. [135]. The data has been converted to the McMillan-Mayer scale, see Chapter 3, using densities from ref. [139] in the case of $MgSO_4$ and using the densities given in [135] for $LiClO_4$. Note that for the data from ref. [137], the osmotic coefficients are not available so the second term in the right hand side of eq (3.6) could not be calculated. This term was therefore omitted in that case, which is a permissible approximation for low concentrations.

The conclusion that can be drawn from the results of Paper V and the discussion above is that the primitive model is unlikely to give a severe misrepresentation of the thermodynamic properties of aqueous 2:2 electrolytes. This state of affairs is fortunate in the sense that it lends support to the notion that conclusions on the basis of the primitive model are applicable to real systems. On the other hand it is unfortunate in that it implies that the thermodynamic properties of electrolytes are insensitive to the details of the

interaction potential. Such an insensitivity implies that little can be learned about those details by the study of the thermodynamic of bulk systems. The situation is the same as that for 1:1 electrolytes, discussed in Section 3.1. This is unfortunate as it makes the physico-chemical origin of "ion-pairing" in electrolytes difficult to ascertain. Despite that the concept of ion-pairs was introduced as a theoretical device in an approximate treatment of the primitive model [21], there is often a tacit assumption that ion-pairing implies the action of some non-electrostatic interaction mechanism. This has caused to considerable confusion in the literature, leading some authors to dismiss the presence of ion-pairing on the basis that experimental data could be well described without assuming any non-electrostatic interaction mechanism [137]. Other authors have cited the presence of ion-pairs as evidence of the presence of chemically well-defined species of associated ions [140], which is hard to reconcile with a purely electrostatic interaction mechanism. The comparison in Paper V between the primitive model and a closely related model where finite-ranged non-electrostatic interactions are taken into account indicate that electrostatic and non-electrostatic interaction mechanisms are difficult to distinguish on the basis of the bulk activity coefficients. Nevertheless, accurate measurements of the activity coefficients for very small concentrations could in principle discriminate between models that are not meaningfully distinguishable for higher concentrations.

A notable feature of the primitive model of 2:2 salts is that the ion sizes are much smaller than would be expected on the basis of the size of hydrated ions. This is so despite that the ion sizes that gives the best fit for the alkaline earth metal halides are commensurate with reasonable hydrated ion sizes [78]. This is consistent with the presence of non-electrostatic attraction between cations and anions, but as the ion sizes obtained in Paper V are in all cases greater than the "bare" ion size they are also consistent with the absence of non-electrostatic attraction. That the ion sizes are smaller in the case of 2:2 electrolytes than for 1:1 and 2:1 electrolytes may well be due to that the anion more readily replaces water in the solvation shell of the cation in the former case. Note that the typical interaction between a cation and a solvating water molecule becomes twice as large when going form 1:1 to 2:2 salt, whereas the interaction between a cation and an anion for a given separation becomes four times as large.

That the primitive model can reproduce bulk thermodynamic data as well as it does suggests that the electrostatic forces are indeed the dominant type of interactions that determine these properties. (The electrostatic interactions cannot be considered in isolation, however. The short-range repulsion between ions, that is approximated in the primitive model by the hard cores,

acts as a cut off for the electrostatic interactions in addition to giving rise to an excluded volume.) This in turn lends credence to the use of the primitive model to study surface properties. Nevertheless it is in interfacial systems that the deficiencies of the primitive model become most clearly visible. In the framework of the naive implementation of the primitive model, where only electrostatic and "hard core" interactions are considered, most ion-specific phenomena are inexplicable. This leaves two options: either the model can be extended in an *ad hoc* fashion, which is the approach taken in this thesis, or the model can be discarded in favor of more detailed models.

Bibliography

[1] Quincke, G. *Pogg. Ann.* **1861**, *113*, 513.

[2] Helmholtz, H. L. F. *Ann. Phys.* **1879**, *7*, 337.

[3] Stillinger, F. H.; Lovett, R. *J. Chem. Phys.* **1968**, *49*, 1991.

[4] LeNeveu, D. M.; Rand, R. P.; Parsegian, V. A.; Gingell, D. *Biophys. J.* **1977**, *18*, 209.

[5] Israelachvili, J. N.; Adams, G. E. *J. Chem. Soc., Faraday Trans. I* **1978**, *74*, 975.

[6] Israelachvili, J. N. *J. Colloid Interface Sci.* **1973**, *44*, 259.

[7] Arrhenius, S. PhD thesis, Uppsala University, **1884**.

[8] Robinson, R. A.; Stokes, R. H. *Electrolyte Solutions;* Dover Publications, 2002.

[9] Grahame, D. C. *Chem. Rev.* **1947**, *41*, 441.

[10] Gouy, G. *J. Phys.* **1910**, *9*, 457.

[11] Chapman, D. L. *Phil. Mag.* **1913**, *25*, 475.

[12] Stern, O. *Z. Electrochem.* **1924**, *30*, 508.

[13] Lyklema, J. *Fundamentals of Interface and Colloid Science, Solid-Liquid interfaces, II;* Academic Press, 1995.

[14] Debye, P.; Hückel, E. *Physik Z.* **1923**, *24*, 185.

[15] Kirkwood, J. G.; Poirier, J. C. *J. Phys. Chem.* **1954**, *22*, 591.

[16] Jönsson, B.; Wennerström, H.; Halle, B. *J. Phys. Chem.* **1980**, *84*, 2179.

[17] Kjellander, R.; Mitchell, D. J. *Chem. Phys. Lett.* **1992**, *200*, 76.

[18] Kjellander, R.; Mitchell, D. J. *Mol. Phys.* **1997**, *91*, 91.

[19] Ramirez, R.; Kjellander, R. *J. Chem. Phys.* **2003**, *119*, 11380.

[20] Stillinger, F. H.; Lovett, R. *J. Chem. Phys.* **1968**, *48*, 3858.

[21] Bjerrum, N. *Z. Electrochem.* **1918**, *24*, 321.

[22] Torrie, G. M. *J. Phys. Chem.* **1992**, *96*, 3772.

[23] Landau, L. D.; Lifshitz, E.; Pitaevskii, L. *Electrodynamics of Continous Media;* Butterworth-Heinemann: Oxford, 2nd ed., 1998.

[24] London, F. *Trans. Faraday Soc.* **1937**, *33*, 8.

[25] Mahanty, J.; Ninham, B. W. *Dispersion Forces;* Academic Press, 1976.

[26] Parsegian, A. *Van der Waals Forces: A Handbook for Biologists, Chemists, Engineers and Physicists;* Cambridge University Press, 2005.

[27] Derjaguin, B.; Landau, L. *Acta Phys.-Chim. U.S.S.R.* **1941**, *14*, 633.

[28] Verwey, E. J. W.; Overbeek, J. T. G. *Theory of the Stability of Lyophobic Colloids;* Elsevier, 1948.

[29] Derjaguin, B. V.; Titijevskaia, A. S.; Abricossova, I. I.; Malkina, A. D. *Discuss. Faraday Soc.* **1954**, *18*, 24.

[30] Lyklema, J.; Mysels, K. J. *J. Am. Chem. Soc.* **1965**, *87*, 2539.

[31] Pashley, R. M. *J. Colloid Interface Sci.* **1981**, *80*, 153.

[32] Kjellander, R.; Marčelja, S.; Pashley, R. M.; Quirk, J. P. *J. Phys. Chem.* **1988**, *92*, 6489.

[33] Kjellander, R.; Marčelja, S.; Pashly, R. M.; Quirk, J. P. *J. Chem. Phys.* **1990**, *92*, 4399.

[34] Kékicheff, P.; Marčelja, S.; Senden, T. J.; Shubin, V. E. *J. Chem. Phys.* **1993**, *99*, 6098.

[35] Israelachvili, J. *Intermolecular and Surface Forces;* Academic Press, 2nd ed., 1991.

[36] Kjellander, R.; Marčelja, S. *Chem. Phys. Lett.* **1987**, *142*, 485.

[37] Attard, P.; Kjellander, R.; Mitchell, J.; Jonsson, B. *J. Chem. Phys.* **1988**, *89*, 1664.

[38] Petrache, H. I.; Zemb, T.; Belloni, L.; Parsegian, V. A. *Proc. Nat. Acad. Sci. U.S.A.* **2006**, *103*, 7982.

[39] Hofmeister, F. *Arch. exp. Patol. Pharmakol.* **1888**, *24*, 247.

[40] Wondrak, E. M.; Louis, J.; Oroszlan, S. *FEBS Lett.* **1991**, *280*, 344.

[41] Nishimura, J.; Narayanasami, R.; Miller, R. T.; Roman, L. J.; Panda, S.; Masters, B. S. S. *J. Biol. Chem.* **1999**, *9*, 5399.

[42] Kim, H.-K.; Tuite, E.; Nordén, B.; Ninham, B. W. *Eur. Phys. J. E* **2001**, *4*, 411.

[43] Baudain, P.; Nohime, F.; Touraud, D.; Neueder, R.; Kunz, W.; Ninham, B. W. *J. Mol. Liq.* **2006**, *123*, 14.

[44] Pashley, R. M.; McGuggian, P.; Ninham, B. W.; Brady, J.; Evans, D. F. *J. Phys. Chem.* **1986**, *90*, 1637.

[45] Lyklema, J. *Adv. Colloid Interface Sci.* **2003**, *100-102*, 1.

[46] Aveyard, R.; Saleem, S. M. *J. Chem. Soc., Faraday Trans. 1* **1976**, *72*, 1609.

[47] Weissenborn, P. K.; Pugh, R. J. *J. Colloid Interface Sci.* **1996**, *184*, 550.

[48] Maheshwari, R.; Sreeram, K. J.; Dhathathreyan, A. *Chem. Phys. Lett.* **2003**, *375*, 157.

[49] Robinson, R. A.; Harned, H. S. *Chem. Rev.* **1941**, *28*, 419.

[50] Lund, M.; Jungwirth, P.; Woodward, C. E. *Phys. Rev. Lett.* **2008**, *280*, 258105.

[51] Hippel, P. H.; Wong, K.-Y. *J. Biol. Chem.* **1965**, *240*, 3909.

[52] Batchelor, J. D.; Olteanu, A.; Tripathy, A.; Pielak, G. J. *J. Am. Chem. Soc.* **2004**, *126*, 1958.

[53] Shimizu, S.; McLaren, W. M.; Matubayashi, N. *J. Chem. Phys.* **2006**, *124*, 234905.

[54] Zhang, Y.; Cremer, P. S. *Curr. Opin. Colloid Interface Sci.* **2006**, *10*, 658.

[55] Ninham, B. W.; Yaminsky, V. *Langmuir* **1997**, *13*, 2097.

[56] Pyper, N. C.; Pike, C. G.; Edwards, P. P. *Mol. Phys.* **1992**, *76*, 353.

[57] Boström, M.; Williams, D. R. M.; Ninham, B. W. *Langmuir* **2001**, *17*, 4475.

[58] Boström, M.; Williams, D. R. M.; Ninham, B. W. *Phys. Rev. Lett.* **2001**, *87*, 168103.

[59] Boström, M.; Tavares, F. W.; Bratko, D.; Ninham, B. W. *J. Phys. Chem. B* **2005**, *109*, 24489.

[60] Boström, M.; Tavares, F. W.; Finet, S.; Skouri-Panet, F.; Tardieu, A.; Ninham, B. W. *Biophys. Chem.* **2005**, *117*, 217.

[61] Moreira, L. A.; Boström, M.; Ninham, B. W.; Biscaia, E. C.; Tavares, F. W. *Colloids Surf., A* **2006**, *282-283*, 457.

[62] Boström, M.; Deniz, V.; Franks, G. V.; Ninham, B. W. *Adv. Colloid Interface Sci.* **2006**, *123-126*, 5.

[63] Boström, M.; Deniz, V.; Ninham, B. W. *J. Phys. Chem. B* **2006**, *110*, 9645.

[64] Moreira, L. A.; Boström, M.; Ninham, B. W.; Biscaia, E. C.; Tavares, F. W. *J. Braz. Chem. Soc.* **2007**, *18*, 223.

[65] Tavares, F. W.; Bratko, D.; Blanch, H. W.; Prausnitz, J. M. *J. Phys. Chem. B* **2004**, *108*, 9228.

[66] Edwards, S. A.; Williams, D. R. M. *Curr. Opin. Colloid Interface Sci.* **2004**, *9*, 139.

[67] Collins, K. D.; Nielson, G. W.; Enderby, J. E. *Biophys. Chem.* **2007**, *128*, 95.

[68] Jungwirth, P.; Tobias, D. J. *Chem. Rev.* **2006**, *106*, 1259.

[69] Boström, M.; Kunz, W.; Ninham, B. W. *Langmuir* **2005**, *21*, 2619.

[70] Padmanabhan, V.; Daillant, J.; Belloni, L.; Mora, S.; Alba, M.; Konovalov, O. *Phys. Rev. Lett.* **2007**, *99*, 086105.

[71] Leontidis, E.; Aroti, A.; Belloni, L. *J. Phys. Chem. B* **2009**, *113*, 1447.

[72] Lund, M.; Jungwirth, P. *J. Phys.:Condens. Matter* **2008**, *20*, 494218.

[73] Harrison, J. A.; Randles, J. E. B.; Schiffrin, D. J. *J. Electroanal. Chem.* **1970**, *25*, 197.

[74] Schiffrin, D. PhD thesis, University of Birmingham, **1965**.

[75] McMillan, W. G.; Mayer, J. E. *J. Phys. Chem.* **1945**, *13*, 276.

[76] Friedman, H. L. *J. Chem. Phys.* **1982**, *76*, 1092.

[77] Forsberg, B.; Ulander, J.; Kjellander, R. *J. Chem. Phys.* **2005**, *122*, 064502.

[78] Abbas, Z.; Ahlberg, E.; Nordholm, S. *J. Phys. Chem. B* **2009**, *113*, 5905.

[79] Torrie, G. M.; Valleau, J. P. *J. Chem. Phys.* **1980**, *73*, 5807.

[80] van Megen, W.; Snook, I. *J. Chem. Phys.* **1980**, *73*, 4656.

[81] Snook, I.; van Megen, W. *J. Chem. Phys.* **1981**, *75*, 4104.

[82] Torrie, G. M.; Valleau, J. P. *J. Phys. Chem.* **1982**, *86*, 3251.

[83] Guldbrand, L.; Jönsson, B.; Wennerström, H.; Linse, P. *J. Chem. Phys.* **1984**, *80*, 2221.

[84] Kjellander, R.; Marčelja, S. *Chem. Phys. Lett.* **1984**, *112*, 49.

[85] Ramanathan, P. S.; Friedman, H. L. *J. Chem. Phys.* **1971**, *54*, 1086.

[86] Friedman, H. L.; Zebolsky, D. M.; Kalman, E. *J. Solution Chem.* **1976**, *5*, 739.

[87] Xu, H.; Friedman, H. L.; Raineri, F. O. *J. Solution Chem.* **1991**, *20*, 739.

[88] Kunz, W.; Belloni, L.; Bernard, O.; Ninham, B. W. *J. Phys. Chem. B* **2004**, *108*, 2398.

[89] Pettitt, B. M.; Rossky, P. J. *J. Chem. Phys.* **1986**, *84*, 5836.

[90] Kusalik, P. G.; Patey, G. N. *J. Chem. Phys.* **1990**, *92*, 1345.

[91] Dang, L. X.; Rice, J. E.; Kollman, P. A. *J. Chem. Phys..* **1990**, *93*, 7528.

[92] Guàrdia, E.; Rey, R.; Padró, J. A. *Chem. Phys.* **1991**, *155*, 187.

[93] Guàrdia, E.; Rey, R.; Padró, J. A. *J. Chem. Phys.* **1991**, *95*, 2823.

[94] Lyubartsev, A. P.; Laaksonen, A. *Phys. Rev. E* **1995**, *52*, 3730.

[95] Lyubartsev, A. P.; Laaksonen, A. *Phys. Rev. E* **1997**, *55*, 5689.

[96] Lyubartsev, A. P.; Marělja, S. *Phys. Rev. E* **2002**, *65*, 041202–1.

[97] Gavryushov, S.; Linse, P. *J. Chem. Phys. B* **2006**, *110*, 10878.

[98] Gavryushov, S. *J. Chem. Phys. B* **2006**, *110*, 10888.

[99] Lund, M.; Vrbka, L.; Jungwirth, P. *J. Am. Chem. Soc.* **2008**, *130*, 11582.

[100] Kjellander, R.; Lyubartsev, A. P.; Marčelja, S. *J. Chem. Phys.* **2001**, *114*, 9565.

[101] Marčelja, S. *J. Phys. Chem. B* **2006**, *110*, 13062.

[102] Hamaker, H. C. *Physica* **1937**, *4*, 1058.

[103] Wertheim, M. *Mol. Phys.* **1973**, *25*, 211.

[104] Lifshitz, E. M. *Soviet Phys. JETP* **1956**, *2*, 73.

[105] Hunter, R. *Foundations of Colloid Science;* Oxford University Press, 2001.

[106] Ninham, B. W.; Parsegian, V. A.; Weiss, G. H. *J. Statis. Phys.* **1970**, *2*, 323.

[107] Dagastine, R. R.; Prieve, D. C.; White, L. R. *J. Colloid Interface Sci.* **2000**, *231*, 351.

[108] Bauernschmitt, R.; Ahlrichs, R. *Chem. Phys. Lett.* **1996**, *256*, 454.

[109] Cossi, M.; Barone, V. *J. Chem. Phys.* **2001**, *115*, 4708.

[110] McQuarrie, D. A. *Statistical Mechanics;* University Science Books, 2000.

[111] Hansen, J.-P.; McDonald, I. R. *Theory of Simple Liquids;* Academic Press, 2006.

[112] Hansen, J.-P.; Verlet, L. *Phys. Rev.* **1969**, *184*, 151.

[113] Ornstein, L. S.; Zernike, F. *Versl. Akad. Wetenschappen* **1914**, *23*, 582.

[114] Van Leeuwen, J. M. J.; Groeneveld, J.; DeBoer, J. *Physica* **1959**, *25*, 792.

[115] Meeron, E. *J. Math. Phys.* **1960**, *1*, 192.

[116] Morita, T. *Progr. Theoret. Phys.* **1960**, *23*, 385.

[117] Rasaiah, J. C.; Card, D. N.; Valleau, J. P. *J. Chem. Phys.* **1972**, *56*, 248.

[118] Levesque, D. *Physica* **1966**, *32*, 1985.

[119] Belloni, L. *J. Chem. Phys.* **1993**, *98*, 8080.

[120] Rossky, P. J.; Dudowicz, J. B.; Tembe, B. L.; Friedman, H. L. *J. Chem. Phys.* **1980**, *73*, 3372.

[121] Carley, D. D. *J. Chem. Phys.* **1967**, *46*, 3783.

[122] Rasaiah, J. C.; Friedman, H. L. *J. Chem. Phys.* **1968**, *48*, 2742.

[123] Lovett, R.; Mou, C. Y.; Buff, F. P. *J. Chem. Phys.* **1976**, *65*, 507.

[124] Wertheim, M. *J. Chem. Phys.* **1976**, *65*, 2377.

[125] Hansen, J.-P.; Torrie, G. M.; Villefosse, P. *Phys. Rev. A* **1977**, *16*, 2153.

[126] Kjellander, R.; Marčelja, S. *J. Chem. Phys.* **1985**, *82*, 2122.

[127] Kjellander, R. *J. Chem. Phys.* **1988**, *88*, 7129.

[128] Kjellander, R. *J. Chem. Phys.* **1988**, *89*, 7649.

[129] Kjellander, R.; Åkesson, T.; Jönsson, B.; Marčelja, S. *J. Chem. Phys.* **1992**, *97*, 1424.

[130] Kjellander, R.; Greberg, H. *Mol. Phys.* **1994**, *83*, 789.

[131] Greberg, H.; Kjellander, R.; Åkesson, T. *Mol. Phys.* **1997**, *87*, 35.

[132] Greberg, H.; Kjellander, R.; Åkesson, T. *Mol. Phys.* **1997**, *92*, 35.

[133] Damaskin, B. B.; Emets, V. V. *Russ. J. Electrochem.* **2001**, *37*, 525.

[134] Gonzáles, R.; Sanz, F. *Electroanalysis* **1997**, *9*, 169.

[135] Barthel, J.; Neueder, R.; Poepke, H.; Wittmann, H. *J. Solution Chem.* **1998**, *27*, 1055.

[136] Marcus, Y. *Ion Properties;* Marcel Dekker, Inc.: New York, 1997.

[137] Malatesta, F.; Zamboni, R. *J. Solution Chem.* **1997**, *26*, 791.

[138] Rard, J. A.; Miller, D. G. *J. Chem. Eng. Data* **1981**, *26*, 33.

[139] Novotný, P.; Söhnel, O. *J. Chem. Eng. Data* **1988**, *33*, 49.

[140] Buchner, R.; Chen, T.; Hefter, G. *J. Phys. Chem. B* **2004**, *108*, 2365.

Paper I

On the effect of image charges and ion-wall dispersion forces on electric double layer interactions

Erik Wernersson and Roland Kjellander[a)]
Department of Chemistry, Göteborg University, SE-412 96 Göteborg, Sweden

(Received 2 August 2006; accepted 1 September 2006; published online 16 October 2006)

Two effects of interactions between polarizable ions and polarizable walls in electric double layers are investigated: ionic image charge forces and ion-wall dispersion forces. The first must be included for a consistent treatment of the wall-wall van der Waals (vdW) interaction, since it contains the effect of screening of the static part of the vdW interaction. The second has been suggested to give rise to ion specificity in double layer interactions. The strength of the ion-wall dispersion forces are estimated from quantum mechanical calculations of ionic polarizability and from experimental data for the dielectric functions of the media. The ion density profiles and the anisotropic ion-ion distribution functions in the double layer are calculated in the highly accurate anisotropic hypernetted chain approximation, which allows the correct treatment of the image charge forces. The double layer interactions are evaluated from these distribution functions. It is found that it is important to include both kinds of ion-wall forces. Quantitative and sometimes even qualitative differences occur in the double layer interactions depending on the ionic species of the electrolyte due to different strengths of the ion-wall dispersion interactions. © *2006 American Institute of Physics*. [DOI: 10.1063/1.2357940]

I. INTRODUCTION

It has been suggested that London-type dispersion interactions between ions and dielectric boundaries may play a role in determining the ion specificity of a range of phenomena related to charged interfaces in electrolytes.[1,2] This hypothesis has been explored in a number of recent publications; for a review see Ref. 3. In particular, the effect of including dispersion forces between ions and interfaces when calculating the potential of mean force between particles has been investigated for both the case of planar walls[4–6] and the case of macroions.[7–9] In the majority of these studies one has neglected that the static electric fields generated by the ions polarize the interfaces between walls and solvent of different dielectric constants. Thus, in such cases the dielectric constant of the walls, ϵ_{wall}, has in effect been set equal to that of the solvent, ϵ_{sol}, while in reality $\epsilon_{\mathrm{wall}} \neq \epsilon_{\mathrm{sol}}$.

The polarization at dielectric discontinuities can be treated by the method of images in, for example, the case of planar walls. We refer to the forces on the ions due to the fictitious image charges as "image forces." These forces must be included in order to obtain a consistent treatment of the van der Waals (vdW) interaction between the walls (see below). This is especially important when the high frequency vdW interactions are weak, as is the case in hydrocarbon/water systems.[10] The image forces can also give rise to other significant contributions to the mean force between colloidal particles when the ion concentration is not very high.

In one study by Boström *et al.*[4] both dispersion and image forces are included, but the latter are treated in an approximate fashion that is on the same level as Onsager-Samaras theory.[2,11] In this approach the screening of the image charges is treated in the Debye-Hückel approximation using, in effect, a screened Coulomb potential from bulk electrolyte solutions. Such an approximation introduces an inconsistency in the treatment of the problem as the postulated screening is not consistent with the ionic concentration profiles and anisotropic ion-ion correlation functions in the double layer. The proper way to include image charges for interacting double layers in planar geometry were described for the general case by Kjellander and Marčelja.[12] Their scheme has been implemented in practical calculations of ionic concentration profiles and ion-ion correlation functions of the double layer using the anisotropic hypernetted chain (AHNC) approximation.[12,13] This is a highly accurate method to calculate double layer properties and it is used in the current work. The AHNC method typically requires much less computational effort than simulations, especially if image forces are to be included. This method produces results in virtually perfect agreement with simulations,[14,15] except at high ionic concentrations, for which there are small systematic errors. The explicit consideration of the ion-ion correlations makes the AHNC method suitable for studying systems where mean field theories, such as the Poisson-Boltzmann approximation, fails to give even qualitatively correct results, as may be the case for systems with divalent ions present.[13,14,16] In this work we will, however, consider only monovalent electrolytes.

As image forces in some cases have a decisive influence on the ionic concentration profiles and the pressure between the walls, it is desirable that they are treated as accurately as possible. It has been shown for the case of uncharged surfaces in absence of ionic dispersion interactions[17] that the self-consistent inclusion of image forces in the treatment of

[a)]Electronic mail: rkj@chem.gu.se

the double layer results in the exact cancellation of the asymptotic term of the static (zero frequency) part of the vdW interaction between planar walls. Therefore, the inclusion of image forces does not only affect the double layer pressure but the vdW pressure as well. The static part of the vdW interaction is screened by the intervening electrolyte and this is contained in the effects of the image forces. This effect will be investigated in the current work.

The presence of dispersion interactions between ions in electrolytes have profound effects on the decay behavior of electrostatic interactions between the ions as function of separation, changing the exponential screening to a power law one.[18,19] In the current work we will only consider ion-wall dispersion interactions and, for simplicity, neglect such interactions between the ions. The latter is expected to be of secondary importance, at least for the system studied here. Thus the electrostatic ion-ion interactions in the electrolyte will be exponentially screened, but the ion-wall dispersion forces will affect the decay of the ion concentration profiles between the walls and indirectly the ion-ion correlation functions. We will see that these dispersion forces give rise to important differences depending on, for example, if the most polarizable ions (e.g., bromide compared to sodium ions in sodium bromide) are counterions or coions of the charged surfaces.

The current primitive model approach does not allow for effects due to the structure of the solvent at the interface. Any ion specificity arising from such effects is therefore missed in the calculations presented below, making the relative importance of these compared to effects due to dispersion forces difficult to assess. Currently, the only reliable methods available for studying solvent-structure dependent ion specificity are laborious simulations. Recent examples of such are found in Refs. 20 and 21.

The outline of the paper is as follows. First the system is described and the interaction potentials are defined. This is followed by an explicit estimation of the strength of the ion-wall dispersion interaction using quantum mechanical calculations. Then the various contributions to the interaction pressure between two planar walls are specified. The calculated wall-wall interaction pressure and ion density profiles are then presented and the results of the paper are discussed.

II. THEORY

A. Model

The system considered is a simple binary electrolyte solution sandwiched between two walls separated by a distance D. The walls are modeled as semi-infinite dielectric slabs with dielectric properties different from those of the solvent. The electrolyte between the walls is assumed to be in thermodynamic equilibrium with a bulk electrolyte solution of concentration $0.5M$. We select a coordinate system with the z axis perpendicular and the x and y axes parallel to the surfaces. The origin is placed at the midplane between the walls. We use the notation $\mathbf{r}=(x,y,z)$.

The pair potential $u_{ij}(\mathbf{r},\mathbf{r}')$ between an ion of species i at coordinate $\mathbf{r}$ and an ion of species j at $\mathbf{r}'$ consists of three contributions,

$$u_{ij}=u_{ij}^{\mathrm{core}}+u_{ij}^{\mathrm{Coul}}+u_{ij}^{\mathrm{im}}, \tag{1}$$

where u_{ij}^{core} is the hard core potential for ions of diameter a, i.e., $u_{ij}^{\mathrm{core}}(\mathbf{r},\mathbf{r}')=\infty$ if $|\mathbf{r}-\mathbf{r}'|<a$ and 0 otherwise, and where

$$u_{ij}^{\mathrm{Coul}}(\mathbf{r},\mathbf{r}')=\frac{q_iq_j}{4\pi\epsilon_{\mathrm{sol}}\epsilon_0|\mathbf{r}-\mathbf{r}'|}, \tag{2}$$

q_i and q_j are the ionic charges, ϵ_{sol} is the dielectric constant of the solvent, and ϵ_0 is the permittivity of vacuum. The contribution u_{ij}^{im} in Eq. (1) is the potential due to image charges, which arises from the presence of the dielectric discontinuities at the two walls. It is a function of the distances of the ions to the surfaces. Due to the planar symmetry we can write its coordinate dependence as $u_{ij}^{\mathrm{im}}(\mathbf{r},\mathbf{r}')=u_{ij}^{\mathrm{im}}(R,z,z'|D)$, where $R=[(x-x')^2+(y-y')^2]^{1/2}$ is the lateral distance and where we have explicitly indicated in the right hand side (rhs) that u_{ij}^{im} depends on the distance D between the wall surfaces. In Fourier space this potential can be written as[12]

$$\hat{u}_{ij}^{\mathrm{im}}(k,z,z'|D)=\frac{q_iq_j}{\epsilon_{\mathrm{sol}}\epsilon_0 k}\left[\frac{\epsilon_D}{e^{kD}-\epsilon_D}\cosh(kz)\cosh(kz')+\frac{\epsilon_D}{e^{kD}+\epsilon_D}\sinh(kz)\sinh(kz')\right], \tag{3}$$

where

$$\epsilon_D=\frac{\epsilon_{\mathrm{sol}}-\epsilon_{\mathrm{wall}}}{\epsilon_{\mathrm{sol}}+\epsilon_{\mathrm{wall}}} \tag{4}$$

and ϵ_{wall} is the dielectric constant of the wall. The notation $\hat{f}(k)$ is used here for the two-dimensional Fourier transform (Hankel transform) of a function $f(R)$. (In real space u_{ij}^{im} is an infinite sum of Coulombic terms due to the presence of multiple image charges from both surfaces.)

The ions are assumed to interact with the walls via dispersion forces as well as hard core exclusion and electrostatic forces. The ion-wall interaction potential $\nu_i(z|D)$ for an ion of species i then consists of four contributions,

$$\nu_i=\nu_i^{\mathrm{core}}+\nu_i^{\mathrm{Coul}}+\nu_i^{\mathrm{im}}+\nu_i^{\mathrm{disp}}, \tag{5}$$

where ν_i^{core} is the ion-wall hard core potential, which is infinite if $|z|>(D-a)/2$ and 0 otherwise, and where ν_i^{Coul} is the electrostatic interaction between an ion and a uniform surface charge density σ on each wall. Since the surface charge densities of the two walls are equal, ν_i^{Coul} is constant in the slit between the surfaces and does not give rise to any forces on the ions there. The contribution ν_i^{im} in Eq. (5) arises due to an ion interacting with its own image charges and is given by

$$\nu_i^{\mathrm{im}}(z|D)=u_{ii}^{\mathrm{im}}(0,z,z|D). \tag{6}$$

The potential for the ion-wall dispersion interactions is set to

$$\nu_i^{\mathrm{disp}}(z|D)=B_i\left(\frac{1}{(z+D/2)^3}+\frac{1}{|z-D/2|^3}\right), \tag{7}$$

where the coefficient B_i is a parameter controlling the strength of the dispersion forces and is defined in Eq. (8) below. It should be remarked that Eq. (7) is only approxi-

mately valid because it only contains the leading contribution from each wall (see below) and, furthermore, it fails to account for wall-ion-wall three-body interactions.

In this work both ion species are assumed to be monovalent, i.e., $q_+=-q_-=e_0$, where e_0 is the elementary charge, and have the same diameter $a=4.6$ Å. The static dielectric constant of the solvent, ϵ_{sol}, is taken to be 78.36, corresponding to that of water at 25 °C and for ϵ_{wall} we use the value 2.54, the static dielectric constant of polystyrene.[22]

B. Estimation of wall-ion dispersion forces

The potential for the dispersion interaction between an ion of species i and a single dielectric discontinuity a distance d away is given by[2]

$$V_i^{\mathrm{disp}}(d) = -\frac{\hbar}{(4\pi)^2\epsilon_0 d^3}\int_0^\infty d\omega \frac{\alpha_i^*(i\omega)}{\epsilon_{\mathrm{sol}}(i\omega)}\epsilon_D(i\omega) = \frac{B_i}{d^3}, \qquad (8)$$

where α_i^* is the excess polarizability of an ion of species i (i.e., the difference in polarizability between an ion surrounded by a solvent and pure solvent) and $\epsilon_D(i\omega)$ has the same meaning as ϵ_D in Eq. (4) except that it is evaluated at the imaginary frequency $i\omega$. The physical interpretation of expression (8) is that it represents the free energy of interaction between a fluctuating point dipole and its dielectric image. This constitutes the leading contribution for large d of the ion-wall dispersion interaction. In reality the distance dependence for small d is more complicated than that of Eq. (8). The singularity of $V_i^{\mathrm{disp}}(d)$ at the wall surface ($d=0$) is unphysical and arises as a consequence of regarding the ions as point-polarizable objects. In our application of Eq. (8) the singularity is never encountered since the ionic size is considered. In Eq. (7) we have $\nu_i^{\mathrm{disp}}(z|D)=V_i^{\mathrm{disp}}(z+D/2)+V_i^{\mathrm{disp}}(|z-D/2|)$, and in practice $|z|\leqslant(D-a)/2$ due to the ion-wall core interactions included in Eq. (5).

The material of the wall is taken to be polystyrene and the representations of the dielectric functions for water and polystyrene, in tabular form for imaginary ω values, were taken from Dagastine *et al.*[23] In order to obtain a reliable estimate of the order of magnitude of B_i in Eq. (8) we chose iodide as a "prototype" for highly polarizable ions. The polarizability of iodide was calculated from the following sum-of-states formula:[10]

$$\alpha(\omega) = \frac{e_0^2}{4\pi\epsilon_0 m_e}\sum_l \frac{f_{0,l}}{\omega_{0,l}^2-\omega^2}, \qquad (9)$$

where m_e is the electron mass, $\omega_{0,l}$ is the frequency, and $f_{0,l}$ is the oscillator strength of the transition from state 0 (the ground state) to state l. These quantities can readily be calculated using time-dependent Kohn-Sham density functional theory (TD-DFT).[24,25]

The calculations were preformed with the GAUSSIAN03 (Ref. 26) package using the B3LYP exchange-correlation functional[27,28] and Dunning's augmented quadruple zeta correlation consistent basis sets[29] (aug-cc-pVQZ) with a relativistic effective core potential.[30] The effects of solvent were included by placing the ion in a cavity in a dielectric continuum and including the reaction field in the Kohn-Sham Hamiltonian using the method of Miertuš *et al.*[31] as implemented in GAUSSIAN03. The default values of 2.250 Å for the cavity radius and 1.776 for the optic dielectric constant of water were used. No attempts were made to include any hydrating water molecules explicitly.

The value that was obtained for the static polarizability, $\alpha(0)$, of iodide in water is 58.7 a.u., to be compared with the experimental value of 50.0 a.u.[32] A numerical evaluation of the integral in Eq. (8) using $\alpha(i\omega)$ as given by Eq. (9) (the bare polarizability) instead of the excess polarizability gave the value -40.2 kJ Å^3 mol^{-1} of B_- for iodide. Considering that the effects of the displacement of water by the ion were neglected and the fact that the static polarizability was overestimated by about one sixth, this number is likely to be an overestimate. This led us to choose B_- values in the range between 0 and -40 kJ Å^3 mol^{-1} for our model anions. We expect that these values are within the range of the typical values of B_- for highly polarizable anions. This view is supported by the fact that values of similar magnitude were obtained by Tavares *et al.*[8] for a range of anions in a similar system using different approximations for $\epsilon_{\mathrm{wall}}(i\omega)$, $\epsilon_{\mathrm{sol}}(i\omega)$, and $\alpha(i\omega)$.

In light of the fact that cations are generally much less polarizable than anions[32] and in order to keep the model simple, B_+ was set to zero in all calculations. We emphasize that we are not aiming to make predictions referring to any particular kind of salt, but rather to investigate the properties of the model presented above for a set of parameters of realistic order of magnitude.

It is somewhat problematic to use the asymptotic form given by Eq. (8) of the potential for the dispersion forces for all separations since it strongly overestimates the interaction for $d\approx 0$ and necessitates the use of a cutoff distance for small d, the exact choice of which may have a large influence on the results. It may therefore be the case that the short-range effects of dispersion forces are exaggerated in the calculations of this paper. Furthermore, it appears likely that a realistic ion-wall potential would also contain contributions of other physical origin, that for short distances may well dominate the contribution due to dispersion forces even for highly polarizable ions.

C. Evaluation of the wall-wall interaction pressure

The net interaction pressure between the walls is the difference between the force per unit area in the slit between the two surfaces, P[slit], and the bulk pressure, P[bulk],

$$P^{\mathrm{net}} = P[\mathrm{slit}] - P[\mathrm{bulk}]. \qquad (10)$$

When the distance D between the walls goes to infinity, $P[\mathrm{slit}]\to P[\mathrm{bulk}]$ and $P^{\mathrm{net}}\to 0$.

The total pressure in the slit is the sum of a contribution from the ions, P^{ion} [defined below in Eq. (14)], and the vdW interaction between the walls

$$P = P^{\mathrm{ion}} + P_{\mathrm{vdW}}^{\mathrm{wall}}. \qquad (11)$$

We have

$$P_{\mathrm{vdW}}^{\mathrm{wall}} = -\frac{A}{6\pi D^3}, \tag{12}$$

where A is the Hamaker constant for the two walls interacting across pure solvent. A can be obtained from Lifshitz theory[10,33] as

$$A = \frac{3k_BT}{2}\sum_{l=0}^{\infty}{}'\sum_{s=1}^{\infty}\frac{\epsilon_D^{2s}(i\omega_l)}{s^3}, \tag{13}$$

where k_B is Boltzmann's constant, T the absolute temperature, the prime on the sum over l indicates that the term corresponding to $l=0$ is to be weighted by one half, and ϵ_D has the same meaning as in Eq. (4) except that it is evaluated at imaginary frequency $i\omega_l$, where $\omega_l = l2\pi k_BT/\hbar$.

We will distinguish the static (zero frequency) part of the vdW interaction from the rest. The former originates from the $l=0$ contribution in Eq. (13) which we will denote as A_0. Note that A_0 contains only the static dielectric constants of the solvent and the walls, the same quantities that determines the magnitude of the image forces [cf. Eq. (3)]. The zero frequency part in Eq. (12) is $P_{\mathrm{vdW}(0)}^{\mathrm{wall}} = -A_0/(6\pi D^3)$. It has a special role in what follows. The high frequency contributions to $P_{\mathrm{vdW}}^{\mathrm{wall}}$ [from the terms with $l>0$ in Eq. (13)] will be denoted as $P_{\mathrm{vdW(hf)}}^{\mathrm{wall}}$.

The pressure due to the ions, P^{ion}, can be decomposed into well defined components,

$$P^{\mathrm{ion}} = P_{\mathrm{kin}}^{\mathrm{ion}} + P_{\mathrm{Coul}}^{\mathrm{ion}} + P_{\mathrm{core}}^{\mathrm{ion}} + P_{\mathrm{im}}^{\mathrm{ion}} + P_{\mathrm{disp}}^{\mathrm{ion}}, \tag{14}$$

the explicit expressions for which are given below. P^{ion} can be evaluated at any plane in the slit between the surfaces (its value is independent of this choice). In the current work it is evaluated at the midplane (at $z=0$) from the ion density profiles, $n_i(z)$, and ion-ion pair distribution functions, $g_{ij}(\mathbf{r},\mathbf{r}')$, in the slit. The planar symmetry of the system allows us to write $g_{ij}(\mathbf{r},\mathbf{r}') = g_{ij}(R,z,z')$. The total correlation function is defined as $h_{ij} = g_{ij} - 1$.

In Eq. (14), $P_{\mathrm{kin}}^{\mathrm{ion}}$ is the pressure due to the thermal motion of the ions, i.e., the momentum transfer across the plane where the pressure is evaluated. It is proportional to the total ion concentration there. At the midplane we have $P_{\mathrm{kin}}^{\mathrm{ion}} = k_BT\Sigma_i n_i(0)$. In the bulk $P_{\mathrm{kin}}^{\mathrm{ion}} = k_BT\Sigma_i n_i^b$, where n_i^b is the bulk concentration.

$P_{\mathrm{Coul}}^{\mathrm{ion}}$ is the pressure contribution from electrostatic interactions due to ion-ion correlations across the midplane and we have

$$P_{\mathrm{Coul}}^{\mathrm{ion}} = -\sum_{i,j}\int_0^{D/2} dz \int_{-D/2}^{0} dz' \int d\mathbf{R} n_i(z) n_j(z') \times h_{ij}(R,z,z')\frac{\partial u_{ij}^{\mathrm{Coul}}(R,z,z')}{\partial z}. \tag{15}$$

The corresponding contribution to the bulk pressure is $-\Sigma_{i,j}\int_{r=a}^{r=\infty} d\mathbf{r} n_i^b n_j^b r h_{ij}^b(r)[du_{ij}^{\mathrm{Coul}}(r)/dr]/6$, where h_{ij}^b is the total correlation function in bulk.

$P_{\mathrm{core}}^{\mathrm{ion}}$ is the pressure contribution from core-core collisions of the ions across the midplane and we have

$$P_{\mathrm{core}}^{\mathrm{ion}} = 2\pi k_BT\sum_{i,j}\int_0^a dz \int_{z-a}^{0} dz' n_i(z) n_j(z')(z-z') \times g_{ij}([a^2-(z-z')^2]^{1/2},z,z'). \tag{16}$$

The corresponding pressure contribution in bulk is $2\pi a^3 k_BT\Sigma_{i,j} n_i^b n_j^b g_{ij}^b(a)/3$, where $g_{ij}^b(a)$ is the core-core contact value of the pair distribution function in bulk.

$P_{\mathrm{im}}^{\mathrm{ion}}$ contains all contributions to the pressure due to image forces,[13]

$$\begin{aligned} P_{\mathrm{im}}^{\mathrm{ion}} = &-2\pi\sum_{i,j}\int_0^{D/2} dz \int_{-D/2}^{D/2} dz' \int_0^{\infty} dk\, n_i(z) n_j(z') \\ &\times \hat{h}_{ij}(k,z,z')k\frac{\partial \hat{u}_{ij}^{\mathrm{im}}(k,z,z'|D)}{\partial z} \\ &-\pi\sum_{i,j}\int_{-D/2}^{D/2} dz \int_{-D/2}^{D/2} dz' \int_0^{\infty} dk\, n_i(z) n_j(z')\hat{h}_{ij}(k,z,z')k \\ &\times \frac{\partial \hat{u}_{ij}^{\mathrm{im}}(k,z,z'|D)}{\partial D} - \frac{1}{2}\sum_i \int_0^{D/2} dz\, n_i(z)\frac{\partial \nu_i^{\mathrm{im}}(z|D)}{\partial z} \\ &-\frac{1}{2}\sum_i \int_{-D/2}^{D/2} dz\, n_i(z)\frac{\partial \nu_i^{\mathrm{im}}(z|D)}{\partial D}. \end{aligned} \tag{17}$$

In bulk there is, of course, no such contribution.

$P_{\mathrm{disp}}^{\mathrm{ion}}$ is the pressure component arising from direct dispersion interactions between ions and walls and is given by

$$\begin{aligned} P_{\mathrm{disp}}^{\mathrm{ion}} = &-\sum_i \int_0^{D/2} dz\, n_i(z)\frac{\partial V_i^{\mathrm{disp}}(z+D/2)}{\partial z} \\ &+\sum_i \int_{-D/2}^{0} dz\, n_i(z)\frac{\partial V_i^{\mathrm{disp}}(|z-D/2|)}{\partial z}. \end{aligned} \tag{18}$$

Each term in the rhs gives the dispersion interaction between the ions on one side of the midplane and the wall on the opposite side. There is no $P_{\mathrm{disp}}^{\mathrm{ion}}$ contribution in bulk.

The zero frequency contribution to the wall-wall vdW interaction pressure, $P_{\mathrm{vdW}(0)}^{\mathrm{wall}}$, is canceled identically for large D by the image force contributions in P^{ion}.[17] The physical result is that $P_{\mathrm{vdW}(0)}^{\mathrm{wall}}$ is screened by the electrolyte in the slit.[34] The high frequency contribution, $P_{\mathrm{vdW(hf)}}^{\mathrm{wall}}$, is, on the other hand, unaffected by the presence of the ions in the slit since they move too slowly to correlate with the rapid quantum fluctuations that give rise to this dispersion force contribution.

In this work the ion density profiles and ion-ion pair distribution functions in the slit were calculated using the AHNC approximation[12] and P[slit] was then obtained from the equations above. P[bulk] was likewise obtained from the pair distribution functions of the bulk phase in the HNC approximation.

Note that in the Poisson-Boltzmann approximation the net kinetic pressure, $\Delta P_{\mathrm{kin}}^{\mathrm{ion}} = k_BT\Sigma_i[n_i(0)-n_i^b]$, and $P_{\mathrm{disp}}^{\mathrm{ion}}$ are the only contributions to P^{ion} that are nonzero.

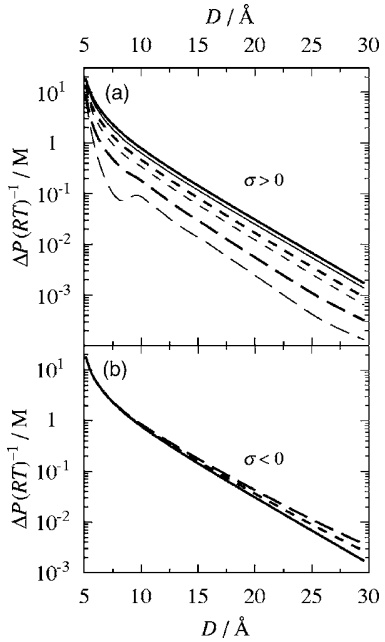

FIG. 1. The net pressure, $\Delta P = P[\text{slit}] - P[\text{bulk}]$, as function of surface separation D between two planar walls with surface charge densities $\sigma = 0.0449$ (upper panel) and -0.0449 C m^{-2} (lower panel), except that the high frequency part of the van der Waals (vdW) wall-wall interaction pressure, $P^{\text{wall}}_{\text{vdW(hf)}}$, is not included. The pressure is plotted as $\Delta P/RT$, where R is the gas constant, in molar units. The electrolyte is a $0.5M$ aqueous solution of monovalent ions with equal diameters $a = 4.6$ Å. The anions have dispersion interactions with the walls of strength $B_- = 0$ (solid lines), -20 (short dashes), and -40 kJ Å^3 mol^{-1} (long dashes), while $B_+ = 0$ throughout. The thick lines show results in the presence of image charge forces. In the upper panel results are shown from the corresponding calculation where image forces are neglected (thin lines). In the lower panel such curves are not shown for clarity, since they lie only slightly below the present curves.

III. RESULTS AND DISCUSSION

AHNC calculations were carried out for a range of wall-wall separations D between 5.1 and 29.6 Å for walls with either positive or negative surface charges in the presence or absence of image forces (in the latter case with $\epsilon_{\text{wall}} = \epsilon_{\text{sol}} = 78.36$). The absolute value of the surface charge was $|\sigma| = 0.0449$ C m^{-2} unless otherwise specified. Three values for B_- were considered: -40, -20, and 0 kJ Å^3 mol^{-1}. Note that the minimal value of D is 4.6 Å, which corresponds to a layer of counterions between the charged surfaces. The principal results of the calculations are presented in Fig. 1, which shows the net pressure between the walls, except that the high frequency vdW pressure, $P^{\text{wall}}_{\text{vdW(hf)}}$, is not included (the latter is the same for all cases shown). The zero frequency part, $P^{\text{wall}}_{\text{vdW(0)}}$, is, however, included for the cases with image forces. When the dielectric discontinuities at the surfaces are neglected, i.e., in absence of image forces, $P^{\text{wall}}_{\text{vdW(0)}}$ is zero since $\epsilon_D = 0$ at zero frequency in these cases. If $P^{\text{wall}}_{\text{vdW(0)}}$ were to be calculated from the actual dielectric constant of the wall material in the latter cases, the model would be inconsistent when image forces are neglected.

There is a dramatic difference between the cases of positive and negative surface charge where the polarizable anions are counterions and coions, respectively. For positive surfaces, the inclusion of dispersion forces significantly decreases the pressure for all separations considered. In the case of negative surfaces the pressure is *increased* at larger separations and remains largely unaffected at small separations when dispersion forces are included. This is the same trend that was recently observed by Boström *et al.*,[5] who treated a similar model within the Poisson-Boltzmann approximation. In their model image forces were neglected but regulation of surface charge at constant pH was taken into account.

As seen in Fig. 1, the absence or presence of image forces can make an important difference. To neglect them makes the pressure less repulsive in all cases, but their relative importance is much greater in the case of positive surfaces with strong ion-wall dispersion interactions than otherwise. In the case of negative surfaces, Fig. 1(b), the neglect of image forces causes only a slight shift downwards of the curves (not shown).

The total net pressure, P^{net} defined in Eq. (10), is obtained by adding the high frequency part of the vdW interaction to the results in Fig. 1. For the polystyrene/water system, which we use as an example of a hydrocarbon/water system, $P^{\text{wall}}_{\text{vdW(hf)}}$ is less than twice the value of $P^{\text{wall}}_{\text{vdW(0)}}$. The high frequency part is often the dominant contribution to the vdW interaction, but in hydrocarbon/water system the zero frequency part is usually of the same order of magnitude as the high frequency part. This is due to the fact that the dielectric properties of water and most hydrocarbons are similar in the UV region of the frequency spectrum[10] while their static dielectric constants differ greatly.

P^{net} is plotted in Fig. 2, which also shows the pressure in absence of various parts of the wall-wall vdW pressure. We first turn our attention to the thick curves in each subfigure [Figs. 2(a)–2(c) (cases with image forces)]. P^{net} turns attractive for large D (see the inserts). This net attraction is due to the high frequency part of the van der Waals attraction, $P^{\text{wall}}_{\text{vdW(hf)}}$, but not the zero frequency part, which is canceled in the net pressure. This can be seen from the fact that the pressure plotted in Fig. 1, which does not contain $P^{\text{wall}}_{\text{vdW(hf)}}$, is entirely repulsive for all of these cases (also plotted as dashed curves in Fig. 2). The cancellation of $P^{\text{wall}}_{\text{vdW(0)}}$, is illustrated by the upper two curves in Fig. 2. The top curve shows $\Delta P^{\text{ion}} = P^{\text{ion}}[\text{slit}] - P^{\text{ion}}[\text{bulk}]$. The second top curve (dashed) equals $\Delta P^{\text{ion}} + P^{\text{wall}}_{\text{vdW(0)}}$. The latter curve is closer to zero and decays faster than ΔP^{ion} in the range shown, despite that it contains $P^{\text{wall}}_{\text{vdW(0)}}$. This is an effect of the cancellation.

The cases without image forces (thin curves) further illustrate this cancellation when compared to the other curves in Fig. 2. The two dashed curves in each subfigure nearly merge with each other when D is increased; despite that the case without image forces shows ΔP^{ion} and the other shows $\Delta P^{\text{ion}} + P^{\text{wall}}_{\text{vdW(0)}}$, i.e., the former does not contain any zero frequency vdW contribution. On the other hand, ΔP^{ion} in the presence of image forces (dashed-dotted line) and ΔP^{ion} in their absence (thin dashed line) differ considerably from each other.

That the neglect of image forces can give a qualitatively wrong result is seen in Fig. 2(a) where P^{net} for the case

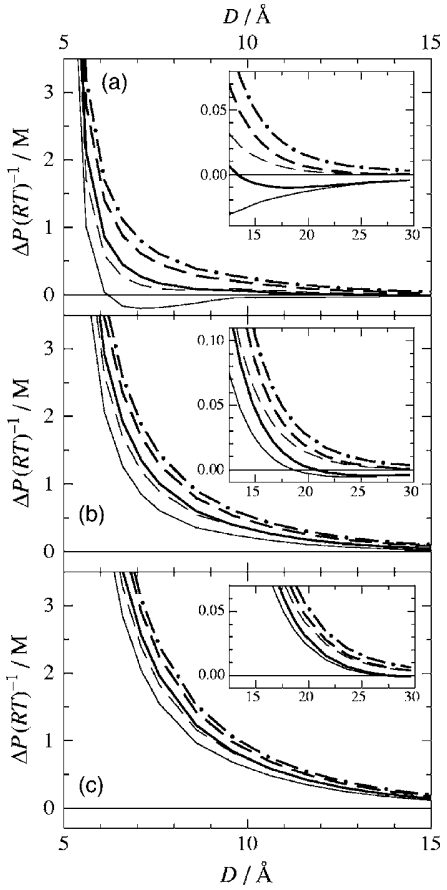

FIG. 2. The total net pressure (full lines) between the walls as a function of D for some of the systems in Fig. 1: (a) $\sigma>0$ and $B_-=-40$ kJ Å^3 mol^{-1}; (b) $\sigma>0$ and $B_-=-20$ kJ Å^3 mol^{-1}; (c) $\sigma<0$ and $B_-=-40$ kJ Å^3 mol^{-1}. The thick lines show the results for systems with image forces (the normal case), while the thin lines show the results in their absence. The dashed-dotted thick curves show ΔP^{ion}, i.e., the net pressure due to only the ions (without any vdW wall-wall interaction pressure). The dashed curves show the net pressure without $P^{\text{wall}}_{\text{vdW(hf)}}$, i.e., the same as the curves in Fig. 1. For the case with image forces this equals $\Delta P^{\text{ion}}+P^{\text{wall}}_{\text{vdW(0)}}$, where the last term is the zero frequency part of the vdW pressure. The latter term is, however, not included when image forces are absent. The inserts show magnified views of the plots for large D.

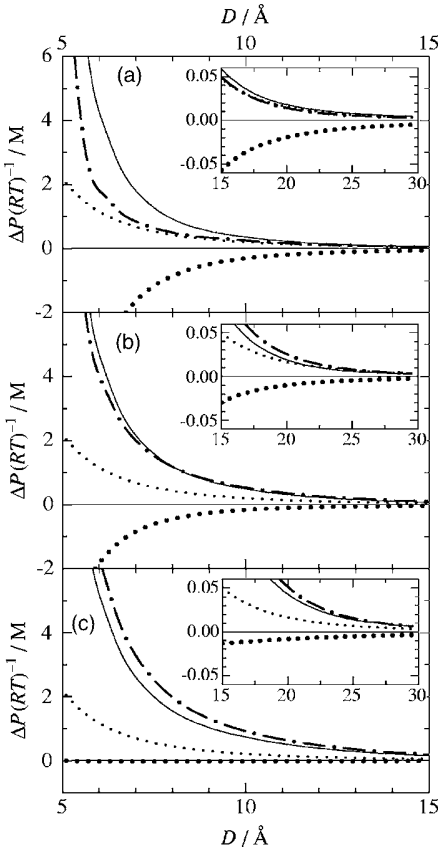

FIG. 3. The net pressure due to ions, ΔP^{ion}, and some of its components defined in Eq. (14) as a function of D for the same systems as in Fig. 2 in the presence of image forces [panels (a), (b), and (c) show the same cases in both figures]. The dashed-dotted curve in each panel represent ΔP^{ion} (the same curve as in Fig. 2), the full curve shows the sum $\Delta P^{\text{ion}}_{\text{kin}}+\Delta P^{\text{ion}}_{\text{Coul}}+\Delta P^{\text{ion}}_{\text{core}}$, the upper dotted curve (small dots) is $P^{\text{ion}}_{\text{im}}$, and the lower dotted curve (large dots) is $P^{\text{ion}}_{\text{disp}}$. The inserts show magnified views of the plots for large D.

without image forces is attractive for intermediate D values, while P^{net} is repulsive there in their presence. If one would include the zero frequency contribution to the vdW pressure as calculated from the dielectric constant of the wall material but neglect image forces, one would have an inconsistent model which would give an artificially large attractive pressure, even larger than in Fig. 2(a). We accordingly conclude that it is very important to have a consistent treatment with the image forces present, at least for cases where $P^{\text{ion}}_{\text{im}}$ constitutes a significant part of the total pressure [as is the case shown in Fig. 2(a), c.f. Fig. 3(a)].

Let us now further examine the case with image forces included. The reasons for the difference between positively and negatively charged surfaces in Fig. 1 can be analyzed by investigating the various pressure components in Eq. (14). Figure 3 shows ΔP^{ion} together with its components $P^{\text{ion}}_{\text{im}}$, $P^{\text{ion}}_{\text{disp}}$, and the sum $\Delta P^{\text{ion}}_{\text{kin}}+\Delta P^{\text{ion}}_{\text{Coul}}+\Delta P^{\text{ion}}_{\text{core}}$ (the former two components have no Δ symbol since they are zero in bulk). In the latter sum the two last contributions are smaller than $\Delta P^{\text{ion}}_{\text{kin}}$ and are about the same in the three cases shown. The kinetic contribution dominates in the sum and it increases somewhat for intermediate D values when going from Fig. 3(a) to Fig. 3(b) and then to Fig. 3(c). This is caused by an increase in total ionic concentration at the midplane. Furthermore, we see that $P^{\text{ion}}_{\text{im}}$ is virtually the same in all three cases.

By comparing Figs. 3(a) and 3(c), which differ only in the sign of the surface charge, we see that the main difference in pressure is due to $P^{\text{ion}}_{\text{disp}}$, which is very small for negative surface charges. The change in $\Delta P^{\text{ion}}_{\text{kin}}$ acts in the same direction and contributes to the increase in ΔP^{ion} when changing the surface charge from positive to negative.

ΔP^{ion} is strongly dependent on the value of B_- when the surface charge is positive since $P^{\text{ion}}_{\text{disp}}$ is large in this case. This is the main reason why ΔP in Fig. 1(a) varies substantially when B_- is changed. The magnitude of $P^{\text{ion}}_{\text{disp}}$ increases faster than linearly with B_- when the latter turns more negative. This is due to the fact that the concentration of negative ions between the walls increases when B_- turns more negative, especially in the region close to the walls (see below). The change in $\Delta P^{\text{ion}}_{\text{kin}}$ also contributes in the same direction as $P^{\text{ion}}_{\text{disp}}$, although to a lesser extent.

When the surface charge is negative ΔP^{ion} is nearly un-

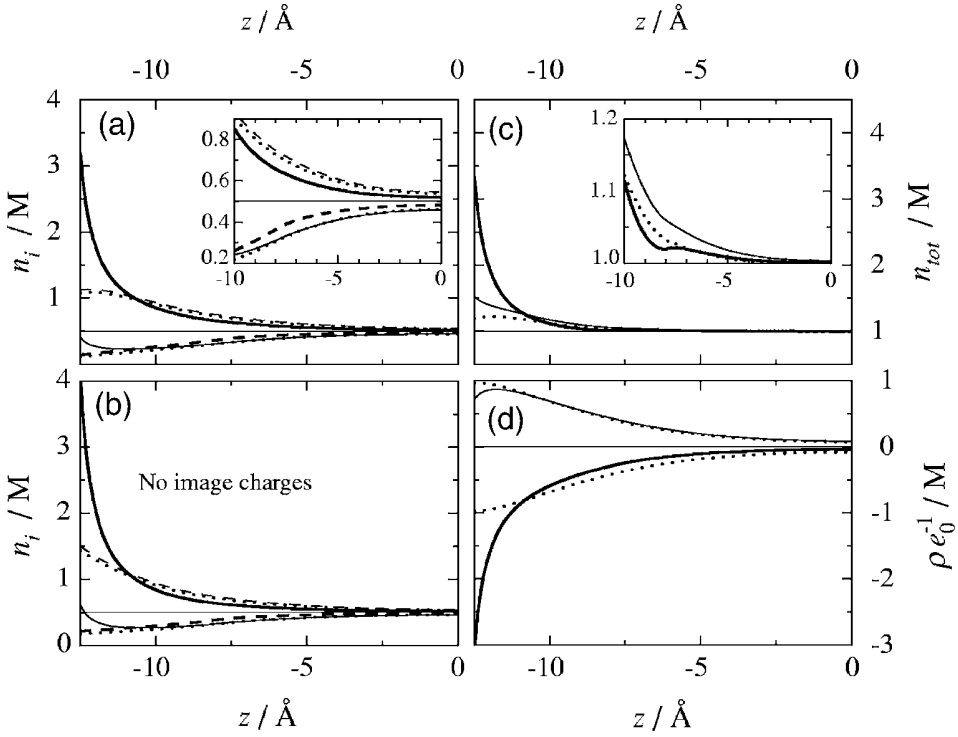

FIG. 4. Number density and charge density profiles in the slit between two walls as functions of coordinate z perpendicular to the surfaces. Only half of each profile is shown; the coordinate $z=0$ denotes the midplane between the walls. The surface separation is $D=29.6$ Å and for $z=\pm 12.5$ Å the ions are in contact with one of the wall surfaces. The dotted curves show the profiles in the absence of ion-wall dispersion interactions, $B_-=0$, while the other curves show cases with $B_-=-40$ kJ Å^3 mol^{-1} [for the latter curves the systems are as in Figs. 2(a) and 2(c)]. Thick curves denote $\sigma>0$ and thin curves $\sigma<0$. (a) Ion density profiles $n_i(z)$ for negative ions (full lines) and positive ions (dashed lines). (b) The same as in (a) but in the absence of image forces. (c) Total number density profiles, $n_{\text{tot}}(z)=n_+(z)+n_-(z)$. (d) Charge density profiles, $\rho(z)=q_+n_+(z)+q_-n_-(z)$, plotted as $\rho(z)/e_0$, where e_0 is the elementary charge. Each insert shows a magnified view of the respective plot near the middle of the slit.

affected by B_- since $P_{\text{disp}}^{\text{ion}}$ is small. In fact, the curves for the case with $B_-=-20$ kJ Å^3 mol^{-1} and negative surface charge (not shown) are virtually the same as Fig. 3(c). The only notable difference is that $\Delta P_{\text{kin}}^{\text{ion}}$ increases slightly when B_- becomes more negative in this case, which is the reason for the differences between the ΔP curves in Fig. 1(b). The reason why $P_{\text{disp}}^{\text{ion}}$ is small for negative surfaces is that the polarizable coions are almost completely expelled electrostatically from the space between the walls for small D. This effect becomes less pronounced when D increases, but even for the largest separation considered $P_{\text{disp}}^{\text{ion}}$ is small compared to the corresponding case with positive surface charge.

Let us now investigate the reasons for these behaviors of $P_{\text{disp}}^{\text{ion}}$ and $\Delta P_{\text{kin}}^{\text{ion}}$. In Fig. 4 density profiles are shown for various cases when $D=29.6$ Å. The profiles in absence of ion-wall dispersion interactions, $B_-=0$ (dotted curves), are compared with the profiles when $B_-=-40$ kJ Å^3 mol^{-1}. We will first focus on the latter.

For the case of positive surface charge (thick curves) there is a large increase in counterion concentration near the surface; see Fig. 4(a). This is hardly surprising as both electrostatic and dispersion forces attract counterions to the surface in this case. The coion profile is not much changed compared to the $B_-=0$ case, but both the counterion and coion densities are closer to zero in the middle of the slit (near $z=0$) when $B_-=-40$ kJ Å^3 mol^{-1}. This is particularly clear in the insert to Fig. 4(a). As a consequence the charge density profile, Fig. 4(d) (thick curve) has large negative values in the region very close to the surface and is rather close to zero in the middle. The small value in the middle compared to the $B_-=0$ case (bottom dotted curve) is a consequence of charge neutrality. The integral of the charge density is constant, independent of the value of B_-, so if the charge density increases in one place it has to decrease somewhere else. Thus it appears justified to claim that a major effect of including dispersion forces is to contract the double layer, thus increasing the electrostatic screening of the surface.

The total number density, Fig. 4(c) (thick curve), is large close to the surface but is somewhat smaller than for the $B_-=0$ case around $z\approx -10$ to -7 Å. The total number of ions in the slit has increased due to the ion-wall dispersion interactions, which attracts the negative ions into the slit while the positive ones follow because of electroneutrality.

For the case of negative surfaces (thin curves) in Fig. 4, we note that although the inclusion of dispersion forces causes a significant increase in the total number density, the charge density is not as strongly affected [see Figs. 4(c) and 4(d)]. An increase in density of the coions near the surface due to the dispersion attraction is seen in Fig. 4(a). This increase must, as before, be followed by an increase in counterion density somewhere due to electroneutrality. The net result is an increased total number density of ions between the walls, explaining the fact that a more negative value for B_- results in a larger $\Delta P_{\text{kin}}^{\text{ion}}$ and hence stronger repulsion for negative surfaces.

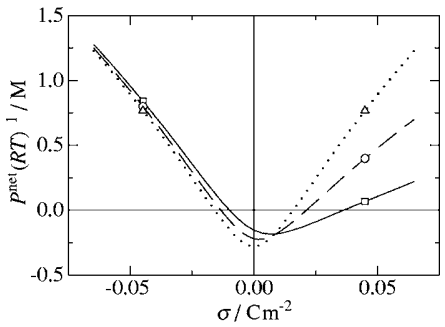

FIG. 5. The total net pressure between the walls at separation $D=9.6$ Å as a function of surface charge density σ for $B_-=0$ (dotted line), −20 (dashed line), and −40 kJ Å^3 mol^{-1} (full line). The systems are otherwise the same as in Fig. 1 (image forces are included). The cases with $\sigma=\pm0.0449$ C m^{-2} are indicated by symbols (they correspond to the cases studied in the other figures).

Let us turn to the effect of image forces. Since these are repulsive, both coion and counterion concentrations close to the surfaces are smaller in Fig. 4(a) than in Fig. 4(b). The density profiles are, however, almost unaffected by the image forces beyond about 5 Å from the surface. The image forces partially counteract the dispersion forces that draw anions into the region near each surface. The neglect of image forces therefore leads to an overestimation of the effects of dispersion forces on the concentration profiles.

The changes in profiles as well as pair correlation functions affect the various pressure components in Eq. (14). However, if we in Fig. 3 would plot $P_{\text{disp}}^{\text{ion}}$ and the sum $\Delta P_{\text{kin}}^{\text{ion}}+\Delta P_{\text{Coul}}^{\text{ion}}+\Delta P_{\text{core}}^{\text{ion}}$ for the cases without image forces, they would in the scale of the figure hardly be distinguishable from those where image forces are included. $P_{\text{im}}^{\text{ion}}$, on the other hand, is obviously zero in the absence of image forces. The conclusion is therefore that the increased repulsion arising from the inclusion of image forces is almost entirely due to P_{im}, rather than due to indirect effects of image forces on the other pressure components via their effects on the concentration profiles and correlation functions.

In Fig. 5 the total net pressure, P^{net}, in presence of image forces is plotted as a function of surface charge density at constant wall separation $D=9.6$ Å. The cases with $\sigma=\pm0.0449$ C m^{-2} that we have investigated so far are indicated by symbols. The curve for $B_-=0$ is, of course, symmetric around $\sigma=0$, while the curves become more and more asymmetric when B_- increases in magnitude. We see that there is in general a large variation in pressure depending on the strength of the counterion-wall dispersion interaction (as apparent for the case $\sigma>0$). The influence of the coion-wall dispersion interaction is much smaller (the case $\sigma<0$).

The difference between the influence of coions and counterions on the pressure make a quantitative and in some cases even a qualitative difference depending on the sign of the surface charge. P^{net} can, for example, be repulsive for negative surface charges and attractive for positive ones. This happens, for instance, when $B_-=-40$ kJ Å^3 mol^{-1} and σ is changed from −0.025 to +0.025 C m^{-2} in Fig. 5. This is entirely due to the ion-wall dispersion interaction since the anions and cations have the same valency and size, but differ in polarizability.

IV. CONCLUDING REMARKS

The results presented above show that in calculations of electric double layer interactions it is important to include both ion-wall dispersion and image charge forces. The former are particularly important when the counterions to the charged surfaces are highly polarizable, such as bromide and iodide ions. The image forces can also give rise to significant contributions to the total pressure. We have demonstrated that, for a certain combination of system parameters, the image forces have such a large effect that the pressure has the wrong sign if they are neglected.

The image forces are intimately connected to the zero frequency contribution of the wall-wall vdW interaction pressure. The screening of the latter by the electrolyte is contained in the action of the image forces via ion-ion correlation effects. If the full vdW pressure, including the zero frequency contribution, is added to the double layer pressure to calculate the total pressure, image forces must be included in order to have a consistent model. This has been explicitly demonstrated in the current work.

Our results support the suggestion that dispersion interactions between ions and interfaces give rise to ion specificity in interfacial phenomena, as discussed by Kunz *et al.*.[3]

The very limited set of calculations presented herein is not sufficient to give the full picture regarding the combined effects of dispersion and image forces, however. Work is currently underway to explore a wider range of systems.

ACKNOWLEDGMENT

This work has received financial support from the Swedish Research Council.

[1] F. A. Long and W. F. McDevit, Chem. Rev. (Washington, D.C.) **51**, 119 (1952).
[2] B. W. Ninham and V. Yaminsky, Langmuir **13**, 2097 (1997).
[3] W. Kunz, P. L. Nostro, and B. W. Ninham, Curr. Opin. Colloid Interface Sci. **9**, 1 (2004).
[4] M. Boström, D. R. M. Williams, and B. W. Ninham, Phys. Rev. Lett. **87**, 168103 (2001).
[5] M. Boström, F. W. Tavares, S. Finet, F. Skouri-Panet, A. Tardieu, and B. W. Ninham, Biophys. Chem. **117**, 217 (2005).
[6] S. A. Edwards and D. R. M. Williams, Curr. Opin. Colloid Interface Sci. **9**, 139 (2004).
[7] M. Boström, D. R. M. Williams, and B. W. Ninham, Biophys. J. **85**, 686 (2003).
[8] F. W. Tavares, D. Bratko, H. W. Blanch, and J. M. Prausnitz, J. Phys. Chem. B **108**, 9228 (2004).
[9] M. Boström, F. W. Tavares, D. Bratko, and B. W. Ninham, J. Phys. Chem. B **109**, 24489 (2005).
[10] J. Mahanty and B. W. Ninham, *Dispersion Forces* (Academic, New York, 1976).
[11] L. Onsager and N. N. T. Samaras, J. Chem. Phys. **2**, 528 (1934).
[12] R. Kjellander and S. Marčelja, J. Chem. Phys. **82**, 2122 (1985).
[13] R. Kjellander and S. Marčelja, Chem. Phys. Lett. **112**, 49 (1984).
[14] R. Kjellander, T. Åkesson, B. Jönsson, and S. Marčelja, J. Chem. Phys. **97**, 1424 (1992).
[15] H. Greberg, R. Kjellander, and T. Åkesson, Mol. Phys. **92**, 35 (1997).
[16] L. Guldbrand, B. Jönsson, H. Wennerström, and P. Linse, J. Chem. Phys. **80**, 2221 (1984).

[17] R. Kjellander and S. Marčelja, Chem. Phys. Lett. **142**, 485 (1987).
[18] R. Kjellander and B. Forsberg, J. Phys. A **38**, 5405 (2005).
[19] R. Kjellander, J. Phys. A **39**, 4631 (2006).
[20] G. Karlström, Phys. Chem. Chem. Phys. **5**, 3238 (2003).
[21] P. Jungwirth and D. Tobias, J. Phys. Chem. B **105**, 10468 (2001).
[22] *Handbook of Chemistry and Physics*, 52nd ed., edited by R. C. Weast (CRC, Cleveland, Ohio, 1971).
[23] R. R. Dagastine, D. C. Prieve, and L. R. White, J. Colloid Interface Sci. **231**, 351 (2000).
[24] R. Bauernschmitt and R. Ahlrichs, Chem. Phys. Lett. **256**, 454 (1996).
[25] M. Cossi and V. Barone, J. Chem. Phys. **115**, 4708 (2001).
[26] M. J. Frisch, G. W. Trucks, H. B. Schlegel *et al.*, GAUSSIAN 03, Revision b.05, Gaussian, Inc., Pittsburgh, PA.
[27] A. D. Becke, J. Chem. Phys. **98**, 5648 (1993).
[28] R. G. Parr, C. Lee, and W. Yang, Phys. Rev. B **37**, 785 (1988).
[29] J. M. L. Martin and A. Sundermann, J. Chem. Phys. **114**, 3408 (2001).
[30] A. Bergner, M. Dolg, W. Kuechle, H. Stoll, and H. Preuss, Mol. Phys. **80**, 1431 (1993).
[31] S. Miertuš, E. Scrocco, and J. Tomasi, Chem. Phys. **55**, 117 (1981).
[32] N. C. Pyper, C. G. Pike, and P. P. Edwards, Mol. Phys. **76**, 353 (1992).
[33] R. Hunter, *Foundations of Colloid Science* (Oxford University Press, New York, 2001).
[34] Section 7.4 in Ref. 10.

Paper II

Image Charges and Dispersion Forces in Electric Double Layers: The Dependence of Wall−Wall Interactions on Salt Concentration and Surface Charge Density

Erik Wernersson and Roland Kjellander*

Department of Chemistry, Göteborg University, SE-412 96 Göteborg, Sweden

Received: June 20, 2007

The interaction pressure between two planar charged walls is calculated for a range of conditions. The diffuse electric double layers between the two wall surfaces are treated with ion−wall dispersion forces and ionic image charge interactions taken into account. Both these interactions are due to dielectric discontinuities at the surfaces. Ion−ion and ion−image charge correlations are explicitly included. The ion−wall dispersion interactions can give rise to appreciable ion specific effects, which are particularly strong when the counterions to the surfaces are highly polarizable. The mechanisms of these effects are investigated, and their influence on the net interaction pressure between the walls is studied for a range of surface charge densities, strengths of the anion−wall dispersion interaction and bulk electrolyte concentrations. When the strength of the anion−wall dipersion interaction is increased, the pressure generally becomes less repulsive (or more attractive) for positive surfaces. The opposite happens in general for negative surfaces but to a much lesser extent. The effects are largest for large surface charge densities and high electrolyte concentrations. The image charge interactions give rise to a considerable depletion attraction between the walls for low surface charge densities.

1. Introduction

The "primitive model" of electrolyte solutions, wherein ions are characterized only by their charge and hard-sphere radius and the solvent enters only via its dielectric constant, forms the basis of much of our present understanding of electric double layers and the interaction of charged particles immersed in electrolyte solutions. In the context of colloidal dispersions, the primitive model is, for example, used in the Derjaguin−Landau−Vervey−Overbeek (DLVO) theory that since more than half a century forms a framework within which a broad range of experimental measurements are interpreted. In this theory, Coulomb and van der Waals interactions are treated as independent and additive. This is not strictly correct but is due to the approximations made. For example, the effects of ion−ion correlations, ionic image charge forces, and ionic polarizabilities are ignored. The importance to include these effects has become more and more apparent during recent years. The ion−ion correlations are not included in the DLVO theory since it is based on the Poisson−Boltzmann approximation, which is a mean field approximation for the ion concentration profiles of the double layer.

It has long been known that the static (zero frequency) part of the van der Waals (vdW) interactions between the colloid particles are screened in electrolytes.[1] The power-law vdW interaction is replaced by an exponentially screened one. This is brought about by the effects of image charge interactions due to the dielectric discontinuity at the particle surfaces, provided the correlations between the ions in the double layer are considered.[2] The high-frequency part of the vdW interactions is, however, not screened. The forces between the ions and the image charges will be referred to as "image forces" below.

Recently, it has been argued that the inclusion of dispersion forces between ions and interfaces in the primitive model is an appropriate measure to improve the model for charged interfaces.[3] In particular, the salt specificity of certain phenomena, such as the salting out of proteins, can partly be explained by dispersion forces acting between ions and interfaces. The effects of the inclusion of such interactions in the treatment of electric double layers and colloidal interactions have been studied by Boström and co-workers[4−11] as well as others; see, for example, refs 12−14. For a recent review, see ref 15. To model the effects of ion−wall dispersion forces, it is common to use the long-distance asymptotic form of these forces. In the current work, we investigate planar "primitive model" double layers where the ion−wall dispersion forces have been included in this approximate manner. The ion−ion correlations and ionic image charge forces are also included. Here, we use the term dispersion forces only when we mean forces that arise due to high-frequency quantum fluctuations (London forces). Compared with the bare Coulomb interactions, the dispersion forces are relatively short-ranged, but they are, on the other hand, relatively long-ranged compared with other non-Coulomb interactions between atoms, molecules, and colloidal particles. Since the Coulomb interactions are screened in electrolytes, the effects of dispersion forces may dominate for large distances but may also give important effects for short distances.

We have calculated the pressure between two parallel walls as a function of distance, surface charge density, and strength of the anion−wall dispersion interaction for a range of bulk electrolyte concentrations by means of the highly accurate anisotropic hypernetted chain (AHNC) approximation.[16,17] Cases with a large difference in anion−wall and cation−wall dispersion interactions are deemed to be of greatest interest. For simplicity, we have assumed that only the anions and not the cations interact with the walls via such forces. This choice was made to reflect the fact that anions tend to have a much greater polarizability than comparable cations[18] and is motivated by a wish to decrease the number of parameters in the model, as we want to place a stronger emphasis on qualitative effects rather

* Corresponding author. E-mail: rkj@chem.gu.se. Phone: +46-31-7722819. Fax: +46-31-7721394.

10.1021/jp0748157 CCC: $37.00
Published on Web 11/21/2007

than quantitative estimates. Apart from the difference in anion−wall and cation−wall dispersion interactions, the electrolyte model is completely symmetric.

The strength of the ion−wall dispersion forces, as well as the wall−wall vdW pressure, has been estimated from Lifshitz theory, wherein both the walls and the solvent are characterized by their frequency dependent dielectric functions and the ions by their dynamic polarizability; see ref 14 for details. Like the Coulomb potential in the primitive model, the large distance asymptotic power law for the dispersion forces is used for all separations beyond contact. Therefore, it may be said that the treatment of electrostatic forces and dispersion forces are on essentially the same level of sophistication.

This paper is a continuation of our previous study,[14] where the interaction between two walls with surface charge density $\sigma = \pm 0.0449$ C m^{-2} were investigated at bulk electrolyte concentration 0.5 M. (Expressed in terms of the number of elementary charges, e_0, per unit area, this surface charge density equals $\pm 0.28\ e_0$ nm^{-2}.) We found that for the model employed there is a dramatic difference between the effects of dispersion forces on the pressure for positively and negatively charged walls.

In the current work, we investigate a wider range of systems in order to obtain a more complete picture of the properties of the model. In section 2, the model and the theoretical methods are presented. The various components of the wall−wall interaction pressure are specified. In section 3, the results are presented and discussed, and finally, in section 4, the main results are summarized and conclusions are presented.

2. Method

2.1. Model. The system studied consists of an electrolyte solution sandwiched between two planar walls (semi-infinite slabs) separated by a distance D and in equilibrium with a bulk electrolyte. We use a coordinate system $\mathbf{r} = (x, y, z)$ with the origin in the plane that lies in the middle between the walls, referred to as the midplane below. The coordinate z is perpendicular to the wall surfaces.

Both the walls and the solvent are modeled as dielectric continua. They have dielectric functions $\epsilon_{\text{wall}}(i\omega)$ and $\epsilon_{\text{sol}}(i\omega)$ respectively, expressed as functions of imaginary frequency, $i\omega$. The static dielectric constants are $\epsilon_{\text{wall}}(0)$ and $\epsilon_{\text{sol}}(0)$.

The electrolyte model considered is a simple primitive model, defined by the ion−ion interaction potential for species i and j

$$u_{ij} = u_{ij}^{\text{core}} + u_{ij}^{\text{Coul}} + u_{ij}^{\text{im}} \tag{1}$$

where u_{ij}^{core} is the hard core potential for ions of diameter a; that is, $u_{ij}^{\text{core}}(\mathbf{r}, \mathbf{r}') = \infty$ if $|\mathbf{r} - \mathbf{r}'| < a$ and 0 otherwise, and where

$$u_{ij}^{\text{Coul}}(\mathbf{r}, \mathbf{r}') = \frac{q_i q_j}{4\pi\epsilon_0\epsilon_{\text{sol}}(0)\,|\mathbf{r} - \mathbf{r}'|} \tag{2}$$

q_i and q_j are the ionic charges and ϵ_0 is the permittivity of vacuum. In this work, the ions are taken to be monovalent, $q_+ = -q_- = e_0$ and have equal diameter a. The term u_{ij}^{im} in eq 1 is the potential for the image forces. The explicit expression for the Hankel transform of u_{ij}^{im} can be found in ref 16. Obviously, this term is zero in bulk solution. Because of the symmetry of the problem, the coordinate dependence of the ion−ion interaction potential can be written $u_{ij}(\mathbf{r}, \mathbf{r}') = u_{ij}(R, z, z')$, where $R = [(x - x')^2 + (y - y')^2]^{1/2}$ is the lateral distance.

The ion−wall potential is given by

$$\nu_i = \nu_i^{\text{core}} + \nu_i^{\text{Coul}} + \nu_i^{\text{im}} + \nu_i^{\text{disp}} \tag{3}$$

where ν_i^{core} is the ion−wall hard core potential, which is infinite if $|z| > (D - a)/2$ and 0 otherwise and where ν_i^{Coul} is the electrostatic interaction between an ion and a uniform surface charge density σ on each wall. Since the surface charge densities of the two walls are equal, ν_i^{Coul} is constant in the slit between the surfaces and does not give rise to any forces on the ions there. The contribution ν_i^{im} in eq 3 arises due to ions interacting with their own image charges, $\nu_i^{\text{im}}(z) = u_{ii}^{\text{im}}(0, z, z)/2$; see ref 16. (Note that a factor 1/2 in front of u_{ii}^{im} is missing in eq 6 of our previous publication, ref 14.) The potential for the ion−wall dispersion interactions is taken to be

$$\nu_i^{\text{disp}}(z|D) = B_i\left(\frac{1}{|z + D/2|^3} + \frac{1}{|z - D/2|^3}\right) \tag{4}$$

where the coefficient B_i is a parameter that controls the strength of the dispersion forces.

Dispersion forces are included only in the ion−wall potential in this work, not in the ion−ion pair potential. Expression 4 is the long-range asymptotic form of a particle−wall dispersion interaction and is only approximately valid for finite distances. Furthermore, it fails to account for the effects of many-body interactions, including the wall−ion−wall three-body interaction. In the calculations presented below, the values 0, −20, and −40 kJ Å^3 mol^{-1} are used for B_-, and B_+ is always set to zero.

The value −40 kJ Å^3 mol^{-1} for B_- is an estimate for iodide in water and was chosen on the basis of the dynamic polarizability of iodide as calculated by quantum mechanical density functional theory (for details, see ref 14). It is appropriate to set $B_+ = 0$ for ions that have roughly the same polarizability as the surrounding water. We have made this choice to reduce the number of parameters in the exploration of qualitative properties of the model. We emphasize that, although the value −40 kJ Å^3 mol^{-1} for B_- was chosen with iodide in mind, the present model does not correspond directly to any real system. It was, however, considered desirable to choose values that are within about the same range as those that might be encountered in real systems.

The choice of B_i parameters made here is only one of many possibilities that lies within the range of values that may be expected to be realistic for some salt. We have chosen B_+ and B_- such that there is a strong asymmetry in the anion−wall and cation−wall dispersion interactions. As anions tend to be more polarizable than comparable cations[18] (i.e., cations with a similar number of electrons); we expect such a large asymmetry to be present in many real systems. That is not to say, however, that the case of B_+ and B_- being roughly equal is either unrealistic or uninteresting, but we defer the study of this case to future works. The choice of equally sized anions and cations is expedient in the present context because it allows the study of a model system where the ion−wall dispersion interaction is the only source of asymmetry.

Recently, an approach similar to that used to calculate dynamic polarizability in ref 14 has been applied to the static polarizability of ions.[19] Both a dielectric continuum representation of the solvent and that of explicit water molecules as well as a hybrid approach were considered and compared. It was found that when the continuum approach was used the polarizability was higher than in vacuum, whereas it came out lower when the approach with explicit water molecules was used. In the hybrid approach, the polarizability was remarkably close to the vacuum value. This lends credence to the suspicion

expressed in ref 14 that the magnitude B_- might have been slightly overestimated by the method of calculation employed therein.

2.2. Anisotropic Hypernetted Chain Approximation. Within the AHNC approximation, the pair correlation functions and concentration profiles for the inhomogeneous electrolyte between the walls are explicitly calculated by numerical solution of the Ornstein−Zernike equation with the approximate HNC closure for the pair correlation functions and an equation for the ionic concentration profiles. In the latter, use is made of the fact that the local excess chemical potential is given within the HNC approximation as a known functional of the pair correlation functions and concentration profiles. The total chemical potential is prescribed to be equal at all points between the walls, which gives a sufficient criterion for determination of the concentration profiles consistent with the correlation functions. A solution with self-consistent correlation functions and concentration profiles is obtained by iteration. Physically, the prescription of a constant chemical potential corresponds to the electrolyte solution in between the walls being in equilibrium with a bulk electrolyte solution of the same chemical potential. The AHNC approximation and the closely related anisotropic reference HNC (ARHNC) approximation have previously been shown to be in very good agreement with simulation results; see refs 20 and 21 and references cited therein. For details regarding the AHNC method and its implementation, see refs 16 and 17.

The AHNC method is particularly suitable for the present problem because it provides a simple way to properly treat the infinite array of image charges needed to take into account the self-consistent polarization of the two walls by the intervening ions. As the image forces are included in the Hamiltonian of the system and the correlation functions are treated consistently, the electrostatic screening of the image charges is included automatically. Hence, there is no need to make any a priori assumptions regarding the screening of the image charges.

2.3. Evaluation of the Wall−Wall Pressure. The pressure between the walls is calculated as described in our previous work,[14] and we employ the same notation here. The pressure due to the ions, P^{ion}, is a sum of five terms of different physical origin,

$$P^{\text{ion}} = P^{\text{ion}}_{\text{kin}} + P^{\text{ion}}_{\text{Coul}} + P^{\text{ion}}_{\text{core}} + P^{\text{ion}}_{\text{im}} + P^{\text{ion}}_{\text{disp}} \tag{5}$$

The term $P^{\text{ion}}_{\text{kin}}$ is the pressure due to the thermal motion of the ions; $P^{\text{ion}}_{\text{Coul}}$ and $P^{\text{ion}}_{\text{core}}$ originate from electrostatic and hard core interactions across the midplane, respectively. $P^{\text{ion}}_{\text{im}}$ originates from the image forces, and $P^{\text{ion}}_{\text{disp}}$ originates from the ion−wall dispersion interactions. The latter is the force per unit area between the ions on one side of the midplane and the wall on the opposite side. See ref 14 for explicit expressions of the pressure components in terms of distribution functions (note that for $P^{\text{ion}}_{\text{im}}$ in eq 17 of ref 14, an additional factor $1/(2\pi)^2$ is missing in front of the first and second sum). The sum of the three terms that are nonzero in bulk solution, $P^{\text{ion}}_{\text{kin}}$, $P^{\text{ion}}_{\text{Coul}}$, and $P^{\text{ion}}_{\text{core}}$, is referred to as the osmotic pressure below and is denoted $P^{\text{ion}}_{\text{osm}}$.

The relevant quantity for comparison with experimental results is the difference between the pressure in the slit between the walls and the bulk pressure $\Delta P^{\text{ion}} = P^{\text{ion}}[\text{slit}] - P^{\text{ion}}[\text{bulk}]$. This applies to most of the pressure components, for example, $\Delta P^{\text{ion}}_{\text{kin}}$, but $P^{\text{ion}}_{\text{im}}$ and $P^{\text{ion}}_{\text{disp}}$ have no counterpart in bulk and are therefore never equipped with a Δ.

The total pressure between the walls can be written as the sum of the pressure due to the ions between the walls and the wall−wall van der Waals pressure,

$$P = P^{\text{ion}} + P^{\text{wall}}_{\text{vdW}} \tag{6}$$

$P^{\text{wall}}_{\text{vdW}}$ is evaluated from Lifshitz theory, and we have explicitly

$$P^{\text{wall}}_{\text{vdW}} = -\frac{k_{\text{B}}T}{4\pi D^3} {\sum_{l=0}^{\infty}}' \sum_{s=1}^{\infty} \frac{\epsilon_D^{2s}(i\omega_l)}{s^3} \tag{7}$$

where

$$\epsilon_D(i\omega_l) = \frac{\epsilon_{\text{sol}}(i\omega_l) - \epsilon_{\text{wall}}(i\omega_l)}{\epsilon_{\text{sol}}(i\omega_l) + \epsilon_{\text{wall}}(i\omega_l)} \tag{8}$$

is evaluated at imaginary frequency $i\omega_l$ where $\omega_l = l2\pi k_{\text{B}}T/\hbar$. The prime on the summation symbol indicates that the $l = 0$ term is to be weighted by one-half.

In the following discussion, it will be necessary to distinguish the term corresponding to $l = 0$ from the rest of the sum in eq 7. The former will be denoted by $P^{\text{wall}}_{\text{vdW(0)}}$ and referred to as the zero frequency vdW pressure, while the latter will be denoted by $P^{\text{wall}}_{\text{vdW(hf)}}$ and referred to as the high-frequency vdW pressure.

It should be remarked that $P^{\text{ion}}_{\text{disp}}$ is based on the approximate ion−wall dispersion interaction in eq 4, so it does not give the proper correction to $P^{\text{wall}}_{\text{vdW(hf)}}$ due to the presence of ions in the medium between the walls. The modification of the dielectric properties of the medium by the ions is not properly treated. For example, many-body effects are neglected. Hence, P^{ion} and $P^{\text{wall}}_{\text{vdW}}$ are not strictly additive. Additivity may nevertheless be a reasonable approximation unless the concentration of ions is too high.

3. Results and Discussion

We have calculated the total interaction pressure between two planar walls as a function of surface separation and surface charge density for three different bulk electrolyte concentrations, 0.500, 0.250, and 0.125 M. The charge and size symmetric electrolyte was monovalent and the ion diameter $a = 4.6$ Å. Three different strengths of the anion−wall dispersion interaction were investigated, $B_- = -40$, -20, and 0 kJ Å^3 mol^{-1}, while the cation−wall dispersion force was neglected throughout, $B_+ = 0$. We have used static dielectric constants $\epsilon_{\text{wall}}(0) = 2.54$ and $\epsilon_{\text{sol}}(0) = 78.36$, which correspond to polystyrene and water[22] at room temperature. $P^{\text{wall}}_{\text{vdW(hf)}}$ was calculated using dielectric function data from White[23] for polystyrene and water.

The results for 0.500 M solutions are shown as contour plots in Figure 1. The pressure as a function of surface separation, D, at constant surface charge density corresponds to a vertical intersection of the diagram. The smallest value of D displayed in the figure is 5.6 Å, while the minimum surface separation is 4.6 Å, which corresponds to one layer of counterions between the walls. Thus, the diagram does not extend down to contact. The pressure eventually becomes repulsive when the surfaces approach contact in all cases with nonzero surface charge, since counterions must remain between the surfaces because of electroneutrality.

The contours of the uppermost panel of Figure 1 are symmetric around $\sigma = 0$ because of the symmetry of the electrolyte in absence of dispersion forces, $B_- = B_+ = 0$. When

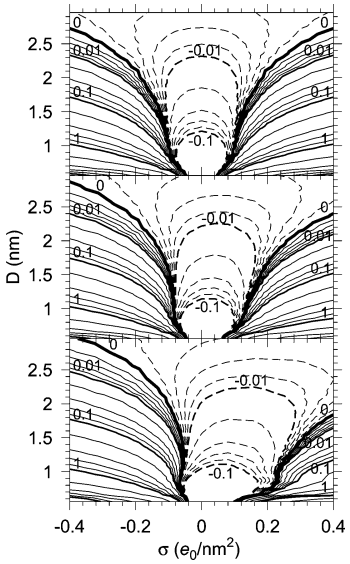

Figure 1. Contour plots showing the net interaction pressure, $\Delta P = P$[slit] $- P$[bulk], between two planar walls as a function of surface charge density, σ, and wall−wall separation, D. The system is in equilibrium with a 0.500 M aqueous electrolyte solution of monovalent ions with equal diameters $a = 4.6$ Å. The upper panel shows the case of no ion−wall dispersion interactions. In the other panels, the anions have such interactions of strength $B_- = -20$ (middle panel) and -40 kJ Å^3 mol^{-1} (bottom panel), while $B_+ = 0$ throughout. The labels of the contours give the pressure as $\Delta P(RT)^{-1}$ in units of M. The thick contours are logarithmically spaced (except, of course, the ones corresponding to zero pressure), while the thin contours correspond to the values $\pm 2 \times 10^m$, $\pm 4 \times 10^m$, $\pm 6 \times 10^m$, and $\pm 8 \times 10^m$ for various integers m. Dashed lines correspond to an attractive pressure, and full lines correspond to a repulsive one. The surface chage density is given as the number of elementary charges, e_0, per unit area.

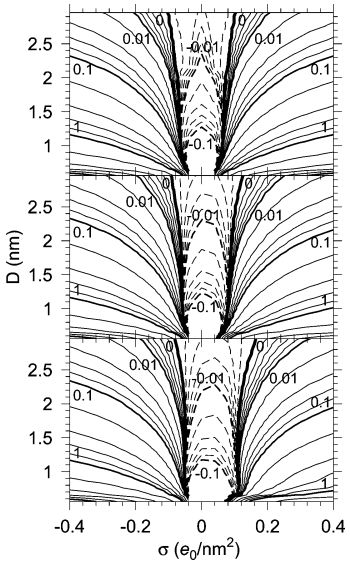

Figure 2. Same as Figure 1 but for bulk concentration 0.250 M.

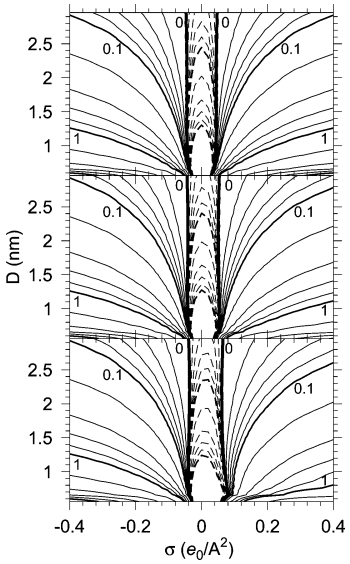

Figure 3. Same as Figures 1 and 2 but for bulk concentration 0.125 M.

B_- is increased in magnitude, the contours turn skewed, more so for more negative B_-.

The contours that corresponds to zero pressure, displayed as extra thick lines in the figure, are particularly interesting as they constitute the "lines of demarcation" between attractive and repulsive pressure and therefore correspond to an extremum in the wall−wall free energy of interaction. When the pressure goes from repulsive to attractive with increasing D, the extremum is a minimum, that is, a stable (or possibly metastable) state. This applies to most parts of the thick lines shown in Figure 1. The free energy minimum is analogous to but not the same as the secondary minimum of DLVO theory. We see in the figure that, when the magnitude of the surface charge is increased, the minimum (the point of zero pressure) shifts to larger D values, which is the same qualitative behavior as in the DLVO theory. (In contrast to the theory we use in this paper, the DLVO theory is, however, only valid as an approximation for double layers at low electrolyte concentrations, low surface charge densities, in absence of image forces, and without ion−wall dispersion forces.)

In the uppermost panel of Figure 1, the attractive region (dashed lines) extends between about -0.10 and 0.10 e_0 nm^{-2} for $D = 10$ Å. In the middle panel, this region has shifted to extend between -0.08 and 0.13 e_0 nm^{-2} for $D = 10$ Å and in the bottom panel to between -0.06 and 0.22 e_0 nm^{-2}. At the right- and left-hand sides of the plot, $\sigma = \pm 0.4$ e_0 nm^{-2}, the positions of the point of zero pressure in the bottom panel differ by more than 1 nm between positive and negative surfaces.

The corresponding plots for bulk electrolyte concentrations 0.250 and 0.125 M are shown in Figures 2 and 3, respectively. The same skewing of the contour of zero pressure and widening of the attractive region are also present in these figures but to a much smaller extent. This is true especially at the lowest concentration, Figure 3, where the pressure does not vary much with B_-. Note that in this figure the contours change the most with increasing magnitude of B_- for large positive surface charge density. The change in the contours for large negative σ values is hardly visible in this case. The latter is true also for the 0.250 M case, Figure 2. For the highest concentration (Figure 1) and large negative σ, there is a slight upward shift in the contours when B_- turns more negative. The trend for positive σ is opposite and larger; there is a downward shift in the contours. The latter is also true in Figures 2 and 3.

By comparing the three panels of Figures 1 to 3, we can conclude that the main effect of increasing the magnitude of B_- is a decreased repulsion (or increased attraction) in the case of positively charged surfaces and that the effect is opposite and smaller for negatively charged surfaces; that is, the repulsion is slightly increased (or attraction decreased) in the latter case. We can also draw the conclusion that these effects are much more pronounced at high bulk electrolyte concentration than low. The fact that the inclusion of ion−wall dispersion forces

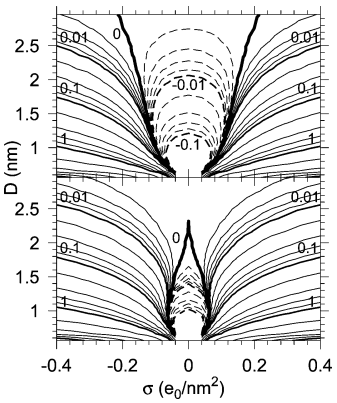

Figure 4. Contour plot showing various sums of pressure components for the same system as in the top panel of Figure 1. No ion−wall dispersion interactions are present. The upper panel shows $\Delta P^{ion}_{osm} = \Delta P^{ion}_{kin} + \Delta P^{ion}_{Coul} + \Delta P^{ion}_{core}$. The lower panel shows the sum of all pressure components apart from $P^{wall}_{vdW(hf)}$, that is $\Delta P^{ion}_{osm} + P^{ion}_{im} + P^{wall}_{vdW(0)}$. The contour plot is constructed in the same way as Figure 1.

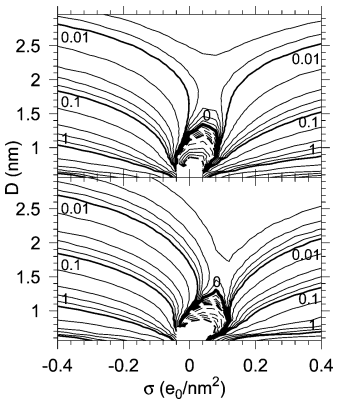

Figure 5. Same as Figure 4 but in presence of ion−wall dispersion interactions of strength $B_- = -40$ kJ Å^3 mol^{-1}. The system is the same as in the bottom panel of Figure 1. The upper panel shows ΔP^{ion}_{osm}, and the lower shows the sum of all pressure components apart from $P^{wall}_{vdW(hf)}$. In this case, the latter sum equals $\Delta P^{ion}_{osm} + P^{ion}_{disp} + P^{ion}_{im} + P^{wall}_{vdW(0)}$.

has opposite effects for positive and negative surfaces has been discussed in our previous publication;[14] see also the work by Boström et al.[7]

The decreased repulsion for positively charged surfaces can to a large extent be explained by the behavior of P^{ion}_{disp}, the pressure component due to direct dispersion interaction between ions and walls. This attractive component increases when the magnitude of B_- is increased for positive surfaces (i.e., when the polarizable anions are counterions). This increase arises both from a larger dispersion interaction for each counterion between the walls and from an increase in the number of ions when counterions are attracted into the slit from the surrounding bulk solution by the dispersion interactions. Furthermore, P^{ion}_{disp} increases with increased positive surface charge density because of the increased number of counterions between the walls needed to maintain electroneutrality.

The anions are attracted to the positive surfaces by both dispersion and electrostatic forces. This causes a decrease in the ion concentration at the midplane compared with the case without dispersion forces and thus causes a decrease in ΔP^{ion}_{kin} in many cases (exceptions occur for large D and for small σ, see below). These changes in P^{ion}_{disp} and ΔP^{ion}_{kin} both act to make the net pressure less repulsive (more attractive).

In the case of negative surfaces, the small increase in double layer repulsion when the magnitude of B_- is increased is due to an increased kinetic pressure between the walls. This arises because the ion concentration in the middle between the walls is increased when ion pairs are drawn into the slit from bulk by dispersion forces acting on the anions. Since the anions are coions to the surfaces in this case, they stay largely in the middle of the slit for moderately large surface separations. Compared with the case of positive surfaces, the total number of anions between the surfaces is much smaller for electrostatic reasons, in particular for short surface separations. Therefore, P^{ion}_{disp} is small and relatively unimportant in this case. In total, the pressure becomes more repulsive (less attractive) for negative surfaces in all cases considered here when B_- turns more negative, but it is a small effect.

These results are further illustrated in Figures 4 and 5, from which the relative importance of various pressure components for the magnitude of the total pressure can be deduced. Both figures are for the case 0.500 M electrolyte and show pressure contributions in absence and presence of ion−wall dispersion interactions, respectively. The pressure component $P^{wall}_{vdW(hf)}$, which is the same in all cases, is not included.

The upper panel of each of these figures shows $\Delta P^{ion}_{osm} = \Delta P^{ion}_{kin} + \Delta P^{ion}_{Coul} + \Delta P^{ion}_{core}$. The latter two contributions in the sum are rather insensitive to the magnitude of B_-, so the difference between the upper panels is mainly due to ΔP^{ion}_{kin}. When we go from Figure 4 to 5, that is, when the ion−wall dispersion interactions is turned on, the contours in the upper panels corresponding to $P(RT)^{-1} = 1.0$ and 0.1 M shift to smaller separations for positive surface charges and to larger separations for negative surfaces in agreement with the discussion above. On the other hand, the $P(RT)^{-1} = 0.01$ M contour shifts to a somewhat larger separation for both positive and negative surfaces. The effect is, however, small for positive surfaces.

In both figures, there is a region where the pressure is attractive. From the upper panel in Figure 4, we see that ΔP^{ion}_{osm} is weakly attractive for a wide range of distances for uncharged to moderately charged surfaces. The attraction is caused by a depletion of ions in the slit due to repulsive image forces. The depletion results in an attractive ΔP^{ion}_{osm} because the electrolyte concentration in the slit is smaller than that in the bulk solution. For uncharged surfaces, the pressure is attractive for all distances, but for charged surfaces, ΔP^{ion}_{osm} turns repulsive for small D. The reason for this is that counterions remain in the slit because of the electroneutrality condition, which prevents all of them from being expelled to bulk.

When ion−wall dispersion forces are included, Figure 5, the attractive region becomes limited to short wall−wall separations and low surface charge densities. ΔP^{ion}_{osm} becomes repulsive at large separations. This is due to the dispersion forces which draw ion pairs into the space between the walls from bulk. These forces have a longer range than the repulsive image forces, which are exponentially screened. (As noted above, for large positive σ, the effect is opposite for small to moderate surface separations. Then, the increase in ΔP^{ion}_{osm} due to disperions forces occurs only for large D.)

Let us now turn to the lower panels in Figures 4 and 5, where we have also included the contributions P^{ion}_{im}, $P^{wall}_{vdW(0)}$, and P^{ion}_{disp} (the latter is zero in Figure 4). Note that whenever P^{ion}_{im} is included in the pressure one should also include $P^{wall}_{vdW(0)}$ since,

as discussed in ref 2, these contributions cancel each other exactly for large wall−wall separations. This cancellation expresses the screening of the zero-frequency vdW pressure by the electrolyte between the walls; that is, $P_{\mathrm{im}}^{\mathrm{ion}}$ contains terms that cancel the power-law decay of $P_{\mathrm{vdW}(0)}^{\mathrm{wall}}$ and replaces it by the screened interaction. For the cases investigated in this paper, $P_{\mathrm{im}}^{\mathrm{ion}}$ was found to be insensitive to the value of B_-, so $P_{\mathrm{im}}^{\mathrm{ion}} + P_{\mathrm{vdW}(0)}^{\mathrm{wall}}$ is about the same in Figures 4 and 5.

The plots in the upper and lower panels of Figure 4 are quite similar except in the region of small σ and large D. Thus, the magnitude of $P_{\mathrm{im}}^{\mathrm{ion}} + P_{\mathrm{vdW}(0)}^{\mathrm{wall}}$ is small compared with $\Delta P_{\mathrm{osm}}^{\mathrm{ion}}$, except in the latter region where the opposite is true. We see that the attractive region for large D in the upper panel is absent in the lower panel. The attraction due to ion depletion is thus counteracted by the repulsive $P_{\mathrm{im}}^{\mathrm{ion}} + P_{\mathrm{vdW}(0)}^{\mathrm{wall}}$ for large D. There remains, however, a region with attractive pressure in the lower panel, where the depletion attraction due to the image forces is quite strong. By comparing Figure 4 with the upper panel of Figure 1, where $P_{\mathrm{vdW(hf)}}^{\mathrm{wall}}$ is included, we see that the magnitude of the depletion attraction for many values of D is comparable to that of the high-frequency vdW attraction, although the former decays more quickly than the latter with increasing D.

By comparing the upper and lower panels of Figure 5, we see that the addition of $P_{\mathrm{im}}^{\mathrm{ion}} + P_{\mathrm{vdW}(0)}^{\mathrm{wall}} + P_{\mathrm{disp}}^{\mathrm{ion}}$ increases the asymmetry already present in the upper panel. This is essentially due to $P_{\mathrm{disp}}^{\mathrm{ion}}$, in agreement with the discussion above. Furthermore, we see that the net attraction for low surface charge densities and short wall−wall separations is slightly enhanced in the lower panel for positive surface charges. The attractive pressure contribution $P_{\mathrm{vdW(hf)}}^{\mathrm{wall}}$, which is included in the bottom panel of Figure 1, makes the attractive region much larger, but a comparison of this plot and both panels in Figure 5 shows that a non-negligible part of the attraction for low surface charge densities and short wall−wall separations originates from $\Delta P_{\mathrm{osm}}^{\mathrm{ion}}$ and $P_{\mathrm{disp}}^{\mathrm{ion}}$.

4. Summary and Conclusions

From the results in this work, we can identify two interdependent mechanisms by which dispersion forces between walls and ions may modify the pressure between walls separated by an electrolyte solution. The first is the direct dispersion interaction between the walls and highly polarizable ions. This results in an attractive pressure that may be regarded as a contribution to the total van der Waals pressure. The magnitude of this pressure contribution is dependent on the total amount of polarizable ions between the walls as well as their spatial distribution. The attraction increases with increased bulk electrolyte concentration and, if the counterions are polarizable, it also increases with increasing surface charge density.

The second mechanism is a change in the concentration profiles due to ion−wall dispersion forces, which leads to an altered osmotic pressure in the slit between the walls. This may result in either a decrease or an increase in net pressure depending on the conditions. Let us assume, as is done above, that the anions are the most polarizable ionic species. A decresed repulsion (or increased attraction) then occurs for large positive surface charge densities (i.e., when the polarizable anions are counterions to the surfaces) and small to moderate surface separations. The dispersion forces then act to draw the anions closer to the surfaces, thereby decreasing the concentration of ions at the midplane between the walls. The opposite pressure change happens for negative surface charge densities or for large surface separations. Then the ion−wall dispersion forces make the osmotic pressure to be more repulsive (or less attractive). In this case, the dispersion forces draw ion pairs from bulk into the slit between the walls, which leads to an increase in ionic concentration at the midplane.

In all cases where an increase in the strength of the dispersion interactions resulted in an increased repulsion, the net effect was found to be small. This can be explained in part by the tendency of the pressure due to direct ion−wall dispersion interactions, that is always attractive, to counteract the change in osmotic pressure.

The image forces due to the dielectric discontinuities at the surfaces give rise to a depletion attraction. For weakly charged surfaces, this is a significant contribution to the pressure for short surface separations. The importance of image forces decreases, however, with increasing surface charge density.

We conclude that ion−wall dispersion forces are of qualitative importance mainly where the counterions to the surface are highly polarizable provided the surface charge density and electrolyte concentration are rather high. For such cases, the direct dispersion interaction between the polarizable counterions and the walls gives rise to a large attractive contribution to the pressure and, in addition, to a decrease in the repulsive osmotic pressure. Taken together, these effects result in a large decrease in net repulsion (or increase in attraction). It is therefore in such cases that a significant influence of dispersion interactions on the total pressure is observed.

Acknowledgment. This work has been supported financially by the Swedish Research Council.

References and Notes

(1) Mahanty, J.; Ninham, B. W. *Dispersion Forces;* Academic Press, New York, 1976.
(2) Kjellander, R.; Marčelja, S. *Chem. Phys. Lett.* **1987**, *142*, 485.
(3) Ninham, B. W.; Yaminsky, V. *Langmuir* **1997**, *13*, 2097.
(4) Boström, M.; Williams, D. R. M.; Ninham, B. W. *Langmuir* **2001**, *17*, 4475.
(5) Boström, M.; Williams, D. R. M.; Ninham, B. W. *Phys. Rev. Lett.* **2001**, *87*, 168103.
(6) Boström, M.; Tavares, F. W.; Bratko, D.; Ninham, B. W. *J. Phys. Chem. B* **2005**, *109*, 24489.
(7) Boström, M.; Tavares, F. W.; Finet, S.; Skouri-Panet, F.; Tardieu, A.; Ninham, B. W. *Biophys. Chem.* **2005**, *117*, 217.
(8) Moreira, L. A.; Boström, M.; Ninham, B. W.; Biscaia, E. C.; Tavares, F. W. *Colloids Surf., A* **2006**, *282*−*283*, 457.
(9) Boström, M.; Deniz, V.; Franks, G. V.; Ninham, B. W. *Adv. Colloid Interface Sci.* **2006**, *123*−*126*, 5.
(10) Boström, M.; Deniz, V.; Ninham, B. W. *J. Phys. Chem. B* **2006**, *110*, 9645.
(11) Moreira, L. A.; Boström, M.; Ninham, B. W.; Biscaia, E. C.; Tavares, F. W. *J. Braz. Chem. Soc.* **2007**, *18*, 223.
(12) Tavares, F. W.; Bratko, D.; Blanch, H. W.; Prausnitz, J. M. *J. Phys. Chem. B* **2004**, *108*, 9228.
(13) Edwards, S. A.; Williams, D. R. M. *Curr. Opin. Colloid Interface Sci.* **2004**, *9*, 139.
(14) Wernersson, E.; Kjellander, R. *J. Chem. Phys.* **2006**, *125*, 154702.
(15) Kunz, W.; Nostro, P. L.; Ninham, B. W. *Curr. Opin. Colloid Interface Sci.* **2004**, *9*, 1−18.
(16) Kjellander, R.; Marčelja, S. *J. Chem. Phys.* **1985**, *82*, 2122.
(17) Kjellander, R. *J. Chem. Phys.* **1988**, *88*, 7129.
(18) Pyper, N. C.; Pike, C. G.; Edwards, P. P. *Mol. Phys.* **1992**, *76*, 353.
(19) Serr, A.; Netz, R. R. *Int. J. Quantum Chem* **2006**, *106*, 2960.
(20) Kjellander, R.; Åkesson, T.; Jönsson, B.; Marčelja, S. *J. Chem. Phys.* **1992**, *97*, 1424.
(21) Greberg, H.; Kjellander, R.; Åkesson, T. *Mol. Phys.* **1997**, *92*, 35.
(22) Weast, R. C., Ed. *Handbook of Chemistry and Physics*, 52nd ed.; The Chemical Rubber Co.: Cleveland, OH, 1971.
(23) Dagastine, R. R.; Prieve, D. C.; White, L. R. *J. Colloid Interface Sci.* **2000**, *231*, 351.

Paper III

Ion correlation forces between uncharged dielectric walls

Erik Wernersson and Roland Kjellander[a)]
Department of Chemistry, University of Gothenburg, SE-412 96 Gothenburg, Sweden

(Received 25 June 2008; accepted 5 September 2008; published online 9 October 2008)

The interaction pressure between two uncharged planar walls immersed in various electrolyte solutions containing mono- and/or divalent ions is investigated. The solution is treated as a primitive model electrolyte, and the wall surfaces constitute dielectric discontinuities. Ionic image charge and ion-wall dispersion interactions are included. The interaction parameters are appropriate for hydrocarbon (polystyrene)/water interfaces, and the electrolyte concentrations considered lie between 0.250*M* and 1.00*M*. The anisotropic hypernetted chain method is used to self-consistently calculate the ion density profiles and the ion-ion correlation functions in the inhomogeneous electrolyte. Thereby, the effects of image charge interactions and dispersion interactions on the pressure and the electrolyte structure are included in a fully consistent manner. The explicit consideration of correlations between the ions in the presence of image charges ensures that the screening of the zero-frequency van der Waals interaction is taken into account. Of special interest are the effects of asymmetries between anions and cations with respect to valency and/or dispersion interaction with the walls. Such asymmetries create an electric double layer in the electrolyte outside each electroneutral surface. This causes the wall-wall interaction for large surface separations to be similar to the interaction between charged surfaces. For intermediate separations, around 1–2 nm, a substantial repulsive peak appears in the ionic pressure. In some cases the repulsion is larger than the van der Waals attraction between the walls, which implies that there is a repulsive barrier in the total pressure despite that the surfaces are uncharged. The strongest repulsion is found for 2:1 electrolytes where the monovalent anions interact strongly with the walls via dispersion forces. In general, ion-wall dispersion forces acting on ions of lower valency have a much greater effect than equally strong dispersion forces acting on ions of higher valency. This is mainly due to the more strongly repulsive image charge forces on ions of higher valency that counteract the attractive dispersion forces. Effects of confinement on the ion-ion correlations also contribute to this difference. For all electrolytes the interaction pressure from the ions is attractive for small surface separations. The main cause is a depletion of ions between the walls from the self-image repulsion and confinement effects. For totally symmetric electrolytes the attractive pressure extends to large separations in most cases. © *2008 American Institute of Physics*. [DOI: 10.1063/1.2990007]

I. INTRODUCTION

Due to its simplicity, the primitive model for electrolyte solutions and for electric double layers has been extensively studied. In this model the ions are treated as charged hard spheres and the solvent as a dielectric continuum. When modeling double layers near macroions, charged walls, or other macroparticles, one usually assumes that the particle surfaces are smooth and uniformly charged. An area of application is statistical mechanical calculations of interactions between various particles, which, for instance, are relevant for the properties and stability of colloidal dispersions and the swelling of clays and surfactant bilayer systems.

The most common approach for the study of electrostatic interactions in electrolyte systems is to use the Poisson–Boltzmann (PB) approximation—a mean field approximation that neglects the ion-ion correlations in the ion atmosphere around the charged particle(s) or surface(s). Such correlations are due to all kinds of interactions between the ions, electrostatic, as well as steric (from finite ionic sizes). The PB theory is quite successful in many cases provided that the typical ionic interactions are not very strong, such as in aqueous monovalent electrolytes at low to moderate concentrations near surfaces that are not too highly charged.

The primitive model has proved useful in explaining the interactions seen between surfaces also in strongly coupled systems, where the PB approximation fails due to the neglect of the effects of ion-ion correlations. For example, the reduced swelling of clays in the presence of calcium ions,[1] the interaction pressure between mica surfaces at high electrolyte concentration,[2] and the cohesion of cement paste[3] can be explained by the primitive model provided its properties are accurately evaluated.

In primitive model treatments of double layer phenomena near walls one assumes in most cases that the dielectric properties of the walls and the solvent are the same. This assumption is not inherent in the model and is done for reasons that are more often technical than physical. Thereby polarization of the dielectric interface by ions (image charge effects) is neglected. This may be a good approximation in many situations, but not necessarily in all cases.

[a)]Electronic mail: rkj@chem.gu.se.

The neglect of surface polarization leads, for example, to inconsistencies in the treatment of the system when the van der Waals forces between the walls are included. Such forces, which usually are added to the double layer interaction to obtain the total wall-wall interaction, incorporate some consequences of different dielectric properties of the walls and the solvent. Unless the same model, including the presence of dielectric boundaries, is used for the double layer calculations one introduces an inconsistency, which incorrectly makes the van der Waals interaction unaffected by the presence of electrolyte. In fact, the correct inclusion in the primitive model of the dielectric polarization induced by the ions at the interfaces leads to a screening of the static (zero-frequency) part of the van der Waals interactions from Lifshitz theory.[4,5] This screening is absent if dielectric boundaries are not properly handled in the treatment of the double layers. The static contribution to the van der Waals interactions constitutes a large part of the total interaction for systems like hydrocarbon particles in water,[6,7] so the screening can have important consequences.

A coupling of the static van der Waals and the double layer interactions is thus inherent in the primitive model when dielectric boundaries are treated consistently. The static polarization of these boundaries by the ions is most easily handled by the method of image charges for simple geometries like planar walls and we therefore will refer to the interactions due to such polarization as "image interactions" or "image forces."

In addition to the static polarizations there are high-frequency fluctuations in polarization of interfaces and ions that give rise to dispersion forces between ions and interfaces. Since the strength of the dispersion force between an ion and an interface depends on the electronic structure of the ion, dispersion interactions have been suggested as a possible source of ion specificity in interfacial phenomena.[8] The dispersion interaction can, as an approximation, be added to the electrostatic and hard core interactions of the primitive model.

The dispersion forces arise when there are differences in the dynamic dielectric properties on either side of an interface and when the polarizability of ions is different from that of the solvent. For sufficiently large wall-ion distances the strength of the dispersion force acting on an ion can be estimated from the frequency dependent dielectric functions of the media and the dynamic polarizability of the ion by Lifshitz theory, as described in Ref. 8. To extend the primitive model in this manner is quite reasonable since one continues to treat the solvent as a dielectric continuum. The dielectric functions can be inferred from spectroscopic data over a wide frequency range,[9] and the dynamic polarizability can be estimated from quantum mechanical calculations[10,11] via the well-known "sum of states" formula for atomic polarizability, cf. Eq. (3.7) in Ref. 4. During recent years, the effects of such dispersion interactions on the ion distribution near interfaces and other properties of double layer systems have been the subject of several studies.[12–26]

In the present work we shall include effects of both image interactions and ion-wall dispersion forces in the calculation of interactions between two planar walls. Our previous results from such calculations[23] for monovalent electrolytes suggest that the influence of surface polarization is largest on a relative scale for small surface charge densities and decreases with increasing magnitude of the surface charge. For this reason, we here study the case with electrolyte in contact with uncharged polarizable walls.

We consider 1:1 and 2:2 charge-symmetric as well as 2:1 and 1:2 charge-asymmetric electrolytes. (The convention used here is that an $m:n$ electrolyte is composed of cations of valency m and anions of valency n.) In all cases the electrolyte is size symmetric, so anions and cations have the same diameter. We will investigate the properties of the systems both in the absence and presence of ion-wall dispersion interactions. In the latter case, we will assume that the anions are much more polarizable than cations. Our main focus concerns qualitative features of the systems and therefore, we have for simplicity neglected the (small) polarizability of the cations, i.e., the latter behave as though their polarizability is equal to that of the surrounding water. We also neglect dispersion interactions between the simple ions.

The relevance of investigations of the effect of electrolyte on interactions between electroneutral walls can be seen in recent experimental studies of the swelling of multilamellar samples of uncharged lipids by Petrache *et al.*[27,28] They measured the pressure between the lipid bilayers as function of lamellar repeat distance using the osmotic pressure technique of Rand and Parsegian.[29] The dependence of the swelling on the type and concentration of monovalent salt was investigated. It was found that the swelling increased with increasing electrolyte concentration and that it was larger for KBr than for KCl at the same concentrations. The concentration dependence was interpreted as due to the screening of the van der Waals attraction by salt. The difference between bromide and chloride was consistent with a weak specific binding of bromide but not of chloride to the bilayer surfaces and the appearance of an electric double layer repulsion in the former case. Petrache *et al.* also included repulsive undulation and "hydration" forces in the analysis and found that the salt effect could not be attributed to changes in these interactions.

These qualitative effects of electrolytes are consistent with the findings in the present work. We do not have any specific adsorption of ions in the model beyond that due to dispersion forces. The binding constant reported in Ref. 28 corresponds to an attraction stronger than but of a similar order of magnitude compared to the anion-wall dispersion force considered in our calculations.[30] We have, however, made no attempt to fit our theoretical results quantitatively to any experimental findings. As stated earlier, our goal here is merely to establish the qualitative features of image interactions and ion-wall dispersion forces for reasonable values of the system parameters. We hope, nevertheless, that the results presented here will in the future prove useful in the interpretation of similar experiments.

Some important objectives of our work are to investigate effects of anion-cation asymmetry and possible relevance for ion specificity in surface phenomena. For the 1:1 and 2:2 electrolytes near uncharged walls, the only source of asym-

metry is the ion-wall dispersion interactions when present. For the 2:1 and 1:2 electrolytes there is also charge asymmetry.

It has been known for a long time that in 2:1 and 1:2 primitive model electrolytes (in the absence of dispersion interactions) there is some degree of charge separation close to an electroneutral wall both in the absence and presence of image forces.[31] Close to the surface the divalent ion concentration is lower than the monovalent one, while the reverse is true some distance away. This difference in the ionic concentration profiles gives rise to a nonzero effective surface charge on the walls, as defined from the asymptotic behavior of the electrostatic potential and ion concentration profiles away from the surface.[32] Any kind of asymmetry between the anions and cations make the electroneutral walls behave as if they were charged, which, as we shall see, has important consequences for the wall-wall interaction when the surface separation is large enough. We shall also see that the simultaneous inclusion of image and dispersion interactions has important consequences for the magnitude of the effects of the latter. We have not attempted to include any effects of unequal hydration of the ions, which is also a source of ionic asymmetry that can bring about a charge separation. Marčelja[33] investigated such effects and the consequences for interactions between bubbles.

To include image forces in models of electric double layers introduces some complications. As the image forces are electrostatic in nature, they are screened by electrolyte. This screening is brought about by ion-ion correlations. It is, for example, not enough to include only the self-image interaction between an ion and the dielectric boundaries since this would lead to an overestimation of the range and magnitude of the effects of image forces. In order to describe the screening of the image interactions in a consistent manner, explicit consideration of the ionic pair correlations of the inhomogeneous electrolyte near the surface is required.

A simple alternative is to include the screening of the image forces *a priori* in some approximate way. A famous example is the Onsager–Samaras theory,[34] where the screening of the image charges is assumed to be equal to the screening of a charge in bulk as given by Debye–Hückel theory. This approach has the obvious disadvantage that the screening ability of an inhomogeneous electrolyte close to a surface need not be very similar to the screening ability of a bulk electrolyte. The ion-ion correlations decay exponentially perpendicularly to the surface (like in bulk), but as a power law in the lateral direction. It is, however, not necessary to use the bulk correlations since in the low coupling limit, where Debye–Hückel theory is valid, analytic expressions for the correlation functions near a dielectric surface can be found in some cases.[35] For systems that are not close to the low coupling limit, Debye–Hückel theory often gives rather poor results, however. More sophisticated approaches, such as simulations or integral equation theory, are appropriate in these cases. If the ion-ion correlations in the inhomogeneous electrolyte are explicitly included in the theory, the screening of image forces will automatically be included at the same level of sophistication as the correlations themselves.

In the present work, ion-ion correlations in the inhomogeneous electrolyte between the walls are calculated with the anisotropic hypernetted chain (AHNC) method,[36,37] which was designed from the outset to correctly treat image interactions. The *only* approximation made is to use the hypernetted chain (HNC) closure for the anisotropic ion-ion correlation functions. These pair correlation functions and the concentration profiles near the surfaces are determined self-consistently by iteration, the former in both ordinary and Fourier space.

For approaches that only consider image interaction in ordinary space, like simulations, the treatment of image interactions for electrolytes between two planar walls can be cumbersome due to the presence of an infinite number of multiple image charges. In the AHNC method this is of no concern since the potential from the multiple images can be written in Fourier space in a closed analytic form.

By the AHNC method, image forces have been shown to give rise to attraction between two uncharged walls immersed in a primitive model electrolyte solution.[5] In addition, the screening of the static component of the van der Waals attraction is automatically included. In the presence of image forces one obtains a repulsive contribution to the ionic pressure that exactly cancels the zero-frequency van der Waals interaction,[5] thus accounting for the screening.

The outline of this paper is as follows. First, the model employed as well as the methods used for calculating pair correlations, concentration profiles, and the interaction pressure are presented. Then the main results are presented for the profiles, the pressure, and its components, which originate from distinct physical mechanisms. The significance of the results is discussed with special emphasis on the dependence of the wall-wall pressure on surface separation, kind of ions, and electrolyte concentration. Finally the major findings of this paper are summarized.

II. METHOD

A. Model

The system under study consists of a primitive model electrolyte solution in a slit between two parallel uncharged walls (semi-infinite dielectric slabs). The electrolyte in the slit is in equilibrium with a bulk electrolyte solution of a specified composition. The bulk concentration of ion species i is denoted n_i^{bulk}. The walls are smooth and separated by a distance, D, that is defined as the distance between the dielectric interfaces, see Fig. 1. The distance of closest approach of the ion centers to each interface is denoted b. We adopt a coordinate system with its origin at the plane in the middle of the slit (the midplane). The z axis is perpendicular to the walls and the x and y axes are parallel to them. The lateral distance along the wall between two points $\mathbf{r}=(x,y,z)$ and $\mathbf{r}'=(x',y',z')$ is denoted $R=[(x-x')^2+(y-y')^2]^{1/2}$.

The interaction potential for a pair of ions of species i and j is given by

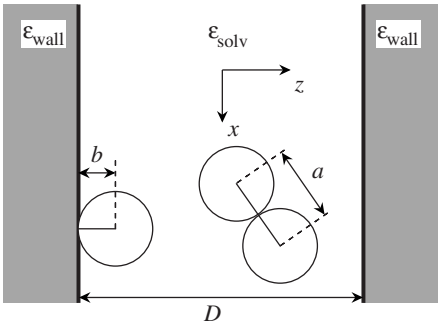

FIG. 1. Two electroneutral walls separated by an electrolyte phase in equilibrium with a bulk solution. The walls and the solvent have different dielectric properties characterized by ϵ_{wall} and ϵ_{solv}, respectively. The wall-wall separation is D as counted between the dielectric discontinuities at the wall surfaces. The distance of closest approach of the ion centers to the surfaces is b. The ion-ion hard core contact distance is a as counted between the ion centers. The coordinate system has its origin at the midplane between the surfaces with the z axis perpendicular and the x and y axes parallel to them.

$$u_{ij} = u_{ij}^{\text{core}} + u_{ij}^{\text{Coul}} + u_{ij}^{\text{im}}, \tag{1}$$

where $u_{ij}^{\text{core}}(\mathbf{r},\mathbf{r}')$ is zero for $|\mathbf{r}-\mathbf{r}'|>a$ and infinite otherwise for all pairs of ions (i.e., the ion centers can approach each other up to a distance a), u_{ij}^{im} is the potential for the image force interactions, see below, and $u_{ij}^{\text{Coul}}(\mathbf{r},\mathbf{r}')$ is the Coulomb potential,

$$u_{ij}^{\text{Coul}}(\mathbf{r},\mathbf{r}') = \frac{q_i q_j}{4\pi\epsilon_{\text{solv}}(0)\epsilon_0|\mathbf{r}-\mathbf{r}'|}, \tag{2}$$

where ϵ_0 is the permittivity of the vacuum, $\epsilon_{\text{solv}}(0)$ is the dielectric function at zero frequency (the dielectric constant) of the solvent, and q_l, $l=i,j$, is the ionic charge. Due to the symmetry of the system in the slit, the coordinate dependence of $u_{ij}(\mathbf{r},\mathbf{r}')$ can be written as $u_{ij}(R,z,z')$. The two-dimensional Fourier transform of u_{ij}^{im} (Hankel transform for variable R) is given by[36]

$$\hat{u}_{ij}^{\text{im}}(k,z,z'|D) = \frac{q_i q_j}{\epsilon_{\text{solv}}(0)\epsilon_0 k}\left[\frac{\epsilon_D(0)}{e^{kD}-\epsilon_D(0)}\cosh(kz)\cosh(kz') + \frac{\epsilon_D(0)}{e^{kD}+\epsilon_D(0)}\sinh(kz)\sinh(kz')\right], \tag{3}$$

where the D dependence of the ion-ion image interaction is shown explicitly. We have defined

$$\epsilon_D(\omega) = \frac{\epsilon_{\text{solv}}(\omega)-\epsilon_{\text{wall}}(\omega)}{\epsilon_{\text{solv}}(\omega)+\epsilon_{\text{wall}}(\omega)}, \tag{4}$$

where $\epsilon_{\text{solv}}(\omega)$ and $\epsilon_{\text{wall}}(\omega)$ denote the frequency dependent dielectric functions of the solvent and the wall, respectively. For the image interactions only the static (zero-frequency) dielectric response matters, but for the van der Waals interactions information about $\epsilon_{\text{solv}}(\omega)$ and $\epsilon_{\text{wall}}(\omega)$ for imaginary ω is needed [cf. Eq. (12) below]. The dielectric constant of the solvent, $\epsilon_{\text{solv}}(0)$, is taken as 78.36, that of pure water at 25 °C. The wall dielectric constant, $\epsilon_{\text{wall}}(0)$, is set equal to 2.54, the static dielectric constant of polystyrene at the same temperature.[38] The hard core contact distance, a, is taken to be 4.6 Å for all ions.

The ion-wall interaction potential is given by

$$\nu_i = \nu_i^{\text{im}} + \nu_i^{\text{disp}} + \nu_i^{\text{core}}, \tag{5}$$

where ν_i^{im} is due to ions interacting with their own images and equals[36]

$$\nu_i^{\text{im}}(z|D) = \tfrac{1}{2}u_{\text{ii}}^{\text{im}}(0,z,z|D) \tag{6}$$

[note that in Eq. (6) of our previous paper,[22] the factor 1/2 is unfortunately missing due to a misprint]. The term ν_i^{disp} in Eq. (5) is the potential due to ion-wall dispersion forces

$$\nu_i^{\text{disp}}(z|D) = B_i\left(\frac{1}{|z+D/2|^3}+\frac{1}{|z-D/2|^3}\right), \tag{7}$$

where B_i gives the strength of the interaction (see below). The ion-wall hard core interaction ν_i^{core} is zero if $|z|\le D/2-b$ and infinite otherwise, with $b=3$ Å for all i. Thus, the ion centers cannot approach the dielectric interface closer than 3 Å, see Fig. 1. Thereby, the unphysical singularities of ν_i^{disp} at $z=\pm D/2$ are avoided. Note that the ion-ion contact distance a, the "ion diameter," is different from $2b$.

In Eq. (7) we have as an approximation set the dispersion interaction potential with two walls equal to the sum of the interactions with each single wall using the long-distance asymptotic form of the ion-wall potential. The coefficient B_i can be calculated from Lifshitz theory as described in Ref. 8. Since we are mainly interested in dispersion forces as a source of asymmetry in the ion model, we restrict ourselves to two combinations of values for B_i: $B_+=0$, $B_-=-40$ kJ Å^3 mol^{-1} and $B_+=B_-=0$. The value $B_-=-40$ kJ Å^3 mol^{-1} is based on quantum mechanical calculations of the dynamic polarizability of iodide,[22] which is taken as an example of a highly polarizable ion. The two combinations of values for B_+ and B_- are intended to correspond to a large and no contribution, respectively, to the anion-cation asymmetry. It should be noted that no net dispersion force is exerted on an ion that has the same polarizability as its surroundings. The choice of $B_i=0$ thus corresponds to the assumption that the ions are as polarizable as water. Electrolyte models with only such ions are referred to as "nonpolarizable" below. Electrolyte models with $B_-\neq 0$ are conversely referred to as "polarizable."

We have modeled the walls as slabs of semi-infinite thicknesses. The results are also valid for walls of finite widths provided the electrostatic interactions across the walls are sufficiently weak, so ions on either side of the walls do not correlate with each other.

B. The AHNC method

In the AHNC method[36] one self-consistently solves a set of equations for the equilibrium concentration profiles, $n_i(z)$, the total pair correlation functions, $h_{ij}(R,z,z')$, and the direct correlation functions, $c_{ij}(R,z,z')$, of an inhomogeneous electrolyte. The set of equations consists of the Ornstein–Zernike equation for inhomogeneous liquids, the HNC closure for the pair correlation functions, and an equation for the density profiles. The latter is obtained from the condition of thermodynamic equilibrium, which specifies that the chemical potential for each species is equal everywhere in the slit. The

mean chemical potential in the slit is set equal to that of a bulk electrolyte of specified composition. Because the excess part of the chemical potential can be expressed as a known functional of the correlation functions within the HNC approximation, the equilibrium density profile can easily be determined once the correlation functions are known. In practice, the problem is solved by solving the closure combined with the Ornstein–Zernike equation for the pair correlation functions by iteration given a fixed set of density profiles. Once a converged set of pair correlation functions is obtained a new set of concentration profiles is calculated from the profile equation, and the correlation functions are then recalculated for the new density profiles. The cycle is repeated until self-consistency is attained.

The accuracy of the AHNC method has been tested against simulations[37,39–42] and was found to be excellent under most conditions. An exception is the situation where the concentration of ions reaches very high values somewhere in the slit. The ion-ion contact values of the pair correlation functions then tend to be overestimated. As this systematic error mainly occurs at very high surface charge densities it is of no concern for the systems that are of interest here. The error can, however, be minimized by including a so-called reference bridge function in the closure[40] if needed.

Of more concern is the fact that the HNC approximation tends to be inaccurate for the restricted primitive model in regions of parameter space that corresponds to 2:2 electrolyte at low concentrations.[43] There are also regions in parameter space where no solution exists for the HNC approximation for bulk electrolyte solutions.[44] This occurs for low temperatures or strong electrostatic interactions (i.e., interaction energies that are large compared to the thermal energy). The problems with the HNC approximation under these conditions are related to the incorrect way the long range tails of the density-density direct correlation functions are handled.[45] These matters are important in the current context because the image charge repulsions make the ion concentration between the walls much smaller than the bulk concentration for small separations. The total interaction between ions is also much larger than in the bulk due to the presence of multiple image charges in close proximity to the wall surfaces when the wall-wall separation is small. The strong image interactions between the divalent ions thus give a situation like that at low temperatures in the bulk. For these reasons, in all cases in this work where divalent ions are present, there exists some minimum separation below which one enters into the part of parameter space where the HNC approximation fails and no solution is found. As we shall see, the failure is not of great concern since in most cases it occurs when there is little electrolyte left in the slit between the walls. Then the ions in the slit do not contribute much to the net wall-wall interaction pressure.

There are indeed similarities in the HNC correlation functions for the cases of inhomogeneous electrolyte for small surface separations and bulk electrolyte at low temperatures. The most striking similarity for low ion concentrations is the appearance of a spurious unphysical peak in the correlation function between like-charged ions for a separation of roughly two ion diameters. In the bulk this peak grows dramatically when one approaches the region where no solution exists by lowering the temperature. The behavior for the inhomogeneous systems with uncharged surfaces in the presence of image charges is very similar when the wall-wall separation approaches the distance where convergence is lost.

The minimum separation for convergence of the HNC approximation is specified for each case investigated below. The results in the close vicinity of this separation should be interpreted with some caution. We will, however, use some analytic limiting results for the density profiles between the walls for short wall-wall separations to bridge the gap where the HNC approximation fails, see Appendix A. As we shall see below, in this regime we have strong net attraction between the walls regardless of the details of the structure of the electrolyte in the slit.

In all other cases considered here, the HNC approximation is reliable. Indeed, for concentrations near the bulk concentrations considered in this work it gives good results even for 2:2 electrolytes.[43]

C. The various contributions to the wall-wall interaction pressure

The total pressure between the walls can be written as a sum of the pressure exerted due to the presence of ions, P^{ion}, and pressure from the van der Waals interactions between the walls, $P_{\text{vdW}}^{\text{wall}}$,

$$P^{\text{tot}} = P^{\text{ion}} + P_{\text{vdW}}^{\text{wall}}. \tag{8}$$

The quantity relevant for the interaction between the walls is the net pressure, i.e., the difference between the pressure in the slit P^{tot} and the pressure in the bulk electrolyte, P^{bulk},

$$\Delta P^{\text{tot}} = P^{\text{tot}} - P^{\text{bulk}}. \tag{9}$$

The bulk pressure contains contributions from the ions only, so the net pressure from ions is equal to

$$\Delta P^{\text{ion}} = P^{\text{ion}} - P^{\text{bulk}}, \tag{10}$$

and we can write

$$\Delta P^{\text{tot}} = \Delta P^{\text{ion}} + P_{\text{vdW}}^{\text{wall}}. \tag{11}$$

The van der Waals pressure is calculated from nonretarded Lifshitz theory[4,46]

$$P_{\text{vdW}}^{\text{wall}} = -\frac{k_B T}{4\pi D^3} {\sum_{l=0}^{\infty}}' \sum_{s=1}^{\infty} \frac{\epsilon_D^{2s}(i\omega_l)}{s^3}, \tag{12}$$

where the prime on the sum over l means that the term $l=0$ should be multiplied by 1/2 and where $\epsilon_D(\omega)$, Eq. (4), is evaluated at imaginary frequency $i\omega_l$, where $\omega_l = l2\pi k_B T/\hbar$. The term corresponding to $l=0$ will be denoted as $P_{\text{vdW}(0)}^{\text{wall}}$ and referred to as "the zero-frequency van der Waals pressure," while the rest of the sum will be denoted as $P_{\text{vdW(hf)}}^{\text{wall}}$ and referred to as "the high-frequency van der Waals pressure."

In this work $P_{\text{vdW}}^{\text{wall}}$ as a function surface separation D is the same in all cases investigated. Only P^{ion}, P^{bulk}, and there-

fore ΔP^{ion} differ. For reasons explained below we will always add $P^{\text{wall}}_{\text{vdW}(0)}$ to the ionic pressure, so we will mostly study

$$\Delta P = \Delta P^{\text{ion}} + P^{\text{wall}}_{\text{vdW}(0)} \tag{13}$$

rather than the total net pressure defined in Eqs. (9) and (11). To obtain ΔP^{tot} we have to add $P^{\text{wall}}_{\text{vdW(hf)}}$, which will be shown separately.

The pressure P^{ion} evaluated at the midplane between the walls can be subdivided into physically distinct contributions according to

$$P^{\text{ion}} = P^{\text{ion}}_{\text{kin}} + P^{\text{ion}}_{\text{Coul}} + P^{\text{ion}}_{\text{core}} + P^{\text{ion}}_{\text{im}} + P^{\text{ion}}_{\text{disp}}. \tag{14}$$

$P^{\text{ion}}_{\text{kin}}$ is the kinetic (ideal) contribution to the pressure given by

$$P^{\text{ion}}_{\text{kin}} = k_B T \sum_i n_i(0), \tag{15}$$

where $n_i(0)$ is the concentration at the midplane. $P^{\text{ion}}_{\text{Coul}}$ and $P^{\text{ion}}_{\text{core}}$ are the contributions due to electrostatic and hard-sphere interactions across the midplane, respectively. $P^{\text{ion}}_{\text{im}}$ is the pressure due to image forces and $P^{\text{ion}}_{\text{disp}}$ originates from the direct dispersion interactions between the ions and walls. The last four pressure contributions are expressed in terms of the ionic distribution functions in Appendix B.

$P^{\text{ion}}_{\text{kin}}$, $P^{\text{ion}}_{\text{Coul}}$, and $P^{\text{ion}}_{\text{core}}$ approach the corresponding components of the bulk pressure for large D. The sum of these three pressure components is sometimes referred to in what follows as the *osmotic pressure*. It is useful to discuss the pressure in terms of these components when one wants to understand the differences between the osmotic pressure of the inhomogeneous electrolyte in the slit and that of the bulk electrolyte. When any of these three components is written with a capital Δ as prefix, it denotes the difference between the value in the slit and in the bulk. For example, $\Delta P^{\text{ion}}_{\text{kin}} = k_B T \Sigma_i [n_i(0) - n_i^{\text{bulk}}]$. These differences obviously all go to zero when $D \to \infty$.

$P^{\text{ion}}_{\text{im}}$ and $P^{\text{ion}}_{\text{disp}}$ do not have any counterparts in the bulk. For large wall-wall separations $P^{\text{ion}}_{\text{im}}$ asymptotically tends to $-P^{\text{wall}}_{\text{vdW}(0)}$.[5] Thus, the sum $P^{\text{ion}}_{\text{im}} + P^{\text{wall}}_{\text{vdW}(0)}$ decays faster to zero than any one of the terms do individually. Physically, this corresponds to the screening of the static van der Waals interactions between the walls by the intervening electrolyte.[4] For this reason we shall in what follows always consider the sum $P^{\text{ion}}_{\text{im}} + P^{\text{wall}}_{\text{vdW}(0)}$. Note that the high-frequency van der Waals term is not screened since it corresponds to fluctuations that are too rapid for the ionic configurations to respond to. The ions do, however, respond by their electronic polarization (which is expressed by their polarizability). This gives rise to the dispersion forces between the ions and the walls.

The total P^{ion} can alternatively be evaluated at one of the wall surfaces. Sometimes this is advantageous, see Appendix B for details.

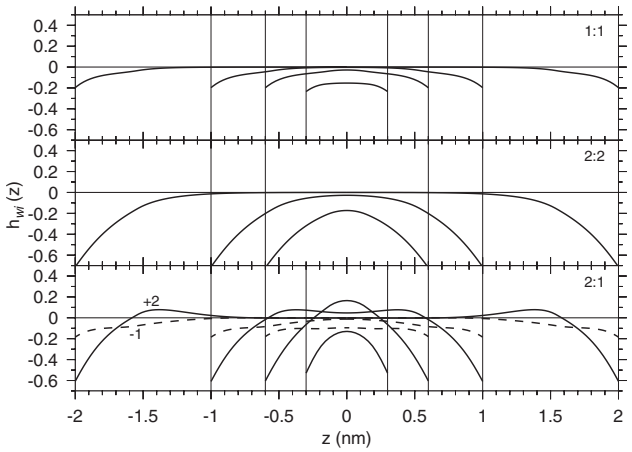

FIG. 2. Ion-wall correlation functions for the cases of 1:1, 2:2, and 2:1 electrolytes with nonpolarizable ions (upper, middle, and lower panels, respectively) at a bulk concentration of 0.500M. The functions are shown for wall-wall separations of 1.2, 1.8, 2.6, and 4.6 nm in the 1:1 and 2:1 cases and for 1.8, 2.6, and 4.6 nm in the 2:2 case. In the charge-symmetric cases the cation and anion correlation functions are identical and are represented by a single (full) curve. In the 2:1 case the full lines correspond to the divalent ion-wall correlation function (marked "+2") and the dashed lines to the monovalent one (marked "−1"). The corresponding curves for the 2:1 electrolyte would look the same, except for a change in the sign of the ions.

III. RESULTS AND DISCUSSION

A. Concentration profiles between the walls

Figure 2 shows concentration profiles for a range of wall-wall separations for various 0.500M electrolytes with nonpolarizable ions (in short "nonpolarizable electrolytes"). The concentration profile for each species of ion is presented as the ion-wall correlation function, i.e., the relative deviation from the bulk concentration of that species of ion,

$$h_{wi}(z) = \frac{n_i(z) - n_i^{\text{bulk}}}{n_i^{\text{bulk}}}. \tag{16}$$

For all systems shown in Fig. 2 there is a depletion of ions close to the surfaces. This is caused by electrostatic interactions: partly from the repulsive image forces and partly due to effects of confinement (the presence of a surface) on the electrolyte structure. The latter effect can be explained as follows. An ion in close proximity to an electroneutral surface is surrounded by a charge density of opposite sign (i.e., its "ion cloud") that is located mainly on the side away from the surface. Therefore the ion is attracted electrostatically by the ion cloud in the direction away from the surface. This effect adds to the repulsion of ions from the surface due to image charges. An electrostatic force due to confinement is a general feature for ions in the neighborhood of both charged of uncharged surfaces since the distribution of ions around each ion must be spatially asymmetric there.[31,32,47] There are also forces from ion-ion core interactions due to excluded volume effects, which are important for high electrolyte concentrations.

From a comparison of the 1:1 and 2:2 electrolyte systems in Fig. 2 it is apparent that there is a much larger degree of depletion close to the surfaces for divalent ions than for monovalent ions. The same dependence of valency can be

seen for the anion and cation profiles for the 2:1 electrolyte systems. These differences in depletion are not surprising in light of the fact that the strength of the self-image interaction, ν^{im}, is proportional to the square of the valency so that it is four times stronger for divalent ions than for monovalent. The confinement effect is also stronger for divalent ions. The asymmetric ion cloud around a divalent ion has twice the charge of that around a monovalent one, so the resulting force away from the surface is stronger in the divalent case.

For the symmetric 1:1 and 2:2 electrolytes the anion and cation profiles are identical because the forces on an anion and a cation are identical for the same distance from the wall. Hence there is no charge separation outside the surface. In the 2:1 case there is charge separation, however, since the magnitude and distance dependence of the force is different for ions of different valency. We see from the concentration profiles that there is a region with excess negative charge close to each wall and an excess of positive charge some distance away. The total charge in the electrolyte phase is, of course, equal to zero. For a 1:2 electrolyte the profiles for monovalent and divalent ions would look exactly the same as those of a 2:1 electrolyte since the surface is uncharged and the anion and cation sizes are the same, but the sign of the charge distribution would be reversed.

Thus, in general, the presence of an electroneutral surface induces a perturbation in the structure of the electrolyte that for small distances is determined by the effective interactions between the ions and the surface. For large distances from the surface the distance dependence of the perturbation is entirely determined by the bulk ion-ion correlations but the magnitude depends on the interactions with the surface.[48–50] For low to medium electrolyte concentrations the decay of the bulk correlations for large distances is exponential with a decay length $1/\kappa$ that tends to the usual Debye length in the limit of zero bulk electrolyte concentration. The ion density profiles away from a surface also have a decay length $1/\kappa$ in most cases (an important exception is totally symmetric electrolytes, see below).

For high concentrations both the bulk correlations and the density profiles change from a monotonic exponential decay to an exponentially damped oscillatory decay. The transition between the two behaviors is determined by the bulk electrolyte and occurs at an electrolyte concentration that depends on the ionic species present. For ions with $a=4.6$ Å the transition between monotonic and oscillatory exponential decay occurs at bulk concentration of $0.73M$ for 1:1, about $0.3M$ for 2:2, and $0.087M$ for 2:1 electrolytes.[51,52] (Close to the surface the ion concentration profiles may, however, have a small number of oscillations even when the decay for large distances is plainly exponential.)

For an uncharged surface these results for the decay do not hold when the electrolyte is totally symmetric (i.e., when anions and cations differ *only* by the sign of their charges). As we have seen, the charge density in the electrolyte is then zero outside the uncharged surface. In this case the ion concentration profiles for large distances from the surface are dominated by a higher order term with shorter decay length (denoted $1/b_S$ in Ref. 51) that is approximately $1/2\kappa$ for low electrolyte concentrations. The term with decay length $1/\kappa$ in the concentration profile does not contribute since its coefficient is zero in this case (in other words, the effective surface charge density of the uncharged walls is zero[53]). As a consequence, the transition to oscillatory decay for the profile occurs at a different bulk electrolyte concentration. For ions with $a=4.6$ Å it takes place[51] at about $1.0M$ for 1:1 electrolyte and above $0.3M$ for 2:2 electrolyte (the precise concentration in the latter case has not been determined). The bulk correlations still have decay length $1/\kappa$, and the profiles would also have this decay length if the surfaces were charged. Note that the wall-wall interaction pressure as a function of D has in general the same decay length for large separations as the concentration profiles.[49]

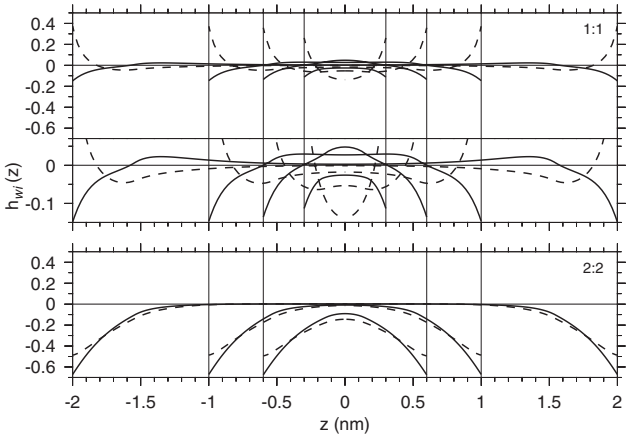

FIG. 3. Ion-wall correlation functions for charge-symmetric electrolytes with polarizable anions at a bulk concentration of $0.500M$. The top and bottom panels show 1:1 and 2:2 electrolytes, respectively, on the same scale, while the middle panel shows the same curves as the upper one on an expanded scale. The functions are shown for wall-wall separations of 1.2, 1.8, 2.6, and 4.6 nm (the smallest separation is not shown for the 2:2 case). The full lines show the cation-wall correlation functions and the dashed lines show the anion-wall functions. The strengths of the ion-wall dispersion interaction are given by $B_-=-40$ kJ Å^3 mol^{-1} and $B_+=0$ (the same values are used for all cases with polarizable ions in this paper).

As soon as the electrolyte has any kind of anion/cation asymmetry the charge density outside an uncharged surface is nonzero. The effective surface charge density of the electroneutral surface is then also nonzero. We shall here explore the consequences the asymmetry brought about by different ion-wall dispersion interactions for anions and cations.

The concentration profiles for $0.500M$ 1:1 and 2:2 electrolytes with polarizable ions (in short "polarizable electrolytes") are shown in Fig. 3. The strength of the anion-wall dispersion interaction is $B_-=-40$ kJ Å^3 mol^{-1}, while the cation-wall dispersion interaction is neglected. There is thus an attractive dispersion force acting on the anions in addition to the repulsive image force. Since the forces on the anions and cations differ, a charge density profile is built up outside each electroneutral surface. The dispersion forces make the amount of anions close to each surface increase compared to the case of the nonpolarizable electrolyte in Fig. 2. For the 1:1 electrolyte in Fig. 3 the anion concentration close to the wall is larger than the bulk concentration. The cation concentration remains below the bulk value there, but it is lifted above the bulk value some distance away from the surface. This is due to an increase in the total number of ions between

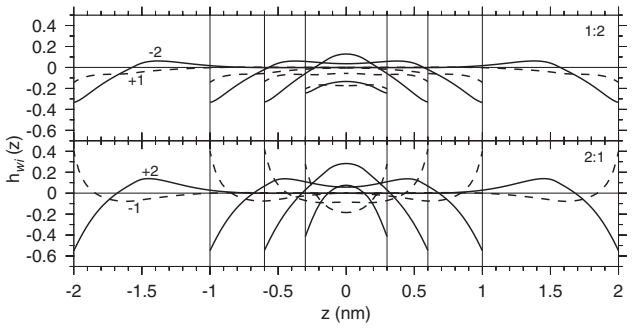

FIG. 4. Ion-wall correlation functions for 1:2 and 2:1 electrolytes with polarizable anions (upper and lower panels, respectively) at a bulk concentration of 0.500*M*. The anions are divalent in the 1:2 electrolyte and monovalent in the 2:1 electrolyte. The functions are shown for wall-wall separations of 1.2, 1.8, 2.6, and 4.6 nm. The full lines correspond to the divalent ion-wall correlation functions and the dashed lines to the monovalent ion-wall functions. These are marked with the appropriate valency in the figure.

the surfaces brought in there from the bulk by the dispersion attraction on the anions. The number of cations then has to increase to maintain electroneutrality.

For the 2:2 electrolyte, on the other hand, the dispersion forces do not change the concentration profiles much compared to the nonpolarizable case. This difference is due to the much stronger repulsive image forces and confinement effect for divalent ions, which dominate here and counteract the attractive dispersion interactions. Also in this case the dispersion forces on the anions cause an increase in the total number of ions between the surfaces, but the effect on the profiles is small.

These kinds of differences between monovalent and divalent ions can also be seen for charge-asymmetric electrolytes in Fig. 4, which shows the profiles for 0.500*M* polarizable 1:2 and 2:1 electrolytes. These profiles correspond to those in the bottom panel in Fig. 2 for the nonpolarizable electrolytes (remember that the profiles for 1:2 and 2:1 electrolytes are identical for the nonpolarizable case apart from the sign of the ionic charges). By comparing Figs. 2 and 4 we see that the dispersion forces on the anions cause an increase in anion concentration close to the walls that is greater for the 2:1 electrolyte compared to the 1:2 electrolyte. In the former case the anions are monovalent while they are divalent in the latter. Concurrent with the increase in anion concentration there is an increase in cation concentration for the same reason as before. This increase is also much greater for the 2:1 electrolyte than for the 1:2 electrolyte.

The decay of the concentration profiles away from the surface for large surface separations contains an exponentially decaying contribution with a decay length determined by the bulk electrolyte, as in the case of nonpolarizable electrolytes. However, for large distances from the surface the decay ultimately goes over to a power-law decay that originates from dispersion interactions coupled to the ion-ion electrostatic interactions. The magnitude of the large distance tail of each profile depends on the ion-wall interactions.

B. Wall-wall interaction pressure

1. Nonpolarizable ions

The pressure between two electroneutral walls has been calculated for 1:1, 2:2, and 2:1/1:2 nonpolarizable electrolytes at bulk concentrations of 0.250*M*, 0.500*M*, and 1.00*M*. The net pressure ΔP is obtained from Eq. (13). Note that for nonpolarizable ions the pressures for a 1:2 and a 2:1 electrolyte are identical since the ions only differ in the signs of the charges, which do not affect the interaction pressure between uncharged walls.

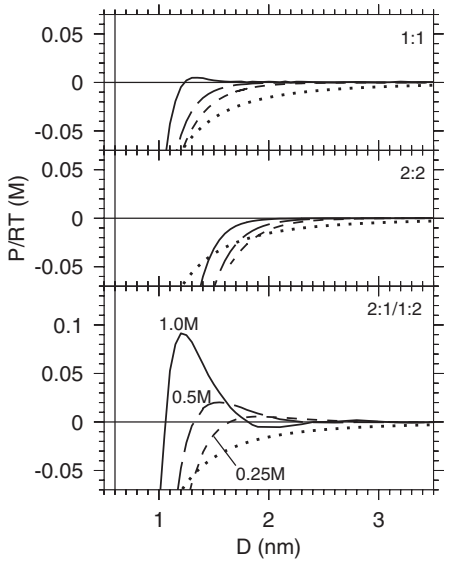

FIG. 5. Net pressure between uncharged walls as function of the wall-wall separation D in the presence of various electrolytes with nonpolarizable ions. The upper panel shows the case of the 1:1 electrolyte, the middle panel the 2:2 electrolyte, and the bottom panel 2:1 and 1:2 electrolytes (which have the same pressure). The bulk electrolyte concentrations are 0.250, 0.500, and 1.00*M* (short-dashed, long-dashed, and full lines, respectively). The dotted lines show the high-frequency van der Waals pressure, $P^{\text{wall}}_{\text{vdW(hf)}}$, which is the same in all cases. The other curves give the remaining net pressure, $\Delta P = \Delta P^{\text{ion}} + P^{\text{wall}}_{\text{vdW(0)}}$, including the zero-frequency van der Waals pressure. Since the ions are nonpolarizable the ions interact with the walls via image forces and "hard wall" interactions only. The full vertical lines denote the smallest separation, 0.6 nm, for which ions can be present between the walls.

Figure 5 shows ΔP as a function of the wall-wall separation D. The high-frequency part of the van der Waals pressure, $P^{\text{wall}}_{\text{vdW(hf)}}$, is shown separately and should be added to obtain the total net pressure ΔP^{tot}. A common feature in all cases is that ΔP is attractive for short surface separations. In some cases the pressure remains attractive for larger separation, while there is a repulsive peak in other.

Let us first consider the behavior of ΔP for short separations. The attraction seen in Fig. 5 actually extends all the way down to wall-wall contact. The limiting value of P^{ion} when $D \to 2b$ (which corresponds to a single layer of ions between the surfaces) can be calculated analytically for electroneutral surfaces. As shown in Appendix A we have

$$\lim_{D\to 2b} P^{\text{ion}} = k_B T (n_+^{\text{bulk}} + n_-^{\text{bulk}}) \gamma_\pm \exp\left[- \frac{q_+ \nu_-(0) + |q_-| \nu_+(0)}{(q_+ + |q_-|) k_B T} \right], \tag{17}$$

where $\gamma_\pm$ is the bulk mean activity coefficient. $P^{\text{wall}}_{\text{vdW(0)}}$ can also be calculated analytically, following Eq. (12). The values of P^{ion} and ΔP for $D = 2b = 0.6$ nm for the various electrolytes are shown in Table I (the HNC values of $\gamma_\pm$ and

TABLE I. Various wall-wall interaction pressures in molar units for the same systems as in Figs. 5 and 6. The concentrations and types of electrolyte are shown in the first two columns, where (*p*) (for polarizable) indicates that the anions interact with the walls via dispersion forces. The following three columns show the net and ionic pressures at surface separation $D=2b=0.6$ nm (the smallest separation for which there are ions between the walls) and the bulk pressure, respectively. The last column shows the smallest separation for which a solution was found, along with the net pressure at that separation (shown in parentheses). A star (*) indicates that the pressure value is listed in column 3. At separation $D=0.6$ nm the zero-frequency van der Waals interaction contributes to $\Delta P/RT$ by an amount of $-0.31M$ in all cases. The high-frequency van der Waals interaction is $-0.57M$ at the same separation.

Conc.	Type	$\Delta P/RT$ $D=0.6$ nm	P^{ion}/RT $D=0.6$ nm	P^{bulk}/RT	D^{min}/nm ($\Delta P/RT$)
0.250	1:1	−0.78	1.5×10^{-2}	0.49	0.60 (*)
	2:2	−0.62	1.3×10^{-7}	0.31	1.65 (−0.047)
	1:2/2:1	−0.97	4.8×10^{-4}	0.66	0.97 (−0.38)
	2:1(*p*)	−0.97	1.1×10^{-3}	0.66	1.05 (−0.15)
0.500	1:1	−1.31	3.1×10^{-2}	1.03	0.60 (*)
	1:1(*p*)	−1.28	5.7×10^{-2}	1.03	0.60 (*)
	2:2	−0.96	2.1×10^{-7}	0.65	1.32 (−0.17)
	2:2(*p*)	−0.96	3.7×10^{-7}	0.65	1.35 (−0.090)
	1:2/2:1	−1.75	9.8×10^{-4}	1.44	0.85 (−0.86)
	1:2(*p*)	−1.75	1.5×10^{-3}	1.44	0.95 (−0.33)
	2:1(*p*)	−1.75	2.2×10^{-3}	1.44	0.95 (−0.18)
1.00	1:1	−2.56	7.6×10^{-2}	2.33	0.60 (*)
	1:1(*p*)	−2.50	1.4×10^{-1}	2.33	0.60 (*)
	2:2	−1.84	3.7×10^{-7}	1.53	1.08 (−0.53)
	2:2	−1.84	6.8×10^{-7}	1.53	1.20 (−0.076)
	1:2/2:1	−3.90	2.6×10^{-3}	3.59	0.74 (−2.04)
	1:2(*p*)	−3.90	3.9×10^{-3}	3.59	0.80 (−0.55)

P^{bulk} have been used in the calculations; the latter is also shown in the table). We see that P^{ion} is small in all cases. This is due to the strongly repulsive image interactions contained in ν_+ and ν_- in the exponent of Eq. (17). Therefore, ΔP for small D is dominated by $P^{\text{wall}}_{\text{vdW}(0)}-P^{\text{bulk}}$, which is strictly negative since $P^{\text{wall}}_{\text{vdW}(0)}<0$ and $P^{\text{bulk}}>0$. In Fig. 5 the surface separation $D=0.6$ nm is marked as a vertical line. For smaller D there can be no ions between the walls, and the interaction pressure for such separations is given simply by $\Delta P=P^{\text{wall}}_{\text{vdW}(0)}-P^{\text{bulk}}$.

As discussed in Sec. II B above, the HNC approximation fails to converge for the systems with divalent ions when the surface separation is so small that there are very strong image charge interactions and a large degree of ion depletion. In this region the net pressure is strongly attractive precisely because of the small concentration of ions in the slit relative to the bulk. In Table I we have listed the surface separation D^{min} down to which we have managed to calculate the pressure in these cases. The corresponding pressures are also shown. For all cases in Fig. 5 except for the $0.25M$ 2:2 electrolyte the problematic region lies well outside the pressure range shown in the figure. The lack of data between D^{min} and 0.6 nm is not of great concern since we know the pressure for $D=0.6$ nm, and the main thing that happens in this interval is that ions leave the slit when D is decreased and ΔP turns more negative (see also the discussion in Sec. III C below).

Let us now turn to the behavior at larger surface separations. In all the charge-symmetric cases except that of $1.00M$ 1:1 salt, the net pressure, ΔP, is attractive for all separations investigated. The main difference between 1:1 and 2:2 electrolytes is that the attraction is stronger in the latter case for a given wall-wall separation and concentration. One reason for the attraction is the depletion of ions due to the repulsive image forces and confinement effects. A depletion is, however, not needed to explain an attractive ΔP. In the Ninham–Parsegian theory[54] for Debye–Hückel screening of zero-frequency van der Waals interactions, it is assumed that the electrolyte concentration in the slit is everywhere equal to that of the bulk. As shown by comparison with AHNC calculations[5] this simple theory performs surprisingly well for 1:1 electrolytes at low concentrations. When ΔP from the Ninham–Parsegian theory is heuristically corrected for the depletion of ions near the surfaces, it gives very good agreement with the AHNC results for the $0.5M$ 1:1 electrolyte when $D>1$ nm. However, for small surface separations the depletion of ions in the whole slit is very important, as we have seen above.

A depletion attraction solely due to confinement (no image interactions) has previously been found between uncharged surfaces by means of grand canonical Monte Carlo simulations.[42,55] In Ref. 55 it was also found that for very high bulk electrolyte concentration the pressure is dominated by ion packing effects and has repulsive peaks. It is the onset of this type of behavior, related to the fact that the concentration profiles turn oscillatory at high concentration, that causes the small repulsion seen in the $1.00M$ 1:1 salt case of the present work.

For the 2:1 and 1:2 electrolytes in Fig. 5 the ionic pressure is repulsive for some range of separations for all concentrations considered. This behavior is in stark contrast to that in the charge-symmetric cases where the pressure is

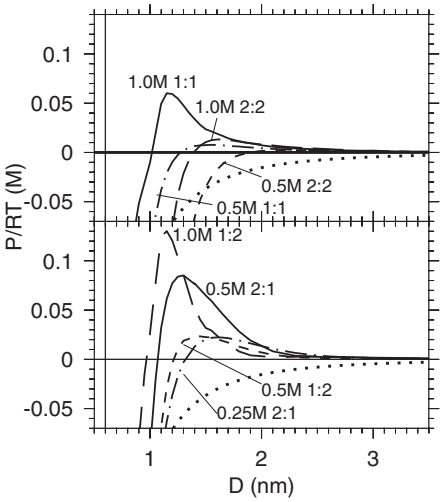

FIG. 6. Same as Fig. 5 but for various electrolytes with polarizable anions. The upper panel shows the cases of 1:1 and 2:2 electrolytes at 1.00*M* concentration (full and long-dashed lines, respectively) and 0.500*M* concentration (dot-dashed and short-dashed lines, respectively). The lower panel shows 2:1 electrolyte at 0.500*M* and 0.250*M* (full and dot-dashed lines, respectively) and 1:2 electrolyte at 1.00*M* and 0.500*M* (long-dashed and short-dashed lines, respectively). The notation is otherwise as in Fig. 5. In all cases the cations interact with the walls via image forces and hard wall interactions only while the anions interact with the walls via dispersion as well as the other forces. For example, in the 1:2 cases the divalent ions interact with the walls via dispersion forces whereas the monovalent does not.

monotonically attractive in most cases. The magnitude of the maximum value of the pressure for charge-asymmetric electrolytes depends strongly on the bulk electrolyte concentration. For the 1.00*M* concentration the ionic pressure gives rise to a repulsion that exceeds the van der Waals attraction for some separations. The qualitative situation is thus similar to that of the familiar Derjaguin-Landau-Verwey-Overbeek (DLVO) theory in the sense that the van der Waals force is balanced by a repulsion originating from the osmotic pressure exerted by the ions between the walls. A crucial difference is of course that in this case no surface charge is needed for the repulsion to arise.

In the region immediately beyond the first peak, the salt concentration dependence of the pressure is opposite to that in the charge-symmetric cases. Whereas increased concentration from 0.500*M* to 1.00*M* results in a decrease in attraction for separations around 2 nm for charge-symmetric electrolytes, the same change in concentration results in a decreased repulsion or increased attraction for charge-asymmetric electrolytes around the same separation. The same is true when going from 0.250*M* to 0.500*M*, but at somewhat larger separations. The pressure curves continue for larger D as exponentially damped oscillations since the bulk concentrations in all three cases are above the value where the bulk pair correlations turn oscillatory.

2. Polarizable ions

In Fig. 6 the pressure-distance profiles are shown for polarizable 1:1, 2:2, 2:1, and 1:2 electrolytes at various bulk concentrations. The concentration of 0.500*M* is included for all cases, while we also show results for 1.00*M* solutions for 1:1, 2:2, and 1:2 electrolytes and 0.250*M* for the 2:1 electrolyte. The reason for including the latter cases is that we want to make comparisons of the different electrolytes at the same concentration of the polarizable anions. In all cases the pressure is more repulsive (or less attractive) for polarizable electrolytes compared to nonpolarizable electrolytes of the same concentration in the separation range shown, cf. Fig. 5.

The net pressure ΔP for small surface separations is attractive in all cases. The situation is very similar to the nonpolarizable electrolyte systems discussed above, and the qualitative conclusions drawn there apply also to the current cases (the relevant quantitative information for all systems is provided in Table I). We therefore focus on the behavior for larger separations in this section.

For the charge-symmetric polarizable electrolytes the pressure turns repulsive above some separation, which is in contrast to the corresponding nonpolarizable cases where the pressure is mostly monotonically attractive. We see in Fig. 6 that polarizable 2:2 and 1:1 electrolytes at the same concentration behave in a qualitatively similar manner, but that the pressure changes sign at a larger separation for the 2:2 cases than for the corresponding 1:1 cases. As a consequence the maximum pressure tends to be smaller for 2:2 electrolytes than for corresponding 1:1 electrolytes. This is a consequence of the more repulsive effective interactions between the surface and the divalent ions.

For the cases with polarizable 2:1 electrolytes, where attractive dispersion forces act on the monovalent anions, the pressure is much more repulsive than for the corresponding nonpolarizable electrolyte for any given separation. For polarizable 1:2 electrolytes, where dispersion forces act on the divalent anions, the difference between polarizable and nonpolarizable electrolytes is not as large on a relative scale. Thus the effects of ionic polarizability are larger for 2:1 than for 1:2 electrolytes, a conclusion that agrees with our findings for the concentration profiles above. The presence of polarizable monovalent anions has made the 0.5*M* 2:1 electrolyte system to show a repulsive peak that exceeds the attractive van der Waals pressure. For the 1:2 electrolyte this happens for the 1.0*M* solution as in the nonpolarizable case.

There are two main effects that give rise to the large difference in the wall-wall pressure for the 0.500*M* 2:1 and 1:2 electrolytes in Fig. 6. The first, somewhat trivial, is that the bulk concentration of polarizable ions is twice as high for the 2:1 electrolyte compared to the 1:2 electrolyte. The second is that divalent ions feel a stronger self-image repulsion and confinement effects which oppose the attractive dispersion forces to a larger degree than for monovalent ions. A consequence of this is, as we have seen, that the increase in the concentration of anions close to the walls relative to the nonpolarizable case is smaller for 1:2 than for 2:1 polarizable electrolytes, cf. Figs. 2 and 4.

The dependence of the pressure on the salt concentration is qualitatively similar for polarizable and nonpolarizable electrolytes. For 2:1 and 1:2 electrolytes the repulsion increases around the pressure maximum with increasing bulk electrolyte concentration, but it decreases in a region further out. For 1:1 and 2:2 electrolytes, on the other hand, the pres-

sure becomes more repulsive (or less attractive) for all distances beyond the maximum as the concentration is increased.

Let us now compare different polarizable electrolytes which have comparable concentrations of the polarizable anions. From Fig. 6 we see that the maximum repulsion is larger for the 0.500*M* 2:1 electrolyte than for the 1.00*M* 1:1 electrolyte. The same is true for the 1.00*M* 1:2 case compared to the 1.00*M* 2:2 case. The same picture emerges when the 0.250*M* 2:1 electrolyte is compared with the 0.500*M* 1:1 case and when one compares the 0.500*M* 1:2 and the 0.500*M* 2:2 cases; the maximum repulsion is in all instances greater in the charge-asymmetric systems. The maximum occurs, however, at different separations in the various cases. The general picture is that in the charge-asymmetric 2:1 and 1:2 cases the pressure tends to be more repulsive than in charge-symmetric 1:1 and 2:2 cases. This observation is hardly surprising in light of the fact that the wall-wall pressure tends to be more repulsive for charge-asymmetric electrolytes compared to charge-symmetric ones also for the nonpolarizable electrolyte.

That the pressure is more repulsive in all cases when the electrolyte is polarizable than when it is nonpolarizable indicates that the larger net osmotic pressure in the former case more than compensates for the attractive pressure component due to ion-wall dispersion forces, $P^{\mathrm{ion}}_{\mathrm{disp}}$, that is only present in the former case. This observation is consistent with the near cancellation between $P^{\mathrm{ion}}_{\mathrm{disp}}$ and the other contributions to ΔP^{ion} that has been observed at large surface separations for systems with charged walls.[22]

C. Pressure components

The components of P^{ion}, as defined in Sec. II C and Appendix B, in the slit between the walls are shown in Fig. 7 for nonpolarizable electrolytes with a bulk concentration of 0.500*M*. $P^{\mathrm{ion}}_{\mathrm{kin}}$ is due to the momentum transfer when ions move across the midplane between the surfaces (the ideal pressure). It is always repulsive. $P^{\mathrm{ion}}_{\mathrm{Coul}}$ comes from the electrostatic forces that arise because ions on one side of the midplane correlate with ions on the other side. It is generally attractive. $P^{\mathrm{ion}}_{\mathrm{core}}$ is due to core-core collisions of ions on either side of this plane and is always repulsive. $P^{\mathrm{ion}}_{\mathrm{im}}$ originates from the ion-image charge interactions (both self-images and images of other ions) and image charge-image charge interactions across the midplane. This component is shown in the figure as $P^{\mathrm{ion}}_{\mathrm{im}}+P^{\mathrm{wall}}_{\mathrm{vdW(0)}}$ in order to highlight the special relation between these two pressure components for large D, as discussed earlier in Sec. II C. It is the negative $P^{\mathrm{wall}}_{\mathrm{vdW(0)}}$ that makes the curve for the sum of all components, $P^{\mathrm{ion}}+P^{\mathrm{wall}}_{\mathrm{vdW(0)}}$, turn negative for small separation. As we have seen, P^{ion} is very small for small D.

In the middle and bottom panels of Fig. 7 the curves do not extend all the way to $D=2b=0.6$ nm. This is due to the lack of convergence for small surface separations ($D<D^{\mathrm{min}}$) caused by the very strong image interactions for divalent ions and the accompanying ion depletion, as discussed in Secs. II B and III B 1. All pressure components can, however, be calculated analytically at $D=0.6$ nm, as

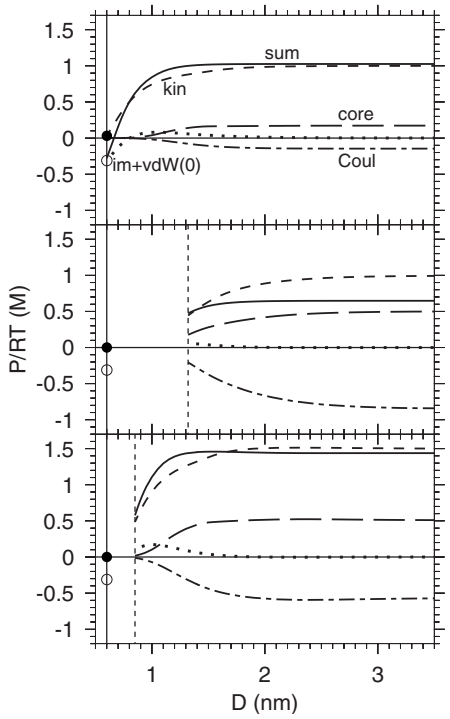

FIG. 7. Components of the pressure in the slit between two uncharged walls as functions of wall-wall separation D in the presence of various electrolytes with nonpolarizable ions. The upper panel shows the case of the 1:1 electrolyte, the middle panel the 2:2 electrolyte, and the bottom panel 1:2 and 2:1 electrolytes (which have the same pressure). The bulk concentration is 0.500*M* throughout. All pressure components are evaluated at the midplane between the walls: kinetic (ideal) pressure $P^{\mathrm{ion}}_{\mathrm{kin}}$ (short-dashed lines), electrostatic ion-ion interaction pressure $P^{\mathrm{ion}}_{\mathrm{Coul}}$ (medium-dashed-short-dashed lines), core-core collision pressure $P^{\mathrm{ion}}_{\mathrm{core}}$ (long-dashed lines), and pressure from image forces and zero-frequency van der Waals attraction $P^{\mathrm{ion}}_{\mathrm{im}}+P^{\mathrm{wall}}_{\mathrm{vdW(0)}}$ (dotted lines). The full curve is the sum of all the pressure components shown, $P^{\mathrm{ion}}+P^{\mathrm{wall}}_{\mathrm{vdW(0)}}$, i.e., the total pressure apart from the high-frequency van der Waals pressure. The dashed vertical lines in the middle and bottom panels denote the smallest separations, D^{min}, for which convergent solution was found, see text. The full vertical lines denote the smallest separation, 0.6 nm, for which ions are present between the walls. The values of the pressure components at this separation are known analytically. These are marked by filled circles for $P^{\mathrm{ion}}_{\mathrm{kin}}$ and open circles for $P^{\mathrm{wall}}_{\mathrm{vdW(0)}}$. The values of $P^{\mathrm{ion}}_{\mathrm{Coul}}$, $P^{\mathrm{ion}}_{\mathrm{core}}$, and $P^{\mathrm{ion}}_{\mathrm{im}}$ are identically zero for $D=0.6$ nm.

demonstrated in Appendix A. For this D value, $P^{\mathrm{ion}}=P^{\mathrm{ion}}_{\mathrm{kin}}$ since all other ionic pressure components are identically equal to zero there. In Fig. 7 the values of $P^{\mathrm{ion}}_{\mathrm{kin}}$ and $P^{\mathrm{wall}}_{\mathrm{vdW(0)}}$ are shown as symbols for $D=0.6$ nm (taken from the data in Table I).

The qualitative behavior of the pressure components appears quite similar in all three cases shown, while the magnitudes of each corresponding component differ depending on the electrolyte. The decrease in $P^{\mathrm{ion}}_{\mathrm{kin}}$ as the separation is decreased corresponds to the exclusion of salt from the slit that accelerates as D becomes smaller. This is partly due to the image repulsion, which increases in magnitude with decreasing D (the multiple images move closer). The exclusion is also caused by the confinement, which results in less opportunity for the ions to arrange themselves in order to lower their free energy compared to the bulk solution. The increasing exclusion continues for small D all the way to $D=2b=0.6$ nm. For the other pressure components in P^{ion}, the

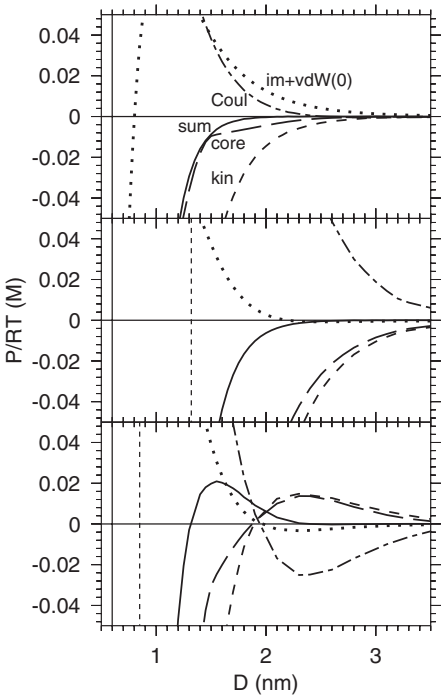

FIG. 8. The components of the net pressure, i.e., the difference between the values in the slit and in the bulk phase, for the same cases as in Fig. 7 but drawn on a different ordinate scale. $\Delta P^{\mathrm{ion}}_{\mathrm{kin}}$, short-dashed lines; $\Delta P^{\mathrm{ion}}_{\mathrm{Coul}}$, medium-dashed-short-dashed lines; $\Delta P^{\mathrm{ion}}_{\mathrm{core}}$, long-dashed lines; and $P^{\mathrm{ion}}_{\mathrm{im}}+P^{\mathrm{wall}}_{\mathrm{vdW(0)}}$, dotted lines. The full lines show their sum $\Delta P=\Delta P^{\mathrm{ion}}+P^{\mathrm{wall}}_{\mathrm{vdW(0)}}$, which is the same as the long-dashed curves in Fig. 5, i.e., the total net pressure apart from $P^{\mathrm{wall}}_{\mathrm{vdW(hf)}}$. The vertical lines have the same meaning as in Fig. 7.

small D behavior can be anticipated from the fact that the components are defined in Appendix B, Eqs. (B3)–(B6), by integrals over an interval that shrinks to zero width, which is the reason why they go to zero when $D\to 0.6$ nm (cf. the discussion in Appendix A). Furthermore, the integrals contain factors n_i that decrease with decreasing D. Note that $P^{\mathrm{ion}}_{\mathrm{Coul}}$ and $P^{\mathrm{ion}}_{\mathrm{im}}$ can be written in terms of charge-charge correlation functions that will remain finite and short ranged, so the influence from the pair distribution functions will not dominate in the integrand. $P^{\mathrm{ion}}_{\mathrm{core}}$ always goes very quickly to zero for vanishing slit width [cf. comment after Eq. (B4)]. Thus all pressure components are expected to simply decrease in magnitude with decreasing surface separation for small D. This is what is seen for the 1:1 electrolyte in Fig. 7.

For these reasons and the results in Fig. 7 it is apparent that the lack of data between the end of the curves and $D=0.6$ nm is not of any great concern since the pressure components most likely just decrease in this region. As the pressure is already appreciably below the bulk pressure for $D=D^{\mathrm{min}}$, the net pressure is unlikely to be anything but attractive until wall-wall contact.

In Fig. 8 the components of the net pressure are shown, i.e., the difference between the pressure in the slit and in the bulk. This way of showing the components gives a clearer picture of how each of them contributes to the total pressure difference. Note the difference in scale between Figs. 7 and 8.

We start with a comparison of the 1:1 and 2:2 electrolytes in the upper two panels of Fig. 8. While the curves for the pressure component sum are similar in these cases, the curve for the 2:2 case appears shifted to greater separations. Furthermore, there are large quantitative differences in the individual net pressure components. For both systems the net kinetic pressure, $\Delta P^{\mathrm{ion}}_{\mathrm{kin}}$, and the net core-core collision pressure, $\Delta P^{\mathrm{ion}}_{\mathrm{core}}$, are attractive for all separations. The net pressure from ion-ion Coulomb interactions, $\Delta P^{\mathrm{ion}}_{\mathrm{Coul}}$, is repulsive for all separations in both cases. The sign of each of these components is due to the fact that the respective value in the slit is smaller (in absolute value) than in the bulk, cf. Fig. 7. This is mainly a consequence of the decreasing number of ions in the slit when D is decreased. The depletion of ions in the slit from repulsive image forces and confinement effects makes this decrease larger than it would be otherwise. The large increase in magnitude of, for example, $\Delta P^{\mathrm{ion}}_{\mathrm{Coul}}$ for small separations is accordingly a consequence of a loss of opportunity for the ions to give electrostatic correlation attraction in the slit rather than some electrostatic repulsion.

For each surface separation D the deviations of $P^{\mathrm{ion}}_{\mathrm{Coul}}$, $P^{\mathrm{ion}}_{\mathrm{core}}$, and $P^{\mathrm{ion}}_{\mathrm{kin}}$ from the respective bulk value are larger for the 2:2 electrolyte than for 1:1, which is caused by the stronger depletion in the former case. These effects of depletion set in at larger surface separations for the divalent electrolyte than for the monovalent one, which can also be inferred from the concentration profile plots, see Fig. 2. The pressure due to the image forces, shown in the figure as the sum $P^{\mathrm{ion}}_{\mathrm{im}}+P^{\mathrm{wall}}_{\mathrm{vdW(0)}}$, contributes to the total net pressure for large D with a repulsion that has a longer range than $\Delta P^{\mathrm{ion}}_{\mathrm{Coul}}$ in the case of the 1:1 electrolyte, but the opposite is true for the 2:2 case. The sum of all these components, $\Delta P=\Delta P^{\mathrm{ion}}+P^{\mathrm{wall}}_{\mathrm{vdW(0)}}$, constitutes the total net interaction pressure between the walls (apart from the high-frequency van der Waals pressure) and is shown in the figure. It decays more quickly to small values than any of the individual components. Therefore it is evident that the different components of the net pressure tend to compensate each other to a large degree.

For the 2:1/1:2 asymmetric electrolyte case in Fig. 8, the pressure components have the same signs as in the charge-symmetric cases only for small separations. The reason for these signs is the same here, namely, depletion of the electrolyte in the slit. However, for the asymmetric electrolyte all net pressure components change sign above a wall-wall separation of about $D=1.9$ nm. The situation is thus the opposite compared to the charge-symmetric cases for separations beyond that. The behavior of the components for large D is, in fact, similar to those for charged surfaces. Due to the charge separation near the uncharged surfaces for asymmetric electrolytes, the electrolyte some distance away from the surfaces "sees" the surfaces as being charged. An electric double layer is formed just in front of the surface, see Fig. 2. This is not the case for totally symmetric electrolytes. The phenomenon of the apparent charging of surfaces due to asymmetry in the electrolyte has been studied previously.[32]

ΔP for the asymmetric electrolyte in Fig. 8 does not change sign at the same separation as the individual components. It becomes repulsive for separations greater than about $D=1.3$ nm and continues as an oscillatory exponentially decaying function when $D\to\infty$ since we are above the bulk

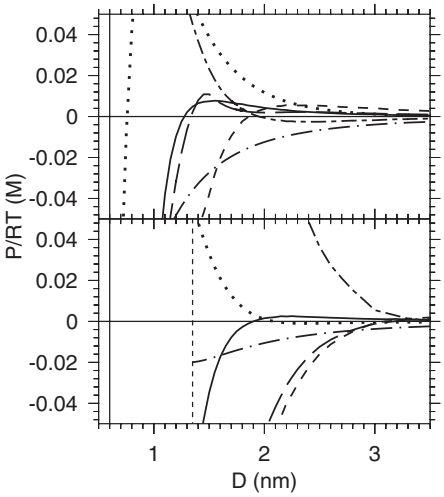

FIG. 9. Components of the net pressure for 1:1 and 2:2 electrolytes with polarizable anions (upper and lower panels, respectively) at a bulk concentration of 0.500M. $P^{\text{ion}}_{\text{disp}}$, dot-dashed lines; $\Delta P^{\text{ion}}_{\text{kin}}$, short-dashed lines; $\Delta P^{\text{ion}}_{\text{Coul}}$, medium-dashed-short-dashed lines; $\Delta P^{\text{ion}}_{\text{core}}$, long-dashed lines; and $P^{\text{ion}}_{\text{im}} + P^{\text{wall}}_{\text{vdW(0)}}$, dotted lines. The full lines show their sum ΔP, which are the same as the corresponding curves in Fig. 6. The vertical lines have the same meaning as in Fig. 7.

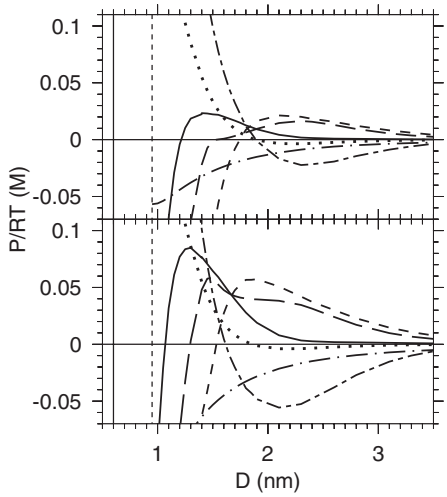

FIG. 10. Components of the net pressure for 1:2 and 2:1 electrolytes with polarizable anions (upper and lower panels, respectively) at a bulk concentration of 0.500M. The anions are divalent in the 1:2 electrolyte and monovalent in the 2:1 electrolyte. The notation is the same as in Fig. 9.

concentration where the pair correlation functions in the bulk turn oscillatory. The main repulsive peak of ΔP occurs where both $\Delta P^{\text{ion}}_{\text{kin}}$ and $\Delta P^{\text{ion}}_{\text{core}}$ are negative. The only repulsive contributions to the net pressure at this separation are $\Delta P^{\text{ion}}_{\text{Coul}}$ and $P^{\text{ion}}_{\text{im}}$. Thus the repulsion is caused by a combination of the repulsive image interactions and a loss of electrostatic correlation attraction compared to the bulk. For larger separations $\Delta P^{\text{ion}}_{\text{kin}}$ and $\Delta P^{\text{ion}}_{\text{core}}$ are repulsive and they are to a large degree counteracted by $\Delta P^{\text{ion}}_{\text{Coul}}$, which is attractive in that region. It is apparent from the figure that ΔP decays more quickly to small values than any of the individual components, which is similar to the charge-symmetric cases.

Let us now turn to the systems with polarizable anions. Figure 9 shows the net pressure components for 1:1 and 2:2 electrolytes. For these charge-symmetric electrolytes we have seen that the presence of ion-wall dispersion forces creates a charge separation in the electrolyte that is more pronounced for the monovalent case than the divalent, cf. Fig. 3. The polarizable electrolyte forms a double layer outside each electroneutral surface and, similar to the charge-asymmetric electrolytes above, the system behaves some distance away from the wall as if the surface were charged. The effective charge of the surface is nonzero. Therefore, it is not surprising that the components of ΔP^{ion} for 1:1 polarizable electrolytes, Fig. 9, at large surface separations D behave qualitatively similar to those for charge-asymmetric electrolytes in Fig. 8. (The pressure at large separations is, however, nonoscillatory here since we are below the bulk concentration where the pair correlations in bulk turn oscillatory.)

Compared to the nonpolarizable electrolytes we have an additional pressure component here, $P^{\text{ion}}_{\text{disp}}$, that originates from the ion-wall dispersion interactions. It is attractive, but the total ΔP^{ion} for the 1:1 case is nevertheless repulsive for intermediate to large separations since $\Delta P^{\text{ion}}_{\text{kin}}$ and $\Delta P^{\text{ion}}_{\text{core}}$ are repulsive. The repulsion is due to the increase in the number of ions between the walls brought in there by the dispersion forces on the anions. For small D the pressure components behave like in all other cases due to the expulsion of ions between the surfaces, as discussed earlier.

For the 2:2 case, where the effects of the ion-wall dispersion forces are smaller than for 1:1 electrolytes, the pressure components in Fig. 9 do not differ as much from the corresponding nonpolarizable electrolyte, see Fig. 8. The sign of ΔP for intermediate to large separations is, however, different from the nonpolarizable case. In the intermediate regime the net repulsion is caused by a positive $\Delta P^{\text{ion}}_{\text{Coul}}$, i.e., a loss of electrostatic correlation attraction compared to the bulk (cf. the charge-asymmetric electrolytes discussed above).

The net pressure components for 1:2 and 2:1 electrolytes with polarizable anions are shown in Fig. 10. For the 1:2 case, where the polarizable ions are divalent, we see that there is not a large difference from the nonpolarizable electrolyte, see Fig. 8. This is yet another example that illustrates the fact that effects of the ion-wall dispersion forces are quite small for divalent ions. Despite that we have an attractive $P^{\text{ion}}_{\text{disp}}$ component here which is not present in the nonpolarizable case, the total ΔP^{ion} is more repulsive (or less attractive) for most D values. This is due to $\Delta P^{\text{ion}}_{\text{kin}}$ and $\Delta P^{\text{ion}}_{\text{core}}$, which are increased compared to the nonpolarizable electrolyte as a consequence of the increased number of ions between the walls brought in there by the dispersion forces on the anions. The increased values of these components more than compensate the attraction from $P^{\text{ion}}_{\text{disp}}$.

For the polarizable 2:1 electrolytes, on the other hand, the ion-wall dispersion forces have a rather large impact on most components, as seen in Fig. 10. ΔP is much more repulsive (or less attractive) than in the nonpolarizable case. This is due to large increases in $\Delta P^{\text{ion}}_{\text{kin}}$ and $\Delta P^{\text{ion}}_{\text{core}}$ for most D values. $\Delta P^{\text{ion}}_{\text{im}}$ is not much affected by the effects of the dispersion forces, while $\Delta P^{\text{ion}}_{\text{Coul}}$ turns much more attractive (or less repulsive). The changes in $\Delta P^{\text{ion}}_{\text{Coul}}$ and the appearance of the attractive $P^{\text{ion}}_{\text{disp}}$ are, however, dominated by the increases

in $\Delta P_{\mathrm{kin}}^{\mathrm{ion}}$ and $\Delta P_{\mathrm{core}}^{\mathrm{ion}}$. These results illustrate the greater importance of the ion-wall dispersion interaction for polarizable monovalent ions than divalent ones.

IV. SUMMARY AND CONCLUSIONS

The ion concentration profiles and interaction pressure between uncharged hard walls immersed in various 1:1, 2:2, 2:1, and 1:2 electrolytes have been investigated. The ions interact with the walls via image charge forces and, when the ions are polarizable, also via ion-wall dispersion forces. Primarily we investigate the net pressure from the ions, including the zero-frequency van der Waals wall-wall interaction pressure, which is screened by the electrolyte. The high-frequency van der Waals wall-wall interaction pressure is the same in all cases and is not included. It is shown separately in Figs. 5 and 6 and can be added to obtain the total pressure. The system parameters for the van der Waals interactions are appropriate for hydrocarbon (polystyrene) particles in water.

For (totally) symmetric nonpolarizable electrolytes (i.e., consisting of nonpolarizable ions with equal sizes and equal absolute values of charges) the pressure is attractive in nearly all cases, as expected from the result of previous work.[5] It is only for high electrolyte concentrations that small repulsive peaks also emerge. For charge-asymmetric (1:2 and 2:1) nonpolarizable electrolytes the behavior is qualitatively different. The interaction pressure is then repulsive for some range of wall-wall separations for all electrolyte concentrations examined. The maximum repulsion is larger in magnitude than the (high-frequency) van der Waals wall-wall attraction between the walls provided the electrolyte concentration is high. The pressure from the ions therefore gives rise to a repulsive barrier against pushing the walls together despite that the surfaces are uncharged.

For small separations the pressure is attractive in all cases. The attraction is to a large extent a depletion interaction caused by the expulsion of ions from the neighborhood of each wall due to repulsive image forces and confinement effects on the ion-ion correlations. The expulsion is larger for divalent ions than for monovalent ones. For the charge-asymmetric case this gives rise to a charge separation in the electrolyte, i.e., an electric double layer is formed outside the electroneutral surface. For symmetric nonpolarizable electrolytes the expulsion of anions and cations is identical, so no charge separation occurs. Therefore, for asymmetric electrolytes the uncharged walls appear from a distance as if they were charged, while this is not the case for totally symmetric electrolytes. This has implications for the behavior of the pressure for large separations between the walls, as discussed in this paper.

Any kind of asymmetry of the electrolyte makes charge separation to appear in the electrolyte outside an electroneutral surface. Examples are 1:1 and 2:2 electrolytes where the anions and cations have different strengths of the ion-wall dispersion interactions. In this work we investigate cases with polarizable anions and negligibly polarizable cations (i.e., the cations are about as polarizable as water). The strength of the dispersion interactions for the anions corresponds approximately to iodide in water. The asymmetry makes charge-symmetric electrolytes with polarizable ions and charge-asymmetric electrolytes to have several features in common. Both behave in many respects as if the surfaces had a charge.

In all cases with polarizable anions, a repulsive pressure due to the ions is seen for intermediate to large wall-wall separations. For small separations the pressure is still attractive in all cases. The point where the pressure changes between repulsive and attractive occurs at greater separations for the 2:2 electrolyte than for the 1:1 electrolyte. The maximal repulsion is stronger for the monovalent case than for the divalent.

The repulsive pressure seen for charge-asymmetric electrolytes is stronger when the anions are polarizable than when they are nonpolarizable. There is, however, a large difference depending on if the anions are monovalent (2:1 case) or divalent (1:2 case). For monovalent anions the maximal repulsion is much stronger for the polarizable case than the nonpolarizable, but for divalent anions there is not a large difference.

One important conclusion is that dispersion forces acting on ions of higher valency have a smaller effect than when they act on ions of lower valency. In part, this can be explained by the presence of self-image charge repulsions which are proportional to the square of the valency. These repulsions are more effective in counteracting the dispersion attraction to the surfaces for ions with high charge than those with low charge. This shows that it is very important to include both image charge and ion-wall dispersion interactions consistently in the theoretical treatment.

The results presented above show that physical phenomena that are commonly neglected in theoretical treatment of colloidal interactions have important implications for the interaction pressure between walls, particularly at high salt concentration. An important example is that an asymmetry of the electrolyte is sufficient to give an appreciable repulsive barrier under conditions where PB theory predicts a contribution to the total pressure that is identically zero. For polarizable ions the barrier in the total pressure occurs at lower concentrations than for nonpolarizable ions, in particular, when the polarizable ions are monovalent. A large repulsive barrier occurs for systems with a large degree of charge separation in the electrolyte near the electroneutral surface, regardless of whether the separation is caused by depletion or enrichment of one ion species with respect to the other in the immediate vicinity of the surface. This shows that repulsive as well as attractive forces may give rise to wall-wall repulsion if they act asymmetrically on the cation and anion.

ACKNOWLEDGMENTS

This work has received financial support from the Swedish Research Council.

APPENDIX A: LIMITING VALUES OF ION DENSITY AND PRESSURE COMPONENTS FOR THIN SLITS

Here we shall investigate the case of thin slits between the electroneutral surfaces. We will consider the limit of

$D \to 2b$, where only a monolayer of ions fits in the slit. We first note that the density profiles are nonzero only in the range $|z| \leq D/2-b$ when $D>2b$ and that they remain finite when $D \to 2b$ since the surfaces are uncharged and the electrolyte in the slit is in equilibrium with a bulk electrolyte solution. While the number of ions between the walls goes to zero in this limit, the concentration remains finite. Both the available volume in the slit and the number of ions go to zero. (For charged surfaces the concentration profile of the counterions must approach infinity in the same limit as the number of counterions between the walls must remain finite in this case due to electroneutrality.)

It is easy to see from the definitions of the pressure components in Appendix B that $P^{\text{ion}}_{\text{Coul}}$, $P^{\text{ion}}_{\text{core}}$, $P^{\text{ion}}_{\text{im}}$, and $P^{\text{ion}}_{\text{disp}}$ all tend to zero in the limit $D \to 2b$ as they contain integrals over a volume that goes to zero while the integrand remains finite. For the same reason, the intrinsic excess chemical potential (the part of the chemical potential that is due to ion-ion interactions) of the ions in the slit goes to zero in this limit, which leads to a simple expression for the ionic concentrations in the same limit.[56] We shall apply this kind of approach for our system and obtain a simple expression for the density in the slit and for $P^{\text{ion}}_{\text{kin}}$, which is proportional to the total ionic concentration at the midplane, see Eq. (15).

Consider a binary electrolyte with mean chemical potential $\mu_{\pm}$ and mean activity coefficient $\gamma_{\pm}$ in the bulk. Without loss of generality the activity coefficient for each ion species in the bulk is taken to be equal to $\gamma_{\pm}$. Equilibrium between the bulk and the slit demands that the chemical potential for species i satisfies

$$\mu_i^{\text{bulk}} = k_B T \ln[\lambda_i^3 n_i^{\text{bulk}} \gamma_{\pm}] = k_B T \ln[\lambda_i^3 n_i(z)] + \nu_i(z) + \mu_i^{\text{ex}}(z) - q_i \Delta\Psi, \tag{A1}$$

where λ_i is the de Broglie thermal wavelength, $\nu_i(z)$ is the ion-wall interaction potential, $\mu_i^{\text{ex}}(z)$ is the intrinsic excess chemical potential at position z in the slit, and $\Delta\Psi$ is the electrostatic potential difference between the slit and the bulk solution needed to maintain electroneutrality in the slit.[57] Note that this potential difference does not affect electroneutral combinations of anions and cations transferred between the bulk and the slit, so $\mu_{\pm}$ is the same everywhere, but each individual ionic chemical potential μ_i in the slit is different from its bulk value when $\Delta\Psi \neq 0$. It follows from Eq. (A1) that the ion density profile in the slit is

$$n_i(z) = n_i^{\text{bulk}} \gamma_{\pm} \exp\left[- \frac{\nu_i(z) + \mu_i^{\text{ex}}(z) - q_i \Delta\Psi}{k_B T} \right]. \tag{A2}$$

Since $\mu_i^{\text{ex}}(z) \to 0$ for all z when $D \to 2b$ we obtain

$$n_i(0) \to n_i^{\text{bulk}} \gamma_{\pm} \exp\left[- \frac{\nu_i(0) - q_i \Delta\Psi}{k_B T} \right]. \tag{A3}$$

Now since electroneutrality demands that we must have $q_+ n_+(0) = -q_- n_-(0)$ in this limit, it follows that $\nu_+(0) - q_+ \Delta\Psi = \nu_-(0) - q_- \Delta\Psi$, where we have used $q_+ n_+^{\text{bulk}} = -q_- n_-^{\text{bulk}}$. Thus, $\Delta\Psi = [\nu_+(0) - \nu_-(0)]/[q_+ - q_-]$ and Eq. (A3) can be written as

$$n_i(0) \to n_i^{\text{bulk}} \gamma_{\pm} \exp\left[- \frac{q_+ \nu_-(0) - q_- \nu_+(0)}{(q_+ - q_-) k_B T} \right]. \tag{A4}$$

Finally we obtain from Eq. (15)

$$\lim_{D \to 2b} P^{\text{ion}}_{\text{kin}} = k_B T (n_+^{\text{bulk}} + n_-^{\text{bulk}}) \gamma_{\pm} \exp\left[- \frac{q_+ \nu_-(0) - q_- \nu_+(0)}{(q_+ - q_-) k_B T} \right], \tag{A5}$$

which is also the limiting value of P^{ion} since the other components are zero at $D=2b$.

APPENDIX B: EVALUATION OF THE WALL-WALL INTERACTION PRESSURE

In this appendix we give explicit formulas for the calculation of the ionic pressure between the walls. At equilibrium, P^{ion} (the perpendicular component of the ionic pressure tensor) is equal everywhere in the slit, i.e., it has the same value at any plane between the walls. Here, we shall consider two possibilities: to calculate P^{ion} at one of the walls and at the midplane between the walls. The relationship between the pressure and the distribution functions is different in the two cases. If one chooses to evaluate P^{ion} at one of the walls, the following expression[36] applies when the two walls are equal:

$$P^{\text{ion}} = k_B T \sum_i n_i^{\text{contact}} - \frac{\sigma^2}{2\epsilon_{\text{solv}}(0)\epsilon_0} - \sum_i \int_{-D/2}^{D/2} dz n_i(z) \times \left[\frac{\partial V_i^{\text{disp}}(D-z)}{\partial D} + \frac{\partial \nu_i^{\text{im}}(z|D)}{\partial D} \right] - \frac{1}{4\pi} \sum_{i,j} \int_{-D/2}^{D/2} dz \int_{-D/2}^{D/2} dz' \int_0^{\infty} dk n_i(z) n_j(z') \hat{h}_{ij}(k,z,z') k \times \frac{\partial \hat{u}_{ij}^{\text{im}}(k,z,z'|D)}{\partial D}, \tag{B1}$$

where the first term contains the contact density of ions at the wall surface, σ is the surface charge density of the wall (zero in our case), and $V_i^{\text{disp}}(d) = B_i/d^3$ denotes the dispersion interaction between an ion and a *single* wall a distance d away, cf. Eq. (7). In our case $n_i^{\text{contact}} = n_i(D/2-b)$ and the ion densities are zero for $|z| > D/2-b$, so the integral limits can be substituted by $\pm(D/2-b)$. Equation (B1) is the so-called *contact theorem* generalized to the presence of ion-wall dispersion and image interactions.

If one instead chooses to evaluate the pressure at the midplane between the walls one obtains a somewhat more complicated expression. It is practical to subdivide P^{ion} into physically distinct contributions according to

$$P^{\text{ion}} = P^{\text{ion}}_{\text{kin}} + P^{\text{ion}}_{\text{Coul}} + P^{\text{ion}}_{\text{core}} + P^{\text{ion}}_{\text{im}} + P^{\text{ion}}_{\text{disp}}, \tag{B2}$$

which are defined below [a similar subdivision is of course possible also for Eq. (B1)].

$P^{\text{ion}}_{\text{kin}}$ is the kinetic (ideal) contribution to the pressure given by Eq. (15). $P^{\text{ion}}_{\text{Coul}}$ and $P^{\text{ion}}_{\text{core}}$ are the contributions to the pressure due to electrostatic and hard-sphere interactions across the midplane, respectively. In terms of the ionic distribution functions $P^{\text{ion}}_{\text{Coul}}$ is given by[37]

$$P^{\text{ion}}_{\text{Coul}} = -2\pi\sum_{i,j}\int_0^{D/2} dz \int_{-D/2}^{0} dz' \int_0^{\infty} dR n_i(z) n_j(z') \times h_{ij}(R,z,z') R \frac{\partial u_{ij}^{\text{Coul}}(R,z,z')}{\partial z}, \tag{B3}$$

and $P^{\text{ion}}_{\text{core}}$ is given by

$$P^{\text{ion}}_{\text{core}} = 2\pi k_B T \sum_{i,j}\int_0^{a} dz \int_{z-a}^{0} dz' n_i(z) n_j(z')(z-z') \times g_{ij}([a^2-(z-z')^2]^{1/2},z,z'), \tag{B4}$$

where the pair distribution function $g_{ij}=h_{ij}+1$ is evaluated at the rim of the hard core exclusion zone of two ions in contact. $P^{\text{ion}}_{\text{core}}$ measures the contact force component perpendicularly to the midplane, which is expressed by the factor $z-z'$. This makes $P^{\text{ion}}_{\text{core}}$ go very quickly to zero when the slit width goes to zero; core-core collisions will then eventually only take place in the lateral direction along the plane.

The pressure due to image forces, $P^{\text{ion}}_{\text{im}}$, contains contributions from both ion-wall and ion-ion interactions and is given by[37]

$$\begin{aligned} P^{\text{ion}}_{\text{im}} = & -\frac{1}{2\pi}\sum_{i,j}\int_0^{D/2} dz \int_{-D/2}^{D/2} dz' \int_0^{\infty} dk n_i(z) n_j(z') \hat{h}_{ij}(k,z,z') k \frac{\partial \hat{u}_{ij}^{\text{im}}(k,z,z'|D)}{\partial z} \\ & -\frac{1}{4\pi}\sum_{i,j}\int_{-D/2}^{D/2} dz \int_{-D/2}^{D/2} dz' \int_0^{\infty} dk n_i(z) n_j(z') \hat{h}_{ij}(k,z,z') k \frac{\partial \hat{u}_{ij}^{\text{im}}(k,z,z'|D)}{\partial D} \\ & -\sum_i \int_0^{D/2} dz n_i(z) \frac{\partial v_i^{\text{im}}(z|D)}{\partial z} - \sum_i \int_{-D/2}^{D/2} dz n_i(z) \frac{\partial v_i^{\text{im}}(z|D)}{\partial D}. \end{aligned} \tag{B5}$$

[This expression replaces Eq. (17) of our previous paper,[22] which contains some misprints.]

$P^{\text{ion}}_{\text{disp}}$ is the pressure contribution due to the direct dispersion interactions between the ions and walls and is given by

$$P^{\text{ion}}_{\text{disp}} = -\sum_i \int_0^{D/2} dz n_i(z) \frac{\partial V_i^{\text{disp}}(z+D/2)}{\partial z} + \sum_i \int_{-D/2}^{0} dz n_i(z) \frac{\partial V_i^{\text{disp}}(|z-D/2|)}{\partial z}, \tag{B6}$$

where, again, $V_i^{\text{disp}}(d)=B_i/d^3$ denotes the dispersion interaction between an ion and a single wall.

The two ways of evaluating the pressure, Eq. (B1) on one hand and Eq. (B2) together with Eqs. (15) and (B3)–(B6) on the other hand, are equivalent (this follows from the Born–Green–Yvon equation). Which one of the two alternatives to use is a matter of preference and numerical expedience. For charged surfaces the pressure evaluation at the midplane is often numerically more reliable than at a wall due to a near cancellation in Eq. (B1) between the term $-\sigma^2/(2\epsilon_{\text{solv}}(0)\epsilon_0)$ and the other terms. In our case, where $\sigma=0$, this is not the case. Instead we find that Eq. (B1) is often numerically more suitable for calculation of the total P^{ion} than the sum of components in Eq. (B2). This is generally the case when only repulsive forces act between the ions and the walls. Therefore we use Eq. (B1) for the total pressure in these cases. When there is attraction between ions and walls a similar problem as in the charged case appears from cancellation between the third term in Eq. (B1) and the other terms. When attractive dispersion forces are present the "midplane formula," Eq. (B2), is therefore often preferable.

[1] R. Kjellander, S. Marčelja, and J. P. Quirk, J. Colloid Interface Sci. **126**, 194 (1988).
[2] P. Kékicheff, S. Marčelja, T. J. Senden, and V. E. Shubin, J. Chem. Phys. **99**, 6098 (1993).
[3] B. Jönsson, A. Nonat, C. Labbez, B. Cabane, and H. Wennerström, Langmuir **21**, 9211 (2005).
[4] J. Mahanty and B. W. Ninham, *Dispersion Forces* (Academic, New York, 1976).
[5] R. Kjellander and S. Marčelja, Chem. Phys. Lett. **142**, 485 (1987).
[6] B. W. Ninham and A. Parsegian, Biophys. J. **10**, 646 (1970).
[7] A. Parsegian and B. W. Ninham, Biophys. J. **10**, 664 (1970).
[8] B. W. Ninham and V. Yaminsky, Langmuir **13**, 2097 (1997).
[9] R. R. Dagastine, D. C. Prieve, and L. R. White, J. Colloid Interface Sci. **231**, 351 (2000).
[10] R. Bauernschmitt and R. Ahlrichs, Chem. Phys. Lett. **256**, 454 (1996).
[11] M. Cossi and V. Barone, J. Chem. Phys. **115**, 4708 (2001).
[12] M. Boström, D. R. M. Williams, and B. W. Ninham, Phys. Rev. Lett. **87**, 168103 (2001).
[13] M. Boström, D. R. M. Williams, and B. W. Ninham, Langmuir **17**, 4475 (2001).
[14] M. Boström, F. W. Tavares, D. Bratko, and B. W. Ninham, J. Phys. Chem. B **109**, 24489 (2005).
[15] M. Boström, F. W. Tavares, S. Finet, F. Skouri-Panet, A. Tardieu, and B. W. Ninham, Biophys. Chem. **117**, 217 (2005).
[16] L. A. Moreira, M. Boström, B. W. Ninham, E. C. Biscaia, and F. W. Tavares, Colloids Surf., A **282–283**, 457 (2006).
[17] M. Boström, V. Deniz, G. V. Franks, and B. W. Ninham, Adv. Colloid Interface Sci. **123–126**, 5 (2006).
[18] M. Boström, V. Deniz, and B. W. Ninham, J. Phys. Chem. B **110**, 9645 (2006).
[19] L. A. Moreira, M. Boström, B. W. Ninham, E. C. Biscaia, and F. W.

Tavares, J. Braz. Chem. Soc. **18**, 223 (2007).
[20] F. W. Tavares, D. Bratko, H. W. Blanch, and J. M. Prausnitz, J. Phys. Chem. B **108**, 9228 (2004).
[21] S. A. Edwards and D. R. M. Williams, Curr. Opin. Colloid Interface Sci. **9**, 139 (2004).
[22] E. Wernersson and R. Kjellander, J. Chem. Phys. **125**, 154702 (2006).
[23] E. Wernersson and R. Kjellander, J. Phys. Chem. B **111**, 14279 (2007).
[24] E. R. A. Lima, E. C. Biscaia, M. Boström, F. W. Tavares, and J. M. Prausnitz, J. Phys. Chem. C **111**, 16055 (2007).
[25] E. R. A. Lima, E. C. Biscaia, M. Boström, F. W. Tavares, and J. M. Prausnitz, J. Phys. Chem. C **112**, 8741 (2008).
[26] M. Boström, E. R. A. Lima, F. W. Tavares, and B. W. Ninham, J. Chem. Phys. **128**, 135104 (2008).
[27] H. I. Petrache, S. Tristram-Nagle, D. Harries, N. Kučerka, J. F. Nagle, and V. A. Parsegian, J. Lipid Res. **47**, 302 (2006).
[28] H. I. Petrache, T. Zemb, L. Belloni, and V. A. Parsegian, Proc. Natl. Acad. Sci. U.S.A. **103**, 7982 (2006).
[29] R. P. Rand and V. A. Parsegian, Biochim. Biophys. Acta **988**, 351 (1989).
[30] In our work the interaction energy between a polarizable ion and a wall in contact is about $0.6k_BT$, whereas the binding constant in Ref. 28 corresponds to a free energy of adsorption of about $1-2k_BT$.
[31] G. M. Torrie, J. P. Valleau, and C. W. Outhwaite, J. Chem. Phys. **81**, 6296 (1984).
[32] J. Ulander, H. Greberg, and R. Kjellander, J. Chem. Phys. **115**, 7144 (2001).
[33] S. Marčelja, J. Phys. Chem. B **110**, 13062 (2006).
[34] L. Onsager and N. N. T. Samaras, J. Chem. Phys. **2**, 528 (1934).
[35] S. L. Carnie and D. Y. C. Chan, Mol. Phys. **51**, 1047 (1984).
[36] R. Kjellander and S. Marčelja, J. Chem. Phys. **82**, 2122 (1985).
[37] R. Kjellander and S. Marčelja, Chem. Phys. Lett. **112**, 49 (1984); **114**, 112(E) (1985).
[38] *Handbook of Chemistry and Physics*, 52nd ed., edited by R. C. Weast (CRC, Cleveland, OH, 1971).
[39] R. Kjellander, T. Åkesson, B. Jönsson, and S. Marčelja, J. Chem. Phys. **97**, 1424 (1992).
[40] H. Greberg, R. Kjellander, and T. Åkesson, Mol. Phys. **92**, 35 (1997).
[41] D. Bratko, B. Jönsson, and H. Wennerström, Chem. Phys. Lett. **128**, 449 (1986).
[42] J. P. Valleau, R. Ivkov, and G. M. Torrie, J. Chem. Phys. **95**, 520 (1991).
[43] P. J. Rossky, J. B. Dudowicz, B. L. Tembe, and H. L. Friedman, J. Chem. Phys. **73**, 3372 (1980).
[44] L. Belloni, J. Chem. Phys. **98**, 8080 (1993).
[45] F. O. Raineri and G. Stell, Condens. Matter Phys. **4**, 621 (2001).
[46] R. Hunter, *Foundations of Colloid Science* (Oxford University Press, New York, 2001).
[47] R. Kjellander and H. Greberg, J. Electroanal. Chem. **450**, 233 (1998); **462**, 273 (1999).
[48] R. Evans, R. J. F. Leote de Carvalho, J. R. Henderson, and D. C. Hoyle, J. Chem. Phys. **100**, 591 (1994).
[49] R. Kjellander and D. J. Mitchell, Mol. Phys. **91**, 173 (1997).
[50] R. Kjellander and D. J. Mitchell, Chem. Phys. Lett. **200**, 76 (1992).
[51] J. Ennis, R. Kjellander, and D. J. Mitchell, J. Chem. Phys. **102**, 975 (1995).
[52] J. Ulander and R. Kjellander, J. Chem. Phys. **109**, 9508 (1998).
[53] J. Ennis, S. Marčelja, and R. Kjellander, Electrochim. Acta **41**, 2115 (1996).
[54] J. Mahanty and B. W. Ninham, *Dispersion Forces* (Ref. 4), Sec. 7.4.
[55] D. Bratko and D. J. Henderson, Phys. Rev. E **49**, 4140 (1994).
[56] D. Bratko, D. J. Henderson, and L. Blum, Phys. Rev. A **44**, 8235 (1991).
[57] R. Kjellander and S. Marčelja, Chem. Phys. Lett. **127**, 402 (1986).

Paper IV

Charge inversion and ion-ion correlation effects at the mercury/aqueous $MgSO_4$ interface: towards the solution of a long-standing issue

Erik Wernersson,[*,†] Roland Kjellander,[†] and Johannes Lyklema[‡]

Dept. of Chemistry, University of Gothenburg, SE-412 96 Gothenburg, Sweden, and Laboratory of Physical Chemistry and Colloid Science, Wageningen University, Dreijenplein 6, 6703 HB Wageningen, The Netherlands

[†]Dept. of Chemistry, University of Gothenburg, SE-412 96 Gothenburg, Sweden

[‡]Laboratory of Physical Chemistry and Colloid Science, Wageningen University, Dreijenplein 6, 6703 HB Wageningen, The Netherlands

Abstract

Charge inversion is the phenomenon that an electric double layer contains more counterions than needed to compensate the surface charge. For colloidal particles this has the consequence that the apparent surface charge, as inferred from electrophoresis or interaction studies, has a sign opposite to that of the actual surface charge, obtainable by titration. This phenomenon has been known for over a century. According to the traditional interpretation, the inversion is caused by (chemical) specific adsorption of ions. However, beginning in the early 80's it has been predicted by a large number of workers that charge inversion should occur as a consequence of many-body ion-ion correlations. For surfaces of sufficiently high surface charge density in the presence of divalent or multivalent counterions, charge inversion is expected to be ubiquitous even in the absence of specific adsorption. Testing this prediction has proved difficult because chemical specific adsorption is a very common phenomenon and can outweigh the effects of ion correlations. So far, no experimental systems have been thoroughly investigated where strong specific adsorption could be *unambiguously* ruled out under conditions where charge inversion due to ion-ion correlations is predicted. Here, we solve this problem by studying the mercury/aqueous $MgSO_4$ interface. This system has the advantage that highly accurate double layer data are available for a variety of conditions, including some where chemical specific adsorption is known to be absent (or at least very weak). From precise data for this system [Harrison, J. A.; Randles, J. E. B.; Schiffrin, D. J. *J. Electroanal. Chem.* **1970**, 25, 197] one can establish the ionic components of charge and surface charge density. To extract quantitative theoretical predictions about the consequences of ion-ion correlations, we use the highly accurate anisotropic hypernetted chain (AHNC) method, where ion-ion correlations in the double layer are taken into account in a fully self-consistent fashion. It is found that for moderate to large negative surface charge densities and not too high concentration, the variation in the ionic components of charge with the surface charge density can to a large extent be quantitatively explained by enrichment of ions close to the surface due to ion-ion correlations. That chemical specific adsorption of Mg^{2+} is negligible is supported by considering the properties of the double layer close to the electrocapillary maximum. In view of the large body of evidence indicating that the counterions tend to specifically adsorb on the mercury surface

for *positive* polarization but not for negative, the agreement between theory and experiment for negative surface charge constitutes strong evidence for ion-ion correlations as the origin of charge inversion.

Keywords: electric double layers, surface and colloid science, primitive model electrolytes, image charges, overcharging, charge reversal

1 Introduction

A phenomenon commonly seen in the study of colloids and interfaces is charge inversion, also called overcharging. This term refers to the situation where more counterions are attracted to a charged surface than needed to neutralize the surface charge. Because of electroneutrality this leads to positive adsorption of co-ions, usually in a region beyond the adsorbed counterions. Thus, the roles of counterions and co-ions appear inverted when viewed from a point sufficiently far from the surface. The traditional way of establishing the phenomenon is by comparing the electrokinetic charge with the surface charge. Electrokinetically, only the outer part of the double layer is measured (outside the "slip plane"). When the electrokinetic charge and bare surface charge have opposite signs, charge inversion has occurred. This is a sufficient but not a necessary condition: charge inversion in the sense in which the term is used here can occur without reversal in sign of the electrokinetic charge. Some aspects of charge inversion are indirectly reflected in colloid interaction; it gives rise to so-called "irregular series" in colloid stability, a phenomenon that has recently be rediscovered in physics and renamed "re-entrant condensation". This is the phenomenon that ion condensation on (mostly) polyelectrolytes first disappears and then re-appears upon some change in conditions.

Stating the phenomenon begs the question what the origin is of overcharging. Traditionally, it is attributed to "specific adsorption", which is due to an affinity of non-electrostatic origin between ions and a surface. If this affinity is strong enough, it can outweigh electrostatic repulsion and hence ions can adsorb against an electric field. The "chemical" origin of such forces can range

from strong chemical bonding, complexation, ligand exchange, hydrophobic bonding to other, rather weak, water structure-mediated attractions. All of this is very well established in colloid and interface science.[1,2] However, computer simulations as well as theory for simple electrolytes near charged surfaces suggest that overcharging can arise even in the absence of any chemical attraction between ions and surfaces.[3–7] In such treatments, where only electrostatic interactions and short-range repulsions are taken into account, the driving force for the extra adsorption is the lowering of the local excess chemical potential close to the surface mainly due to many-body correlations and, to some extent, excluded volume effects due to ionic size (both are aspects of ion-ion correlations in the electric double layer). For aqueous systems at room temperature electrostatic correlations are important predominantly for divalent and multivalent electrolytes.

The resulting state of the art is that two alternative interpretations for the same phenomenon are available. In a sense, this is a luxury problem. The two alternatives are not mutually exclusive; the question is rather which mechanism, if any one, is most important for a system under given conditions. That overcharging *can* be explained by one of these mechanisms, does not mean that it *is* caused in that way. One must show that the proposed adsorption mechanism is in action and is sufficiently strong to explain the experimental observations. What is generally done in colloid and interface science is to interpret any adsorption that cannot be explained by traditional diffuse double layer theory in terms of an ion-free layer and chemical specific adsorption.

For the inquiring academic mind the option of the ion-correlation interpretation may look more attractive because of its more *ab initio* nature, but so far it has not been unequivocally shown by experiments that this mechanism really is dominant in any case. In fact, most of the available experimental evidence points to chemical specific adsorption. At best there are observations that might have been caused by ion-ion correlations, but does not constitute rigorous tests of that mechanism. By way of illustration, in two recent reviews[8,9] a variety of overcharging cases were collected and attributed to ion-ion correlations but where closer inspection showed that chemical specific adsorption was the driving force. Chemical phenomena that may easily outweigh the effects of correlations include hydrophobic bonding, adsorption of hydrolyzing species (hydroly-

sis can reduce the valency but increase the adsorbability) and adsorption of polymeric substances (adsorption energies per segment of only 0.2 - 0.3 k_BT suffice to let the chain attach almost irreversibly). Recent experiments that have been invoked as indications for overcharging by ion-ion correlations[10–12] are not clear-cut either, because either or both the surface charges and electrokinetic potential could not be controlled, let alone measured, and/or the pH was not systematically studied, so that the hydrolysis state of the multivalent ionic species was not rigorously established.

Similar comments can be given about interpretations of experimental data based on the Poisson-Boltzmann (PB) mean field approximation. In this approximation the statistical mechanical treatment of the theoretical model is simplified by replacing the potential of mean force for an ion with the mean electrostatic potential times the charge of an ions. Here and in what follows we make a sharp distinction between the model for a system, i.e. the assumed form of the intermolecular interactions, and the approximations made when evaluating the properties of the model. The PB approach carries the cost that many features of the model (to be described later) are not accurately taken into account. The range of applicability of Gouy-Chapman (GC) theory, which is the application of the PB approximation to planar surfaces, is rather restricted. As suggested by a wide range of experiments, this approximation is valid only for low surface charge densities and low electrolyte concentrations. The vast majority of all experiments apply to ranges far beyond these limits, so that improvements of the theory are mandatory. These improvements fall into two principal classes: improvements of the approximations made in the treatment of a given model and changes in the model itself. The most common member of the second class is the incorporation of a Stern layer,[13] entailing corrections for counterion size and/or specific adsorption in a first layer, adjacent to the surface, only. In many cases this is a quite effective improvement, indicating that it is not the approximations of CG theory but the assumptions about the ion-surface interactions that are mainly at fault in these cases. Typically, the ion-surface interactions have a range that is much shorter than the thickness of the double layer. It is for this reason that the inclusion of these interactions as a Stern layer is often appropriate. Because GC theory is not exact, however, deviations between experimental data and GC predictions do not *necessarily* mean that one must invoke Stern

type mechanisms to explain discrepancies between theory and experiment: the assumptions made in the model of the system may be sufficiently close to reality, and the deviations from experiments may instead be caused by the approximations inherent in GC theory. In fact, ion-ion correlations, that are entirely neglected in the GC approximation, are sometimes important for the behavior of simple electrolytes. For instance, this is the case when the electrostatic interactions are strong and/or the electrolyte concentration is high. In these cases, it is improvements of the theoretical treatment of the diffuse part of the double layer that are needed.

Any kind of asymmetry between anions and cations (including but not limited to the magnitude of their charges) causes differences in ion-ion correlations between the two ionic species that can lead to appreciable effects when the asymmetry is sufficiently large. For instance, even outside an uncharged inert surface, e.g. a hard wall, there appears a charge separation for asymmetric electrolytes even in absence of any specific ion adsorption. Therefore an electric double layer will be spontaneously formed. Ion correlations could in principle account for the influence of electrolytes on the location of the point of zero charge, a phenomenon that is usually attributed exclusively to specific chemical adsorption, depending on the details of the system. As we can see from these examples, the term "specific adsorption" for adsorption due to direct surface-ion interactions is somewhat unfortunate because adsorption due to ion-ion correlations can also be specific in the sense that it depends on the species of ions present. However, as the term has long been in use as referring to adsorption due to direct chemical interactions between the ions and the surface, we will nevertheless use it here in the latter sense. In cases where ambiguity may arise we shall write "chemical specific adsorption," etc.

Although it is not direct evidence of ion adsorption due to ion-ion correlations, the possible relevance of such correlations has been demonstrated by the measurement of attractive double layer interaction between surfaces with equal surface charge density.[14–16] This interaction is attractive for small surface separations in presence of divalent counterions, while it is repulsive at any distance for monovalent ions. The attraction can be explained by electrostatic ion-ion correlation attraction between the charged surfaces (neglected in the PB approximation),[17–19] and is often

much stronger than any reasonable van der Waals interaction. Obviously, GC mean field theory cannot account for that phenomenon.

The connection to the phenomenon of charge inversion is that the switch from repulsion to attraction with increase in counterion valency is caused by a large *decrease in the repulsive contributions* to the double layer interaction, that makes the attractive correlation interaction dominant. This occurs because divalent counterions are much more strongly attracted to the surface region than monovalent ones, which gives rise to a much lower ionic concentration in the middle between the surfaces in the divalent case. The dominance of the attractive forces can occur when the number of adsorbed counterions is less than what is required for charge inversion, so appearance of double layer attraction can happen under milder conditions. Note that the ion-ion correlation attraction between the surfaces is not very different for monovalent and divalent ions, so it is not a variation in the attractive contribution to the force that explains the switch.[17,19] According to the theoretical treatment the ion-ion correlations cause both the attractive contribution to the double layer interaction and the strong attraction of multivalent ions to the surfaces.

Again, the interpretation of the experiments is not unambiguous because ions can be attracted to the surfaces by chemical specific adsorption. When the two interacting surfaces do not have exactly the same charge density and distribution, induction in combination with charge regulation can also cause attractions.[20] However, in this latter way double layer attractions cannot be accounted for when the two surfaces are identical. Then the question is whether identity of the two surfaces is established and whether the surface charge density is high enough for the attraction due to ion correlations to become substantial. It is a pity in many of these types of experiments the surface charge was insufficiently controlled, implying that the issue is not yet fully resolved.

A system where the action of ion correlations can unequivocally be shown to be the dominant factor for charge inversion has to satisfy a number of constraints. The surface charge must be accurately measurable and high, multivalent ions must be found that do not adsorb chemically and the hydrolysis state of these ions (determined by the pH) must be well-established. These are severe restrictions; they exclude at least two of the classical model systems of colloid science:

oxides are too complex because the surface charge and the state of hydrolysis are simultaneously changing with pH, and silver iodide because high surface charges are not attainable.

One system that does satisfy these requirements is the mercury/aqueous electrolyte interface. From an experimental standpoint, this system has many advantages. By employing dropping mercury electrodes the surface is continually rejuvenated and consequently very clean. For this interface, using a Lippmann electrometer, the interfacial tension can readily be measured as a function of the applied potential. Differentiation gives the surface charge density from the Lippmann equation, and the result can be confirmed by integration of directly measured capacitances, using a bridge method.[21] Consequently, very high quality data can be obtained. For these reasons this system has been widely studied experimentally. Because the charge on the surface is controlled by an externally applied potential, the surface charge density and the concentration and composition of the electrolyte can be varied independently. From the surface tension and charge a wealth of information can be obtained via relations obtained from the Gibbs adsorption isotherm. Particularly, the ionic components of charge are directly obtainable (see Section 2) and these quantities will play a central role in our analysis. Another relevant advantage is that relatively high surface charges are obtainable by polarization of the interface (absence of Faradaic current). Finally, the chemical specific adsorption of both cations and anions is generally low at sufficiently negative surface charge density,[22] though many anions adsorb specifically for positive surface charge. Hence, for a suitable electrolyte, all elements for anticipating a convincing theoretical interpretation of charge inversion in terms of ion correlations are fulfilled.

Here, we attempt to clarify the role of ion-ion correlations in electrical double layers by modeling the mercury/aqueous $MgSO_4$ solution interface and comparing this model with published data for the same system. This constitutes a quantitative test of the accuracy of the model predictions, including but not limited to the prediction that charge inversion should occur for double layers with divalent counterions at sufficiently high surface charge densities. While there exists a vast body of experimental data for weakly coupled system, i.e. for 1:1 salts, and a fair amount of data for 2:1 and 1:2 salts, experimental data for systems characterized by stronger ionic interactions, such as

3:1 and 2:2 salts, are scarce. In fact, the only example of a comprehensive, high quality data set for a 2:2 salt that we were able to find were the electrocapillary and capacitance measurements by Harrison, Randles and Schiffrin[23,24] on $MgSO_4$ solutions.

2 Electrocapillary Measurements

Let us consider a system consisting of a dropping mercury electrode and a reference electrode immersed in a solution of a binary salt. The latter electrode is reversible to either the cation (+) or the anion (−). For this system the Gibbs adsorption isotherm reads[25]

$$-d\gamma = \sigma dE_{\pm} + \Gamma_{\mp} d\mu^{salt} \tag{1}$$

where γ is the interfacial tension, σ is the surface charge density, $E_{\pm}$ is the electrostatic potential difference between the mercury electrode and the reference electrode,[26] Γ_i is the Gibbs adsorption excess for species *i* relative to the dividing surface for the solvent and μ^{salt} is the chemical potential of the salt. The subscript $\pm$ on E indicates that the reference electrode is reversible to either cations or anions.

The surface charge density is related to the interfacial tension and the electrostatic potential by the well known Lippmann equation

$$\sigma = -\left.\frac{\partial \gamma}{\partial E_{\pm}}\right|_{T,\mu^{salt}}, \tag{2}$$

where subscripts T and μ^{salt} indicate that the temperature and the chemical potential of the salt are to be held constant. The differential capacitance, C, is the derivative of the surface charge density with respect to the applied potential,

$$C = \left.\frac{\partial \sigma}{\partial E_{\pm}}\right|_{T,\mu^{salt}}. \tag{3}$$

As both γ and C are accessible from experiments where the applied potential is controlled, the surface charge density can be obtained by two routes that are independent apart from an integration constant. The range of surface charge densities that is experimentally available extends between about -20 to 25 μC/cm^2.

The surface excess of the ionic species with respect to which the reference electrode is *not* reversible can be obtained as

$$\Gamma_{\mp} = -\left.\frac{\partial \gamma}{\partial \mu^{salt}}\right|_{T,E_{\pm}}, \tag{4}$$

The components of charge, σ_i, i.e. the individual contributions to the countercharge to the surface that is due to adsorption or depletion of ion species i, can be defined from the surface excess as

$$\sigma_{\pm} = Z_{\pm} F \, \Gamma_{\pm}, \tag{5}$$

where $Z_{\pm}$ is the valency of the species of ion, with sign, and F is Faraday's constant. Electroneutrality requires that

$$\sigma = -(\sigma_{+} + \sigma_{-}). \tag{6}$$

Complete information about the components of charge for a binary electrolyte can therefore be obtained from experiments by use of reference electrodes reversible to one of the ionic species.

The components of charge are directly related to the ionic concentration profiles through

$$\sigma_{\pm} = Z_{\pm} F \int_{-\infty}^{\infty} [n_{\pm}(z) - n_{\pm}^{bulk} \Theta(z - z^{solv})] \, dz, \tag{7}$$

where $n_i(z)$ is the concentration profile of species i, z is the coordinate perpendicular to the surface, $\Theta(z - z^{solv})$ is one for positive arguments and zero for negative arguments and z^{solv} is the coordinate of the Gibbs plane for the solvent. For this reason electrocapillary measurements are suitable for testing theoretical predictions derived from the concentration profiles.

3 Modeling of the Double Layer

In this work we model the electrical double layer by specifying all relevant interactions in the system and solving the resulting statistical-mechanical model. Such a model is defined by the assumptions about the potentials describing all the interactions in the system. These assumptions may be regarded as approximations to the true interaction potentials. What we refer to below as "approximations" are of another type: approximations made to simplify the non-trivial problem of deriving thermodynamic observables from a given set of interaction potentials. In order to be able to make a comparison with Gouy-Chapman-Stern (GCS)[1] theory we adopt a model that is based on the same physical assumptions about the interactions in the system. The difference between our approach and the GCS theory lies entirely in the mathematical approximations made in the treatment of the model. In what follows, we will distinguish between the "diffuse" and the "inner" parts of the double layer in essentially the same way as is done within GCS theory. We acknowledge that this distinction is somewhat artificial; in a complete treatment of the problem all the details of the continuous transition between aqueous solution and liquid metal would be taken into account in the form of concentration profiles of all species present.

The fundamental assumptions in the model that we employ are that the solvent behaves as a dielectric continuum solely characterized by its dielectric constant. Each ion is spherical, has a short-range repulsive interaction potential (we will use a hard core potential) and has a point charge at the center. The mercury surface is assumed to be smooth and have a uniformly smeared out surface charge density σ. Here we will only consider planar surfaces. The interior of the mercury is a assumed to be a continuum with an infinite permittivity since it is a conductor. The surface then constitutes a dielectric discontinuity and the ions in the electrolyte experience so-called image charge forces from the surface polarization charge.

The PB approximation, which is used in GCS theory to treat the diffuse part of the double layer, ignores ion-ion correlations.[27] Such correlations include the effects of all kinds of ion-ion interactions, both electrostatic ones and those caused by non-zero ion sizes (core-core collisions). According to the PB approximation, the ions are treated as being point-like and the electrostatic

interactions amongst the ions are solely due to the electrostatic potential from the average charge distribution of the double layer (the "mean electrostatic potential"). In the underlying model it is, however, essential that ions have non-zero sizes, because otherwise the model would fall victim to the "Coulomb catastrophe", where negative and positive point charges would fall on top of each other, resulting in the unphysical situation of infinite negative potential energy. Because all interactions except electrostatic ones are neglected in the GC approximation a large class of models will give identical results when treated in that approximation. In GCS theory, the properties of diffuse double layers are unaffected by the excluded ion volume, for instance. Some effects of finite ion size are contained the Stern layer, but as such they will only affect the properties of the inner layer.

The presence of a dielectric discontinuity at the planar interface does not affect the structure of the diffuse part of a GCS double layer. One can show that the lateral translational symmetry of the charge distributions implies that the mean electrostatic field in the diffuse layer originating from the surface region (including the polarization charges) only depends on the total amount of charge per unit area of the surface and the dielectric constant of the solvent. Expressed in terms of image charges, the field in the diffuse layer due to the image of the entire planar double layer is zero (the total charge of the image is zero). The self-image interactions of the ions cannot be introduced into the Boltzmann factor simply as an *ad hoc* "correction" to the GC theory since the neglect of the ion-ion correlations implies that the screening of the image charge will not be taken into account. In order to treat this screening consistently it is essential that the interaction between ions is taken into account on a level beyond PB mean field theory. Ref. 28 and references therein contain early attempts to do so.

In GCS theory all deviations from ideality are contained in the ionic interactions with the mean electric field. As the mean field in bulk is zero the bulk electrolyte is treated as an ideal gas. We therefore expect deviations from GCS theory if the deviation from ideality in bulk is large. Close to a charged surface the concentration of counterions is large even for dilute electrolyte solutions. If the counterions interact strongly, the force on an ion in the double layer is not well represented by

the force from the mean electric field because each ion significantly perturbs its local environment, i.e. ion-ion correlations are important, and we expect deviations from GCS theory also in this case.

When ion-ion correlations are taken into account in the treatment of the diffuse layer, we will use the term "ion-correlation (IC) theory" for any accurate approach irrespectively of how (and if) a Stern layer is included in the model. To emphasize that a Stern layer *is* included we use the term "ion-correlation-Stern (ICS) theory". This is similar to the use of the term "GC theory" for a PB mean field treatment of the diffuse part of the double layer and "GCS theory" for a treatment that includes a Stern layer.

For any comparison between ICS and GCS theory to be meaningful, the same assumptions about the Stern layer must be made in both theories. As our main objective is to study the effects of ion-ion correlations in the diffuse layer, we will model a situation where the ion-surface interactions are as simple as possible, i.e. where specific adsorption is negligible. In the GCS as well as the ICS theory, the system should then have (at most) an ion-free layer, a zeroth order Stern layer. When we specifically refer to GCS theory with a zeroth order Stern layer we append a zero in parenthesis to the acronym. That is, we use the acronym GCS(0) to denote GCS theory with the constraint that only a zeroth order Stern layer is allowed. Similarly, we denote ICS theory with the Stern layer limited to zeroth order as ICS(0).

It is important to keep in mind that the inclusion of a Stern layer does in no way constitute a correction to the mathematical approximations used in the treatment of the diffuse part of the double layer but is a separate model assumption. Therefore, the validity of any conclusion regarding the Stern layer hinges on the validity of the theory used to treat the diffuse part of the double layer. The comparison between the ICS(0) theory and experimental data for a particular system therefore serves to establish whether there is any need to introduce a more sophisticated Stern layer for that system. The conclusion of such an analysis is of course dependent on the quality of the model for the diffuse double layer and may be subject to change on further refinement of that model. Nevertheless we expect that as long as the ion model includes, with reasonable accuracy, the interactions that are important in real systems, the qualitative conclusion will be robust. In order to ensure

that this is the case we use ion sizes that gives reasonable agreement with experimental activity coefficients when the model is applied to the bulk solution, see Section 4.4.

With the assumption of a charge-free Stern layer, the equations relating the inner and diffuse parts of the double layer in GCS theory, see ref. 1, are simplified and take on the form of the equations below, that are valid for both ICS(0) and GCS(0) theory. In the general case where the Stern layer *does* contain charge one must distinguish between the charge in the inner, σ^i, and in the charge in diffuse, σ^d, parts of the double layer. These are related to the surface charge density by $\sigma = -(\sigma^i + \sigma^d)$. As σ^i is always zero in this work, the need for this symbol is eliminated and the only surface charge density that needs to be considered is σ. To keep the number of symbols as small as possible, all equations below are therefore written in terms of σ.

Let us select a coordinate system with the z axis perpendicular to the mercury interface and with the origin at the plane of closest approach of the ion centers to the surface, at the coordinate z^{ion}, so that by this convention $z^{ion} \equiv 0$. The surface charge is assumed to be located at a plane at $z = z^{\sigma}$. We make no assumption about z^{σ} other than that $z^{\sigma} < z^{ion}$. In the case where image charges are considered we place the dielectric discontinuity at the coordinate z^{diel}, see Figure 1. The zeroth order Stern layer has a width of $|z^{ion} - z^{solv}|$,[29] where z^{solv} is the location of the Gibbs surface of the solvent, and its contributions to the components of charge are given by

$$\sigma_{\pm}^{i} = -Z_{\pm} F n_{\pm}^{bulk} (z^{ion} - z^{solv}) \tag{8}$$

Note that z^{solv} is not known *a priori* and must be determined from experimental data.

The diffuse parts of the components of charge are given by

$$\sigma_{\pm}^{d} = Z_{\pm} F \int_0^{\infty} (n_{\pm}(z) - n_{\pm}^{bulk})\, dz. \tag{9}$$

The inner and diffuse contributions to the components of charge are additive,

$$\sigma_{\pm} = \sigma_{\pm}^{i} + \sigma_{\pm}^{d}, \tag{10}$$

as a consequence of the separation of the inner and diffuse parts of the double layer by a sharp dividing surface. Note that as we only have a zeroth order Stern layer in the GCS(0) and ICS(0) theories, we have

$$\sigma = -(\sigma_+^d + \sigma_-^d). \tag{11}$$

since $\sigma_+^i + \sigma_-^i = \sigma^i = 0$. In the general case, Equation (6) has to be used.

The diffuse potential ψ^d, i.e. the difference in mean electrostatic potential between the point of closest approach for the ions to the surface and a point in the bulk solution, is given by

$$\psi^d = -\frac{F}{\varepsilon\varepsilon_0}\sum_i Z_i \int_0^\infty n_i(z)\, z\, dz. \tag{12}$$

This the same expression as in GC theory but the concentration profiles are in general different from the GC concentration profiles. In the ICS(0) theory the diffuse layer capacitance is given by

$$\frac{1}{C^d} = \frac{d\psi^d}{d\sigma}. \tag{13}$$

This expression is valid also in GCS(0) theory, but *not* in the general case of GCS theory where it has to be replaced by eq. (3.6.33) of ref. 1. In the current work the differential capacitance C^d for the ICS(0) theory is calculated numerically as a finite difference ratio from the variation in ψ^d due to a small change in σ. The capacitances of the charge-free inner and diffuse parts of the double layer act as capacitors in series, so that

$$\frac{1}{C} = \frac{1}{C^i} + \frac{1}{C^d}. \tag{14}$$

where C^i is the capacitance of the inner layer.

4 Model and Method

4.1 The Primitive Model Interaction Potential

The primitive model (PM) for electrolyte solutions is defined by the pair interaction potential u_{ij}, where i and j are species indices, given by

$$u_{ij} = u_{ij}^{core} + u_{ij}^{Coul} + u_{ij}^{im}, \tag{15}$$

where u_{ij}^{im} is the image charge potential, that is relevant only near a surface (see below), $u_{ij}^{core}(r)$ is the hard core potential, that is infinite for $r < d_{ij}$ and zero otherwise, and $u_{ij}^{Coul}(r)$ is the Coulomb potential. The latter is given in units of k_BT (with $\beta = 1/k_BT$, where k_B is Boltzmann's constant) by

$$\beta u_{ij}^{Coul}(r) = \frac{Z_i Z_j e_0^2}{4\pi\varepsilon\varepsilon_0 k_B T\, r} = \frac{Z_i Z_j l_B}{r}, \tag{16}$$

where Z_l, $l = i, j$, is the ionic valency (with sign) and e_0 is the unit charge. In the right hand side (rhs) we have introduced the Bjerrum length, $l_B = e_0^2/(4\pi\varepsilon\varepsilon_0 k_B T)$, i.e. the distance between unit charges for which their interaction energy is equal to k_BT. The value of the the relative permittivity ε (dielectric constant) is taken as that of the pure solvent. For water at 25 °C it is[30] 78.36 and therefore the Bjerrum length is 0.715 nm.

The contribution u^{im} to the pair potential is due to the fact that the interface is polarized by the presence of ions both due to shifts in electron density at the mercury surface and orientations of water molecules. It is zero in bulk solution. In models with a sharp dielectric discontinuity at a planar interface the potential from the polarization is easily treated by the method of images. For two ions located at coordinates $\mathbf{r}_1$ and $\mathbf{r}_2$, where $\mathbf{r}_\nu = (x_\nu, y_\nu, z_\nu)$, the contribution to the ion-ion pair potential from the image charges of the ions is given by

$$\beta u_{ij}^{im}(\mathbf{r}_1, \mathbf{r}_2) = \frac{\varepsilon_D Z_i Z_j l_B}{[(z_1 + z_2 - 2z^{diel})^2 + R_{12}^2]^{1/2}} \tag{17}$$

where $R_{12} = [(x_1 - x_2)^2 + (y_1 - y_2)^2]^{1/2}$ is the lateral distance, $\varepsilon_D = (\varepsilon - \varepsilon_w)/(\varepsilon + \varepsilon_w)$ and ε_w is the relative permittivity of the wall material. For a conductor such as a metal, ε_w is infinite and $\varepsilon_D = -1$. Unless otherwise stated we take $z^{diel} = -0.3$ nm, which corresponds roughly the diameter of a water molecule, in all cases where image charges are considered.

When the PM is applied to interfacial systems the interface has to be modeled as well as the ions. The approach that is applicable to ICS(0) theory is to assume that the surface is a uniformly charged plane that is impenetrable to the ions. It is likely that the mercury/water interface at negative polarization is very close to this idealization, as the excess charge on the mercury then stems from an excess of electrons. The ion-wall interaction is given by

$$v_i = v_i^{core} + v_i^{Coul} + v_i^{im}, \tag{18}$$

where the ion-"hard wall" interaction potential $v_i^{core}(z)$ is infinite when $z < z^{ion}$ and zero otherwise. We have here assumed that that anions and cations can approach the surface equally closely, a constraint that we shall relax in Section 5.3.3. The electrostatic interaction energy $v_i^{Coul}(z)$ of the ions with the surface charge density σ in a plane located at z^σ is given by

$$\beta v_i^{Coul}(z) = -\frac{Z_i e_0 \sigma}{2\varepsilon\varepsilon_0 k_B T}|z - z^\sigma|. \tag{19}$$

Note that since $z^\sigma < z^{ion}$ the value of z^σ does not affect the properties of the diffuse part of the double layer as all such values gives rise to the same forces on each ion there. The term v_i^{im} is the one-body image contribution to the interaction potential, the self-image interaction, i.e. the interaction between each ion and its own image charge

$$\beta v_i^{im}(z) = \frac{\varepsilon_D}{4}\frac{Z_i^2 l_B}{z - z^{diel}}. \tag{20}$$

It is of course far from certain that the forces between an ion and the interface are well represented by the continuum picture that forms the basis for the method of images, but this level of

sophistication is commensurate with the assumptions inherent in the PM so it is considered here.

4.2 GC Theory for the Diffuse Layer

The GC theory may be regarded as an approximate theory for the treatment of the PM. In this approximation the PM is indistinguishable from other members of a wider class of models where the interactions between ions are given by the sum of the Coulomb potential and some short-range potential. This is so because only the electrostatic interactions contribute to the mean field. In the GC theory the effect of the dielectric boundary drops out from the treatment of the planar diffuse double layer due to the symmetry of the charge distribution, as noted in Section 3. For completeness, the GC theory expressions used in GCS(0) theory for some relevant quantities are presented and briefly discussed in this section. The results are given here as functions of the bare surface charge density σ for easy comparison with the ICS(0) theory.

In GC theory for *Z:Z* electrolytes, the diffuse layer potential ψ^d as a function of surface charge density is

$$\psi^d = \frac{2RT}{ZF}\sinh^{-1}(p\sigma) = \frac{2RT}{ZF}\ln\left([(p\sigma)^2+1]^{1/2}+p\sigma\right) \tag{21}$$

where $p=(8\varepsilon\varepsilon_0 n^{bulk}RT)^{-1/2}$, R is the gas constant, T is the absolute temperature, n^{bulk} is the bulk concentration of salt and Z is the absolute value of the ionic valency. In the case of zeroth order Stern layer the surface charge density σ can be identified with the corresponding quantity in eq. (2). The expression would have to be modified to be valid in the presence of ionic charges in the Stern layer, see ref. 1.

The capacitance corresponding to eq. (21) is given by

$$C^d = \varepsilon\varepsilon_0\kappa[(p\sigma)^2+1]^{1/2} \tag{22}$$

where ε is the relative permittivity of the solvent, ε_0 is the permittivity of vacuum and κ is the inverse Debye length as defined by $\kappa^2 = 2(ZF)^2 n^{bulk}/(\varepsilon\varepsilon_0 RT)$. At the point of zero charge the capacitance is $\varepsilon\varepsilon_0\kappa$ whereas at high surface charge densities it approaches $\varepsilon\varepsilon_0\kappa|p\sigma|$. The valencies

of the ions of the electrolyte only enters the expression via κ.

The components of charge from the diffuse layer, $\sigma_{\pm}^{d}$, are in the GC theory given by

$$p\sigma_{\pm}^{d} = \pm\frac{1}{2}\left([(p\sigma)^2+1]^{1/2} \mp p\sigma - 1\right). \tag{23}$$

Very notably, for symmetric electrolytes they do not depend on the valencies of the ions. Thus, GC theory predicts that the components of charge are fully determined by the bulk electrolyte concentration and surface charge density, whatever the valency of the electrolyte. At the point of zero charge the components of charge are both zero, whereas at high positive $p\sigma$ it follows that $p\sigma_{-}^{d} \sim -(|p\sigma| - 1/2)$ and $p\sigma_{+}^{d} \sim -1/2$. For high negative surface charge densities $p\sigma_{-}^{d} \sim 1/2$ and $p\sigma_{+}^{d} \sim |p\sigma| - 1/2$. Another way to express these relations for aqueous systems at room temperature is to say that when the concentration is expressed in M, the component of charge for the co-ions will approach a plateau value of $-\mathrm{sign}(\sigma)$ 5.866 $(n^{bulk})^{1/2}$ μC/cm^2 as the surface charge density increases.[1] Thus, in the PB approximation there is always depletion of co-ions in the diffuse part of the double layer near charged surfaces and less counterions than needed to neutralize the surface charge. At the point of zero charge there is neither excess nor depletion of salt; small increments of charge are compensated on a 50-50% base by positive adsorption of one ion type of ion and negative adsorption of the other.

4.3 The AHNC Method for Calculation in the Ion Correlation Theory

Any method in statistical mechanics that treats ion-ion correlations with sufficient accuracy can be used to extract the true predictions of IC theory. In this work we use the anisotropic hypernetted chain (AHNC) method,[18,31] which is a procedure for the calculation of pair correlation functions and concentration profiles of an inhomogeneous fluid self-consistently within the HNC approximation for pair correlation functions. Close to a surface the pair correlation functions are anisotropic, which is taken into account in the AHNC method.

In the AHNC method, the Ornstein-Zernike equation for inhomogeneous fluids is solved nu-

merically by iteration for a trial set of concentration profiles, which gives the correlation functions. A new set of concentration profiles is then calculated from the equilibrium condition of equal chemical potential everywhere that can be written as

$$n_i(z) = n_i^{bulk} e^{-\frac{v_i(z)+\mu_i^{ex}(z)-\mu_i^{ex,bulk}}{k_B T}}, \tag{24}$$

where $\mu_i^{ex}(z)$ is the excess chemical potentials at z, calculated from the pair correlation functions and the trial profiles, and $\mu_i^{ex,bulk}$ is the chemical potential in bulk. Here one utilizes the fact that in the HNC approximation μ_i^{ex} can be expressed as a simple, known functional of these functions. New trial profiles are thus obtained and the procedure is iterated until the correlation functions and concentration profiles are fully self-consistent. In this work the concentration profiles and correlation functions are calculated for an electrolyte solution in a slit between two parallel, identical walls that are sufficiently far from each other so that the solution in the middle of the slit is very close to bulk conditions.

So far, the AHNC method has been tested against simulations for several systems and in most cases it shows excellent agreement.[18,19,32–34] Deviations between AHNC and simulations are found (i) for very high ionic densities that occur locally close to the wall for large surface charge densities or when the bulk concentration is very high and (ii) for situations with high electrostatic coupling and low bulk concentration, where the HNC equation has been shown[35] not to have a solution for the PM.

In case (i) the effects of short-range repulsions between counterions become very important and the agreement between AHNC calculations and simulations for identical systems are qualitative rather than quantitative. In the present work this shortcoming is expected to be of minor importance as the surface charge densities where this discrepancy is important are not reached in this work. Should it be necessary, this problem can be minimized by improving the closure, for instance by using a reference bridge function as done in ref. 34.

Failing (ii) is relevant in this case as the 2:2 system with the rather small ion sizes considered

here is sufficiently strongly coupled for us to expect that there is a concentration range in which no solution exists. In effect, this places a lower limit on the range of bulk concentrations for which convergent solutions can be found. The boundaries of this concentration range have been thoroughly investigated[35] in the PM for bulk electrolytes with anions and cations of equal size (the "restricted primitive model"). The boundaries applicable for inhomogeneous PM systems with unequal ionic sizes are, however, not known.

For the $MgSO_4$ solutions considered in this work we were able to obtain HNC solutions for the bulk electrolyte down to about 0.14 M. For the inhomogeneous system no solution could be found for the system in equilibrium with a 0.2 M bulk electrolyte, which is probably caused by the fact that the local concentration near the surface becomes so low that the regime in which there is no solution is entered. (For the system with larger ions, cf. Section 5.3.2, HNC solutions could be obtained for lower concentrations.) Since we limit ourselves to bulk concentrations above 0.5 M, the results from the AHNC method should be very accurate.

4.4 Modeling of $MgSO_4$ by the Primitive Model

As stated in Section 3 we need to determine reliable values for the ion-ion hard core contact distances d_{ij} (the "ion sizes") in the PM in a way that is independent of the description of the double layer. We therefore turn to calculations of the activity coefficients of bulk solutions of $MgSO_4$.

The expectation is that d_{+-} is by far the most critical distance and that small deviations in d_{++} and d_{--} are relatively unimportant, at least for volume fractions that are far from close packing. This is so because d_{+-} has a strong effect on the "ion pairing" between anions and cations whereas the sizes associated with like-charged pairs are less important because the Coulomb repulsion, at least for volume fractions that are not too large. Considering that our aim is not perfection, but merely adequacy, in the description of the ion-ion interactions, we make the assumption that the radii are pairwise additive in order to limit the number of adjustable parameters. The diameter of the anion, d_{--}, is taken to be equal to the crystallographic diameter[36] and d_{+-} is used as the fitting

parameter. The diameter of the cation, d_{++}, is then calculated from $d_{+-} = (d_{++} + d_{--})/2$.

The criterion for our choice of d_{+-} is agreement between experimental[37] and theoretical (PM) values of the mean activity coefficient, $f_{\pm}$, as a function of electrolyte concentration. The theoretical $f_{\pm}$ is calculated in the hypernetted chain (HNC) approximation for bulk electrolytes. The range of concentrations considered is between 0.20 and 2.5 M. Densities from ref. 38 are used to convert the experimental data from Lewis-Randall (molal concentration) scale to McMillan-Mayer (molar concentration) scale, appropriate for the PM, according to the procedure given in ref. 39. We find that the diameters $d_{++} = 0.30$, $d_{--} = 0.46$ and $d_{+-} = 0.38$ nm give the activity coefficient in good agreement with the experimental values, see Figure 2 where results for three values of d_{+-} are shown. As can be seen, the selected value of 0.38 nm gives the best agreement for low concentrations, that must be given most weight in the comparison as it is for low concentrations that the assumptions that defines the PM can reasonably be expected to be justified. The osmotic coefficients are in comparable agreement with experimental data (not shown). For the upper end of the concentration range the experimental $f_{\pm}$ data lie between the 0.38 and 0.355 nm curves, indicating that giving more weight to this region would result in a slightly smaller cation diameter than the selected value. From these results it is clear, however, that d_{+-} should not exceed 0.38 nm.

The choice of the excess chemical potentials in the form of activity coefficients, i.e. $\mu_i^{ex} = k_B T \ln f_i$, as the bulk properties to be used in the selection criterion for the ion model is justified by the fact that the concentration profiles are inextricably linked with the local excess chemical potential through the equilibrium condition of equal chemical potential everywhere, eq. (24). We argue that by ensuring that the excess chemical potential of the salt model is approximately correct in bulk, we improve the chances that it will give realistic concentration profiles. This criterion is also somewhat similar to the thermodynamic consistency criterion derived in ref. 40.

While an acceptable agreement with bulk thermodynamic data is certainly a necessary criterion for accepting an electrolyte model as realistic, it is not a sufficient one. The somewhat limited agreement of the present model with bulk thermodynamic data does not imply that the PM gives a

detailed representation of the short-range interaction between ions. For this reason we emphasize that the ion diameters that give the best agreement with thermodynamic data need not reflect the actual, geometric sizes of the hydrated ions.

The value for $d_{++} = 0.30$ nm obtained here is not transferable between different magnesium salts. For the halides, for instance, d_{++} around 0.6 nm gives reasonable agreement with experiments.[41] That the optimum Mg^{2+} radius differ between salts of different valence type illustrates the fact that the ion sizes in the context of the primitive model are not necessarily geometric properties of the hydrated ions but rather effective sizes that reflect all short-ranged pairwise interaction between ions. One might rationalize the small size of Mg^{2+} in $MgSO_4$ by the argument that the strong electrostatic attraction at anion-cation contact leads to a degree of ion association that mimics the "ion pairing" that is believed to occur in aqueous $MgSO_4$.[42] From a chemical point of view it is not at all unreasonable to expect the oxygens of sulfate to displace water molecules in the solvation shell of Mg^{2+}, which would imply a Mg^{2+}-SO_4^{2-} pair distance that is smaller than the sum of the hydrated radii. The most realistic set of ion diameters should thus be non-additive. Indirect support for this notion is given by recent simulations studies[43,44] where it was found that the effective cation-anion diameter was smaller than the mean of the cation-cation and anion-anion diameters in all the cases examined. Unfortunately for our purposes, while Mg^{2+} was among the cations examined neither SO_4^{2-} nor any other divalent anion was considered in that work, so the conclusions cannot be applied directly to the present problem. In addition, it is known from simulation studies that the interactions between ions in a molecular solvent have an oscillatory component, which becomes important for separations less than about 1 nm.

Nevertheless, the fact that the primitive model *does* perform as well as it does in our case can likely be ascribed to a major influence of the Coulomb interactions. We can thus be relatively confident that the primitive model does properly contain the dominant interactions.

5 Predictions of the Ion Correlation Theory

5.1 Potential and Capacitance

The diffuse layer potential, ψ^d, and its derivative with respect to σ, the inverse differential capacitance $1/C^d$ (cf. equation (14)), are shown as a function of the surface charge density in Figure 3. The potential passes through zero very close to $\sigma = 0$, which is a consequence of the fact that the electrolyte is not far from being symmetrical with respect to both ion-ion and ion-surface interactions. The maximum of $1/C^d$ therefore lies very close to $\sigma = 0$. (In the GC and therefore GCS(0) theory one always has $\psi^d = 0$ when $\sigma = 0$, but in ICS(0) theories this is not the case in general.)

For large negative σ the inverse capacitance turns negative, which corresponds to the existence of a minimum in ψ^d. This phenomenon is well known for PM electrolytes with parameters corresponding to divalent counterions in water at room temperature where ψ^d as a function of σ exhibits an extremum (maximum for positive surface charge densities, minimum for negative) beyond which the magnitude of the potential decreases with increasing magnitude of the surface charge density.[3,45] This behavior is seen here for all concentrations investigated.

An overall negative capacitance is incompatible with thermodynamic equilibrium. However, for complicated double layers, in which more than one capacitance can be distinguished, it is possible that one of the capacitances is negative, provided it is (over)compensated by the other one(s); Ref. 46 gives an experimental example of this. In our case, a negative sign of the diffuse layer capacitance does not preclude thermodynamic equilibrium if the inner layer capacitance is positive and smaller in magnitude, cf. equation (14). For the mercury/aqueous electrolyte interface, the magnitude of the diffuse layer capacitance as calculated from the PM is never smaller than a few thousands of μF/cm^2 in those cases where it is negative. Typical measured values of the total capacitance are in the order of tens of μF/cm^2 .[21] Under these circumstances, the occurrence of a negative diffuse layer capacitance implies that the overall capacitance must be larger than the inner layer capacitance.

As the diffuse layer capacitance is so large, the absolute value of any differences in inverse

capacitance for the different bulk concentrations is very small except around $\sigma = 0$. Because the experimental inner layer capacitance is so much smaller in magnitude, the variation in diffuse layer capacitance with concentration for this model corresponds to a negligible variation of the total capacitance. For the same reason, discriminating between the theoretical capacitances from GC and IC theories on the basis of experimental values is a very insensitive test of the relative merits of the two theories. Also a comparison on the basis of the effect of electrolytes does not work because the dependence on salt concentration is not qualitatively different between the two theories. For such a comparison the demands on the quality of experimental data is simply too high. So, on the basis of capacitance data it is virtually impossible to discriminate between the two models, even though there are dramatic differences between them.

5.2 Concentration Profiles and Components of Charge

The concentration profiles of Mg^{2+} and SO_4^{2-} for four bulk concentrations between 0.5 and 2.0 M for two surface charge densities are shown in Figure 4 and Figure 5 (with and without image charge interactions respectively). Let us first analyse the behavior in absence of images, Figure 5. For low surface charge density, $\sigma = -0.95$ μC/cm^2, there is depletion of electrolyte near the wall for all concentrations, in excess to the co-ion depletion that would be expected on the basis of GC theory due to the charge on the surface alone. This can be seen clearly from the fact that close to the walls, the concentration of *counterions* is smaller than the bulk concentration. This is an effect of ion-ion correlations. In the bulk solution the ionic atmosphere around *each individual ion* is spherically symmetric, while close to a wall it is not. The wall prevents the ion from being surrounded by other ions on one side, so when an ion is close to a wall its ionic atmosphere is distorted. With most of its countercharge on the solution side, each ion is subject to a net electrostatic force that pulls the ion in the direction away from the wall. When the force from the surface charge is weak or absent the result is a depletion of ions close to the surface. This mechanism is different from the exclusion of co-ions due to repulsion from the surface charge.

In the presence of attractive image charge interactions with the mercury surface, Figure 4, the

depletion for low surface charge densities is less pronounced but still visible at a short distance from the surface. By comparing Figure 4 and Figure 5 we see that the image charge interactions cause both the co-ion and counterion concentration to be higher near the surface compared to the case of no images. The peak at contact is due to the self-image charge interactions. In our case these are equally strong for both species of ions as the electrolyte is symmetric. Each ion close to the surface also interacts with the images of all other ions in its neighborhood. Due to ion-ion correlations, the net image charge interaction is screened and decays steeply with increasing distance from the surface (the decay length is half the decay length of the ion-ion correlations).

For the larger surface charge density, $\sigma = -9.95$ μC/cm^2, see the bottom panels in Figure 4 and Figure 5, there is not much difference between the profiles with and without image interactions. In the former case the concentrations are somewhat higher close to the surface. In both cases the concentration profiles show significant structure. The co-ion peak around $z = 0.5$ nm is typical for situations where there is overcharging. As seen in the figure, there are more co-ions (i.e. anions) than counterions (cations) in the region to the right of the first point where the co-ion and counterion concentration profiles cross each other (around $z = 0.3$ - 0.5 nm; this is most clearly seen for the three highest concentrations). Therefore the total charge in this region is negative (same sign as σ). Overall electroneutrality is maintained since this charge is neutralized by an excess of countercharge, due to depletion of co-ions and enrichment of counterions, near the surface (to the left of the crossing point).

The presence of an excess of countercharge near the surface is an effect of ion-ion correlations, as the model does not include chemical specific adsorption. When the surface charge density is increased the counterion concentration near the surface also increases. The correlation from the repulsion between counterions then gives an increasingly important contribution to the mean force on any given counterion. When a counterion is located close to the charged surface, other counterions are depleted from the region between the surface and the ion. Some of this depletion is due to electrostatic forces, but a significant part comes from hard core (excluded volume) interactions. In the GC theory neither of these two effects are considered, which means that there are

more counterions in the region between the ion and the surface than if ion-ion correlations were properly taken into account. These intervening ions weaken the net attraction between the ion and the surface charge. Thus, when correlations *are* considered, a larger part of the surface charge is "exposed" than in GC theory, which causes each counterion to be more strongly attracted to the surface region in the presence of correlations.[47,48]

Ionic core-core collisions that push counterions towards the surface give an additional, but relatively small, contribution to the attraction between the counterions and the surface. Together, these effects lead to a large build-up of countercharge near the surface. Likewise, the co-ions are more strongly repelled from the region near the surface than predicted by the GC theory. Therefore, the co-ions that must be present to compensate for the excess counterions are located predominantly at some distance from the surface, seen as the co-ion peak in Fig. Figure 4.

Most of the countercharge and the accompanying co-ion layer are located within a few tenths of a nanometer from the surface. For the 0.5 M case the concentration profiles decay monotonically to the bulk concentration for $z > 1$ nm, while for the higher bulk concentrations there are oscillations in the concentration profiles that continue in the region some distance from the surface. The amplitude decays exponentially with increasing distance from the surface. In some cases this can be seen in Figure 5 while in other cases the amplitude is so small that only the first peak is visible. Such oscillations are related to the conditions in the bulk solution and occur when the concentration is sufficiently large. The wave length of the oscillation is determined by (and the same as) that of the pair correlation functions in bulk, i.e. not by the properties of the interface. For low concentrations both the profile and the bulk correlation functions are monotonically decaying, but a region with excess countercharge and an accompanying co-ion peak still appears if the surface charge density is sufficiently high; the co-ion peak *is* a property of the interface even though the details of how the concentration profiles decay to bulk concentration are determined by the bulk correlations.

We will now consider the diffuse parts of the components of charge in the double layer as defined in eq. (9). These quantities reflect the (positive or negative) surface excesses of anions and

cations in the diffuse part of the double layer. For a given σ the anionic and cationic components of charge are related via equation (11) and are therefore coupled quantities. The anionic components of charge for several bulk concentrations are shown as a functions of the surface charge density in Figure 6 for both the cases with and without image charge interactions. The values from the GC theory are also shown.

Consider first the situation at and near the point of zero charge. We see that σ_-^d for the IC theory is positive in this region for all concentrations investigated. This behavior is in sharp contrast with the qualitative behavior in the GC theory according to which the components of charge are predicted to be exactly zero at the point of zero charge. As a positive value of σ_-^d corresponds to depletion of anions, which must be accompanied by an equal amount of cation depletion when $\sigma = 0$, there is salt depletion at the point of zero charge. For the system considered here, where the electrolyte is symmetric, the IC theory shares the feature with GC theory that close to the point of zero charge the surface charge is compensated by increased depletion of co-ions and enrichment of counterions in equal measures. Furthermore, image charge interactions attract both anions and cations towards the surface to the same degree. For these reasons the IC theory curves in panel (a) are similar to those in panel (b) apart from a vertical displacement around $\sigma = 0$; they have about the same derivative in the region $-2 < \sigma < 2$ μC/cm^2.

Consider next the situation for more negative surface charge densities. When the negative surface charge density is made larger in magnitude, the depletion of anions (that are co-ions to the surface) initially increases but reaches a maximum and then decreases with more negative surface charge density for all electrolyte concentrations. This tendency is most prominent in the absence of image charge interactions. Again, the results when ion correlations are taken into account are in sharp contrast to those from GC theory, according to which the depletion of co-ions should tend asymptotically to a plateau value. A decrease in σ_-^d, i.e. $\Delta\sigma_-^d < 0$, with increasingly negative σ implies a relative enrichment of salt in the diffuse part of the double layer. Both co-ions and counterions are brought in, the latter to a larger extent than needed to compensate for the increase in negative surface charge. This can be seen from from equation (11), which implies that

$\Delta\sigma_+^d + \Delta\sigma = -\Delta\sigma_-^d$, where the rhs is positive in the current case so $\Delta\sigma_+^d > |\Delta\sigma|$ when σ decreases.

5.3 Sensitivity to System Parameters

5.3.1 Dielectric Permittivity

In this section we consider the effect of varying the dielectric permittivity of the wall as well as the solvent. In Figure 7 the anionic components of charge for three values of the wall permittivity are shown, corresponding to the extreme cases of a "vacuum" wall and a "conducting" wall as well as the case where the wall permittivity is the same as that of the solvent. The distance of closest approach between the ions and the dielectric discontinuity is 0.3 nm ($z^{diel} = -0.3$ nm) in all calculations. The salt depletion for small surface charge densities is largest for the $\varepsilon_w = 1$ case and smallest in the $\varepsilon_w = \infty$ case. This can be explained by the self-image interaction between the ions and the wall that is repulsive when $\varepsilon_w = 1$ and attractive when $\varepsilon_w = \infty$, corresponding to image charges of the same and the opposite sign as that of the real charge, respectively.

For large negative surface charge densities the rate of decrease in the depletion with increasingly negative surface charge density is largest in the $\varepsilon_w = 1$ case and smallest in the $\varepsilon_w = \infty$ case. This is not surprising as the image charges of an ion also interacts with all other ions, hence the contribution to the ionic pair potentials. The image interactions increase the repulsion between counterions close to the wall for $\varepsilon_w = 1$, enhancing ion enrichment due to correlations. The opposite is the case when $\varepsilon_w = \infty$, the value that is applicable to the mercury surface. For highly charged surfaces the contribution from image charges to the pair potential thus has an effect on the components of charge that is opposite to that due to the self-image interaction.

In Figure 8 the permittivity of the wall is assumed to be the same as for the solvent, i.e. there are no image charges. The anionic components of charge as a function of surface charge density are shown for solvent permittivities 2.0, 1.5, 1.25, 1.0, 0.9 and 0.8 times that of water. As we see in the figure, a decrease in permittivity leads to an increase in the co-ion depletion for σ near zero and a decrease for large negative σ. This is expected since the deviation from the GC theory should increase as the ion-ion interactions becomes stronger. Both the overcharging for large

negative surface charge densities and the depletion for small surface charge densities are enhanced as the surface charge density is increased. This explains why the curves for different values of the permittivity cross each other. It is not obvious, however, why this should happen at about the same point for all the curves, which is the case. It is notable that the surface excess appears to depend more strongly on the permittivity for low permittivities than for high. Compare, for instance, the pair corresponding to 2 and 1.5 times the permittivity of water and the pair corresponding to 1 and 0.8. Changing the solvent permittivity changes the correlations in bulk as well as close to the surface whereas changing the wall permittivity only gives rise to changes in the correlations close to the surface. Our results in Figure 8 are consistent with those of Boda and coworkers.[49]

In the partition function for the PM, the temperature enters in βu_{ij} and βv_i only as the product εT (the products βu_{ij}^{core} and βv_i^{core} are independent of T because these potentials are either zero or infinite). Since the product εT for water *decreases* by about 14 % as the temperature increases from 0 to 100 °C, only two of the curves in Figure 8, the ones corresponding to 1 and 0.9 times the permittivity of water, lie within the range that is expected to be experimentally relevant for the aqueous $MgSO_4$ system. For other systems, such as salts of other valence types and/or non-aqueous solvents, a larger range of electrostatic coupling strengths may be relevant, however. While solvents with a dielectric permittivity exceeding that of water by a factor above 1.5 are virtually non-existent, the strength of the electrostatic interactions that correspond to divalent salt in a high permittivity medium is similar to that corresponding to a monovalent salt in a low permittivity medium.

5.3.2 Ion Size

In this section we compare the results obtained with a computation in which the cation diameter is doubled, i.e. $d_{++} = 0.60$, $d_{--} = 0.46$ and $d_{+-} = 0.53$ nm. Although this set of diameters gives very poor values for the activity coefficients, and therefore can be rejected as a satisfactory model of $MgSO_4$, this choice of cation diameter is not completely arbitrary. For several magnesium salts with monovalent anions the diameter $d_{++} = 0.60$ nm gives good agreement with experimental

activity coefficients, as mentioned in Section 4.4 above.

In Figure 9 the concentration profiles are shown for two surface charge densities. For a concentration of 0.5 M and small surface charge density, $\sigma = -0.95$ μC/cm^2, there is some depletion close to the wall. For 1.0 M solutions there happens to be about as much depletion of anions as there is enrichment of cations, a situation similar to the GC theory predictions for low surface charge density. The detailed behavior of the concentration profiles is, however, not like that expected from the GC theory since the concentration profiles are non-monotonic. For higher concentrations, 1.5 and 2.0 M, there is a large degree of enrichment close to the wall and the profiles show perceivable structure up to about 1 nm from the wall. For the higher surface charge density, -9.95 μC/cm^2, the oscillatory structure of the concentration profiles is very pronounced for these concentrations. Careful investigation of the concentration profiles reveal that oscillations are present in all cases, but they are hard to see on the scale of the figure for the lowest concentrations. Since the oscillatory structure is induced by the bulk correlations, oscillations are present for all surface charge densities, but they are less prominent in the upper panel. The large enrichment close to the walls at high concentrations and the oscillations in the concentration profiles make the structure superficially reminiscent of that a hard sphere fluid close to a hard wall,[50] at least for small surface charge densities and large concentrations. This illustrates that excluded volume constraints are important for the structure of the electrolyte in this case. The analogy with the hard-sphere system must not be carried too far, however.

In Figure 10 the anionic component of charge is shown as a function of surface charge density for the "big cation" model. The differences with respect to the "small cation" model, Figure 6, are striking. Only for 0.5 M concentration there is a maximum and the curve beyond that is almost flat. Fortuitously, at a concentration of 1.0 M the degree of depletion is qualitatively similar to that predicted by GC theory. For higher concentrations there is not depletion but enrichment of salt at the point of zero charge (not shown). In these cases, the negative surface charge density on the wall has to be very high to cause any depletion of anions.

It is instructive to compare the results for the "small cation" and "large cation" situation because

they can be identified as stemming from two different regimes: The "small cation" model belongs to the "electrostatic" regime where electrostatic interactions dominate whereas the "large cation" model at high concentrations belongs to the "core" regime where the packing constraints for the repulsive hard cores become dominant. In the latter regime one would not expect the assumption to hold that d_{+-} is the diameter that dominates the system properties. The electrostatic regime is characterized by depletion of salt near a weakly charged interface whereas the core regime is characterized by enrichment. Using this classification, the 1.0 M concentration of the "large cation" model would fall right at the boundary between the two regimes. Bulk activity coefficients are useful to illustrate the characterization of the system along these lines. An activity coefficient of less than one (negative excess chemical potential) indicates that attractive interactions dominate in bulk whereas a value of greater than one indicates predominance of repulsive interactions (positive excess chemical potential). A wall prevents nearby ions from interacting with other ions, simply because there can be no ions inside the wall. The excess chemical potential should thus be expected to decrease in magnitude but retain its sign as ions are brought close to an uncharged interface. This would give rise to an effective repulsive force between the wall and the ions in the electrostatic regime but an effective attractive force in the core regime. The difference between the correlations in bulk and those close to the surface thus gives a contribution to the total potential of mean force that may counteract, or work in concert with, any direct interaction between ions and walls. As the total potential of mean force depends on the interactions and concentration profiles in a complicated way, not much more can be said in general about the details of its distance dependence on the basis of bulk chemical potentials only. Conversely, no definite conclusion can be drawn about the direct interactions between ions and walls in systems where the deviation from ideality is large unless that deviation is taken into account in the determination of the concentration profiles.

The large differences between the "small cation" and the "large cation" models indicate that the properties of a model double layer is sensitive to the properties of the salt model, especially for the rather large concentrations studied here. With respect to components of charge, the two models predict deviations from GC theory that for the larger concentrations are in opposite directions. This

sensitivity highlights the importance of using rational criteria in the selection of the parameters for the salt model, as we have done in Section 4.4.

5.3.3 Distance of closest approach of ions to the surface

In this section we relax the constraint that the anions and the cations have the same distance of closest approach to the surface. See Figure 11 for a sketch of the system considered here. The origin of the coordinate system is placed at the plane of closest approach of the *cations*, that we write with a subscript as z_+^{ion}. We allow the anions to approach the surface up to the Gibbs plane of the solvent, that we for purpose of illustration take to be located at $z_-^{ion} = z^{solv} = -0.3$ nm. To avoid an unphysical singularity of the self-image interaction, the dielectric discontinuity must be placed at $z < z_-^{ion}$. For this reason we consider the values -0.4, -0.5 and -0.6 nm for z^{diel} rather than take $z^{diel} = -0.3$ nm as we do elsewhere. This range of values for z^{diel} is considered in order to establish the sensitivity of the model predictions with respect to this parameter.

The anionic components of charge are shown in Figure 12. In the cases with $z_-^{ion} \neq z_+^{ion}$ and $z^{diel} = -0.6$ and -0.5 nm (the upper two thick curves in the figure), the components of charge for moderate and large negative surface charge densities are quite similar to the cases with equal distance of closest approach (thin curves). For small surface charge densities the dashed thin curve, for which case no image charge interactions are included, is not very similar to the other three curves.

The most extreme case, with $z_-^{ion} = -0.3$ nm and $z^{diel} = -0.4$ nm (the bottom thick curve), displays much less depletion close to the point of zero charge than any of the other cases. Note that $z^{diel} = -0.4$ nm corresponds to just 0.1 nm between the dielectric discontinuity and the plane of closest approach for the anions. Since the radius of sulfate is 0.23 nm this would correspond to a significant portion of the charge distribution on a real sulfate ion being inside the metal. In this situation the assumption that the force on the ion is well represented by the image charge force on a point charge at the ion center is not a reasonable model, but will severely overestimate the strength of these forces. Even in this case, however, the components of charge for large negative

surface charge densities are remarkably similar to those from the other variants of the model.

We can thus conclude that the predictions of the model for large negative surface charge densities are insensitive to the details of the wall-ion interaction investigated in this section. Otherwise stated, any conclusion based on comparison to experimental data for such surface charge densities is robust.

6 Comparison with Experimental Data

In this section results from capacitance and electrocapillary measurements from refs.[23] and[24] are presented and compared with results from the GCS(0) and ICS(0) theories. As we make no attempt to model chemical specific adsorption we will mainly focus on the subset of the data that corresponds to zero or negative surface charge, where specific adsorption is expected to be weak or absent. (Below we shall investigate whether this expectation is justified.) Our main focus will be to determine which features of the data can be explained for reasonable parameter values within the framework of ICS(0) theory in its present form and which features cannot.

6.1 Components of Charge

Experimental data for the cationic component of charge for a mercury/$MgSO_4$ solution interface is given in ref. 23 for $MgSO_4$ concentrations 0.1, 0.2, 0.5, 1.0, 1.5 and 2.0 M and for surface charge densities down to about -17 μC/cm^2. The thickness of the zeroth order Stern layer, here defined as $|z^{ion} - z^{solv}|$,[29] is used as an adjustable parameter to fit the ICS(0) results to the experimental data. This thickness only affects the contribution σ_-^i from the inner part of the double layer, equation (8). In practice we vary z^{solv} since $z^{ion} \equiv 0$ here. The same thickness is then used for the GCS(0) interpretation. Note that the ionic sizes have been determined from bulk data, see Section 4.4, so no additional fitting parameter was needed.

A comparison between the experimental data and the theoretical results from GCS(0) and ICS(0) calculations is made in Figure 13, where the anionic component of charge is presented.

We consider the four concentrations where results were obtained from AHNC calculations (cf. end of Section 4.3). The anionic and the cationic components of charge and the total surface charge density are related via eq. (6) (this equation was used to obtain the experimental σ_- from σ_+). It is preferable to plot σ_- for negative surfaces since the co-ion component of charge varies considerably more slowly than the counterion component. Therefore, differences between the experimental data and the theoretical predictions are more clearly visible. Note, however, that the range of surface charge densities in the figure extends somewhat into the positive range, where the anions become counterions.

As seen in Figure 13, the ICS(0) result for 0.5 M bulk concentration with $z^{solv} = -0.35$ nm agrees with the experimental data within the experimental uncertainty for $\sigma < -1$ μC/cm^2. The value $z^{solv} = -0.35$ nm was used here for all ICS(0) and GCS(0) curves. Changes in z^{solv} have the effect of shifting each σ_- curve vertically in proportion to the bulk electrolyte concentration, cf. equation (8). The value of z^{solv} may in principle depend on the concentration, but this is not considered in our fit. It is therefore the shapes of the curves rather than their absolute values in any point that are to be given most weight in the comparison with the experimental data. The 1.0 and 1.5 M results agree reasonably well with the experiments in the same interval, while there are quite large deviations for the 2.0 M case. The main message from these graphs is that ICS(0) results are able to predict the experimentally found maximum, which is impossible in GCS(0) theory. For the lower part of the concentration range, the agreement is even quantitative. The only way in which the maxima can be explained in terms of a mean field GCS theory is by assuming that Mg^{2+} adsorbs specifically in conjunction with a relatively thick ion-free layer, which would be rather artificial and hence difficult to justify, especially so since there is no positive evidence for specific adsorption of Mg^{2+} ions at the point of zero charge (see below). Thus, our results clearly demonstrate the action of ion-ion correlations in the electric double layer.

In the original experimental paper,[24] much of the variation of σ_- with concentration was explained by assuming a thickness of about 0.44 nm for the ion-free layer. The anionic component of charge from solely such a layer (shown in Figure 13), i.e. σ_-^i, as a function of σ is always a

horizontal line, hence the maxima cannot be accounted for in this way. The discrepancy between this thickness and our estimate 0.35 nm is due to the fact that some depletion of anions is in the ICS(0) theory accounted for in σ_-^d and arises from the ion-ion correlations in the diffuse part of the double layer.

The ICS(0) curves in Figure 13 are calculated in presence of image charge effects. In Figure 14 we show the corresponding results without image charges. Here, we have selected $z^{solv} = -0.30$ nm, which gives a reasonable agreement with the experimental data for $\sigma < -4$ μC/cm^2 for the 0.5 and 1.0 M cases. If instead we had chosen $z^{solv} = -0.35$ nm, the agreement for the 1.0 M case would have deteriorated somewhat while that for 1.5 M would have improved (not shown). The difference of 0.05 nm in z^{solv} is sufficient to accommodate a large part of the differences between the curves in panels (a) and (b) of Figure 6. The larger salt depletion in the absence of attractive image charge interactions is to a large extent compensated by a thinner ion-free layer. Thus, excluding image charge effects does not have a large effect on the possibility to obtain a fit between theory and experiment. The behavior of σ_- for small negative surface charge densities is better described when images are included. On the other hand, the trend in the experimental data for large negative surface charge densities appears to be better reproduced by the model without images. Because the scatter is so large in the experimental data set, the data can be accommodated by both the "image" and "no image" variant of ICS(0) theory. No definite conclusion can thus be drawn about their relative merits.

The magnitude of the effect of image charges depends on the location of the dielectric discontinuity via the parameter z^{diel} in eqs. (17) and (20). As mentioned earlier, we have selected the value -0.3 nm for z^{diel}, corresponding to a dielectric discontinuity 0.3 nm from the plane of closest approach of the ions. One must remember that the various distances and ion sizes used in the PM are merely effective parameters that do not necessarily give precise information about the geometrical distances, but it is important that these parameters have reasonable magnitudes.

For positive surface charge densities, we see in Figure 13 that the experimental σ_- value decreases very strongly with increasing σ; more strongly than the ICS(0) theory predicts for the

parameters used. In order to show the behavior of the components of charge over a range that also includes larger positive surface charge densities, the *cationic* component of charge, σ_+, is shown as a function of surface charge density in Figure 15. For negative surface charges the agreement between the ICS(0) and experimental values is very good except for the 2.0 M case (eq. (6) implies that the deviations must be as large as in Figure 13). However, for positive surface charges the theoretical results deviate very strongly from the experimental data. In fact, for large positive σ this deviation is much larger than the difference between the results of the GCS(0) and ICS(0) theories. Even if one would allow anions to enter into the inner layer as in Section 5.3.3, one would not obtain good agreement between the ICS(0) theory and experiment for positive surface charges (not shown). All of this suggests that strong specific chemical adsorption of SO_4^{2-} ions on positively charged mercury surfaces[51] has to be taken into account. As will be seen below, the behavior of the potential at the point of zero charge also supports to this notion.

6.2 Potential at the Electrocapillary Maximum

The potential at the electrocapillary maximum (point of zero charge) for the mercury/$MgSO_4$ solution interface with respect to the sulfate-reversible $Hg|Hg_2SO_4|$ reference electrode, i.e. for the cell $Hg|Hg_2SO_4|MgSO_4(n^{bulk})|Hg$, is given in ref. 23 for ten concentrations of $MgSO_4$. In order to compare the position of the electrocapillary maximum between different concentrations, the potential scale must be such that the reference electrode is unaffected by changes in electrolyte concentration. From the data in ref. 23 we have therefore calculated the potential with respect to the reference electrode $Hg|Hg_2SO_4|MgSO_4(1M)|$ by subtracting the potential of the concentration cell $Hg|Hg_2SO_4|MgSO_4(n^{bulk})||MgSO_4(1M)|Hg_2SO_4|Hg$, calculated via the Nernst equation. We used activity coefficients taken from ref. 37, which we converted to the molarity scale using densities from ref. 30. Here, n^{bulk} denotes the concentration of the solution in contact with the mercury electrode. The results are shown in Figure 16. It can be seen in this figure that the potential decreases with concentration in an almost perfectly linearly fashion, changing at a rate of about -8.5 mV/M.

A negative shift of the position of the electrocapillary maximum on an increase in concentration is often quoted as evidence for chemical specific adsorption of anions. The argument is that specific chemical adsorption of anions tends to induce a positive surface charge on the mercury, so that a more negative potential must be applied to attain the point of zero surface charge density than in their absence.[22] This approach contains the implicit assumption that, as predicted by GC theory, the diffuse layer potential at the point of zero charge does not depend on the bulk concentration. However, when correlation effects are taken into account in the calculation of the diffuse layer potential this needs not be the case. In the present case with a nearly symmetric electrolyte the diffuse layer potential at the point of zero charge is indeed almost constant over the range of concentrations considered, as can be seen from Figure 3. Thus, to take ion-ion correlations into account does not invalidate this criterion for detecting specific adsorption *in this case*. The tentative conclusion is therefore that sulfate ions are chemically specifically adsorbed at the point of zero charge but that magnesium ions are not (or at least much less strongly so). It must be kept in mind that this conclusion may be subject to change with further refinement of ICS model of the diffuse layer. A difference in the distance of closest approach to the surface between anions and cations, such as the one considered in Section 5.3.3, could conceivably explain much of the shift in the point of zero charge, for instance.

The conclusion that sulfate is specifically adsorbed at the point of zero charge is consistent with the interpretation of experiments on Na_2SO_4.[51] The conclusions reached in that work have, however, been contested.[52,53] The objections raised are not applicable to the potential data considered in the present work, despite that the experiments are very similar. The crucial difference is that in ref. 51 potential scale conversions are carried out by use of an approximately calculated cell potentials for cells with a liquid junction potentials, whereas in ref. 23 measured cell potentials are used. Note that the approximations used in ref. 51 may affect both the conclusions about the shift of the electrocapillary maximum with concentration and those regarding the components of charge in that work.

7 Concluding Remarks

The results above show that for concentrations up to about 1.5 M and surface charge densities more negative than about -1 μC/cm^2, the properties of the double layer at the Hg/aqueous $MgSO_4$ interface are well described by ICS(0) but not by GCS(0) theory. The ICS(0) theory correctly predicts the feature of the experimental data in ref. 23 that the anionic component of charge reaches a maximum and then decreases with increasingly negative surface charge density. GCS theory would be unable to give an explanation of these experimental features of the components of charge unless a sophisticated Stern layer is included. The combination of a zeroth order Stern layer and adsorption due to ion-ion correlations in the diffuse layer naturally accommodates the experimental behavior with only one fitting parameter (the width of the Stern layer), that simply adds a constant shift (proportional to the bulk concentration) of the theoretical curves. In our view, this constitutes strong evidence of the importance of ion-ion correlations in electrical double layers. As far as we are aware this is the first unambiguous experimental demonstration of the action of ion-ion correlations in this context.

Image charges give rise to some enrichment near the surface that compensates for the depletion due to ion-ion correlations. This is particularly important mainly close to the point of zero charge. For larger surface charge densities the image charges partly counteract charge inversion by weakening the ion-ion correlations close to the surface. These conclusions are valid for materials with an infinite permittivity, as for a metal. Had the permittivity been much smaller than that of water, a very common situation, the reverse would apply.

For positive surfaces the deviation between the model and experimental components of charge are attributed to chemical specific adsorption of sulfate. This is an interesting distinction: at the positive side the double layer seems to be dominated by adsorption in the Stern layer, whereas on negative surfaces the ICS(0) model prevails. Although we do not model the adsorption on positive surfaces here, we do expect that the ICS theory can be extended to treat the specific adsorption of ions, e.g. by the inclusion of a short-range non-electrostatic adsorption potential for the ions, which gives rise to the Stern layer of adsorbed ions. The equilibrium between free and adsorbed

ions will then automatically be taken into account in the model. When ion-ion correlations are considered in the modeling of chemically specifically adsorbed ion layers, one has the advantage that the effect of lateral interactions within that layer as well as correlations with all ions would be included automatically. Actually, such an approach would help to overcome the most-evasive problem in Stern theory, viz. establishing the mean potential at the inner Helmholtz plane. If the IC model and the choice of the parameters are adequate such an analysis is expected to lead to a chemical specific adsorption Gibbs energy that is independent of the surface charge.

Deviations from GCS behavior become stronger with increasing strength of the electrostatic interactions. Electrolytes with ions of higher valency than two would therefore be more promising when one wants to quantify deviations from PB theory and make comparisons with the predictions of theories containing ion-ion correlations. The practical impediment is that trivalent ions tend to hydrolyze, producing strongly chemically adsorbing complexes. Hence, in practice realistic opportunities for testing the model remain scarce and the elaboration given here may appear to be one of the few feasible.

As the long-range electrostatic interactions depend only on the ionic valencies and the solvent and wall permittivities, one would expect that it is possible to find chemically dissimilar systems where the electrostatic interactions are similar. If this is indeed the case, it would provide an opportunity for further tests of the validity of ion-ion correlations as a mechanism for overcharging. As the strength of the electrostatic interactions can be changed either by changing the valency of the electrolyte or the relative permittivity of the solvent, non-aqueous electrolytes might be appropriate for testing the generality of the conclusions drawn above. For instance, one would expect that an electrolyte consisting of a 1:1 salt in a solvent with relative permittivity of about 20 would behave as a 2:2 salt in water. Similarly a double layer with monovalent counterions in a solvent of relative permittivity 20 would be similar to a double layer with divalent counterions in water of twice the surface charge density. The dropping mercury electrode appears to be a suitable setup, perhaps also for experiments employing non-aqueous electrolyte. In fact there are some examples of such experiments in the literature.[54,55] Another option may be to study the double layer on dispersed

oxides in the presence of non-hydrolyzing multivalent electrolyte. Awaiting such applications the system investigated by us remains unique for the reasons stated in the last paragraphs of Section 1.

Acknowledgments

We would like to thank Professor David Schiffrin for making the data from his PhD thesis, ref. 23, available to us. E. W. would also like to thank Dr. Zareen Abbas for fruitful discussions regarding the modeling of bulk electrolytes. This work has received financial support from the Swedish Research Council.

References

(1) Lyklema, J. *Fundamentals of Interface and Colloid Science, Solid-Liquid Interfaces, II*; Academic Press, 1995.

(2) Lyklema, J. *Fundamentals of Interface and Colloid Science, Particulate Colloids, IV*; Academic Press, 2005.

(3) Torrie, G. M.; Valleau, J. P. *J. Phys. Chem.* **1982**, *86*, 3251.

(4) Lozada-Cassou, M.; Saavedra-Barrera, R.; Henderson, D. *J. Chem. Phys.* **1982**, *77*, 5150.

(5) Outhwaite, C. W.; Bhuyian, L. B. *J. Chem. Soc.: Faraday Trans. 2* **1983**, *79*, 707.

(6) Carnie, S. L.; Torrie, G. M. *Adv. Chem. Phys.* **1984**, *56*, 141.

(7) Torrie, G. M.; Valleau, J. P.; Outhwaite, C. W. *J. Chem. Phys.* **1984**, *81*, 6296.

(8) Attard, P. *Curr. Opin. Colloid Interface Sci.* **2001**, *6*, 366.

(9) Grosberg, A. Y.; Nguyen, T. T.; Shklovskii, B. I. *Rev. Modern Phys.* **2002**, *74*, 329.

(10) Martin-Molína, A.; Quesada-Peréz, M.; Galisto-González, F.; Hidalgo-Álvarez, R. *J. Phys.: Condens. Matter* **2003**, *15*, S3475.

(11) Jönsson, B.; Nonat, A.; Labbez, C.; Cabane, B.; Wennerström, H. *Langmuir* **2005**, *21*, 9211.

(12) Besteman, K.; Zevenbergen, M. A. G.; Lemay, S. G. *Phys. Rev. E* **2005**, *72*, 061501.

(13) Stern, O. *Z. Electrochem.* **1924**, *30*, 508.

(14) Kjellander, R.; Marčelja, S.; Pashley, R. M.; Quirk, J. P. *J. Phys. Chem* **1988**, *92*, 6489.

(15) Kjellander, R.; Marčelja, S.; Pashly, R. M.; Quirk, J. P. *J. Chem. Phys.* **1990**, *92*, 4399.

(16) Kékicheff, P.; Marčelja, S.; Senden, T. J.; Shubin, V. E. *J. Chem. Phys.* **1993**, *99*, 6098.

(17) Guldbrand, L.; Jönsson, B.; Wennerström, H.; Linse, P. *J. Chem. Phys.* **1984**, *80*, 2221.

(18) Kjellander, R.; Marčelja, S. *Chem. Phys. Lett.* **1984**, *112*, 49.

(19) Kjellander, R.; Åkesson, T.; Jönsson, B.; Marčelja, S. *J. Chem. Phys.* **1992**, *97*, 1424.

(20) Lyklema, J.; Duval, J. F. L. *Adv. Colloid Interface Sci.* **2005**, *114-115*, 27.

(21) Grahame, D. C. *Chem. Rev.* **1947**, *41*, 441.

(22) Hunter, R. *Foundations of Colloid Science*, 2nd ed.; Oxford University Press: New York, 2001; See section 7.4.

(23) Schiffrin, D. Ph.D. thesis, University of Birmingham, 1965.

(24) Harrison, J. A.; Randles, J. E. B.; Schiffrin, D. J. *J. Electroanal. Chem.* **1970**, *25*, 197.

(25) Hunter, R. *Foundations of Colloid Science*, 2nd ed.; Oxford University Press: New York, 2001; See section 7.2.

(26) More strictly $-e_0E_{\pm}$, where e_0 is the elementary charge, equals the difference in the electrochemical potential for electrons in electrical leads of the same kind of metal connected to the electrodes.

(27) Jönsson, B.; Wennerströn, H.; Halle, B. *J. Phys. Chem.* **1980**, *84*, 2197.

(28) Levine, S.; Outhwaite, C. W. *J. Chem. Soc.: Faraday Trans. 2* **1978**, *74*, 1670.

(29) The thickness of the Stern layer is often taken as the distance between the surface charge and the plane of closest approach of the ions. Because the location of the surface charge and that of the Gibbs surface of the solvent need not coincide this creates some ambiguity. We have chosen to define the thickness in terms of the Gibbs surface of the solvent because our main interest is in the comparison with the experimental components of charge.

(30) *Handbook of Chemistry and Physics*, 52nd ed.; Weast, R. C., Ed.; The Chemical Rubber Co.: Cleveland, OH, 1971.

(31) Kjellander, R.; Marčelja, S. *J. Chem. Phys.* **1985**, *82*, 2122.

(32) Bratko, D.; Jönsson, B.; Wennerström, H. *Chem. Phys. Lett.* **1986**, *128*, 449.

(33) Valleau, J. P.; Ivkov, R.; Torrie, G. M. *J. Chem. Phys.* **1991**, *95*, 520.

(34) Greberg, H.; Kjellander, R.; Åkesson, T. *Mol. Phys.* **1997**, *92*, 35.

(35) Belloni, L. *J. Chem. Phys.* **1993**, *98*, 8080.

(36) *Ion Properties*; Marcus, Y., Ed.; Marcel Dekker, Inc.: New York, NY, 1997.

(37) Rard, J. A.; Miller, D. G. *J. Chem. Eng. Data* **1981**, *26*, 33.

(38) Novotný, P.; Söhnel, O. *J. Chem. Eng. Data* **1988**, *33*, 49.

(39) Pailthorpe, B. A.; Mitchell, D. J.; Ninham, B. W. *J. Chem. Soc. Faraday Trans.* **1984**, *80*, 115.

(40) Gonzáles, R.; Sanz, F. *Electroanalysis* **1997**, *9*, 169.

(41) Abbas, Z.; Ahlberg, E.; Nordholm, S. *J. Phys. Chem. B* **2009**, *113*, 5905.

(42) Buchner, R.; Chen, T.; Hefter, G. *J. Phys. Chem. B* **2004**, *108*, 2365.

(43) Gavryushov, S.; Linse, P. *J. Phys. Chem. B* **2006**, *110*, 10878.

(44) Gavryushov, S. *J. Phys. Chem. B* **2006**, *110*, 10888.

(45) Torrie, G. M. *J. Phys. Chem.* **1992**, *96*, 3772.

(46) Lyklema, J. *Trans. Faraday Soc.* **1963**, *59*, 418.

(47) (a) Kjellander, R.; Greberg, H. *J. Electroanal. Chem.* **1998**, *450*, 233; (b) Erratum: Kjellander, R.; Greberg, H. *J. Electroanal. Chem.* **1999**, *462*, 273.

(48) Kjellander, R. *J. Phys.: Condens. Matter* **2009**, in press.

(49) Boda, D.; Henderson, D.; Chan, K.-Y.; Wasan, D. T. *Chem. Phys. Lett.* **1999**, *308*, 473.

(50) Kjellander, R.; Sarman, S. *J. Chem. Soc., Faraday Trans.* **1991**, *87*, 1869.

(51) Payne, R. *J. Electroanal. Chem.* **1975**, *60*, 183.

(52) Daghetti, A.; Trasatti, S. *J. Electroanal. Chem.* **1984**, *162*, 327.

(53) Payne, R. *J. Electroanal. Chem.* **1984**, *162*, 333.

(54) Jastrzębska, J. *Elecrochim. Acta* **1971**, *16*, 1693.

(55) Fawcett, W. R.; Filho, R. C. R.; Doubova, L. M. *J. Chem. Soc. Faraday Trans.* **1991**, *87*, 2967.

Figure Captions

Figure 1: Illustration of how the interface between mercury and an aqueous $MgSO_4$ solution is modeled. The mercury phase is modeled as an ideal conductor (i.e. $\varepsilon_w = \infty$) and the solvent as a dielectric continuum with relative permittivity ε. The dielectric discontinuity is located at z^{diel}, indicated by a dashed vertical line. The vertical line at z^{ion} indicates the position of the plane of closest approach of the ion centers. The dashed-dotted vertical line at z^{σ} indicates the location of the surface charge and the vertical full line at z^{solv} indicates the position of the Gibbs dividing plane of water. Note that z^{diel} is specified *a priori* while z^{solv} is used as a fitting parameter. No special assumptions are made about the relation between z^{diel}, z^{σ} and z^{solv} although we expect that they should be close to each other for the model to be realistic. The curves are sketches of ionic concentration profiles and the horizontal dashed line shows the bulk concentration of electrolyte.

Figure 2: Comparison between experimental (symbols) and primitive model, PM, (curves) activity coefficients, $f_{\pm}$, of aqueous $MgSO_4$ solutions for various values of d_{+-}. The PM values are calculated within the HNC approximation. The distances of closest approach between the cations and anions, d_{+-}, are indicated in the figure. The diameter of the anions d_{--} is taken to be 0.46 nm throughout and the diameter of the cations, d_{++}, follows from the assumed additivity of the radii. The value 0.38 nm is the one used for d_{+-} in the calculations in this work unless otherwise stated.

Figure 3: The diffuse layer potential ψ^d (panels a and c) and the inverse of the corresponding capacitance C^d (panels b and d) as functions of surface charge density for the system described in Figure 1 for the bulk electrolyte concentrations indicated. The thick curves are from IC theory, calculated using the AHNC method with the PM pair interaction potential, see Figure 2. The thin curves are from GC theory. Panels (a) and (b) show the results for a mercury surface (image charge interactions included) while panels (c) and (d) show the corresponding results without image charge interactions.

Figure 4: Concentration profiles in the diffuse part of the double layer from IC theory for the

system with image charges considered in Figure 3 for the bulk electrolyte concentrations indicated. In panel (a) $\sigma = -0.95$ μC/cm^2 and in panel (b) $\sigma = -9.95$ μC/cm^2. The full curves denote $n_+(z)$, the cation (counterion) concentration profile, and the dashed curves denote $n_-(z)$, the anion (co-ion) concentration profile, respectively.

Figure 5: Same as Figure 4, but the dielectric constant on both sides of the charged surface is set equal to that of water, i.e. no image charge interactions are included.

Figure 6: Diffuse layer part of the anionic component of charge, σ_-^d, as a function of surface charge density for the $MgSO_4$ bulk concentrations indicated. (a) Results for a mercury surface (image charge interactions included). (b) Corresponding results without image charge interactions. The bold curves are from IC calculations whereas the thin ones are from GC theory. Systems as in figs. Figure 4 and Figure 5. (Note that the abscissa scale has negative polarization to the left and positive to the right contrary to the usual convention in electrochemistry.)

Figure 7: Diffuse layer part of the anionic component of charge as a function of surface charge density for 1.0 M concentration for wall permittivities corresponding to vacuum, water and a perfect conductor, as indicated in the figure. The dielectric discontinuity is assumed to lie 0.3 nm from the plane of closest approach of the ions.

Figure 8: Diffuse part of the anionic component of charge as a function of surface charge density for 1.0 M $MgSO_4$ solutions with dielectric constants 2, 1.5 1.25, 1, 0.9 and 0.8 times that of water, ε. Image charge interactions are *not* included. Except for the full curve, corresponding to the dielectric constant of water, longer dashes means higher permittivity. Selected values of the permittivity are shown in the figure.

Figure 9: Same as Figure 5, but for large ions. The ionic diameters used are $d_{++} = 0.60$, $d_{--} = 0.46$ and $d_{+-} = 0.53$ nm.

Figure 10: Same as the IC results in Figure 6 b, but for larger cations. Same ionic sizes as in Figure 9.

Figure 11: Illustration of the variants of the double layer model considered in Section 5.3.3. In contrast to the system considered elsewhere in this paper, presented in Figure 1, the coordinates of the plane of closest approach of the anions, z_-^{ion}, and the cations, z_+^{ion}, are different. Otherwise, the symbols have the same meaning. The origin of the coordinate system is placed at z_+^{ion}, i.e. $z_+^{ion} \equiv 0$. The Gibbs surface of the solvent is assumed to coincide with the plane of closest approach of the anions and is taken to be located at $z = -0.3$ nm, i.e. $z^{solv} = z_-^{ion} = -0.3$ nm. For z^{diel}, the values -0.6, -0.5 and -0.4 nm are considered (marked in the figure as dashed vertical lines).

Figure 12: The thick curves show the anionic components of charge (total, not only the diffuse part) for a model where the anions can approach the surface as close as up to the Gibbs plane of the solvent, here taken to be located at $z^{solv} = -0.3$ nm, cf. Figure 11. The bulk $MgSO_4$ concentration is 0.5 M and $z^{diel} = -0.6$ nm (long-dashed curve), $z^{diel} = -0.5$ nm (medium-dashed curve) and $z^{diel} = -0.4$ nm (short-dashed curve). The thin curves correspond to the 0.5 M curves from Figure 6, with (full curve) and without (dashed curve) image charges, with z^{solv} taken as -0.3 nm. The vertical line is the the Stern layer contribution to the components of charge corresponding to this value.

Figure 13: Anionic component of charge, σ_-, for the mercury/$MgSO_4$ solution interface as a function of surface charge density for the electrolyte concentrations indicated. The symbols are experimental data from ref. 23, small symbols correspond to σ_- calculated from capacitance measurements and large symbols to σ_- from electrocapillary curves. The dashed lines are the predictions of GCS(0) theory and the full lines are ICS(0) results. Image charge interactions with the mercury surface are included. The contribution to σ_- from a zeroth order Stern layer (an ion free layer) of thickness 0.35 nm has been added to the theoretical curves, i.e. $z^{solv} = -0.35$ nm, cf. eq. (8). The thin, horizontal lines correspond to the contribution to σ_- solely from an ion free layer of thickness 0.44 nm, as assumed in ref. 24, see text. (Note that the abscissa scale has negative polarization to the left and positive to the right contrary to the usual convention in electrochemistry.)

Figure 14: Same as figure Figure 13 but without image charge interactions. The thickness of the Stern layer is 0.30 nm, $z^{solv} = -0.30$ nm, for the theoretical curves.

Figure 15: Cationic component of charge, σ_+, as a function of surface charge density for the same system as in figure Figure 13 (the same notation is used in both figures).

Figure 16: Measured potential of the electrocapillary maximum with respect to a $Hg|Hg_2SO_4|MgSO_4(1M)|$ reference electrode as a function of the concentration of $MgSO_4$. Data taken from ref. 23.

Figures

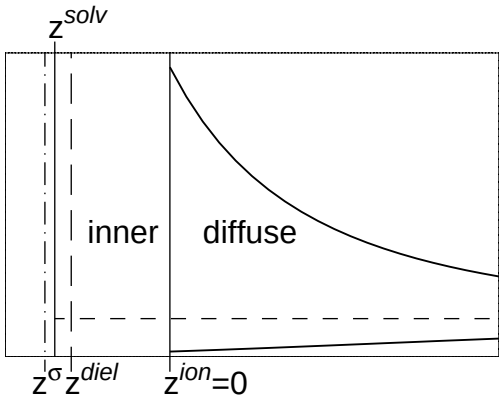

Figure 1

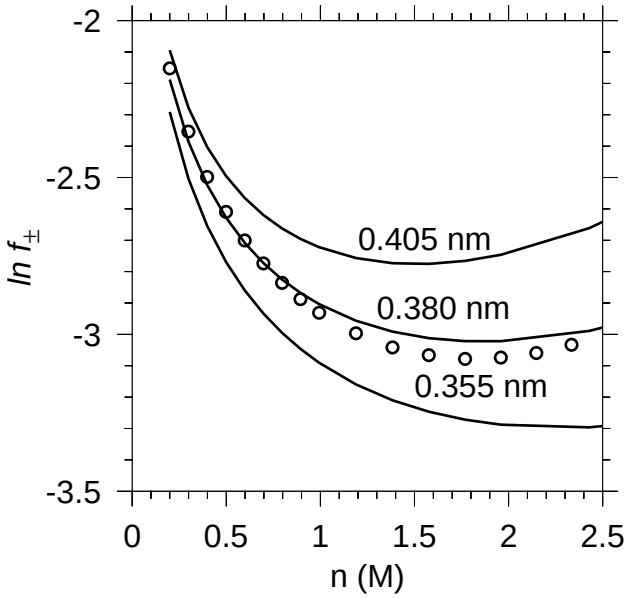

Figure 2

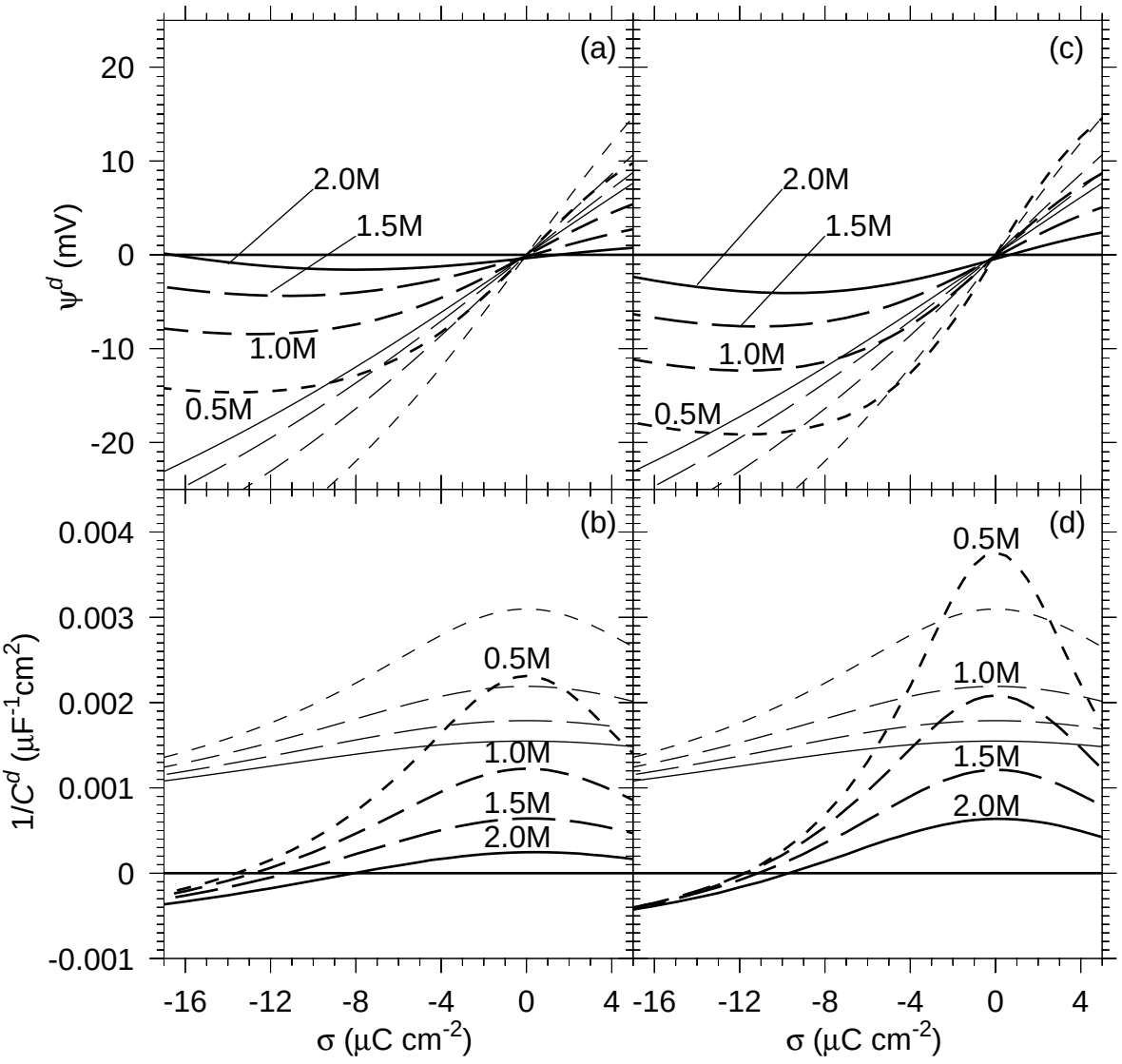

Figure 3

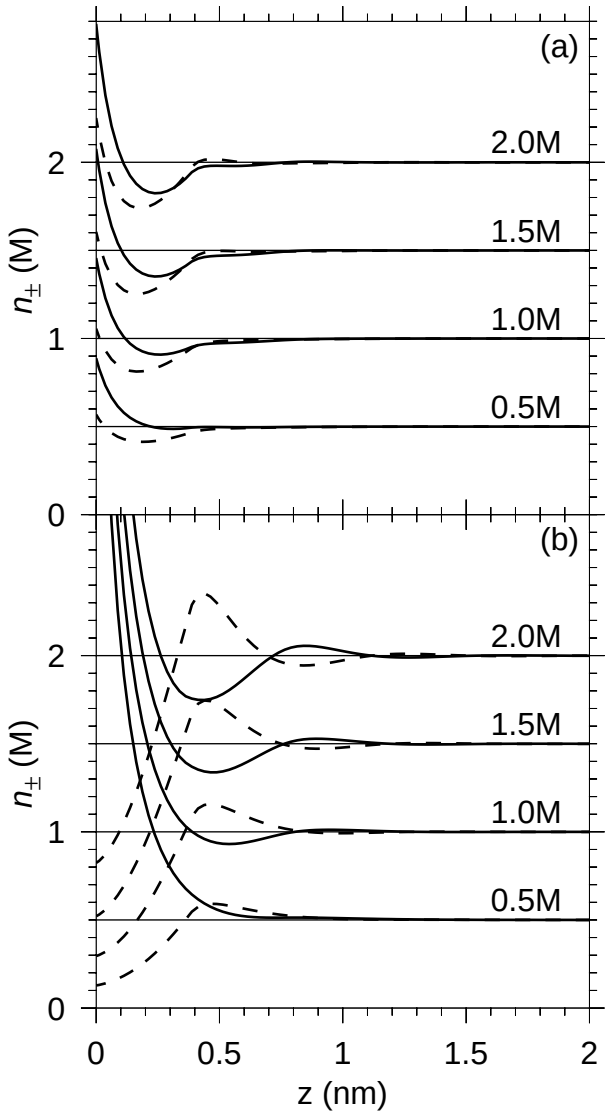

Figure 4

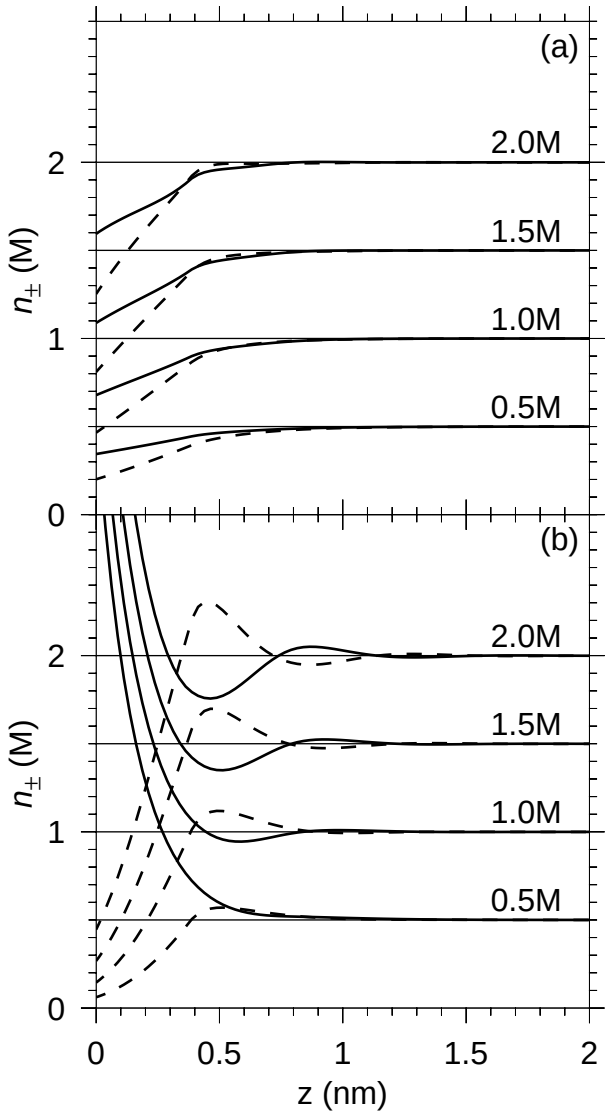
(a)
2.0M
1.5M
1.0M
0.5M
$n_{\pm}$ (M)
0
1
2
(b)
2.0M
1.5M
1.0M
0.5M
$n_{\pm}$ (M)
0
1
2
0
0.5
1
1.5
2
z (nm)

Figure 5

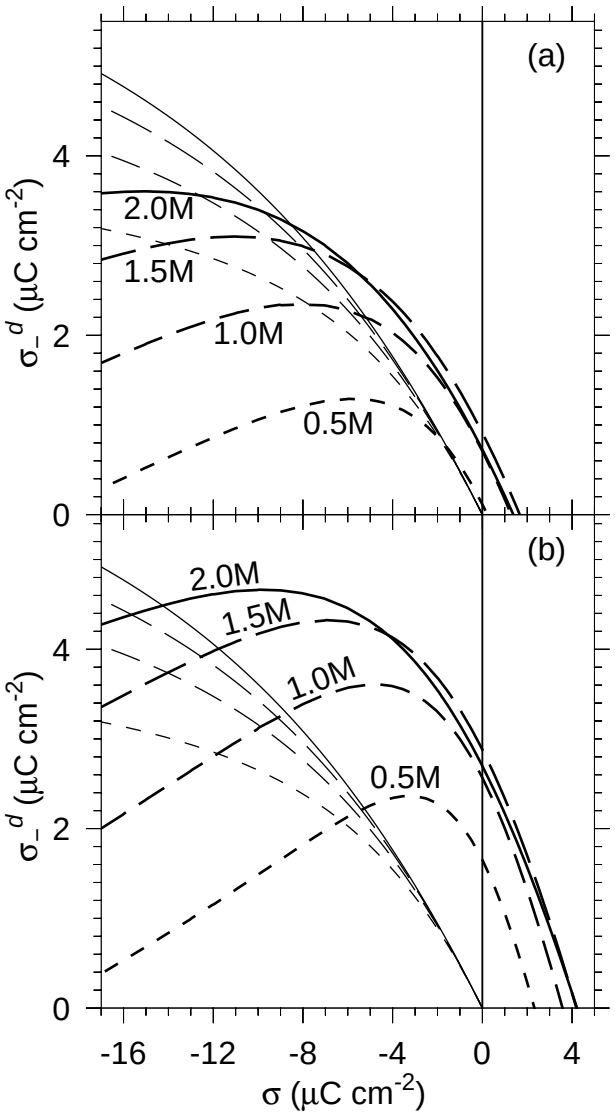

Figure 6

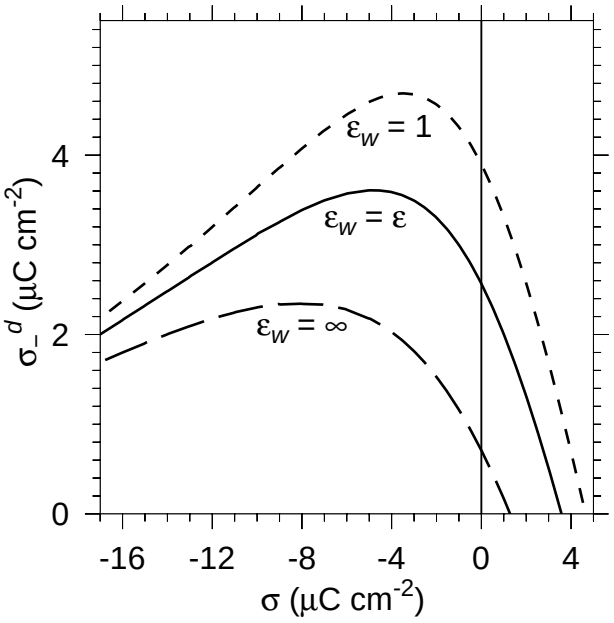

Figure 7

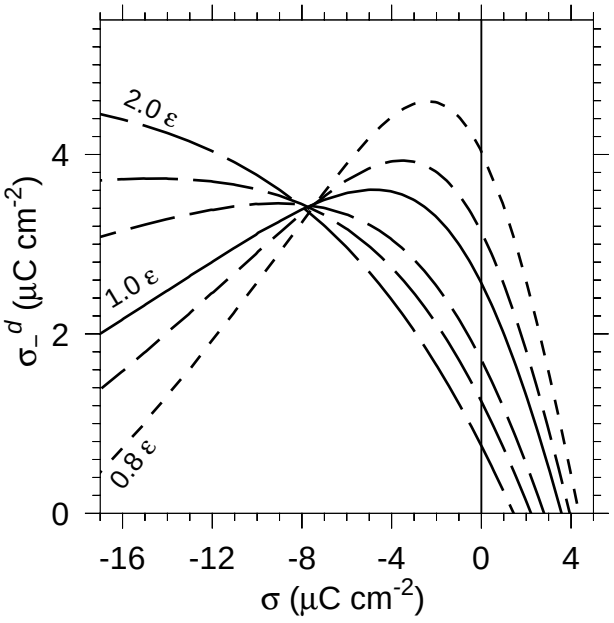

Figure 8

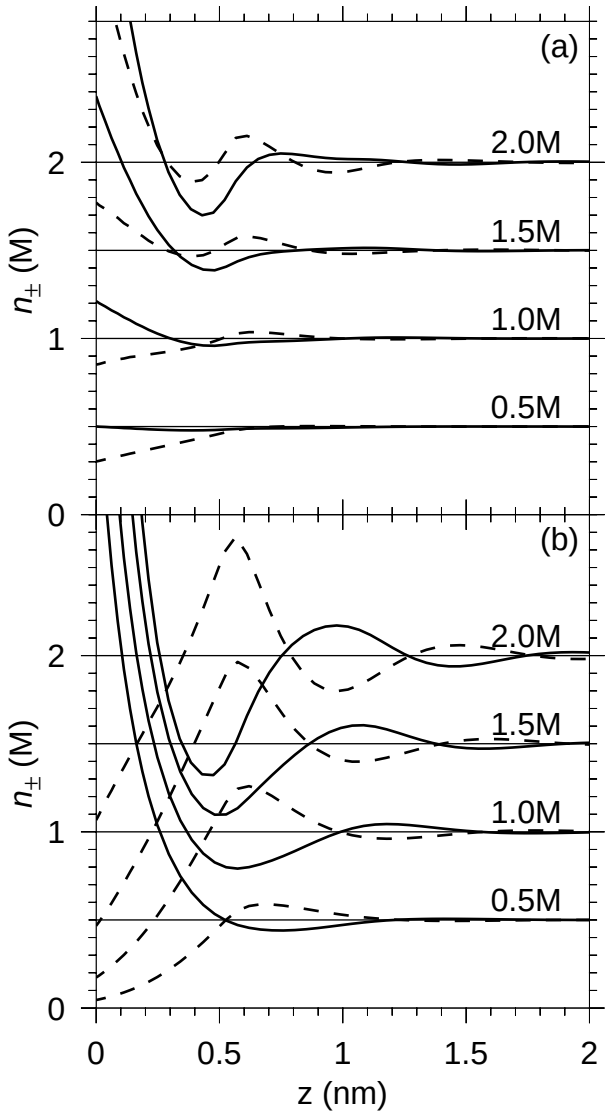

Figure 9

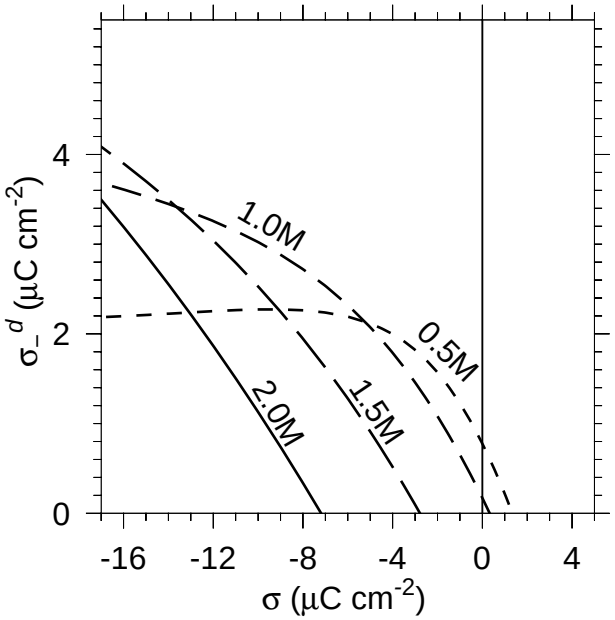

Figure 10

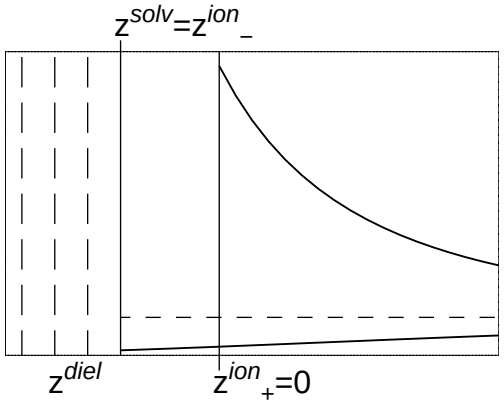

Figure 11

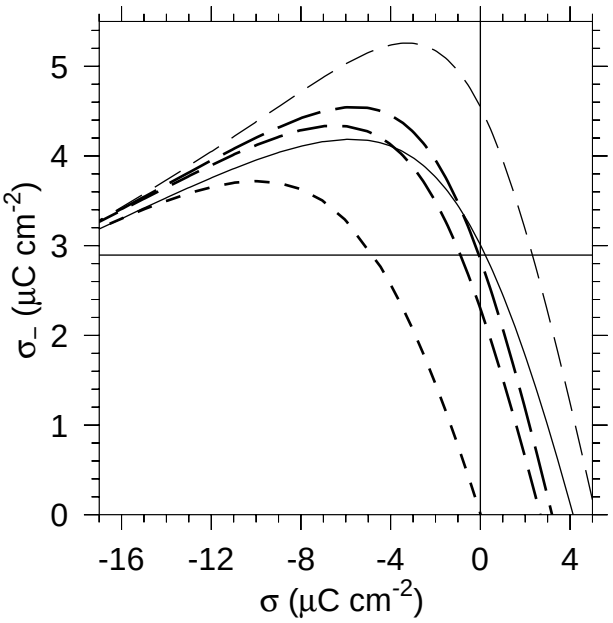

Figure 12

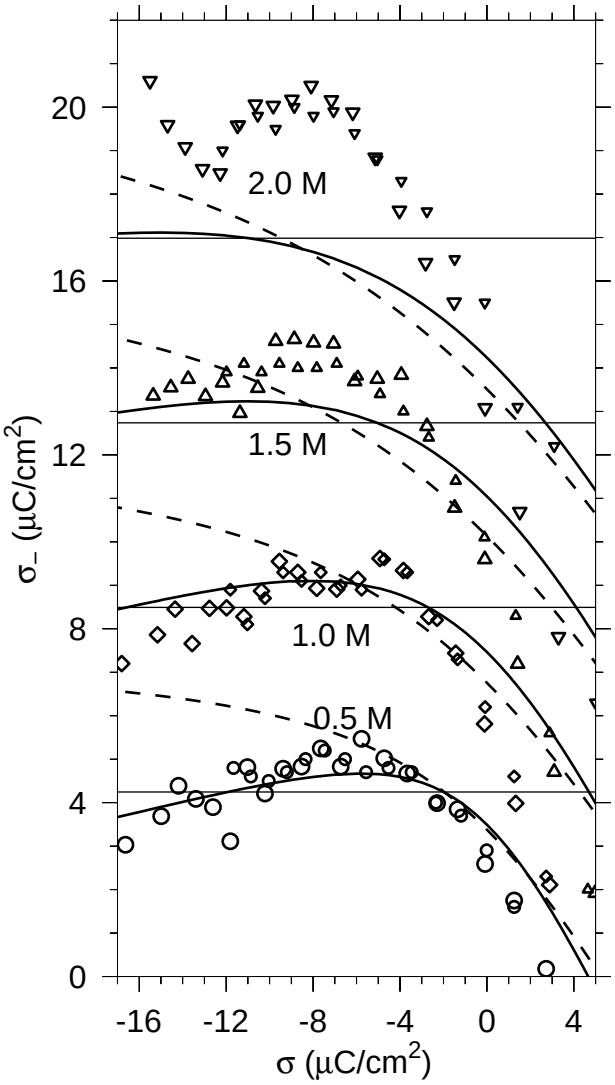

Figure 13

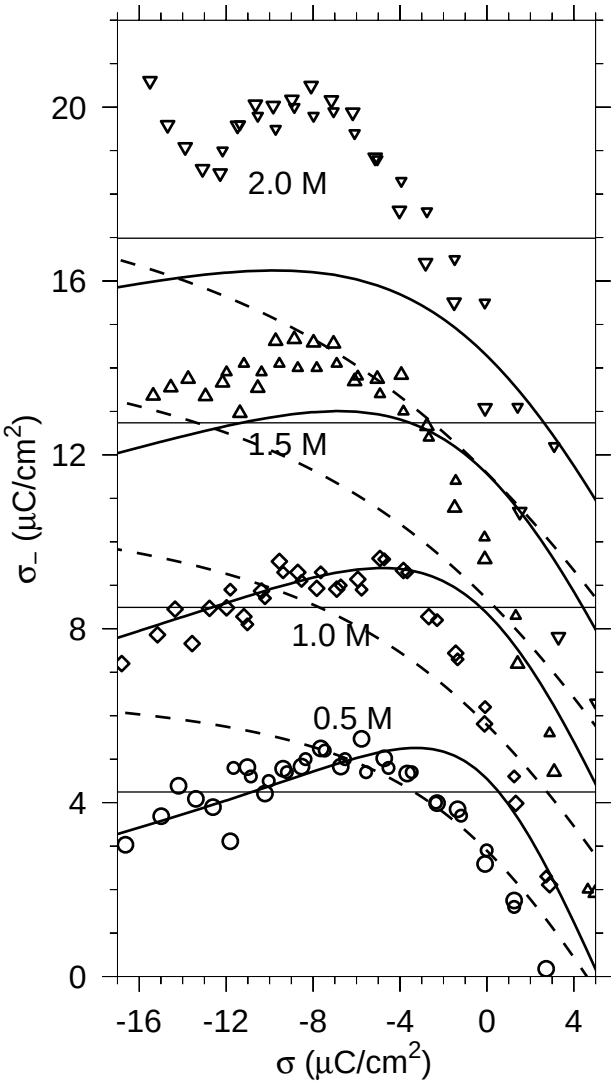

Figure 14

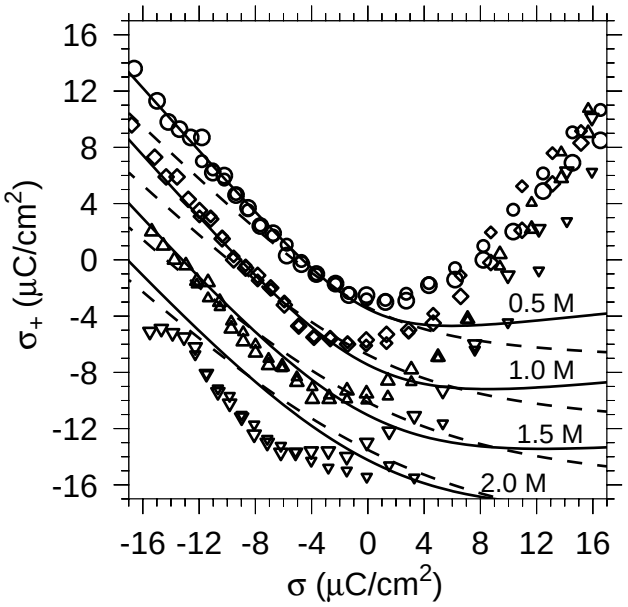

Figure 15

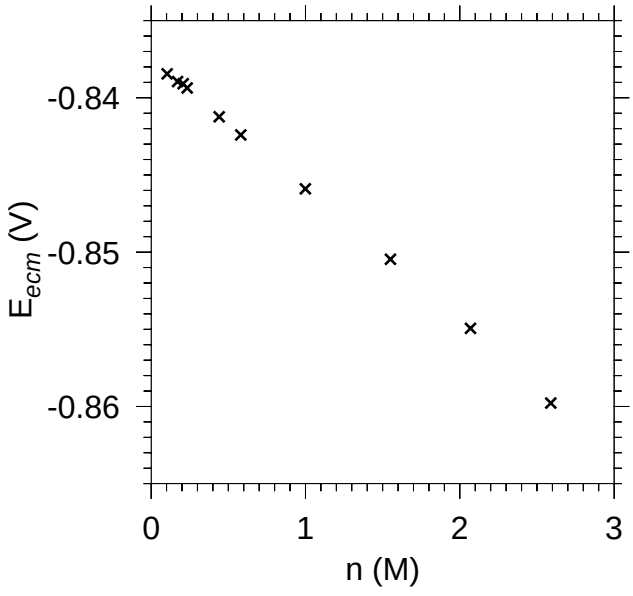

Figure 16

Paper V

On the applicability of simple electrolyte models to solutions of divalent metal sulfates

Erik Wernersson,* and Zareen Abbas

Department of Chemistry, University of Gothenburg SE-412 96 Gothenburg, Sweden

Abstract

The ability of the primitive model and a closely related model to reproduce the experimental activity coefficients of aqueous solutions of several divalent metal sulfates is investigated. Both models gave a fair representation of the variation of the activity coefficients over the range where reliable experimental data are available. However, the two models predicted significantly different values of the absolute activity coefficients. These observations are reconciled by noting that the variation of the activity coefficients at low concentrations (< 10 mM) is different in the two models. This reveals that the thermodynamic properties of 2:2 electrolytes are sensitive to the form of the interaction potential even for low concentrations. The ion diameters that give the best agreement between the experimental and calculated activity coefficients are found to be significantly smaller than the expected geometric size of hydrated cations. There is a tendency towards smaller cation size with increasing atomic number, but some exceptions to this trend were also found.

Keywords: primitive model electrolytes, sulfates, ion pairing, Monte Carlo simulation, hypernetted chain approximation

1 Introduction

Many sulfates with divalent metal cations (referred to as "divalent sulfates" below) are very soluble, although calcium sulfate (gypsum) and barium sulfate are well known examples of the contrary. The bulk thermodynamic properties of solutions of divalent sulfates show large deviations from ideal solution behavior and are remarkably similar for different cations. Close inspection of the activity coefficients for the aqueous solutions of divalent sulfates of beryllium, magnesium, manganese, nickel, copper, zinc and cadmium reveals a systematic (though not completely universal) trend towards a lower activity coefficient for a given concentration with increasing atomic number of the cation. Atomic number correlates with many properties that are potentially important for ionic interactions, such as ionic size and polarizability. From a fundamental point of view, it would be of great interest to elucidate the details of the solvent averaged ion-ion interactions that give

rise to the differences in thermodynamic properties and how these interactions vary with the cation properties.

Accurate modeling of aqueous electrolytes for all but the most dilute concentrations is a difficult problem. This is especially true for electrolytes of high valence types where the strong electrostatic interactions between ions give rise to association, "ion pairing". For symmetric electrolytes in aqueous solution at room temperature, the divide seems to lie between 1:1 and 2:2 electrolytes: 1:1 electrolytes *usually* do not exhibit significant ion pairing whereas 2:2 electrolytes invariably do. Following Bjerrum, ion pairing is frequently described in terms of an equilibrium between "free" and "paired" ions, characterized by an equilibrium constant.[1] This leads to a description where the ion-pair is formally treated as a separate chemical species.

In apparent contradiction to this view are models that contain only the free ions, interacting by some set of pair potentials that define the details of the model. The contradiction is apparent rather than real because ion pairing arises as a consequence of the interactions in the latter approach, showing up as a strong peak in the anion-cation pair distribution function. This requires proper, non-linear treatment of the electrostatic interactions. Thus, in approximate theories where the electrostatic interactions are treated in a linear, Debye-Hückel-like fashion ion pairing cannot be treated correctly. It is instructive to recall that Bjerrum theory in its original form is an approximate theory for the primitive model (PM) of electrolyte solutions, wherein the ions are modeled as charged hard spheres and the solvent as a dielectric continuum, intended to remedy this problem. To describe ion paring in terms of a chemical equilibrium (or set of equilibria) is to sacrifice a detailed representation of the ion-ion distribution functions for an approximate, conceptual simpler one. Although such a description is capable of fitting experimental data, it does not imply the presence of any attractive interaction in addition to the electrostatic one. On the other hand, the presence of such non-electrostatic interactions is hard to preclude. What can be said with certainty is that if the ion pairing can be described in terms of a chemical equilibrium, the cation-anion interaction is strong compared to the thermal energy.

The PM is able to give a reasonable fit to the experimental activity coefficients of $MgSO_4$ for

moderate electrolyte concentrations with the ion sizes used as fitting parameters.[2] Since the PM only contains the Coulomb interactions and the ionic size, it is presumably not a very faithful representation of the details of the inter-ionic potential. This immediately raises questions about just how sensitive the model predictions are to the details of the behavior of the interaction potential for short to intermediate distances, where the deficiencies of the PM are likely to be the most severe. Experience with 1:1 electrolytes shows that it is relatively easy to find a model that approximately reproduces the thermodynamic properties of real solutions.[3] It is possible to acquire similar agreement with experimental thermodynamic data with models having dramatically different structural properties.[4] Clearly, the relative ease of fitting bulk thermodynamic data is more of a liability than an asset in the search for the "true" pair potential. (The word "true" is in quotation marks because the full solvent-averaged interaction potential is known to contain many-body terms.[5] There is no guarantee that there is such a thing as a unique best interaction potential that is limited to pairwise terms, except, of course, in the limit of infinite dilution.) Thus, the most one can reasonably hope for when trying to determine the inter-ionic interaction potentials by fitting experimental data is to find the broad, qualitative features of the interaction potential.

For some applications it is essential to know the interaction potential explicitly. The theoretical treatment of electrical double layers and inhomogeneous electrolyte solutions is an example of this. See ref. 6 for an example of such an application. It is worth noting that while a description of electrolytes containing ions of high valency in terms of Bjerrum-type ion pairing is likely to give a reasonable description of the bulk properties, it is certain to be misleading for electrical double layers. Due to the excess of counterions in the vicinity of any charged surface, a simple ion pairing picture cannot be expected to give an accurate description of the deviations from ideality. The deviations from ideality in that situation originate mainly from repulsion between counterions (to the surface) rather than attraction between ions of opposite charges. This example shows that it is important to construct models in terms of explicit interaction potentials in order to make correct generalizations. A simple and robust model with few fitting parameters is preferable in this context to a highly parametrized, less robust model, even if the latter type of models can

give a better description of the properties of the bulk solution. This is in contrast to the task of simply describing experimental data in a compact form that allows easy interpolation. For this purpose highly parametrized expressions such as the Pitzer equation[7] are suitable and the increased computational effort needed to treat models with explicit interaction potentials is hardly justified.

The modeling of electrolytes on the level of ionic interactions may also offer improved prospects for putting activity coefficients on the absolute scale. What is meant by absolute scale here is a scale with a non-interacting standard state, where the solution is taken to be ideal. The set of tabulated activity coefficients generally considered most reliable[8] have been obtained by isopiestic determination of the osmotic coefficients from which the activity coefficients are obtained by integration of the Gibbs-Duhem equation. This integration gives the difference in excess chemical potential from the value at the lower bound range of integration, corresponding to 0.1 m concentration in ref. 8. For the activity coefficients to be given on an absolute scale the integration has to be carried out all the way from zero concentration, where the solution is truly ideal. This is a source of great uncertainty in the determination of the standard chemical potential: even for high quality data this quantity is often not accurately known. This limitation does not detract from the validity of the activity coefficients for most purposes, because only differences in (chemical) potential have physical significance. However, from a fundamental point of view it is somewhat unsatisfying to be unable to compare the activity coefficients on the absolute scale. Such a comparison would be necessary to fully quantify the differences between the different divalent sulfates.

By fitting one (or more) parameter(s) appearing in a model to osmotic coefficient data and subsequently calculating the activity coefficients from the theory with the same parameters, the absolute activity coefficients can be obtained. Indeed, this strategy is commonly used to treat experimental data, see for instance ref. 9 where the Pitzer equation is used and ref. 10 where the problem is treated in terms of a Bjerrum-like chemical equilibrium model. The strategy of using theory in this way to extract absolute activity coefficients from measured osmotic coefficients is a somewhat risky one. This is so because it is in effect an interpolation of the osmotic coefficient as a function of concentration over a range in which the function varies quickly. For this reason,

it is important that the theory that is used has a sound physical basis. (Debye-Hückel theory is of limited applicability in practice for 2:2 electrolytes, despite that this theory is an exact limiting law. The reason is that the concentration range in which this theory is valid is very narrow compared to the range over which the interpolation has to be made.) Conversely, the ability, or lack of such, of a model to furnish a good extrapolation to lower concentrations can be used as a test of the model.

Measurements of the electromotive force (EMF) of electrochemical cells can be used for this purpose. The EMF is directly related to the chemical potential of the salt through the Nernst equation. Thus, this method is experimentally independent from isopiestic measurements of the osmotic coefficients. EMF measurements are possible down to concentrations that are orders of magnitude smaller than those amenable to isopiestic experiments and are therefore useful for testing theories in the low concentration regime. However, for EMF measurements to yield activity coefficients on an absolute scale, the EMF for zero concentration has to be determined through extrapolation. Over the last century, many attempts have been made to determine activity coefficients of divalent sulfates on the basis of such data.[11–20] The extrapolation to zero concentration in refs. 13,18–21 relies on the use of the PM, evaluated using various approximate theories, which are only valid for low concentrations. The validity of the PM thus directly affects the reliability of this extrapolation. In the experimental setup used in refs.[18–20] an alternative route for the determination of the activity coefficients on an absolute scale was used. This method is based on relating the absolute activity coefficients of the electrolyte of interest to those of a set of auxiliary electrolytes. Thus, the activity coefficients given in these papers must be considered more reliable than those from the older studies.

The primary goal of the current paper is to investigate the ability of the PM as well as another, closely related, model to reproduce the experimental activity coefficients for solutions of a range of divalent sulfates. Such an analysis enables the ability of the models to accommodate the difference between chemically distinct but physically similar salts to be tested. The comparison between two similar models enables estimation of the sensitivity of the thermodynamic properties to the assumptions about the form of the interaction potential. Special emphasis is placed on the ability

of each model to furnish a reliable extrapolation to low concentrations with parameters determined from experimental data for moderate to high concentrations.

A secondary goal is to test the accuracy of the hypernetted chain (HNC) approximation for electrolyte models that give realistic values for the activity coefficients. Whenever no great error is incurred by doing so, it is preferable to use integral equation theory over simulation, as the former requires much less computational effort, for evaluating the properties of a given model. The HNC approximation have been tested before[22] , showing great promise as a quantitative theory *in some regions of parameter space*, though not in others.[23] There is even a region in parameter space where no physical solution exist for the PM.[24] As the region in parameter space that is relevant for 2:2 salts in water partly overlaps with the region where HNC theory is inaccurate, comparison with simulation is necessary to establish the applicability range in concentration, for the actual ion sizes used.

The outline of this paper is as follows: First, the pair potentials defining the two model interaction potentials that we consider are given. Then, the theoretical methods used, Monte Carlo simulation and HNC theory, are presented. The procedure for fitting the parameters of the model potentials to experimental osmotic coefficients at moderate concentration is then described, followed by the results of the fitting procedure for each of the model potentials. The activity coefficients for low concentrations for the same parameter values are then calculated and compared with experimental data from EMF measurements.

2 Modeling of Sulfates

2.1 The Primitive Model

The PM is defined by the pair interaction potential $u^{PM}(r)$, that is given by

$$u_{ij}^{PM}(r) = u_{ij}^{Coul}(r) + u_{ij}^{core}(r) \tag{1}$$

where $u_{ij}^{core}(r)$ is a hard sphere potential that is zero for $r \geq d_{ij}$ and infinite for $r < d_{ij}$, where d_{ij} is the diameter associated with the interaction between an ion of species i and one of species j and $r = |\mathbf{r} - \mathbf{r}'|$ where $\mathbf{r}$ and $\mathbf{r}'$ are the positions of the ions. The term $u_{ij}^{Coul}(r)$ is the Coulomb potential given by

$$u_{ij}^{Coul}(r) = \frac{Z_i Z_j e_0^2}{4\pi\varepsilon\varepsilon_0 r} \tag{2}$$

where Z_l, $l = i, j$, is the ionic valency (with sign), e_0 is the unit charge, ε_0 is the permittivity of vacuum and ε is the relative permittivity of the solution. The value of the relative permittivity is taken as that of the pure solvent, 78.36 for water at 25 °C.[25]

Here, we make the assumption that the ionic diameters are additive so that $d_{+-} = (d_{++} + d_{--})/2$. Note that as the ion sizes in the PM are not necessarily geometric sizes, but rather serves to approximate the repulsive forces between pairs of ions, this additivity is not self evident. It is our expectation that d_{+-} is the by far most important parameter in the model as it determines the strength of the Coulomb interaction at contact and thereby the degree of ion pairing. Here, we keep d_{--} fixed to the crystal diameter of sulfate, 4.6 Å,[26] and use d_{++} as a fitting parameter; d_{+-} follows from additivity. This prescription is motivated by the expectation that the cation is more strongly hydrated than the anion.

While the PM may be regarded as the simplest member of a class of models composed of the generic long-range Coulomb interaction and a specific short-range interaction, it is just one member of an infinite set of possible ones. We think it is prudent to consider also another member of this class of models, described in section 2.2 below, in order to guard against the possibility that the PM may be a pathological case in one way or another.

2.2 The Solvent Structure Primitive Model

Simulations consistently show that the ionic interaction has an intermediate-range oscillatory component arising from ordering of the solvent. This is the case both for the short-range part of the potential of mean force[27–31] and that of the effective potential that reproduces the true pair correla-

tion functions.[32–34] The details of this potential are of course dependent on the force-field used in the simulation, but the qualitative conclusion about the existence of an oscillatory contribution to the interaction potential is robust. The approach in the current work is to adopt a simple expression that has the expected qualitative features. Instead of using the ion sizes to fit experimental data, a parameter in the short range potential, the explicit expression for which is given below, serves this purpose.

A very simple expression that reproduces the expected qualitative behavior of the short ranged part of the potential of mean force between cations and anions is

$$u_{ij}^{s}(r) = \alpha_{ij} \frac{d_s \cos\left(2\pi \frac{r-d_{ij}}{d_s}\right) \exp\left(-\frac{r-d_{ij}}{d_s}\right)}{r}, \tag{3}$$

where d_{ij} is the ion diameter, d_s is a length scale associated with the solvent and α_{ij} gives the energy scale. We refer to the model defined by adding eq. (3) to the PM interaction potential, eq. (1), as the "solvent structure primitive model", abbreviated "SSPM". (The same value of d_{ij} is used in eq. (3) and for the hard cores.) This name is due to the role of the solvent in creating the oscillatory behavior of the potential of mean force that eq. (3) seeks to mimic. In principle, all of the parameters of eq. (3) could be used as fitting parameters. For a binary electrolyte this would correspond to no less than seven parameters. While a large number of fitting parameters does not automatically disqualify a model, this is clearly an inappropriately large number if comparison with the one-parameter version of the PM considered here is to be meaningful.

The size parameters for ions and solvent, d_{ij} and d_s, are constrained to values obtained from independent information. The length scale parameter of the solvent, d_s, was taken as 2.76 Å, the typical inter-atomic spacing in liquid water.[26] The ion diameters d_{ij} were taken as $2d_+^b + d_s$ for d_{++}, $2d_-^b$ for d_{--} and $d_+^b + d_-^b + d_s/2$ for d_{+-}, with d_i^b denoting the "bare" radius. In all cases the value of d_i^b was taken as the recommended value for the crystallographic ion diameter from ref. 26. The energy scale parameter α_{+-} is used as a fitting parameter and α_{++} and α_{--} are set to zero. This prescription is motivated by the expectation that the anion-cation interaction is the

most important interaction in the system. This choice of diameters together with the form of $u^s_{ij}(r)$ ensures that a anion-cation pair closer than $d^b_+ + d^b_- + d_s$ will be repelled due to the short-ranged part of the pair potential. Between $d^b_+ + d^b_- + d_s/2$ and $d^b_+ + d^b_- + d_s$ there is a soft repulsion from $u^s_{+-}(r)$ and smaller distances are forbidden by the infinitely repulsive hard cores. This is meant to model the free energy cost of displacing water molecules from the first solvation shell of the cations. The diameters associated with interactions between like-charged ions may be considered a compromise to maintain additivity.

We emphasize that the model defined by eq. (3) together with the prescriptions for the ion sizes above is not predicted by any theory but is an ansatz made on the basis of our qualitative expectations of the appearance of the potential. While the qualitative features that the form of eq. (3) seeks to mimic are features that are consistently seen in simulation, the details are unlikely to be faithfully represented; this potential is at best a sketch of the true interaction potential. The reason why we investigate such a model is rather to establish to what extent the ability to fit experimental data depends on the actual form of the potential. We note that the form used here is analogous to the one used in[35] for 1:1 electrolytes, but that the pre-factor and the prescriptions for what ion-sizes to use differ.

In Figure 1 the interaction potentials between Zn^{2+} and SO_4^{2-} are shown for the PM and SSPM, see Section 4.1 below. Note that the Coulomb potential is the dominant contribution to the total potential even in the SSPM. The extra potential u^s_{+-} nowhere accounts for more than half the value of the potential, which is the case at contact, and appears completely unimportant beyond 10 Å. Of course, u^s_{+-} gives rise to a large change in the *force* between ions for some separations, particularly close to anion-cation contact. The fact that u^s_{+-} gives a modest contribution relative to the total interaction potential does not necessarily mean that this contribution is unimportant. On the contrary, a weak attraction superimposed on a strong attraction may have a larger effect than the weak interaction alone. The reason is that the interaction potential enters the Boltzmann factor and thus the response in density due to a change in potential is dependent on the strength of the original interaction potential in a non-linear way.

3 Theoretical Methods

3.1 The HNC Approximation

The Ornstein-Zernike (OZ) equation for a bulk system is given by

$$h_{ij}(r) = c_{ij}(r) + \sum_m n_m \int h_{im}(|\mathbf{r} - \mathbf{r}'|) c_{mj}(|\mathbf{r}'|) d\mathbf{r}', \tag{4}$$

where $h_{ij}(r)$ is the total correlation function and $c_{ij}(r)$ is the direct correlation function for ion species i and j. The total correlation function is related to the pair distribution function, $g_{ij}(r)$, by $g_{ij}(r) = h_{ij}(r) + 1$. The hypernetted chain (HNC) approximation has the form of a relation between $h_{ij}(r)$ and $c_{ij}(r)$,

$$c_{ij}(r) = -\beta u_{ij}(r) + h_{ij}(r) - \log[1 + h_{ij}(r)]. \tag{5}$$

Together, these two relations between $h_{ij}(r)$ and $c_{ij}(r)$ form a system of equations from which these functions can be calculated given $u_{ij}(r)$. Here, the standard procedure of solving the set of equations composed of (4) and (5) by Picard iteration is employed.[36] The numerical difficulties caused by the long-range Coulomb interactions are handled by the method described in ref. 37. Briefly, for a starting guess for the set of c_{ij}'s eq. (4) is solved with respect to the set of h_{ij}'s by taking the Fourier transform of this equation. Due to the convolution theorem eq. (4) then takes the form of an algebraic equation that is solved for the Fourier transform of the set of h_{ij}'s. Then the inverse Fourier transforms are calculated and a new guess for the set of c_{ij}'s is obtained from eq. (5). The procedure is repeated until convergence.

The accuracy of the HNC approximation tends to be good for ionic systems. A known exception is systems with strong, attractive electrostatic interactions at low density. For PM electrolytes there is a region where there is no solution for the HNC approximation. This region has been mapped out for the "restricted primitive model", i.e. the PM with the constraints $d_{++} = d_{--} = d_{+-}$ and $Z_+ = -Z_-$.[24] In the vicinity of the region of no solution there are systematic errors in the total

correlation functions. For the anion-cation correlation function the height of the peak at contact is then too low; the degree of ion pairing in the system is underestimated. In the like-charged ion correlation functions the errors of the HNC approximations show up as a spurious peak about one ion radius from the contact distance.[38] At higher concentrations both these errors are less important: the peak height in the unlike-charged ion correlation function is better represented and the peak in the like-charged ion correlation function is here a true feature of the system. The error in the HNC approximation is that this peak does not disappear for low concentrations. For aqueous 2:2 electrolytes with sizes around those considered here, the region where this problem becomes severe starts at concentrations below about 0.2 M and rapidly gets worse for lower concentrations. Moreover, the HNC approximation also shows a more severe inconsistency between the compressibility and virial routes for calculation of thermodynamic properties for 2:2 salts than for 1:1 and 1:2 salts. The accuracy of the HNC approximation thus cannot be taken for granted in the present case. For this reason, MC simulations are employed to test the predictions about the activity coefficients from HNC theory. Note that the HNC approximation is thermodynamically consistent in the limited sense that the "energy" route to thermodynamic properties is consistent with the "virial" route.[39,40] Because of the presence of a region where no solution exist the compressibility route is unpractical for the calculation of osmotic coefficients and activity coefficients on an absolute scale for the PM of solutions of divalent sulfates. For this reason all thermodynamic quantities presented in this work are calculated via the energy/virial route.

3.2 MC Simulation

All simulations presented in this work are performed using the standard Metropolis Monte Carlo method for the canonical ensemble using 242 pairs of ions with the concentration determined by the box size. Periodic boundary conditions with the minimum image convention were used. The simulation was run for 50 million configurations of equilibration followed by 150 million configurations. The long equilibration was performed in order to guard against the possibility that non-representative configurations formed by the initial random placement of the particles would

persist for many steps due to the strong forces acting in 2:2 salts.

The excess chemical potential was evaluated using a variant of the Widom insertion method. The basic implementation of this method is that a trial insertion of a particle is made at random into the simulation box and the interaction with all other particles is evaluated. The excess free energy in units of k_BT is simply the ensemble average of the Boltzmann factor associated with the insertion of a particle at a random location. In charged systems, the naive implementation of this method displays very poor convergence with increasing system size. This is because the insertion gives rise to a non-electroneutral system. To remedy this problem an approximate but accurate modification of this scheme was used.[41]

3.3 Fitting to Experimental Data

Experimental activity coefficients and osmotic coefficients of sulfates with the cations Be^{2+}, Mg^{2+}, Mn^{2+}, Ni^{2+}, Cu^{2+}, Zn^{2+} and Cd^{2+} were taken from ref. 8. To cast the osmotic coefficient in a form that is compatible with the definition of this quantity in McMillan-Mayer type models the data was converted from Lewis-Randall to McMillan-Mayer scale according to the procedure described in.[42] Empirical expressions for the densities of the salt solutions from ref. 43 were used.

The activity coefficient data are based on isopiestic measurements of the osmotic coefficient for concentrations above some lowest concentration m_0, 0.1 mol/kg in this case, followed by integration according to the Gibbs-Duhem equation according to

$$-\ln\gamma_{\pm}(m) = -\ln\gamma_{\pm}(m_0) + \int_{m_0}^{m}(1-\phi(m'))d\ln m'. \tag{6}$$

The osmotic coefficients and activity coefficients thus contain essentially the same information. The accuracy of the absolute value of the activity coefficient is dependent on the activity coefficient for concentration m_0. If $\gamma_{\pm}(m_0)$ is not reliably known, only the *ratio* of activity coefficients (or equivalently, difference in excess chemical potential) to that for a given concentration can be calculated. For this reason, the osmotic coefficient was used to determine the optimal parameters

for each model. In ref. 8, $\gamma_{\pm}(m_0)$ is simply set to 0.150 (on the Lewis-Randall scale, though the difference between the McMillan-Mayer and Lewis-Randall scale are insignificant for this concentration) for all the divalent sulfates. (See ref. 44 for details.)

In order to obtain meaningful information about the ionic interactions from such a fit the number of parameters must be kept to a minimum. Otherwise, there is a risk that the model becomes so flexible that a good fit can be obtained regardless of any resemblance between the model potential and the true potential. What number of parameters is reasonable ultimately depends on the number of independent pieces of information that has to be simultaneously fitted. Because we limit ourselves to a single type of information here, we consider it prudent to use a single fitting parameter, as described in Sections 2.1 and 2.2.

The root mean square deviation between the experimental and theoretical osmotic coefficients,

$$\delta = \left[\frac{\sum_m^N (\phi(n_m) - \phi^{exp}(n_m))^2}{N} \right]^{1/2} \tag{7}$$

where $\phi(n_m)$ and $\phi^{exp}(n_m)$ are the theoretical (from the HNC approximation) and experimental osmotic coefficient for concentration n_m and N is the number of different concentrations considered, was used as the figure of merit for the fit. We have used the HNC approximation in order to calculate the model osmotic coefficient because the accurate evaluation of osmotic coefficients from simulations would require very long runs. The value of the fitting parameter that minimized δ was considered best. The results thus obtained are subsequently validated by comparison of the activity coefficients to the results from simulations for the optimal parameters. The nine data point corresponding to 0.2 to 1.0 m concentration was used, i.e. $N = 9$. It is not reasonable to expect McMillan-Mayer type models to be applicable for concentrations much higher than 1 or 2 M, although the limit of the range of validity cannot be known *a priori*. The lower limit of 0.2 m is imposed due to the fact that the HNC approximation is not accurate for the PM at low concentrations under conditions of high electrostatic coupling. Solutions of different divalent sulfates have different density. Thus the osmotic coefficients are not calculated at exactly the same concentration

interval in terms of molar concentrations. However, the difference between the salts in the width of the concentration interval is small, less than one percent, and not likely to skew the comparison between the fits for different cations.

4 Results

4.1 Determination of Model Parameters

4.1.1 The PM

For all divalent sulfates considered here the cation diameter was adjusted to the value that minimized δ while the anion diameter was fixed to 4.6 Å, the crystallographic diameter of a sulfate ion. The results are summarized in Table 1. The optimal values of δ are in the order of one to a few percent of the typical values of the osmotic coefficients in the concentration range considered. A more detailed comparison between theory and experiment is made in Figure 2. While the PM shares with the experimental data the feature that the osmotic coefficient goes through a minimum in the concentration range of the figure, the position of that minimum is well reproduced only in the case of $BeSO_4$. For the other salts, the minimum in the model is consistently placed at too low concentrations.

The theoretical activity coefficients, presented in the figure as $\ln f_{\pm}/f_{\pm}^{ref}$ where $f_{\pm}^{ref}$ is the activity coefficient for 0.2 m concentration, appear to reproduce the experimental trends more faithfully. The deviations are quite insignificant up to concentrations around 1.5 M but for concentrations larger than that the agreement rapidly deteriorates (Figure 2). The apparently better agreement between theoretical and experimental activity coefficients than between theoretical and experimental osmotic coefficients is not due to any thermodynamic inconsistency, but is merely a consequence of the way in which the activity coefficients and osmotic coefficients are related by the Gibbs-Duhem equation. That $\ln f_{\pm}$ varies more quickly with concentration than ϕ is a consequence of that the osmotic coefficient appears in the integrand of eq. (6). The same rela-

tive deviation between theory and experiment for $\ln f_{\pm}$ is thus less conspicuous than that for ϕ on the scales of the figures for most of the concentration range. (Note that eq. (6) is written in terms of molalities rather than molarities. This does not affect the argument, however.) The PM systematically underestimates the osmotic coefficient for the lower concentrations considered and overestimate it for higher concentrations. This has the consequence that the error incurred in the activity coefficient from the integration in the lower half of the concentration range is canceled to some degree by the error from the upper half. The level of agreement for the experimental and theoretical activity coefficients for concentrations around 1 M may thus be improved by cancellation of errors and may therefore give an overly favorable impression of the model.

4.1.2 The SSPM

Here both the cation and anion sizes are held constant and the energy scale parameter α_{+-} is used as a fitting parameter, as explained in detail in section 2.2. The parameters that optimize δ are shown in Table 2. Typically the values of δ are lower than the corresponding ones for the PM by a factor of two to three. Only for $BeSO_4$ the agreement is slightly worse than for the PM. Note that for this salt, the cation diameter used here is similar to the cation radius that gives the best fit for the PM. In light of this it is not surprising that the optimal value of α_{+-} is small: for this salt the PM and SSPM are very similar.

In Figure 3 the osmotic and activity coefficients obtained from the model are compared to their experimental counterparts. The main merit of the SSPM compared to the PM is that it reproduces the position of the minimum in the osmotic coefficient as a function of concentration quite faithfully. While the agreement between theory and experiment does extend to higher concentrations than for the PM for $MgSO_4$, $MnSO_4$, and $CdSO_4$, this is not so for $BeSO_4$. The activity coefficients are in better agreement with experiment for concentrations up to about 1 M for the SSPM than for the PM. However, the concentration range in which theory and experiment are in agreement is not very different for the PM and the SSPM models.

4.2 Test of the HNC approximation against simulation

In Figure 4 the mean activity coefficients calculated in the HNC approximation for the PM are compared with those from simulation. The agreement is remarkably close for the entire concentration range, especially so in light of that the criterion of thermodynamic consistency between the compressibility and energy/virial routes for calculation of thermodynamic quantities is not fulfilled to a very high accuracy for 2:2 salts.[45] The agreement between HNC and simulations for the activity coefficients indicates that the energy/virial route is definitely preferable over the compressibility route in terms of accuracy. This is fortunate because the energy/virial route is also more computationally expedient. A corresponding comparison for the SSPM is made in Figure 5. Note that this model does not seem to share with the PM the problem that it lacks a solution in the region of parameter space corresponding to 2:2 salts at moderate concentrations. The agreement between theory and simulation is good up to about 1 M, but above this concentration there is a considerable deviation. Fortuitously, and fortunately, the upper concentration limit of the range where the HNC approximation is accurate coincides with the upper concentration limit of the range where the model agrees with the experimental data. For low concentrations the agreement between the HNC approximation and simulation is fair, but the activity coefficients are slightly overestimated by the HNC theory. This is especially true for the concentration range of about 1 mM to 100 mM, where the deviation is at most a few percent.

Figure 6 shows a comparison between the pair distribution functions calculated for the SSPM in the HNC approximation and by simulation. It is clear that deficiencies of the HNC approximation that are well documented for the soft-core analogue of the PM[23] are also present for the SSPM. For example, the height of the peak in $g_{+-}(r)$ is underestimated by ten to twenty percent in the concentration range considered. Good agreement between the activity coefficients obtained by simulation and theory is found for the SSPM at small concentrations ($<$ 100 mM). This is surprising in light of the deficiencies in $g_{+-}(r)$ from the HNC approximation. Nevertheless, the consistency between the virial and compressibility routes for calculating the osmotic coefficients is comparable to that for the PM (not shown). This suggests that the energy/virial route to thermo-

dynamic observables is subject to some cancellation of errors that compensates for the structural deficiencies of the theory. Indeed, this conclusion is consistent with the observation made in ref. 23 that closures that improve the predictions for structural properties over the HNC approximation do not necessarily give improved predictions for thermodynamic quantities.

4.3 Comparison With Experiments

In Figure 7 the mean activity coefficients of $ZnSO_4$ obtained from the PM and the SSPM are compared with two experimental studies for $ZnSO_4$. $ZnSO_4$ is chosen as the main example because this salt has been widely studied experimentally. The experimental data sets, from refs.[11] and,[18] which are shown in the figure, are not the only ones available in the literature. Those sets were chosen because they cover a wide range of concentrations and show a large degree of mutual agreement despite the fact that different types of cells were used. In ref. 21 the same cell is used as in ref. 11. There is good agreement between the results obtained in these studies for concentrations of 5 mM and above. However, when the activity coefficients are presented on a scale that is intended to be absolute, there is limited agreement. This is the case for different experimental data sets as well as between experiment and theory. The discrepancies between the experimental data sets can reasonably be explained by that the values of the experimental activity coefficients on an absolute scale are dependent on an extrapolation to zero concentration. Such an extrapolation is very sensitive to the data points for very small concentrations, where the experimental errors are likely to be the largest. The good agreement between experimental data sets for low concentration in panel (a) of Figure 7 is an illusion created by strong weight of the inaccurate low concentration points in the extrapolation. By representing the data as the ratio of the activity coefficient to that for a finite concentration, the data can be compared without having to take into account the accuracy of the extrapolation procedure. We emphasize that these two representations have the exact same physical significance. For concentrations between 10 mM and about 1 M (see also Figure 3 and Figure 2) the PM and the SSPM do not show large differences when compared in this way. In fact, the difference between the models is smaller than the experimental error. Nevertheless, the absolute

values of the logarithm of the activity coefficients are different in this region by about ten percent. This difference implies that the behavior of the two models must be quite different in the low concentration region to fulfill the condition that the activity coefficient is one at infinite dilution. This dependence on the details of the interaction potential for low concentration is unfortunate: it calls into question the reliability of the practice of using "theory assisted extrapolation" to put the the activity coefficients on an absolute scale. This conclusion is underlined by the comparison between model and experimental activity coefficient data for $MgSO_4$ and $CdSO_4$ in Figure 8 and Figure 9. For $MgSO_4$ the SSPM is apparently superior to the PM whereas for $CdSO_4$ the opposite is true. As the PM and SSPM are just two members of a wide class of models of comparable plausibility it is our opinion that it is hardly meaningful to speculate which one, if any, can be considered best in general without additional information.

5 Discussion and Conclusions

The cation diameters that give the best fit between the results from PM and experiments are much smaller than the expected geometric size of hydrated divalent cations. Furthermore, there is a general, but not universal, trend that the the ionic radius decreases with increasing atomic number. This would appear to suggest that the optimal PM diameter has an inverse relation to the "bare" diameter. If the selected diameters from ref. 26 are to be taken as accurate our results do not support such a relationship, except in as much that the ion with the smallest bare ion size has the largest value of d_{++} and vice versa. Obviously, caution must be applied in drawing conclusions about the size of ions in solution on the basis of apparent sizes in crystals. This is especially true in this case, where a small relative error in the size of the ions might change the conclusion.

The small cation sizes obtained here are in most cases much closer to the bare ion diameter than any reasonable "hydrated" size. Note, however, that for the magnesium halides a cation diameter commensurate with strong hydration was obtained using a fitting procedure similar to the one used here.[46] This clearly illustrates that the effective diameters of ions in the PM is really a property of

the interaction between pairs of ions rather than geometric properties of individual hydrated ions. This carries the implication that it might be possible to improve the agreement with experiments by making the ion sizes non-additive, so that the distance of closest approach between a magnesium ion and a sulfate ion need not be the arithmetic mean of the distance of closest approach between two magnesium ions and two sulfate ions. Since the Coulomb interaction between like charged ions causes the ions to stay well separated on average, regardless of their distance of closest approach, this would likely only have a large effect for high concentrations.

For the SSPM the value of α_{+-} increases with increasing atomic number, with the values for the first row transition metal cations being approximately equal. Note that α_{+-} does *not* carry the interpretation as some "strength of hydration". The effect of the first hydration shell is assumed to be included first and foremost in the ion sizes, that are selected on the basis of geometrical considerations only. There are good reasons to suspect that the cations considered here are strongly hydrated: even the largest one, Cd^{2+}, is smaller than Na^{+}, and has twice the charge. If one accepts the notion that the strength of solvation should be roughly proportional to the field strength at the surface of the ion, as is often argued, see for instance ref. 47, the conclusion must be that Cd^{2+} is more strongly solvated than Na^{+}, which is itself strongly solvated. It is, however, not unreasonable to expect that the sulfate oxygens might replace water molecules in the hydration shell of the cation, thereby allowing smaller cation-anion distances. The feature of u^{s}_{+-} that is probably most important is the attractive well constituted by the first minimum in this oscillatory potential. The peak in g_{+-} coincides closely with this minimum, but in its absence g_{+-} would have a cusp at anion-cation contact. Thus, a larger value of α_{+-} has the main effect that the potential in this region is more negative. In that sense the fits for the PM and SSPM are commensurate: a smaller d_{++} and a larger α_{+-} both gives rise to stronger attraction between anions and cations. The conclusion is thus that the pair potential is more repulsive or less attractive for ions of light elements than for heavy. (Although no definite trend could be discerned within the set of first row transition metals considered.)

Comparison between the fits obtained with the PM and SSPM illustrate that these two models

can be made to agree with experimental data to a similar extent, in terms of the relative activity coefficients, over a large concentration range even though the cation sizes are in some cases very different. However, the two models give rather different results for the *absolute* activity coefficients. Table 3 shows the activity coefficient at 0.1 M concentration and for the purpose of this discussion that may be taken as insignificantly different from the 0.1 m concentration which is the lowest one considered in ref. 8 , for which the activity coefficient is taken to be 0.150 for all divalent sulfates considered therein. (The difference between the Lewis-Randall and McMillan-Mayer scales is hardly significant for this concentration.) The activity coefficients predicted by the PM and SSPM differ greatly for this concentration. Therefore, the PM and SSPM must also disagree about the absolute activity coefficients at higher concentrations. This reveals a subtlety in the modeling of 2:2 electrolytes: the thermodynamic properties are sensitive to the details of the short- and intermediate-range interaction potential down to very small concentrations. Thus, in order to understand the relative importance of Coulomb and non-Coulomb interactions in determining the thermodynamic behavior of electrolytes, reliable information about the activity coefficient in the range 0.1-10 mM is needed for a range of salts.

In refs.[13,18–21] the PM was used for the extrapolation to infinite dilution, evaluated using various approximate theories valid for low concentrations. The ion sizes that were found in those works to give the best fit to experimental data are roughly commensurate with those obtained here. The values of d_{+-} corresponding to our cation sizes are only by a few tenth of an Å from any of those obtained in refs.[13,18–21] for the same cation. The difference between the sizes obtained in the different works is of similar magnitude. The comparison with experiment in section 4.3 indicates that the activity coefficients from the PM agree reasonably well with experiments down to about 10 mM concentration. For lower concentrations the agreement between different experiments is not good enough for any definite conclusion to be drawn. However, if the more recent data from ref. 18 are to be believed the agreement is at least fair for the entire experimental range. The data from ref. 11 closely follows the SSPM curve but the data from ref. 21 (not shown) for the same cell are closer to the data from ref. 18. Comparison with experimental data for different salts yield

the same conclusion, i.e. down to a few mM the PM and SSPM are not meaningfully distinguishable by comparison of the relative activity coefficients (to those for 0.2 m concentration), and for smaller concentration experimental uncertainty makes it hard to choose between them. Nevertheless, both models agree fairly well with experiments over at least three orders of magnitude. The behavior of the relative (but not the absolute) activity coefficient also appears to be insensitive to the details of the interaction potential as the SSPM gives a fit comparable to that of the PM except for very low concentrations. We expect that this is the case not only for the two models considered here but also for a wider class of models.

The expectation that the PM is unable to fit the entire concentration range for which solutions can be prepared[48] is borne out in that the activity coefficients for concentrations much above 1 M are poorly reproduced by the sizes that give a reasonable fit at lower concentrations. Nevertheless, the optimum ion size is roughly the same over at least three orders of magnitude. The PM should thus be regarded as a crude but fairly life-like model up to concentrations of about 1-1.5 M, where the agreement with experiment quickly deteriorates with increasing concentration, see Figure 2. In our opinion, it is hardly meaningful to try to extend the concentration range where a fit can be obtained to higher concentrations as the assumption underlying the PM are hard to justify for high

References

(1) Bjerrum, N. *Z. Electrochem.* **1918**, *24*, 321.

(2) Lund, M.; Jönsson, B.; Pedersen, T. *Mar. Chem.* **2003**, *80*, 95.

(3) Ramanathan, P. S.; Friedman, H. L. *J. Chem. Phys.* **1971**, *54*, 1086.

(4) Friedman, H. L.; Zebolsky, D. M.; Kalman, E. *J. Solution Chem.* **1976**, *5*, 1976.

(5) McMillan, W. G.; Mayer, J. E. *J. Phys. Chem.* **1945**, *13*, 276.

(6) Wernersson, E.; Kjellander, R.; Lyklema, J. *J. Phys. Chem. C* **2009**, submitted.

(7) Pitzer, K. S. *J. Phys. Chem.* **1973**, *77*, 268.

(8) Robinson, R. A.; Stokes, R. H. *Electrolyte Solutions*; Dover Publications, 2002.

(9) Rard, J. A.; Miller, D. G. *J. Chem. Eng. Data* **1981**, *26*, 33.

(10) Pitzer, K. S. *J. Chem. Soc., Faraday Trans. 2* **1972**, *68*, 101.

(11) Bray, U. B. *J. Am. Chem. Soc.* **1927**, *49*, 2372.

(12) Getman, F. H. *J. Phys. Chem.* **1930**, *34*, 1454.

(13) La Mer, V. K.; Parks, W. G. *J. Am. Chem. Soc.* **1931**, *53*, 2040.

(14) Masaki, K.; Ikkatai, T. *Bull. Chem. Soc. Japan* **1932**, *7*, 238.

(15) Demassieux, N.; Fedoroff, B. *Ann. de Chimie, Ser. 11* **1941**, *16*, 215.

(16) Fedoroff, B. *Ann. de Chimie, Ser. 11* **1941**, *16*, 154.

(17) Davies, W. G.; Otter, R. J.; Prue, J. E. *Disc. Faraday Soc.* **1957**, *24*, 103.

(18) Malatesta, F.; Zamboni, R. *J. Solution Chem.* **1997**, *26*, 791.

(19) Malatesta, F.; Carbonaro, L.; Fanelli, N.; Ferrini, S.; Giacomelli, A. *J. Solution Chem.* **1999**, *28*, 593.

(20) Malatesta, F.; Trombella, S.; Fanelli, N. *J. Solution Chem.* **2000**, *29*, 685.

(21) Copperthwaite, I. A.; La Mer, V. K. *J. Am. Chem. Soc.* **1931**, *53*, 4333.

(22) Valleau, J. P.; Cohen, L. K.; Card, D. N. *J. Chem. Phys.* **1980**, *72*, 5924.

(23) Duh, D.-M.; Haymet, A. D. J. *J. Chem. Phys.* **1992**, *97*, 7716.

(24) Belloni, L. *J. Chem. Phys.* **1993**, *98*, 8080.

(25) *Handbook of Chemistry and Physics*, 52nd ed.; Weast, R. C., Ed.; The Chemical Rubber Co.: Cleveland, OH, 1971.

(26) Marcus, Y. *Ion Properties*; Marcel Dekker, Inc.: New York, 1997.

(27) Dang, L. X.; Rice, J. E.; Kollman, P. A. *J. Chem. Phys.* **1990**, *93*, 7528.

(28) Guàrdia, E.; Rey, R.; Padró, J. A. *Chem. Phys.* **1991**, *155*, 187.

(29) Guàrdia, E.; Rey, R.; Padró, J. A. *J. Chem. Phys.* **1991**, *95*, 2823.

(30) Gavryushov, S.; Linse, P. *J. Phys. Chem. B* **2006**, *110*, 10878.

(31) Gavryushov, S. *J. Phys. Chem. B* **2006**, *110*, 10888.

(32) Lyubartsev, A. P.; Laaksonen, A. *Phys. Rev. E* **1995**, *52*, 3730.

(33) Lyubartsev, A. P.; Laaksonen, A. *Phys. Rev. E* **1997**, *55*, 5689.

(34) Lyubartsev, A. P.; Marělja, S. *Phys. Rev. E* **2002**, *65*, 041202–1.

(35) Ciccarello, S.; Gazzillo, D. *J. Chem. Soc., Faraday Trans. 2* **1985**, *81*, 1163.

(36) Rasaiah, J. C.; Friedman, H. L. *J. Chem. Phys.* **1968**, *48*, 2742.

(37) Ng, K.-C. *J. Chem. Phys.* **1974**, *61*, 2680.

(38) Rossky, P. J.; Dudowicz, J. B.; Tembe, B. L.; Friedman, H. L. *J. Chem. Phys.* **1980**, *73*, 3372.

(39) Morita, T. *Prog. Theor. Phys.* **1960**, *23*, 829.

(40) Schlijper, A. G.; da Gama, M. M. T.; Ferreira, P. G. *J. Chem. Phys.* **1993**, *98*, 1534.

(41) Svensson, B. R.; Woodward, C. E. *Mol. Phys.* **1988**, *64*, 247.

(42) Pailthorpe, B. A.; Mitchell, D. J.; Ninham, B. W. *J. Chem. Soc. Faraday Trans.* **1984**, *80*, 115.

(43) Novotný, P.; Söhnel, O. *J. Chem. Eng. Data* **1988**, *33*, 49.

(44) Robinson, R. A.; Stokes, R. H. *Trans. Faraday Soc.* **1949**, *45*, 612.

(45) Rasaiah, J. C. *J. Chem. Phys.* **1972**, *56*, 3071.

(46) Abbas, Z.; Ahlberg, E.; Nordholm, S. *J. Phys. Chem. B* **2009**, *113*, 5905.

(47) Collins, K. D.; Nielson, G. W.; Enderby, J. E. *Biophys. Chem.* **2007**, *128*, 95.

(48) Rasaiah, J. C. *J. Solution Chem.* **1973**, *2*, 301.

Tables

Table 1: Optimizes cation diameters for the PM.

cation	d_{++} (Å)	d_{+}^{b} (Å)^{a}	$10^2 * \delta$
Be^{2+}	3.14	0.72	0.34
Mg^{2+}	2.77	1.44	1.28
Mn^{2+}	2.30	1.66	1.48
Ni^{2+}	2.11	1.38	1.57
Cu^{2+}	2.07	1.46	0.76
Zn^{2+}	2.25	1.50	1.06
Cd^{2+}	2.01	1.90	0.85

[a] The selected values of the ion diameter in crystals from ref. 26.

Table 2: Optimized interaction strength parameter for the SSPM.

cation	$\frac{\alpha_{+-}}{k_B T}$	d_{++} (Å)^{a}	$10^2 * \delta$
Be^{2+}	2.5	3.48	0.43
Mg^{2+}	4.4	4.20	0.72
Mn^{2+}	5.2	4.42	0.55
Ni^{2+}	5.1	4.14	0.62
Cu^{2+}	5.2	4.22	0.38
Zn^{2+}	5.0	4.26	0.33
Cd^{2+}	5.8	4.66	0.38

[a] See Section 2.2.

Table 3: Theoretical activity coefficients for 0.1 M concentration.

cation	$f_{\pm}^{PM}(0.1\ \mathrm{M})$	$f_{\pm}^{SSPM}(0.1\ \mathrm{M})$
Be^{2+}	0.156	0.166
Mg^{2+}	0.146	0.165
Mn^{2+}	0.132	0.160
Ni^{2+}	0.129	0.155
Cu^{2+}	0.125	0.155
Zn^{2+}	0.131	0.159
Cd^{2+}	0.122	0.157

Figure Captions

Figure 1: The best-fit potential of the PM (full curve) and SSPM (dashed curve) in units of k_BT for $ZnSO_4$, see Table 1 and Table 2 in Section 4.1.

Figure 2: In panel (a) the osmotic coefficient as a function of concentration is shown. In panel (b) the logarithm of the the mean activity coefficient relative to its value at 0.2 m is shown. The symbols are experimental data from ref. 8 and the lines are calculated from the primitive model (PM) in the HNC approximation. The circles and short-dashed curves are for $BeSO_4$, diamonds and medium-dashed curves are for $MgSO_4$, triangles and long dashed curves for $MnSO_4$ and stars and full curves $CdSO_4$. $NiSO_4$, CuSO4 and $ZnSO_4$ have been omitted to avoid cluttering the figure. The curves corresponding to these salts would all fall between those for $MnSO_4$ and $CdSO_4$. The cation sizes are chosen to give optimal agreement between PM osmotic coefficients in the range 0.2 to 1.0 m, see Table 1. Points corresponding to higher concentrations are not considered in the fit.

Figure 3: Same as Figure 2, but with interaction potential parameters taken from Table 2. Here, it is α_{+-} rather than d_{++} that is used as a fitting parameter.

Figure 4: Comparison between the HNC approximation (curves) and MC simulation (symbols) for the PM with four different cation diameters. The circles and short-dashed curves are for $d_{++} =$ 3.14 Å (the size that gives the best fit for $BeSO_4$), diamonds and medium-dashed curves are for $d_{++} = 2.77$ Å ($MgSO_4$), triangles and long dashed curves for $d_{++} = 2.30$ Å ($MnSO_4$) and stars and full curves for $d_{++} = 2.01$ Å ($CdSO_4$). See Table 1.

Figure 5: Comparison between the HNC approximation and MC simulation for the SSPM for four different divalent sulfates. The circles and short-dashed curves are for the parameters that gives the best fit for $BeSO_4$, diamonds and medium-dashed curves are for $MgSO_4$, triangles and long dashed curves for $MnSO_4$ and stars and full curves for $CdSO_4$. See Table 2. Note that the abscissa is in log-scale in the upper pannel.

Figure 6: Comparison between the HNC approximation (curves) and MC simulation (symbols) for the pair distribution functions $g_{ij}(r)$ for the SSPM with parameters corresponding to $ZnSO_4$, see section 2.2 and table Table 2. Panel a is $g_{+-}(r)$ shown on a log-linear plot and panel b is $g_{+-}(r)$ (full curves and filled circles) and $g_{++}(r)$ (dashed curves and open circles) on a linear-linear plot. The data is shown in this way to enable comparison both for the strongly peaked $g_{+-}(r)$ and the slowly varying $g_{++}(r)$. Curves and symbols for $g_{--}(r)$ are not shown because these would be indistinguishable from $g_{++}(r)$ on the scale of the figure.

Figure 7: Comparison between simulations for the PM (full lines) and the SSPM (dashed lines) and experimental data (circles and triangles for data from refs.[11] and,[18] respectively) for the mean activity coefficient of $ZnSO_4$. In panel (a) the data is presented as given in the original reference while in panel (b) the data is shifted to bring the value to zero for 0.2 m concentration, in effect making the excess chemical potential for this concentration that of the standard state.

Figure 8: Comparison between simulations for the PM (full lines) and the SSPM (dashed lines) and experimental data (symbols), from ref. 18, for the mean activity coefficient of $MgSO_4$.

Figure 9: As Figure 8, but for $CdSO_4$. Data from refs. 19 (triangles) and 13 (circles).

Figures

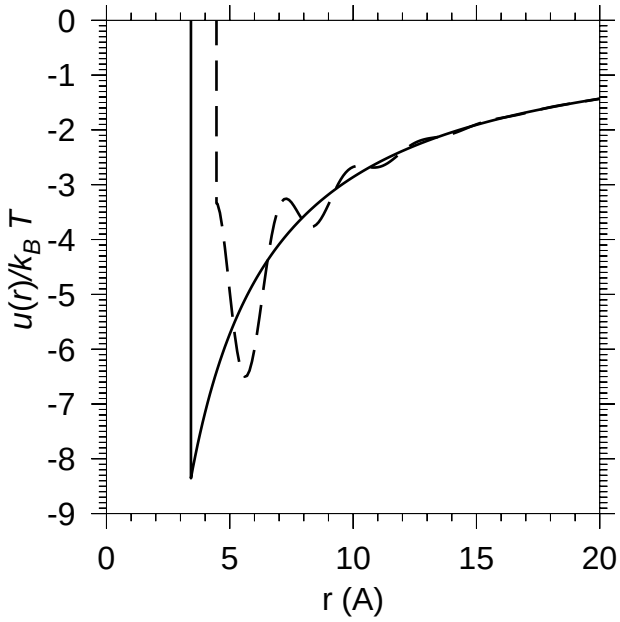

Figure 1

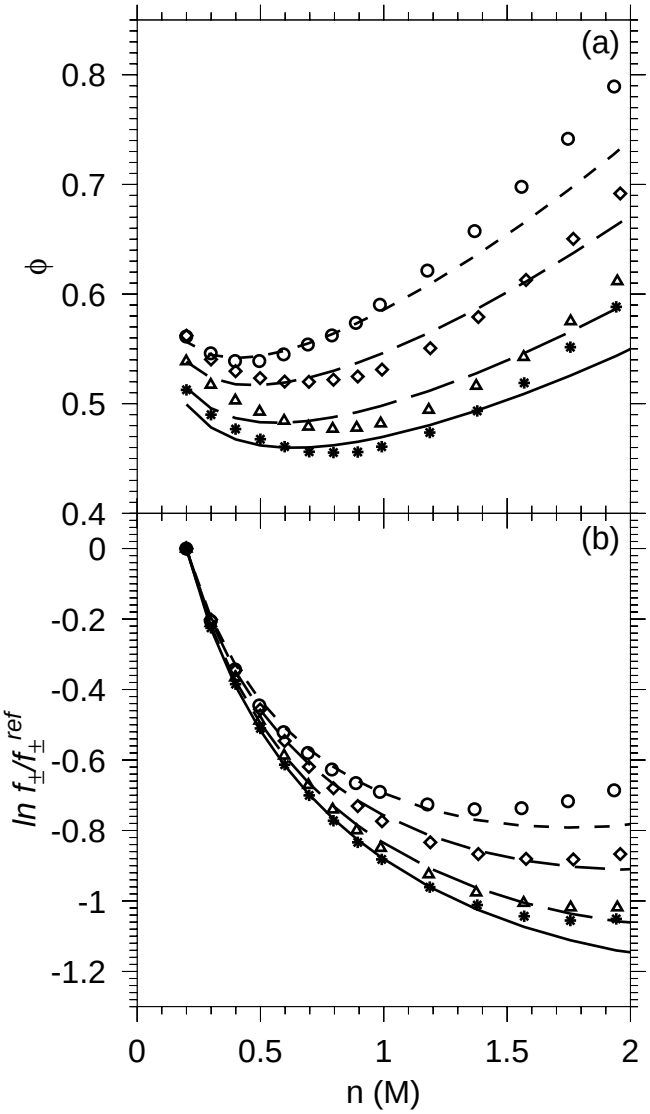

Figure 2

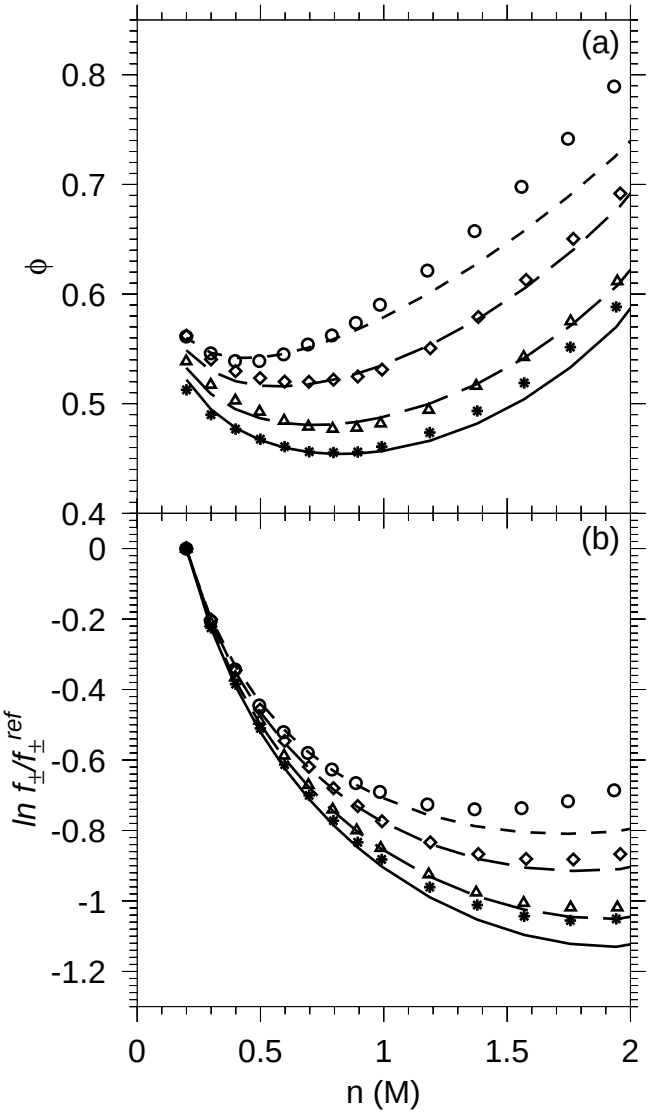

Figure 3

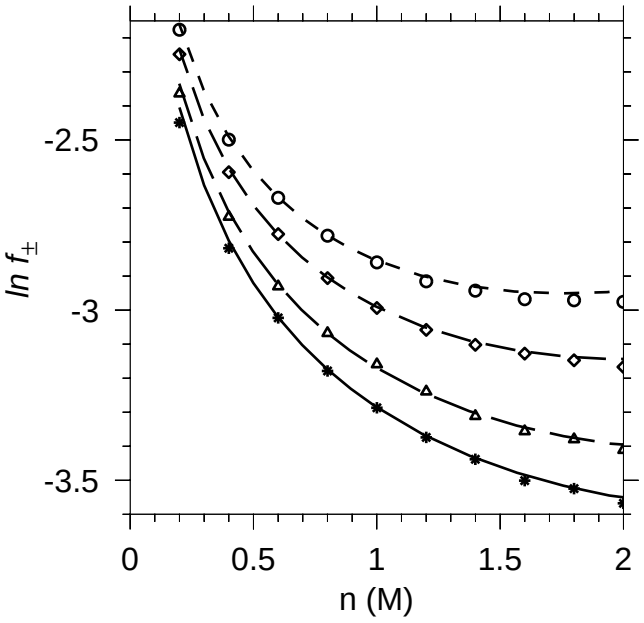

Figure 4

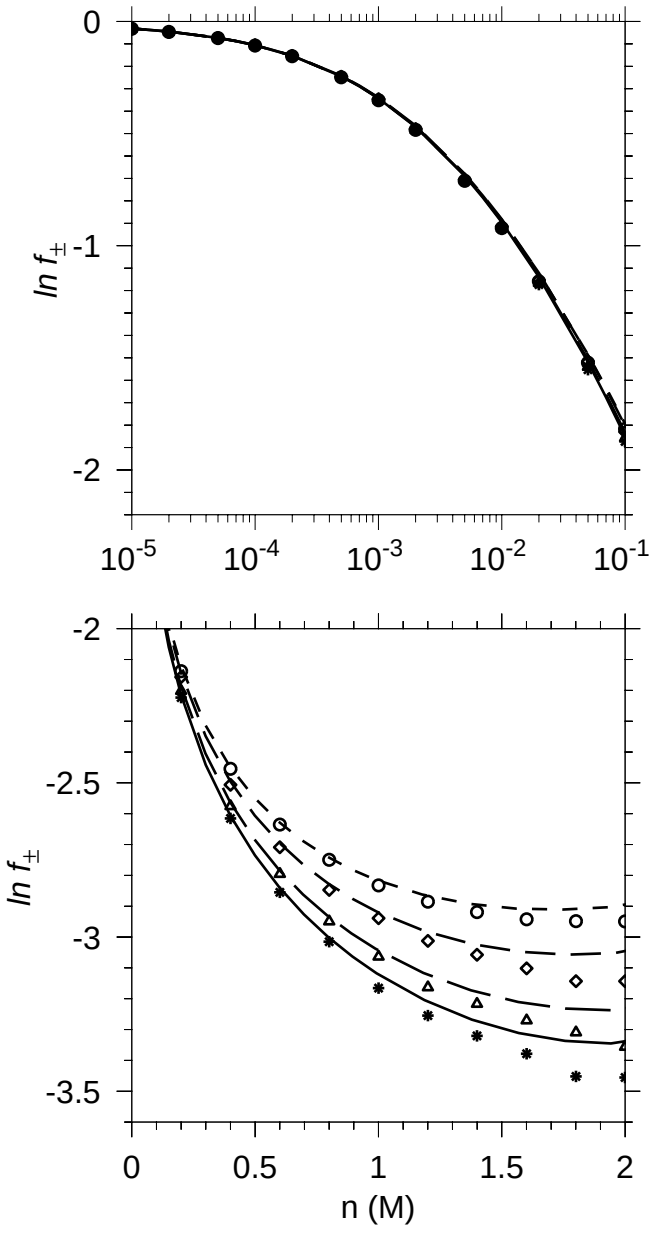

Figure 5

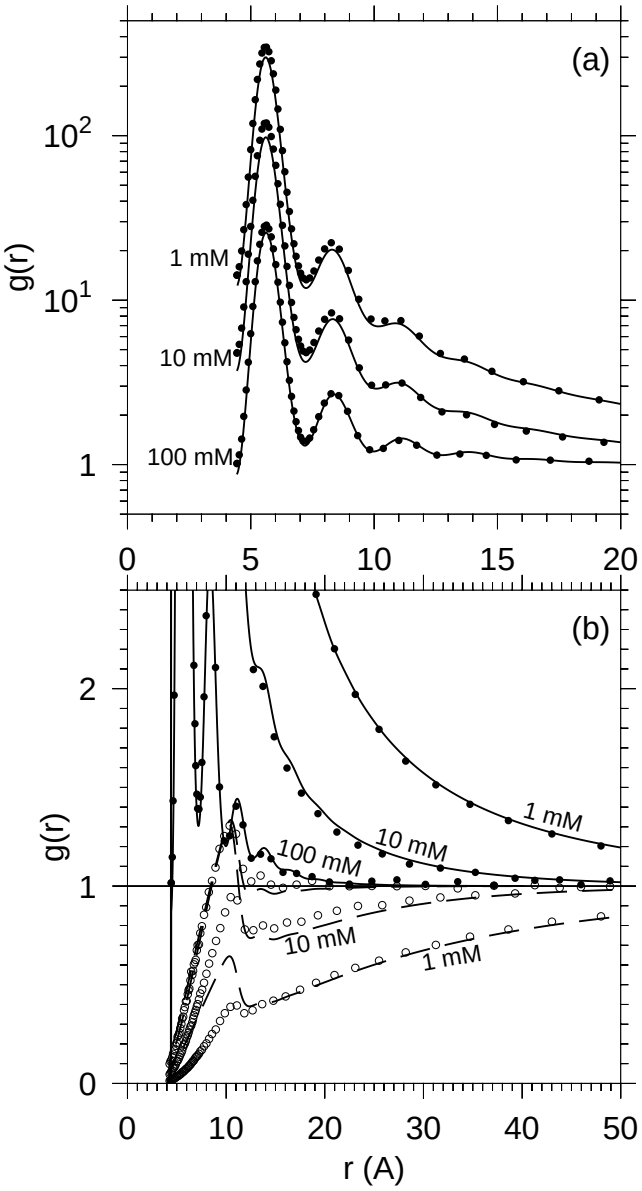
(a)
g(r)
10^2
10^1
1
1 mM
10 mM
100 mM
0
5
10
15
20
(b)
g(r)
2
1
0
1 mM
10 mM
100 mM
10 mM
1 mM
0
10
20
30
40
50
r (A)

Figure 6

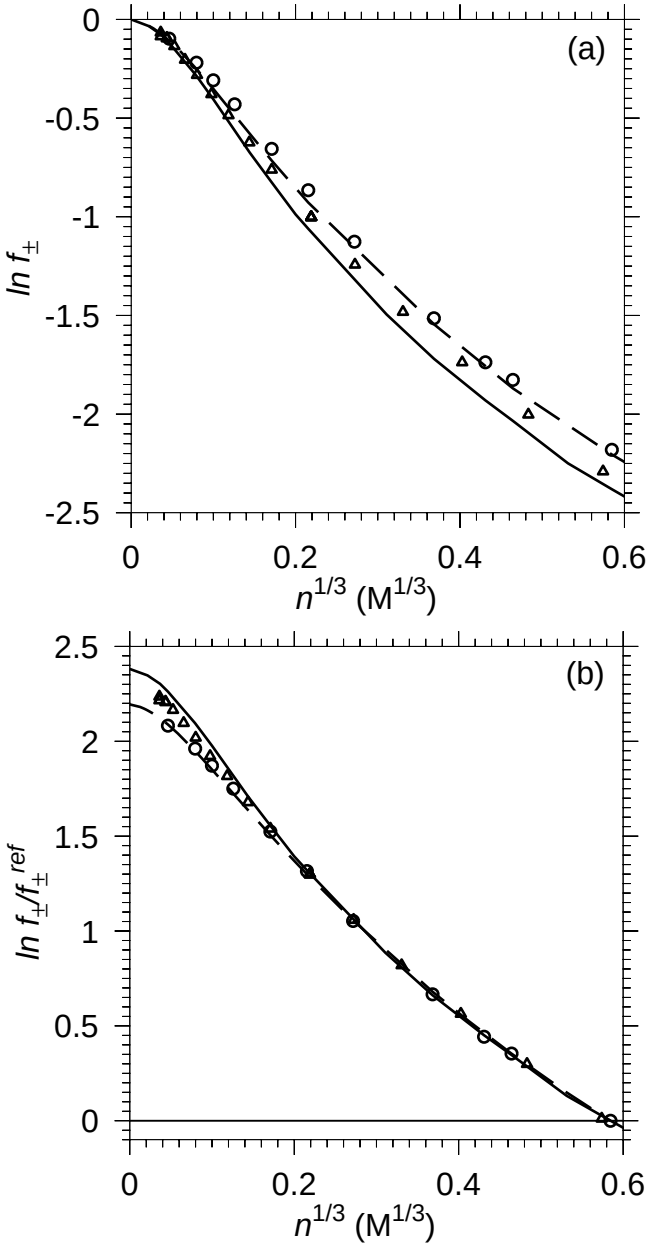
(a)
0
-0.5
-1
-1.5
-2
-2.5
ln f±
0
0.2
0.4
0.6
n1/3 (M1/3)
(b)
2.5
2
1.5
1
0.5
0
ln f±/f± ref
0
0.2
0.4
0.6
n1/3 (M1/3)

Figure 7

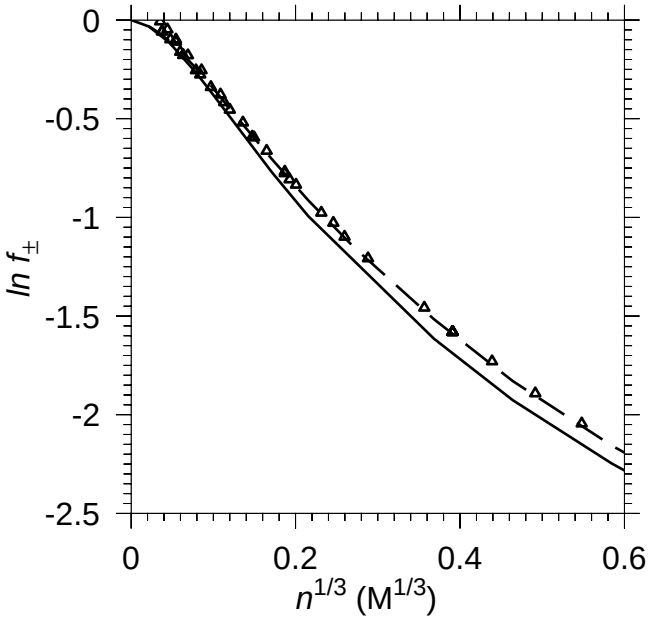

Figure 8

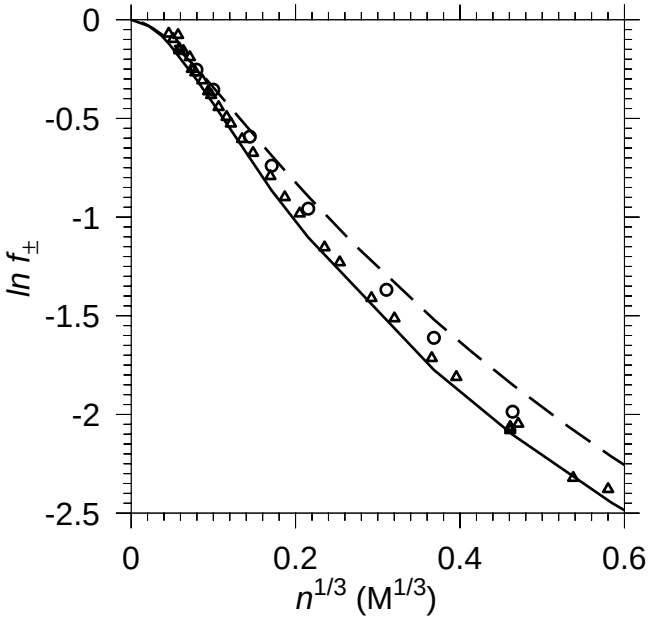

Figure 9